Synthesis and Structural Studies of Metallacarboranes

Greig Scott

Submitted for the degree of Doctor of Philosophy at Heriot-Watt University, on completion of research in the School of Engineering and Physical Sciences.

February 2015

Abstract

The properties of some new metallacarboranes are described in this thesis, along with the results of a study to determine structural patterns in compounds published by others.

Chapter 1 introduces heteroborane cluster compounds and a description of the bonding in these compounds. The synthesis and structure of supraicosahedral heteroboranes are discussed in detail with reference to literature examples throughout. A brief description of the trans influence is also given.

Chapter 2 describes the synthesis and structures of a series of thirteen vertex indenyl cobaltacarboranes and a single fourteen vertex bimetallic indenyl cobaltacarborane. The crystallographically-determined orientation of the exo-polyhedral indenyl ligand in each compound is used to probe the relative strengths of the metal-carborane bonds. Rotation of a related exo-polyhedral ligand about 360º is explored computationally and the results used to help rationalise the orientations of the indenyl ligands.

Chapter 3 describes the synthesis and structures of a single twelve vertex and a series of thirteen vertex naphthalene ruthenacarboranes. As for the isoelectronic indenyl cobaltacarboranes, the orientations of the naphthalene ligands are explored crystallographically and computationally. The details of some unexpected side products are also discussed.

Chapter 4 is an analysis of the results of a crystallographic database search which showed clear structural patterns in previously published metallacarboranes. Cage atoms which are relatively weakly bonded to the metal tend to lie trans to exo-polyhedral ligands which are relatively strongly bonded to the metal.

Chapter 5 describes the structures of thirteen and fourteen vertex bimetallic pentamethylcyclopentadienyl ruthenacarboranes with unconventional electron counts, which were synthesised by metallation followed by direct electrophilic insertion. The structures of an exo-polyhedral metal-bound species and three solvent-bound zwitterionic

metallacarboranes prepared from attempted direct electrophilic insertion reactions are also presented.

Chapter 6 gives the experimental procedures used to synthesise and purify each new compound and provides details of how they were characterised.

Appendix 1 lists the crystallographic data relevant to each compound.

Appendix 2 gives details of the literature structures found during the structural database search described in chapter four.

Appendix 3 (electronic appendix - see CD-ROM) contains rtf and CIF files (crystallographic data) for all compounds (where available).

Appendix 4 (electronic appendix - see CD-ROM) contains CIF and mol2 files for all literature compounds discussed in chapter four.

Acknowledgements

I would firstly like to thank my supervisor Professor Alan Welch for his help and guidance during my PhD. Throughout my time at Heriot-Watt he has always taken the time to answer my questions and provide support. His enthusiasm for boron chemistry is boundless, and I could not imagine having a better supervisor. I am also grateful to the EPSRC for funding.

I would also like to thank Dr David Ellis for his help, both during his time as a postdoc and running the NMR service. His patience in answering my queries and his suggestions of solutions to experimental problems were greatly appreciated. I would also like to thank Dr Winnie Man, with whom I collaborated on the work described in chapter five. Her helpfulness and friendliness made the last year of my time in the lab all the more enjoyable. The work described in chapter one would not have been possible without the help and support of Dr Amelia McAnaw, who showed me the ropes in the Boron Lab. Amelia's guidance and encouragement when we worked together was invaluable.

I also thank former Boron Group members Ross, Hugo, Brian, Gobika and Chris - all of whom helped me at some point in my research and contributed to a great environment in the lab. All the former Boron Group members also deserve acknowledgement, as I have consulted their research for ideas and experimental details during my PhD, as do the current group members who have been very friendly and supportive whilst I have been writing up. Lastly from the Boron Group I would like to thank Lisa Elrick (who helped with the work in chapter four) and Sam Powley, the two project students who I worked with. I enjoyed working with both of them (and hope I, in turn, was tolerable to work with).

The computational calculations detailed in chapters two and three were performed by Dr David McKay and his contribution to this work is much appreciated. Thanks is also due to Dr Georgina Rosair for her role as the *X*-ray crystallographer and for running the mass spectrum service, but also for all the help which she gave me in refining my structures. I am also grateful to Dr Koenraad Collart and Christina Graham for elemental analysis, Mary Pratt for helping me in stores, Dr Alan Boyd for NMR spectra and the chemistry department staff, most of whom I bothered with some question(s) about my research at some point or another.

Finally, I would like to thank my family for their support and patience during my PhD.

Table of contents

Chapter 6 – Experimental Section

Appendix 1

Appendix 2

Appendix 3 (electronic appendix - see CD-ROM)

Crystallographic data for all compounds (where available)

Appendix 4 (electronic appendix - see CD-ROM)

CIF and Mol2 files for chapter four literature compounds

Abbreviations

2c-2e	two centre two electron
3c-2e	three centre two electron
Å	Ångström, $1x10^{-10}$ m
ABMO	Anti-Bonding Molecular Orbital
ADP	Anisotropic Displacement Parameter
bipy	2,2′-bipyridine, $C_{10}H_8N_2$
BMO	Bonding Molecular Orbital
br	broad
[BTMA]Cl	benzyltrimethylammonium chloride, $[PhNMe_3]Cl$
CHN	elemental analysis
Cp	cyclopentadienyl (C_5H_5)
Cp^*	pentamethylcyclopentadienyl (C_5Me_5)
CPF	Crystal Packing Force
Δ	designates heating of a compound/reaction
δ	chemical shift
d	doublet
DCM	dichloromethane
DEI	Direct Electrophilic Insertion
DFT	Density Functional Theory
Dip	2,6-diisopropylphenyl
DSD	Diamond-Square-Diamond
EHMO	Extended Hückel Molecular Orbital
EI	Electron Impact
ELO	Exo-polyhedral Ligand Orientation
EPL	Exo-Polyhedral Ligand
Et	ethyl
e.s.d.	estimated standard deviation
EWG	Electron Withdrawing Group
FMO	Frontier Molecular Orbital
HOMO	Highest Occupied Molecular Orbital
LUMO	Lowest Occupied Molecular Orbital

m	muliplet
M^+	parent ion
Me	methyl
mmol	millimoles
MS	Mass Spectrometry
M_w	molecular weight
n-BuLi	*n*-butyl lithium
NMR	Nuclear Magnetic Resonance
p-cymene	1-methyl-4-isopropyl-benzene
Ph	Phenyl
ppm	parts per million
PSE	Polyhedral Skeletal Electron
PSEP	Polyhedral Skeletal Electron Pair
R_f	retention factor
RTE	Rotational Trans Effect
s	singlet
t	triplet
THF	tetrahydrofuran
TLC	Thin Layer Chromatography

Abbreviations for specific compounds

1 4-(η-C_9H_7)-4,1,6-*closo*-$CoC_2B_{10}H_{12}$

2 1,6-Me_2-4-(η-C_9H_7)-4,1,6-*closo*-$CoC_2B_{10}H_{10}$

3 4-(η-C_9H_7)-4,1,8-*closo*-$CoC_2B_{10}H_{12}$

4 1,8-Me_2-4-(η-C_9H_7)-4,1,8-*closo*-$CoC_2B_{10}H_{10}$

5 4-(η-C_9H_7)-4,1,12-*closo*-$CoC_2B_{10}H_{12}$

6 1,12-Me_2-4-(η-C_9H_7)-4,1,12-*closo*-$CoC_2B_{10}H_{10}$

7 4-(η-C_9H_7)-4,1,10-*closo*-$CoC_2B_{10}H_{12}$

8 1,14-(η-C_9H_7)$_2$-1,14,2,10-*closo*-$Co_2C_2B_{10}H_{12}$

9 3-(η-$C_{10}H_8$)-3,1,2-*closo*-$RuC_2B_9H_{11}$

10 3-(η-EtPh)-3,1,2-*closo*-$RuC_2B_9H_{11}$

11 4-(η-$C_{10}H_8$)-4,1,6-*closo*-$RuC_2B_{10}H_{12}$

12 4-(η-$C_{10}H_8$)-4,1,8-*closo*-$RuC_2B_{10}H_{12}$

13 4-(η-$C_{10}H_8$)-4,1,10-*closo*-$RuC_2B_{10}H_{12}$

14 4-(η-$C_{10}H_8$)-4,1,12-*closo*-$RuC_2B_{10}H_{12}$

15 4-(η-C_8H_{10})-4,1,6-*closo*-$RuC_2B_{10}H_{12}$

16 4-(η-$C_{10}H_{12}$)-4,1,6-*closo*-$FeC_2B_{10}H_{12}$

17 7-(THF)-3-(η-C_5Me_5)-3,1,2-*closo*-$RuC_2B_9H_{10}$

18 4,5-(η-C_5Me_5)$_2$-4,5,1,6-*closo*-$Ru_2C_2B_9H_{11}$

19 4,5-(η-C_5Me_5)$_2$-4,5,2,11-*closo*-$Ru_2C_2B_9H_{11}$

20 8-(n-BuO)-4,5-(η-C_5Me_5)$_2$-4,5,1,6-*closo*-$RuC_2B_9H_{10}$

21 3,6-(η-C_5Me_5)$_2$-3,6,?,?-*closo*-$RuC_2B_{10}H_{12}$*

22 3,6-(η-C_5Me_5)$_2$-3,6,2,?-*closo*-$RuC_2B_{10}H_{12}$*

23 (μ^3-dicarba-*closo*-dodecaborane-B^1,B^2,B^3,H^1,H^2,H^3)-(μ^3-ethylidyne)-tris(η^5-pentamethylcyclopentadienyl)-triruthenium*

24 5-(THF)-2,3-(CH_2)$_3$-1-(η-C_5Me_5)-1,2,3-*closo*-$RuC_2B_{11}H_{10}$

25 11-(THF)-2,3-(CH_2)$_3$-1-(η-C_5Me_5)-1,2,3-*closo*-$RuC_2B_{11}H_{10}$

I 3-(η-C_9H_7)-3,1,2-*closo*-$CoC_2B_9H_{11}$

II 8-Me-4-(η-C_9H_7)-4,1,8-*closo*-$CoC_2B_{10}H_{11}$

III 1,2-Me_2-4-(η-C_9H_7)-4,1,2-*closo*-$CoC_2B_{10}H_{10}$

IV 1,2-(CH_2)$_3$-4-(η-C_9H_7)-4,1,2-*closo*-$CoC_2B_{10}H_{10}$

V 3,3-(PPh_3)$_2$-3-H-3,1,2-*closo*-$RhC_2B_9H_{11}$

VI 3-(κ^2-NO_3)-3-(PPh_3)-*closo*-3,1,2-$RhC_2B_9H_{11}$

VII 3,3-(PPh_3)$_2$-3-(κ^1-NO_3)-3,1,2-*closo*-$RhC_2B_9H_{11}$

VIII 4,5-(η-C_5Me_5)$_2$-4,5,2,3-*closo*-$Ru_2C_2B_9H_{11}$

IX 4,5-(η-C_5H_5)$_2$-4,5,2,3-*closo*-$Fe_2C_2B_9H_{11}$

* For these compounds one or both of the cage carbon atoms could not be located during crystallographic refinement.

Chapter 1
Introduction

1.1 Boron and boron hydrides

The element boron was discovered in 1808 by the reduction of boric acid.[1] The word boron comes from the mineral ore borax ($Na_2B_4O_7 \cdot 10H_2O$), one of the principle sources of the world's boron. Boron can exist as several allotropes, all of which (including two of the most common ones, α- and β-rhombohedral) contain B_{12} icosahedra (polyhedron with twelve vertices). Boron has two naturally occurring stable isotopes ^{10}B (19.78%) and ^{11}B (80.22%), both of which are NMR active. NMR spectroscopy of the heavier, more abundant ^{11}B isotope is used routinely to help characterise boron-containing compounds.

While carbon can obtain a full octet by forming four covalent 2c-2e bonds, which is the basis of much of organic chemistry, boron has only three valence electrons, and so cannot obtain its octet by forming three (non-dative) covalent 2c-2e bonds. Fortunately the electron deficiency of boron compared to its neighbour carbon allows for fascinating polyhedral clusters with BH vertices. One boron atom can bond to three hydrogen atoms by electron precise bonding, leaving an unoccupied p-orbital perpendicular to the BH_3 plane (figure 1.1.1).

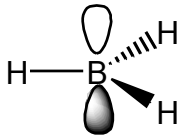

Figure 1.1.1 BH_3, with the empty p-orbital shown.

BH_3 does not normally exist as a discrete molecule, it either coordinates to a Lewis base to give an adduct or dimerises to give B_2H_6 (figure 1.1.2).[2] B_2H_6 takes advantage of 3c-2e B-H-B units to give a structure which satisfies the octet of the boron atoms.[3] In BX_3 (X = π-donor) electron density from the π-donor can be donated to the boron atom's unoccupied p-orbital to stabilise the molecule.

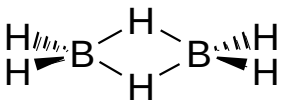

Figure 1.1.2 B_2H_6, the dimeric form of BH_3.

Boron hydrides such as B_2H_6 are called boranes, and while the simplest member of this family is too small to be a polyhedral cluster/cage (the terms cluster and cage are used interchangeably), addition of BH vertices/electrons builds up the $[B_nH_n]^{2-}$ polyhedral clusters and related open-faced clusters which are more highly negatively charged ($[B_nH_n]^{4-}$/$[B_nH_n]^{6-}$) and often made neutral by the binding of protons to the open face (B_nH_{n+4}/ B_nH_{n+6}).

The icosahedral boron hydride with twelve cage vertices was predicted[4] to be dianionic, and the isolation of the potassium salt $K_2[B_{12}H_{12}]$ confirmed this.[5] $[B_{12}H_{12}]^{2-}$ is very robust, being able to withstand temperatures above 800 ^oC and exhibiting inertness toward many reagents with the notable exception of strong bases.[6]

Borane chemistry first found major application in the late 1940s when B_2H_6, B_5H_9 and $B_{10}H_{14}$ were explored for use as rocket fuels.[6] Ultimately this use of boranes never really came to fruition due to problems with the presence of boron combustion products and boranes being overtaken by other non-borane advances in rocket fuel chemistry. However large stockpiles of certain boranes had been prepared for rocket fuel research and attention turned to exploring the chemistry of these compounds. This included the incorporation of other elements as vertices in borane clusters to give heteroboranes.

Current applications of heteroboranes[6] include: the cancer treatment boron neutron capture therapy (BNCT)[7a] (figure 1.1.3 (a)); catalysis - in, for example, olefin hydrogenation/isomerisation[7b] (figure 1.1.3 (b)); extraction of radioactive nucleotides; least coordinating anions; incorporation into polymers[7c] (figure 1.1.3 (c)); HIV protease inhibitors; neutron capture in nuclear reactors; supramolecular chemistry/molecular machines; and superacid compounds.

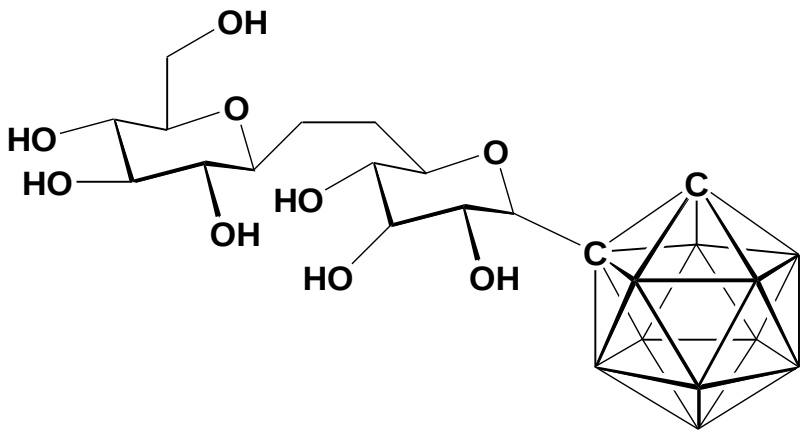

(a)

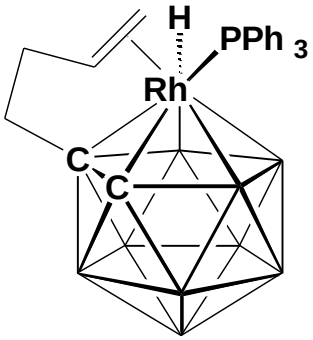

(b)

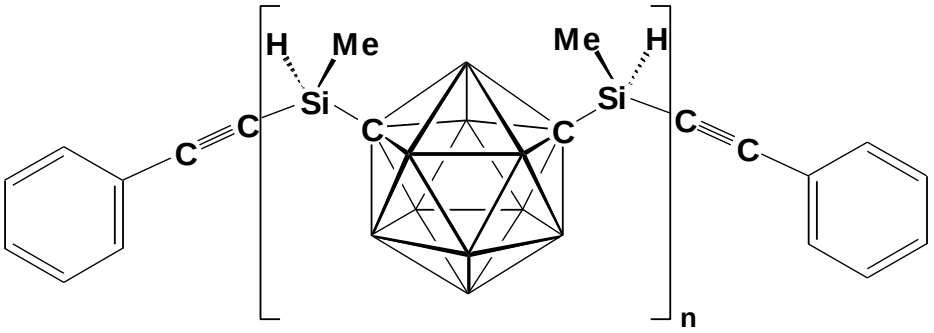

(c)

Figure 1.1.3 Structures of: (a) a glycoside-carborane compound identified as a good candidate for BNCT; (b) a 1-*n*-butenyl-substituted rhodacarborane which is an effective alkene hydrogenation catalyst; (c) a phenylacetylene-terminated *m*-carboranyl polymer.

1.2 Bonding in boranes

One of the first approaches[8] to rationalising the bonding in boranes involved solving three simultaneous equations, given below, the variables for which are the number of: 3c-2e B-B-B bonds (t); 2c-2e B-B bonds (y); 3c-2e B-H-B bonds (s); BH_2 vertices (x), and the values n and m for a borane of formula B_nH_{n+m}:

$$t + y = n - m/2 \qquad s + x = m \qquad s + t = n$$

This bonding approach was called the styx rules, and was quite effective for smaller boranes, but the equations were not able to accurately predict the structures of the larger boranes.

A better description of the bonding in boranes was given by Polyhedral Skeletal Electron Pair theory (PSEP theory, also known as Wade's rules).[9] This theory uses equation **1** to assign the number of cluster bonding electrons provided by any main group vertex, the total of which for the whole cluster (plus any negative charges/bridging hydrogens, each of which contribute one electron), divided by two, gives the number of PSEPs:

$$s = v + x - 2 \qquad (\mathbf{1})$$

v = the number of valence electrons of the vertex atom, and x = the number of electrons provided by exo-polyhedral groups.
Number of cluster bonding electrons for a {BH} vertex $\rightarrow$ $s = 3 + 1 - 2 = 2$
The number of PSEPs relative to the number of vertices (n), gives the type of structure:

n + 1 = *closo*
n + 2 = *nido* (i.e. one $[BH]^{2+}$ vertex removed)
n + 3 = *arachno* (i.e. two $[BH]^{2+}$ vertices removed)
n + 4 = *hypo* (i.e. three $[BH]^{2+}$ vertices removed)
n + 5 = *klado* (i.e. four $[BH]^{2+}$ vertices removed)
n = *hypercloso* (usually a closo-like structure which is stable with only n PSEPs)

Closo is the prefix for a closed, totally deltahedral cluster, whereas nido and arachno structures contain open faces. For $[closo\text{-}B_nH_n]^{2-}$ the following structures are predicted for the

n = 5-12 clusters: $[B_5H_5]^{2-}$, trigonal bipyramid; $[B_6H_6]^{2-}$, octahedron; $[B_7H_7]^{2-}$, pentagonal bipyramid; $[B_8H_8]^{2-}$, dodecahedron; $[B_9H_9]^{2-}$, tricapped trigonal prism; $[B_{10}H_{10}]^{2-}$, bicapped square antiprism; $[B_{11}H_{11}]^{2-}$, octadecahedron; $[B_{12}H_{12}]^{2-}$, icosahedron (figure 1.2.1).

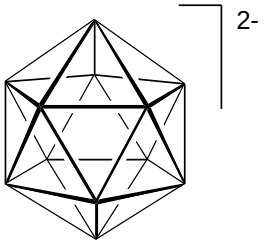

Figure 1.2.1 Icosahedral structure of [*closo*-$B_{12}H_{12}]^{2-}$.

PSEP theory is based in MO theory, as can be seen by the example of [*closo*-$B_6H_6]^{2-}$, which has at every vertex one available radial and two tangential orbitals. The tangential orbitals form the surface of the cluster - overlapping to give six BMOs and six ABMOs, whilst the radial orbitals point inwards, to form five ABMOs, and one BMO (figure 1.2.2 (left)). Filling all of the BMOs requires fourteen electrons, or n + 1 electron pairs, where n is the number of boron vertices (six in this case).

The removal of a $[BH]^{2+}$ vertex (a decapitation) leads to retention of the overall polyhedral structure, albeit minus one vertex, as the electrons have been retained by the cluster and the symmetry of the resulting nido species ensures that the number of BMOs is the same (although the energies are not, as can be seen figure 1.2.2 (right)).[9,10]

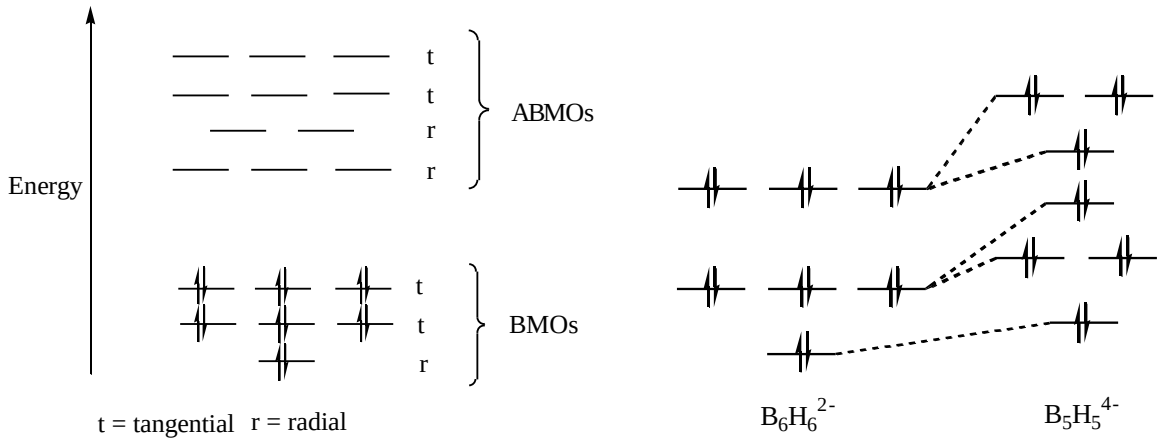

Figure 1.2.2 Cluster molecular orbital diagram for (left) [*closo*-$B_6H_6]^{2-}$ and (right) change in energy of BMOs in going from [*closo*-$B_6H_6]^{2-}$ to [*nido*-$B_5H_5]^{4-}$.

The nido and arachno fragments of the [*closo*-B_nH_n]$^{2-}$ n = 10-13 boranes are shown in figure 1.2.3 in part of a scheme called the Wade-Williams-Rudolph structural matrix.[10]

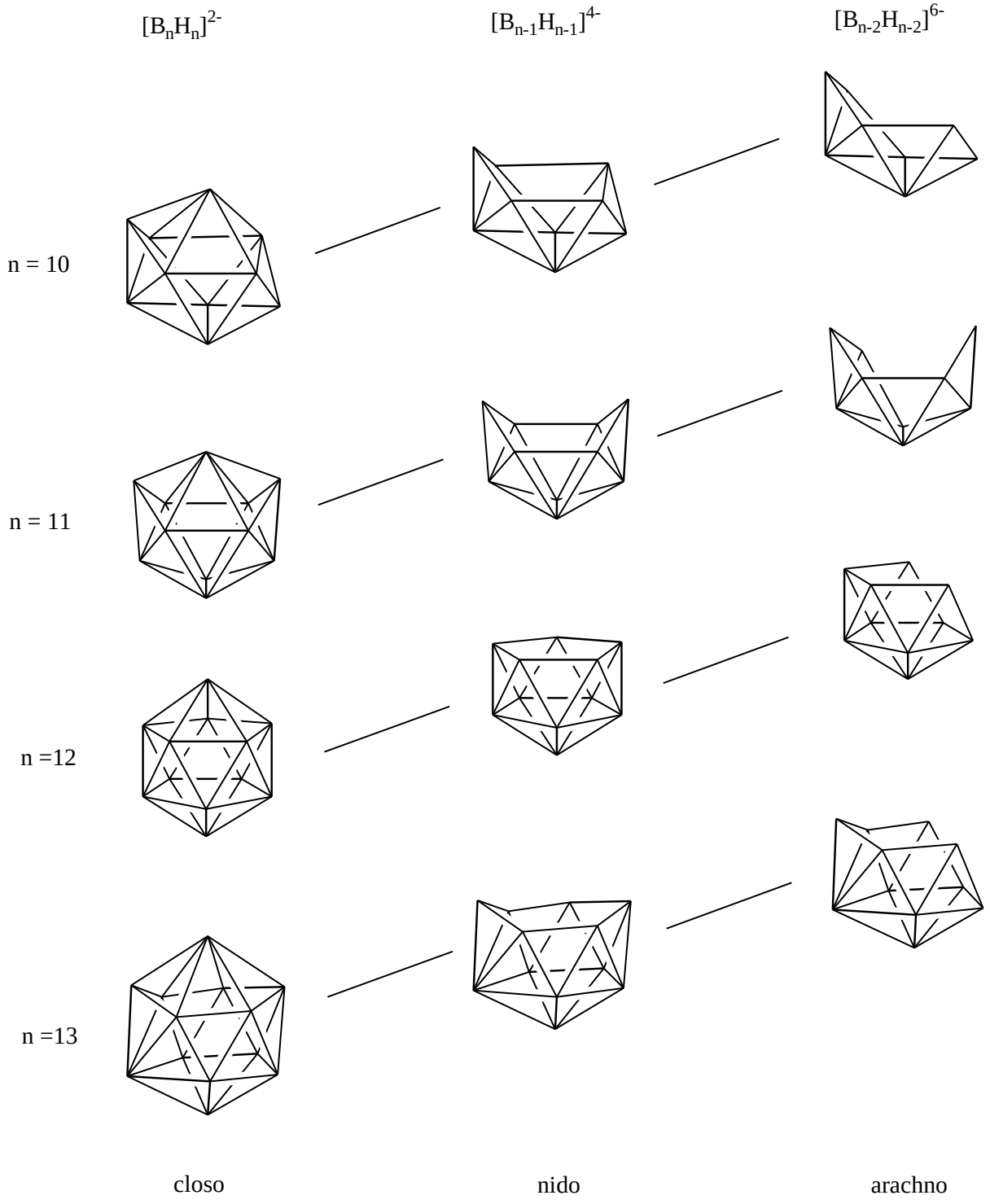

Figure 1.2.3 Selected portion of the Wade-Williams-Rudolph structural matrix, showing the result of one and two $[BH]^{2+}$ removals from [*closo*-B_nH_n]$^{2-}$ (n = 10-13).

The nido/arachno species form salts with cations such as Li^+/Na^+, but they can also bind protons, reducing the overall negative charge and giving more stable species, such as *nido*-B_6H_{10}[11a] and *arachno*-B_4H_{10}.[11b] The protons tend to add to the nido/arachno structure's open face in bridging positions[11c] and to individual boron atoms to give BH_2 groups. For BH_2 groups the extra B-H bond is considered endo to the cluster and so the electrons in this bond are available for cluster bonding, meaning the {BH_2} fragment contributes three cluster bonding electrons altogether.

Whilst PSEP theory is generally good at describing the structures of clusters based on the number of PSEs, some exceptions do exist. Ab initio/semi-empirical calculations are often helpful when the structure predicted by PSEP theory and the observed structure do not agree. Some of the exceptions to PSEP theory (called 'non-Wadian' species) arise when vertices other than boron, and/or when exo-polyhedral species other than hydrogen are introduced to the cluster and have different electronic/steric demands to {BH}. For example in some closo boron halide clusters the usual n + 1 PSEP requirement is reduced to an n PSEP requirement. It is thought that this is because the halide atoms donate electron density to the cage.[12]

B_4H_4 (T_d symmetry) is predicted to be another example of a non-Wadian species. It has been calculated[12,13] to be stable with only n or n + 2 PSEPs, but not with n + 1 PSEPs. This is because with n + 1 PSEPs two electrons would reside in a degenerate set of orbitals (of E symmetry), causing paramagnetism in the triplet state and a symmetry-lowering Jahn-Teller distortion in the singlet state. Some closo boranes which do not belong to degenerate point groups have been calculated[12] to be stable with n PSEPs (hypercloso), as the occupation of the HOMO in the $[B_nH_n]^{2-}$ (n + 1 PSEPs) species is not essential to the stability of the molecule. Hypercloso metallacarboranes are known[14] and are discussed further in chapter five.

PSEP theory can also be used to predict the structures of many transition metal and main group clusters, and structures of heteroboranes with metals incorporated as vertices into the polyhedral framework (metallaboranes/metallacarboranes, see section 1.7). The number of cluster bonding electrons provided by a metal fragment is:

s = v + x - 12 (for 18 electron species)
s = v + x - 10 (for 16 electron species)

In addition to there being discrete polyhedral borane clusters, there also exist boranes that have more than twelve vertices and are stable, but have structures based on the fusion of two clusters with twelve or fewer vertices.[15] These species, designated as conjuncto-, share a common edge, face or vertex between the two clusters, and commonly contain structures based on fused fragments of icosahedral polyhedra (for example[16] [*conjuncto*-$B_{21}H_{18}]^-$, figure 1.2.4).

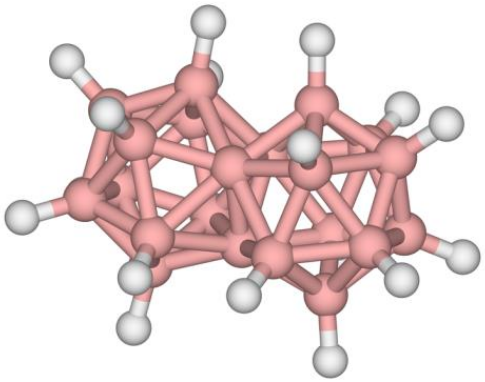

Figure 1.2.4 Structure of the face-sharing [*conjuncto*-$B_{21}H_{18}]^-$.

The PSEP rules were further expanded to include these boranes composed of fused polyhedra to give the mno rules,[17] which predict the number of cluster electrons required for a stable structure based on certain parameters. For structures without open faces the parameters are: m = number of polyhedra; n = number of vertices; o = number of single-vertex-sharing condensations, and m + n + o = the number of electron pairs required for a stable structure. Similar equations can be applied to fused structures which have open faces.

1.3 Boranes and carboranes

Diborane is made by reaction of $NaBH_4$ with $BF_3{\cdot}OEt_2$ and is an important starting material for making subicosahedral (polyhedra with less than twelve vertices)/icosahedral boranes.[18a] Closo icosahedral and subicosahedral boranes are commonly made by condensation reactions (e.g. reaction of $B_{10}H_{14}$ and Et_3NBH_3 gives $[B_{12}H_{12}]^{2-}$) or by pyrolysis (e.g. heating $[B_3H_8]^-$ gives $[B_9H_9]^{2-}$ + $[B_{10}H_{10}]^{2-}$ + $[B_{12}H_{12}]^{2-}$ + $[BH_4]^-$).[18b]

The protonated neutral nido/arachno boranes can be made from thermolysis of B_2H_6/$[B_3H_8]^-$ or other boranes, or by cluster expansion/degradation starting from an appropriate precursor.[18a,b] Cluster expansion can be performed by addition of B_2H_6 or $[BH_4]^-$ and cluster degradation can be performed by addition of a strong base such as $[OH]^-$. The protonated nido/arachno species can generally be deprotonated by addition of a suitable base.[18b]

Some common reactions[18b] of boranes include: halogenation by adding a strong base plus an appropriate halogen containing compound, electrophilic substitution of protons at the cage vertices; and certain cage reductions (e.g. reduction of *nido*-$B_{10}H_{14}$ with sodium metal gives [*arachno*-$B_{10}H_{14}]^{2-}$).

Carbon (in the form of a CH vertex) can be incorporated into the cluster to give a carborane. Carbon is of similar size/electronegativity to boron, but has three electrons available for cluster bonding, meaning {CH} is not electronically the same as {BH}, but $\{CH\}^+$ is. For example replacement of two BH vertices with CH vertices in [*closo*-$B_{12}H_{12}]^{2-}$ gives neutral *closo*-$C_2B_{10}H_{12}$. Twelve vertex species with one CR ($[CB_{11}H_{12}]^-$)[19a] and four CRs ($Me_4C_4B_8H_8$, formed from the oxidative fusion of $(Me_2C_2B_4H_4)_2CoH$ or $(R_2C_2B_4H_4)_2FeH_2$)[19b] are both known, the latter having open faces to give a nido-like structure in order to accommodate the extra electrons from the carbon atoms.

The closo carboranes have a general formula $[C_nB_xH_{n+x}]^{(2-n)-}$ and offer a degree of chemoselectivity to the cluster, with sites of nucleophilic attack becoming more likely at vertices closer to the relatively electronegative carbon atoms, and sites of electrophilic attack becoming more likely at vertices further away. The relatively acidic protons on CH vertices can be removed and replaced with various groups,[20a,b] a key factor in the development of supraicosahedral compounds (polyhedra with more than twelve vertices, see section 1.6).

Numbers prefixing the C_nB_x part of the molecular formula denote the positions of the cage heteroatoms and are designated based on the numbering schemes in figure 1.3.1 (for the twelve to fourteen vertex closo structures and the eleven and twelve vertex nido structures). The numbering schemes of thirteen and fourteen vertex structures are introduced in figure 1.3.1, but for discussion of these structures see sections 1.5-1.7.

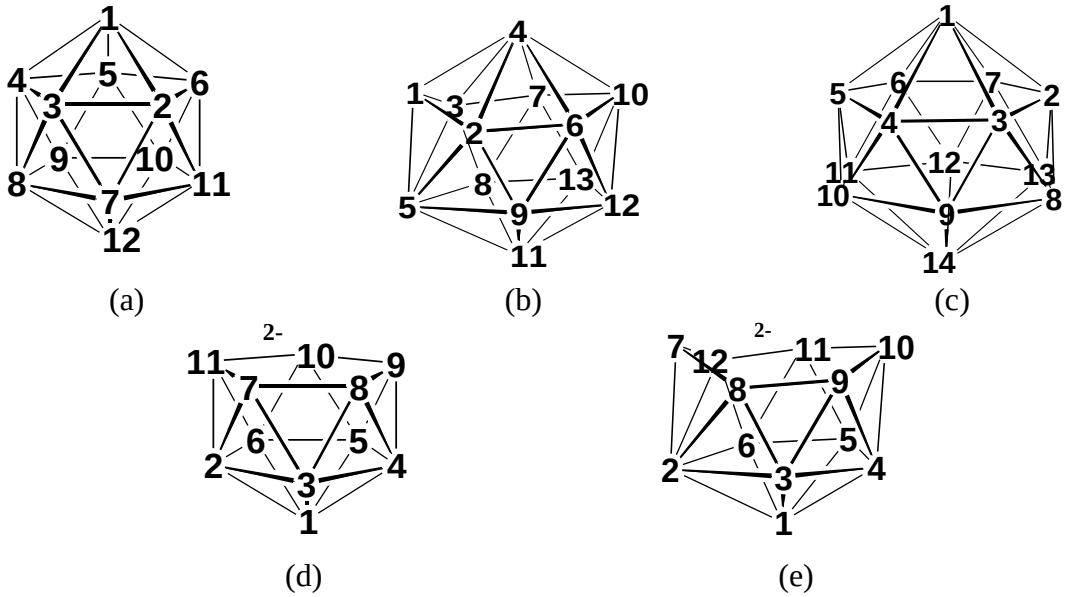

Figure 1.3.1 Numbering schemes for: (a) twelve vertex closo structure, icosahedron; (b) thirteen vertex closo structure, docosahedron; (c) fourteen vertex closo structure, bicapped square antiprism; (d) eleven vertex nido structure; (e) twelve vertex nido structure.

Any exopolyhedral substituents are listed before the numbers prefixing C_nB_x and are themselves prefixed by the number of the vertex to which they are joined. For example the compound in figure 1.3.2 has the formula 1,12-Me_2-1,12-*closo*-$C_2B_{10}H_{10}$. The omission of prefixing numbers indicates that a general compound and not specific isomers are being discussed.

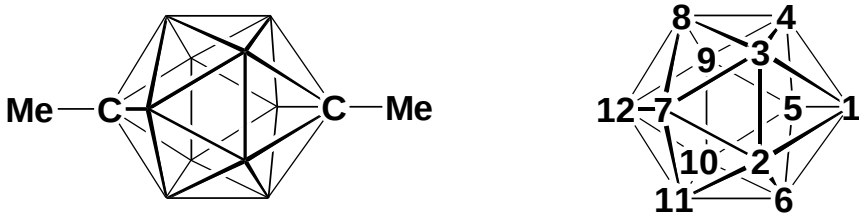

Figure 1.3.2 Structure of 1,12-Me_2-1,12-*closo*-$C_2B_{10}H_{10}$.

The main method used to synthesise carboranes is to treat nido boranes with alkynes, often in the presence of a Lewis base catalyst. For example reaction of *nido*-$B_{10}H_{14}$ with two

equivalents of a suitable Lewis base causes cage opening to an *arachno*-$L_2B_{10}H_{12}$ species, then adding an alkyne gives 1,2-*closo*-$C_2B_{10}H_{12}$[21a] (figure 1.3.3). The alkyne can also be inserted directly into *nido*-$B_{10}H_{14}$ in biphasic ionic liquid/toluene mixtures.[21b] The method of alkyne insertion is an efficient way of preparing carboranes, but does not work if the substituents on the alkyne are bulky or strongly EWGs.[21c]

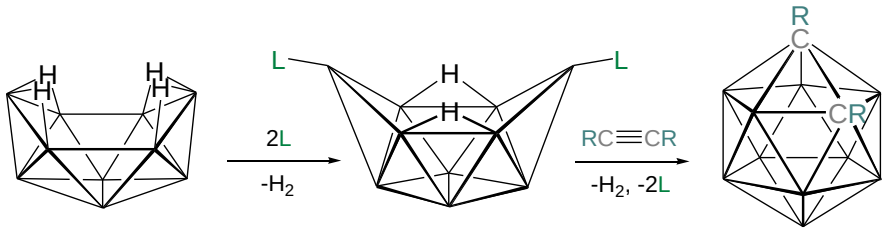

Figure 1.3.3 Alkyne insertion into an arachno borane to give 1,2-R_2-1,2-*closo*-$C_2B_{10}H_{10}$.

The icosahedral compound [*closo*-$CB_{11}H_{12}$]$^-$ can be made by insertion of dichlorocarbene into the open five-membered face of [*nido*-$B_{11}H_{14}$]$^-$ in strongly basic media.[19a] However reaction of [*nido*-$B_{11}H_{11}$]$^{4-}$ with alkynes/other sources of two carbon atoms (e.g. 1,2-dichloroethene) has never been reported, nor has the reaction of dianionic nido carboranes such as [*nido*-$C_2B_{10}H_{12}$]$^{2-}$ (which has a six-membered open face) with diboron sources such as B_2H_6/B_2Cl_4 or $R_2B_2H_2$/R_2B_2[22,23] (R = :C{N(Dip)CH}$_2$).

When considering the bonding of individual vertices of a heteroborane with the rest of the cage, a {BH}/{CH} fragment can be considered to be capitating a ring of atoms within the heteroborane.[24] Figure 1.3.4 shows the interaction of the orbitals of two CH/BH fragments with the orbitals of a four-membered ring in an octahedral cluster, and in this the two capitating vertices are said to be degree four (spanning four-membered ring).

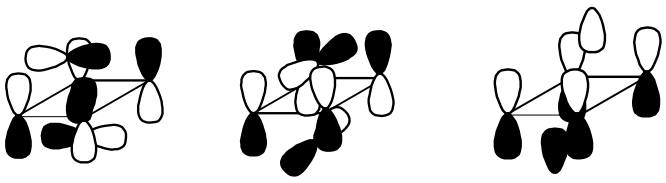

(a) (b)

Figure 1.3.4 (a) π- and (b) σ- interaction of the orbitals of two {CH} or {BH} fragments with the orbitals of a four-membered ring.

The size of the capitating vertices orbitals ultimately determines how large a ring it will be able to capitate, and therefore its preferred number of connectivities. It has been calculated[24]

that boron prefers ring sizes in the order 5 > 4 >> 3 ≈ 6, while carbon (less diffuse orbitals than boron) prefers ring sizes in the order 4 > 3 > 5 >> 6. Icosahedral carboranes/boranes appear to be especially stable, and have all degree five vertices. For this reason, when a cage vertex is not degree five it is said to be a defective vertex.[11c] The 'ring-cap' principle goes some way towards explaining the difficulty in preparing supraicosahedral carboranes which contain defective degree six vertices.

Closo-$C_2B_{10}H_{12}$ has three isomers - 1,2-*closo*-$C_2B_{10}H_{12}$, 1,7-*closo*-$C_2B_{10}H_{12}$ and 1,12-*closo*-$C_2B_{10}H_{12}$ - shown in figures 1.3.5 (a), (b) and (c) respectively. These isomers are often referred to as ortho-, meta- and para- carborane respectively.

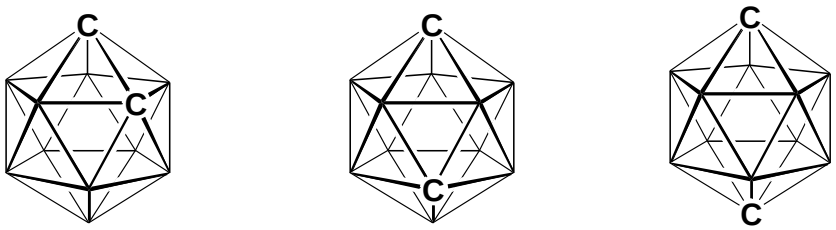

(a) (b) (c)

Figure 1.3.5 The three isomers of *closo*-$C_2B_{10}H_{12}$: (a) 1,2-*closo*-$C_2B_{10}H_{12}$; (b) 1,7-*closo*-$C_2B_{10}H_{12}$; (c) and 1,12-*closo*-$C_2B_{10}H_{12}$.

In the icosahedron all of the vertices are degree five and so the relative energies of the three isomers is not related to CH/BH vertices being in their respective preferred connectivities, but rather how far apart the relatively electronegative carbons are. The further apart the cage carbon atoms are, the energetically lower the isomer will be.

When closo carboranes are reacted with a strong base, one of the BH vertices can be removed to form a nido structure. For example for 1,2-*closo*-$C_2B_{10}H_{12}$ or 1,7-*closo*-$C_2B_{10}H_{12}$ the [7,8-*nido*-$C_2B_9H_{12}]^-$ and [7,9-*nido*-$C_2B_9H_{12}]^-$ structures are formed respectively upon reaction with KOH in EtOH.[25] The extra proton which bridges the open face can easily be removed, giving an open faced structure which can bond to a metal in a similar fashion to $[Cp]^-$. For [*nido*-$C_2B_9H_{11}]^{2-}$, the FMOs of the open faced carborane are bent inwards by 22.6 degrees, whereas for $[Cp]^-$ the FMOs are perpendicular to the plane of the C_5 ring[26] (figure 1.3.6). When a carborane is coordinated as a ligand to a metal fragment the resulting compound is known as a metallacarborane, and these types of compound are discussed further in section 1.7.

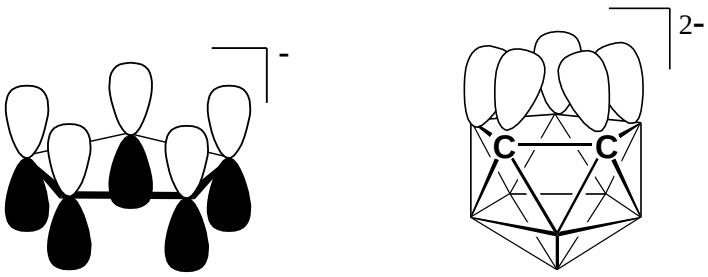

(a) (b)

Figure 1.3.6 One of the FMOs of (a) $[C_5H_5]^-$ and (b) [7,8-*nido*-$C_2B_9H_{11}]^{2-}$.

1.4 Isomerisation in icosahedral carboranes

As noted *closo*-$C_2B_{10}H_{12}$ can exist as three different geometric isomers. These isomers are thermally[27a] and electrochemically accessible.[27b] The 1,7- isomer can be converted to the 1,2- isomer by two electron reduction followed by oxidation, and the 1,12- isomer can convert to the 1,7- isomer by reduction followed by oxidation (figure 1.4.1). The 1,2 isomer converts to the 1,7 isomer at 450°C, and the 1,7 isomer converts to the 1,12 isomer at 700°C (figure 1.4.1). These temperatures are generally too high to be able to isolate intermediates, so there remains some ambiguity as to the exact isomerisation mechanism.

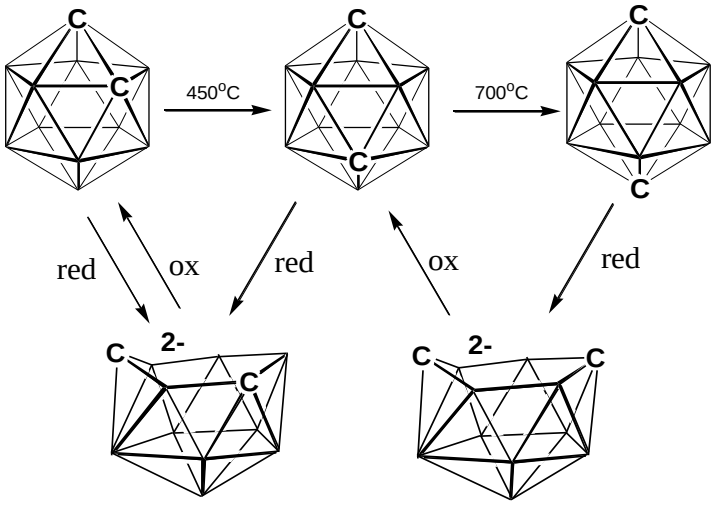

Figure 1.4.1 Thermal and redox isomerisations of *closo*-$C_2B_{10}H_{12}$.

Electrostatic repulsion between the carbon atoms is the driving force behind the thermal isomerisations. Several different mechanisms have been proposed to explain the isomerism in icosahedral carboranes, the first of which was a diamond-square-diamond (DSD) type process.[28a] The two triangular faces in figure 1.4.2 make a diamond shape in which vertices 2 and 3 are connected.

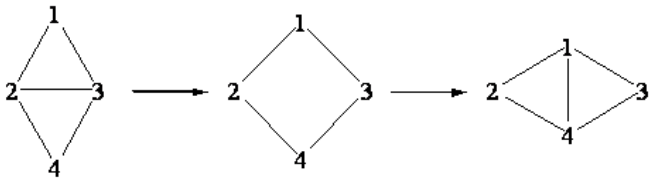

Figure 1.4.2 Diamond-square-diamond (DSD) mechanism.

In the 1,2 isomer, the two carbons are at vertices 2 and 3 in the initial diamond. The mechanism involves the two carbon atoms separating until the B_2C_2 diamond is a square,

with the carbon atoms at opposite corners. During this process the connectivity between the carbon atoms elongates until the point of breaking, then a connectivity is formed between the two boron atoms. The 1,2 to 1,7- isomerisation mechanism was suggested to proceed through a concerted hextuple DSD process occurring through a cubeoctahedral intermediate (figure 1.4.3).

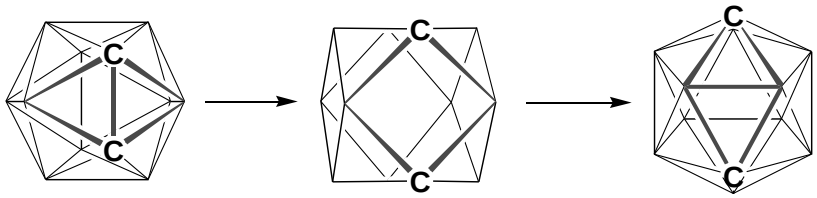

Figure 1.4.3 Initially proposed hextuple DSD isomerisation mechanism for conversion of 1,2-*closo*-$C_2B_{10}H_{12}$ to 1,7-*closo*-$C_2B_{10}H_{12}$, proceeding through a cubeoctahedral intermediate.

This mechanism accounts for the transformation of the 1,2- to the 1,7- isomer, but not for the 1,7- to the 1,12- isomer, and subsequent calculations[28b] have shown that the formation of the cubeoctahedral intermediate is unlikely due to it being too high in energy.

Another mechanism proposed for the isomerism is Triangular Face Rotation (TFR)[29] where triangular faces are rotated by angles of 120° (figure 1.4.4).

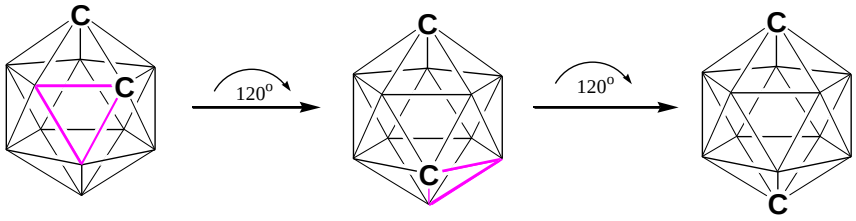

Figure 1.4.4 Proposed triangular face rotation mechanism.

While the exact mechanism of isomerisation remains elusive, recent calculations[30] have shown that the lowest energy 1,2- to 1,7- isomerisation pathway is a TFR mechanism which proceeds through a transition state with three square faces, which is the equivalent to a concerted triple DSD process. The lowest energy 1,7- to 1,12- isomerisation pathway proceeds through a transition state with two quadrilateral faces (or possibly a hexagonal open face) by an adjacent, concerted double DSD process to give an unstable closo intermediate, which then goes through another transition state with two quadrilateral faces by an adjacent, concerted double DSD process to give the 1,12- isomer.

1.5 Supraicosahedral boranes

The icosahedral shape tends to give especially stable clusters in borane/carborane chemistry because it has no defective vertices and high symmetry. This stability makes the synthesis of supraicosahedral heteroboranes challenging, as the icosahedral shape is lost upon cage expansion beyond twelve vertices. This is reflected in the fact that the largest known discrete $[B_nH_n]^{2-}$ borane remains $[B_{12}H_{12}]^{2-}$.

Despite this, calculations[31a,b] have predicted that supraicosahedral $[B_nH_n]^{2-}$ boron clusters where n = 13-17, are capable of stable existence. The predicted structures for the $[B_nH_n]^{2-}$ (n = 13-17) boron clusters are given in figure 1.5.1. Calculations[31b] on cumulative {BH} addition energies predict endothermic steps for $[B_{12}H_{12}]^{2-}$ to $[B_{13}H_{13}]^{2-}$ and $[B_{14}H_{14}]^{2-}$ to $[B_{15}H_{15}]^{2-}$, and exothermic steps for $[B_{13}H_{13}]^{2-}$ to $[B_{14}H_{14}]^{2-}$, $[B_{15}H_{15}]^{2-}$ to $[B_{16}H_{16}]^{2-}$ and $[B_{16}H_{16}]^{2-}$ to $[B_{17}H_{17}]^{2-}$ (figure 1.5.2). The compounds $[B_nH_n]^{2-}$ (n = 13-15) are all predicted to be thermodynamically less stable than $[B_{12}H_{12}]^{2}$, but $[B_{16}H_{16}]^{2-}$ and $[B_{17}H_{17}]^{2-}$ are predicted to be thermodynamically more stable.

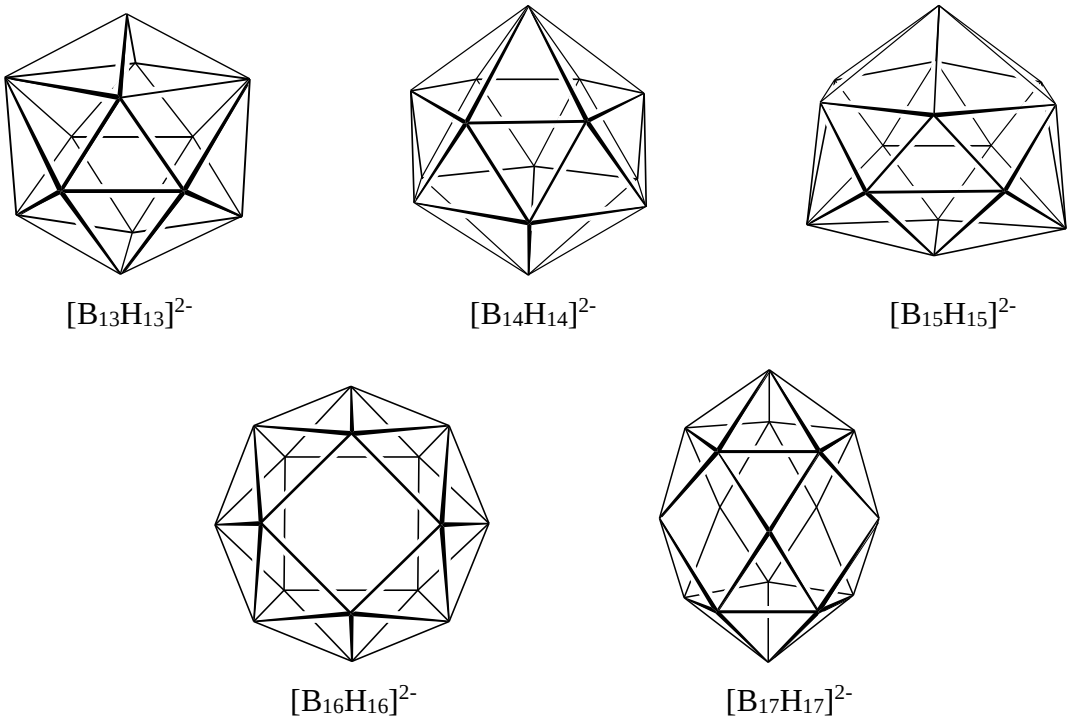

Figure 1.5.1 **P**redicted structures for the $[B_nH_n]^{2-}$ (n = 13-17) boranes.

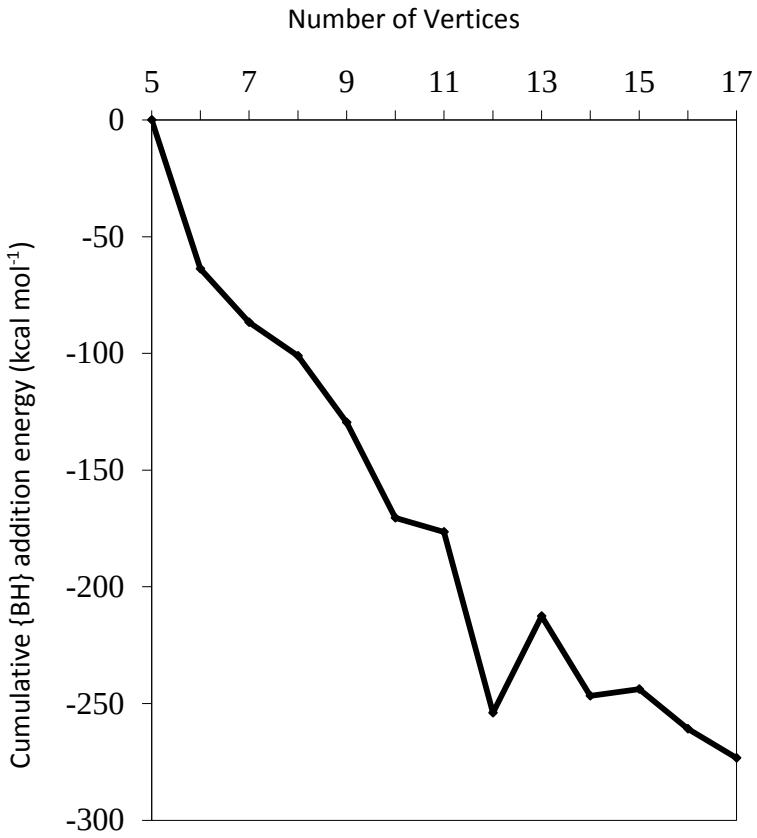

Figure 1.5.2 Plot of cumulative {BH} addition energy (kcal mol^{-1}) vs n for $[B_nH_n]^{2-}$.

These calculations are based on the deltahedral (i.e. all triangulated faces) structures for *closo*-$[B_nH_n]^{2-}$ n = 12-15, then non-deltahedral structures for n = 16 and 17. The calculated stability of $[B_{16}H_{16}]^{2-}$ and $[B_{17}H_{17}]^{2-}$ reflects a decrease in the coloumbic repulsion as the size of the polyhedron is increased, but a smooth increase in stability form $[B_{12}H_{12}]^{2-}$ to $[B_{17}H_{17}]^{2}$ is not observed as there are a number of defective vertices present in the structures of the *closo*-$[B_nH_n]^{2-}$ n = 13 - 15 boranes. The structures predicted for n = 16 and n = 17 have open faces in order to avoid defective vertices.

The computational study[31b] also predicts that if subicosahedral boranes are formed during the attempts to make supraicosaheral boranes, disproportionation reactions between the sub- and supraicosahedral species could lead to the formation of $[B_{12}H_{12}]^{2-}$. It therefore seems that the non-existence of the larger boranes is linked to the especially stable icosahedral $[B_{12}H_{12}]^{2-}$ and the relative instability of the n = 13 to n = 15 clusters in between $[B_{12}H_{12}]^{2-}$ and $[B_{16}H_{16}]^{2-}$/$[B_{17}H_{17}]^{2-}$.

$[B_nH_n]^{2-}$ clusters tend to have 3-D aromaticity,[32] with the degree of electron delocalisation dependent on the number of vertices in the cluster and the symmetry of the cluster. Larger clusters with high symmetry are predicted to afford the most electron delocalisation. Calculations[31b] for $[B_nH_n]^{2-}$ (n = 13-17) show that the twelve and seventeen vertex clusters are the most aromatic structures, the twelve vertex because it is highly symmetric, and the seventeen vertex because it is large and relatively symmetric (D_{5h}).

1.6 Supraicosahedral carboranes

The electron counting rules discussed in section 1.2 imply that addition of an electron pair to a C_2B_n carborane will give a nido dianon with an open face and the structure of the decapitated C_2B_{n+1} carborane. Two electron reduction of 1,2-*closo*-$C_2B_{10}H_{12}$ or 1,7-*closo*-$C_2B_{10}H_{12}$ (usually using sodium or lithium, often in the presence of naphthalene (forms sodium/lithium naphthalenide, an effective charge transfer agent)) gives [7,9-*nido*-$C_2B_{10}H_{12}]^{2-}$, an air sensitive species which is prone to re-oxidation[33] (figure 1.6.1).

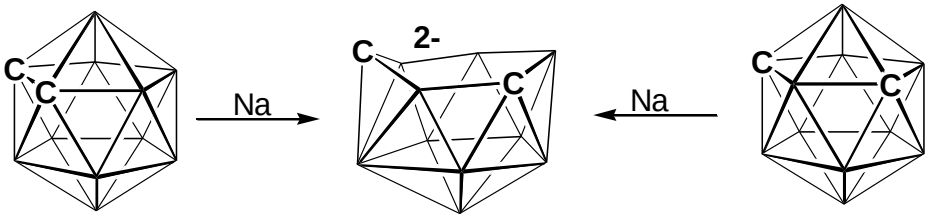

Figure 1.6.1 Reduction of 1,2-*closo*-$C_2B_{10}H_{12}$ or 1,7-*closo*-$C_2B_{10}H_{12}$ to [7,9-*nido*-$C_2B_{10}H_{12}]^{2-}$.

Upon re-oxidation of this nido species the closo 1,2- isomer is formed exclusively. The re-oxidation of the 7,9- nido species back to the closo 1,2- isomer has been calculated[34] to be lower in energy than re-oxidation back to the closo 1,7- isomer.

Attempts[35] to make supraicosaheral carboranes have centred around the capitation of reduced twelve vertex carboranes with a boron fragment of the form $\{BR\}^{2+}$ (which tends to come from BRX_2, R = H, aryl, alkyl, X = Cl, Br, I). The borane $[B_{12}H_{12}]^{2-}$ cannot be used in these reduction/capitation reactions as it is already dianionic, and the adding of additional electrons is unlikely to occur.

The reduction/capitation approach to making supraicosahedral species was first used with a degree of success[36] when BI_3 was added to reduced 1,2-*closo*-$C_2B_{10}H_{12}$. From this reaction was isolated 3-I-1,2-*closo*-$C_2B_{10}H_{11}$ and 1,2-*closo*-$C_2B_{10}H_{12}$, indicating that the capitation had initially been successful, but that the thirteen vertex product was presumably not stable and degrades via loss of a BH or BI vertex back to 1,2-*closo*-$C_2B_{10}H_{12}$ or 3-I-1,2-*closo*-$C_2B_{10}H_{11}$.

It was noted that the cage carbon atoms move apart during the reduction step, but that the degradation of the initially formed thirteen vertex species is associated with the cage carbon atoms becoming adjacent again. It was thought that if the cage carbon atoms could be prevented from separating in the reduction step (and so not move after capitation), then this would potentially avoid the degradation back to the twelve vertex species.

This led to the development of 'ortho tethering', where 1,2-*closo*-$C_2B_{10}H_{12}$ is deprotonated (at the carbons atoms) and then an exo-polyhedral tether added to stop the carbon atoms moving apart during reduction (the reduced species is now the nido 7,8- isomer). This led to the isolation of the first thirteen vertex carborane[36] 1,2-μ-($C_6H_4(CH_2)_2$)-3-Ph-1,2-*closo*-$C_2B_{11}H_{11}$ and subsequently other thirteen vertex carboranes with different tethers/cage substituents[37] (figure 1.6.2). The ortho tether of the nido 7,8- isomer seems to prevent the degradation of the capitated product seen for the nido 7,9- isomer.

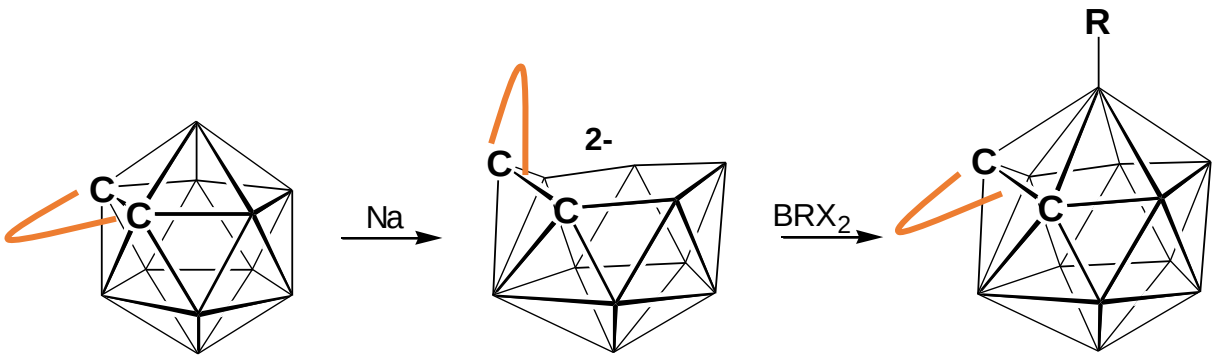

Figure 1.6.2 Ortho tethering method which led to the first supraicosahedral carborane.

Calculations[38] have shown that the barrier to re-oxidation is higher for the nido 7,8- isomer than the nido 7,9- isomer (figure 1.6.3). This makes the former a less powerful reducing agent, and it has been suggested[39] that this may make the nido 7,8- isomer easier to capitate as the dianion is less likely to reduce the boron fragment which is being used for the attempted capitation. It is not clear whether the nido 7,8- isomer can be capitated because it prevents the degradation of the initially capitated product (which occurs for the capitated nido 7,9- isomer), or because it is a less powerful reducing agent than the nido 7,9- isomer, or some combination of these two properties.

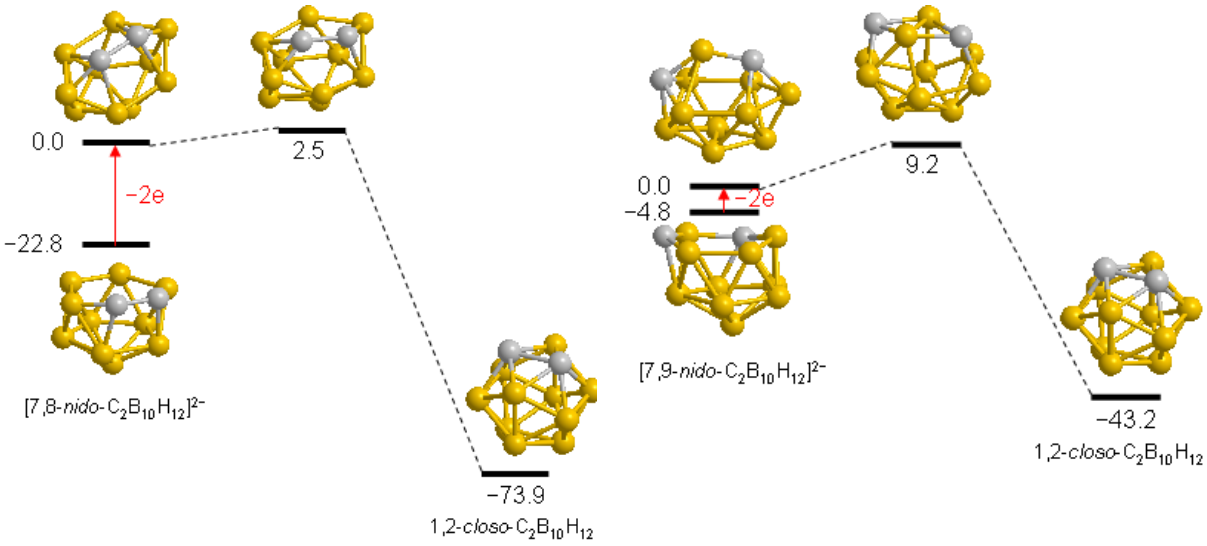

Figure 1.6.3 Calculated barriers of re-oxidation (kcal mol^{-1}) to 1,2-*closo*-$C_2B_{10}H_{12}$ from [7,9-*nido*-$C_2B_{10}H_{12}]^{2-}$ and [7,8-*nido*-$C_2B_{10}H_{12}]^{2-}$.

The shape adopted by the tethered thirteen vertex carboranes is henicosaheral (figure 1.6.4), which is similar to docosahedral, but with the breaking of a single connectivity to give a quadrilateral face, two degree four vertices and one degree six vertex (the docosahedron has one degree four and two degree six vertices). This structure is presumably adopted in order to allow the two carbon atoms (which are forced to be adjacent by the tether) to occupy favourable degree four vertices, whilst making one of the degree six boron vertices a more favourable degree five boron vertex.

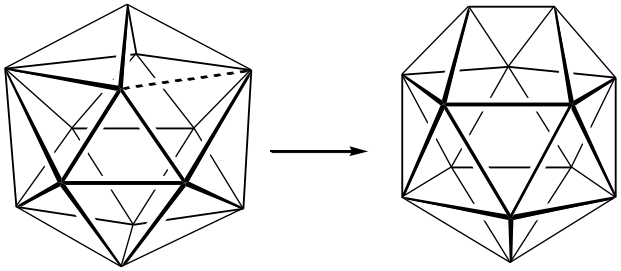

Figure 1.6.4 Breaking of a connectivity in a thirteen vertex docosahedron (left) gives a henicosahedron (right).

For the compound 1,2-μ-($C_6H_4(CH_2)_2$)-3-Ph-1,2-*closo*-$C_2B_{11}H_{11}$ the added BPh vertex is assumed to initially capitate a six-membered face, but the thirteen vertex species must then undergo cage rearrangement as the crystal structure of this compound shows the BPh vertex occupying a degree five site and one of the BH vertices occupying the degree six site.

A further development in the use of ortho tethering is the synthesis of 1,2-μ-($CH_2SiMe_2CH_2$)-1,2-*closo*-$C_2B_{10}H_{10}$, a carborane with a removable silane tether[40] (figure 1.6.5). After reduction/capitation of the twelve vertex tethered carborane, the tether was removed by putting the compound down a silica column (leaving methyl groups on the cage carbon atoms). The henicosahedral thirteen vertex product, which is the 1,2- isomer, was heated to reflux in toluene which led to isomerisation to the thermodynamically more stable docosahedral structure, accompanied by cage carbon separation (becoming the 1,6-isomer). This modification to the ortho tether approach means that the tether is not restricting the carbon atoms movement during subsequent experiments using the thirteen vertex products.

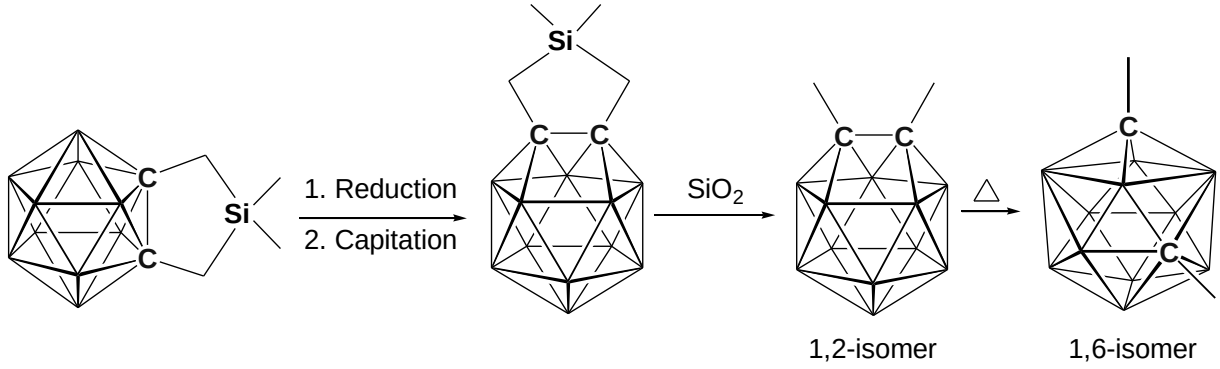

Figure 1.6.5 Reduction/capitation of 1,2-μ-($CH_2SiMe_2CH_2$)-1,2-*closo*-$C_2B_{10}H_{10}$ followed by tether removal to give 1,2-Me_2-1,2-*closo*-$C_2B_{11}H_{11}$, thermal isomerisation of which gives 1,6-Me_2-1,6-*closo*-$C_2B_{11}H_{11}$.

The docosahedral isomer was also made in small yield by the reduction capitation of 1,2-Me_2-1,2-*closo*-$C_2B_{10}H_{10}$.[40] It is not known why capitation of the reduced dimethyl carborane is possible, but not reduced 1,2-*closo*-$C_2B_{10}H_{12}$.

Fourteen vertex carboranes can be made two ways. The first method,[39,41] as shown in figure 1.6.6, involves reduction of 1,2-μ-$(CH_2)_3$-1,2-*closo*-$C_2B_{10}H_{10}$ (or another suitably tethered carborane) with lithium to give a tetraanionic species with open five and six-membered faces, followed by capitation with two equivalents of an appropriate boron reagent (12 (vertices) + 2 (capitations)). The second method[39,41] involves reduction/capitation of 1,2-μ-$(CH_2)_3$-1,2-*closo*-$C_2B_{11}H_{11}$ or 1,X-Me_2-1,X-*closo*-$C_2B_{11}H_{11}$ (X = 2 or 6) carboranes (13 + 1). When the $(CH_2)_3$ tethered carboranes are used (for 12 + 2 or 13 + 1 reactions) the initially formed fourteen vertex product can be reduced and then re-oxidised to give a second isomer, whereas when the other tethered carboranes are used both isomers are formed during the initial

reaction. One isomer is formed when the untethered 1,6- isomer is used, and three isomers are formed when the untethered 1,2- isomer is used.

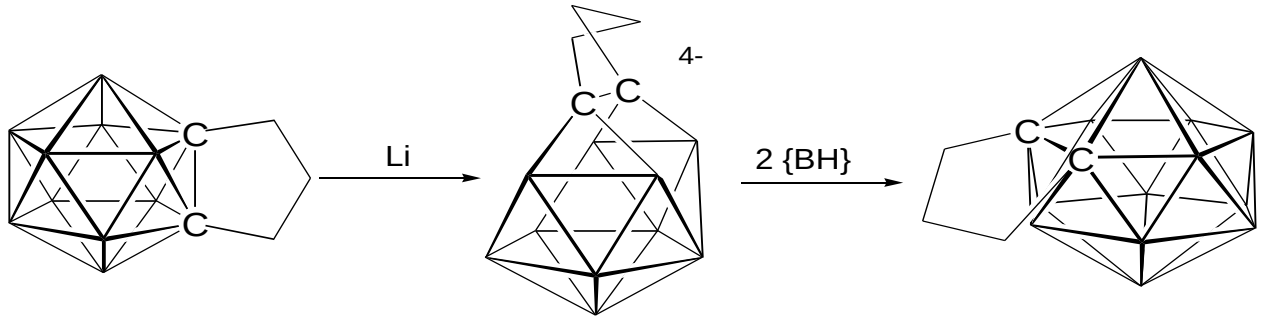

Figure 1.6.6 Reduction/double capitation (12 + 2) of 1,2-μ-$(CH_2)_3$-1,2-*closo*-$C_2B_{10}H_{10}$ to give a fourteen vertex carborane.

1.7 Metallacarboranes

Most elements have been incorporated as polyhedral vertices into borane clusters (figure 1.7.1),[42a,b,c] with the exception of the nobel gases/halogens.[6] Many main group element (both metallic and non-metallic) heteroboranes are known, the most widely studied being carboranes. The f- and d-block metals have also been incorporated into boranes/carboranes, the latter more routinely so, to give metallaboranes/metallacarboranes.

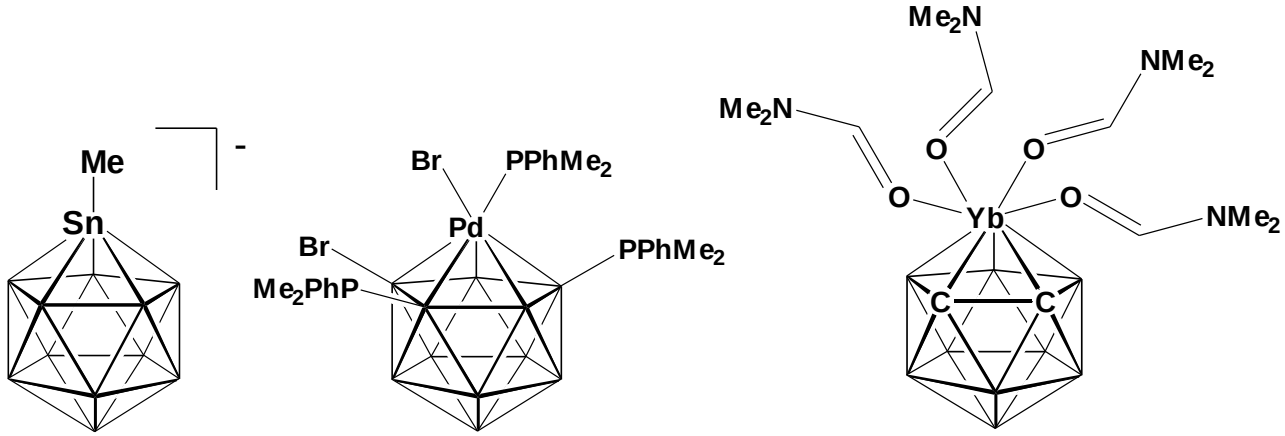

(a) (b) (c)

Figure 1.7.1 Structures of (a) a stannaborane (tin vertex), (b) a palladaborane (palladium vertex) and (c) a ytterbacarborane (ytterbium vertex).

Many subicosahedral metallaboranes/metallacarboranes are known, but relatively few icosahedral metallaboranes exist compared to the numerous examples of icosahedral metallacarboranes.[6] Similarly there are a number of examples of supraicosahedral metallacarboranes known with 13-15 vertices[6] (with the number of examples decreasing as the number of vertices increases), but only two supraicosahedral metallaboranes are known,[43] although these two do constitute two of the largest heteroboranes known.

Certain transition metal fragments are isolobal[44] with {BH} fragments, in that they have similar symmetry properties, approximate energies, extents in space, and electron occupation of their frontier molecular orbitals. For example {BH} and $\{Os(CO)_3\}$ are isolobal. Commonly used metal fragments which are isolobal with {BH} include {Ru(arene)} and {CoCp}. Transition metal fragments have enabled the synthesis of supraicosahedral compounds as they have more diffuse orbitals than carbon/boron and so are better suited to occupying degree six vertices.

Examples of subicosahedral metallacarboranes incorporating a range of types of metal fragment, number of metal fragments and size of cage have been reported.[6] These compounds are typically made by either direct insertion of a metal into a closo carborane[45a] or by metal insertion into the open face of a nido/arachno (charged or made neutral by the addition of protons) carborane.[45b]

Closo metalladicarboranes have a molecular formula of the general type $MC_2B_nH_{n+2}$. For the numbers denoting the positions of the cage heteroatoms which prefix $MC_2B_nH_{n+2}$, the position of the metal atom(s) precedes the positions of the cage carbon atoms. However for exo-polyhedral substituents the positions of those bonded to carbon atoms precedes those bonded to metal atoms. For example the compound in figure 1.7.2 has a cobalt atom with an exo-polyhedral Cp group at vertex 3, and carbon atoms with exo-polyhedral methyl groups at vertices 1 and 2, and so is given the molecular formula 1,2-Me_2-3-Cp-3,1,2-*closo*-$CoC_2B_9H_9$.

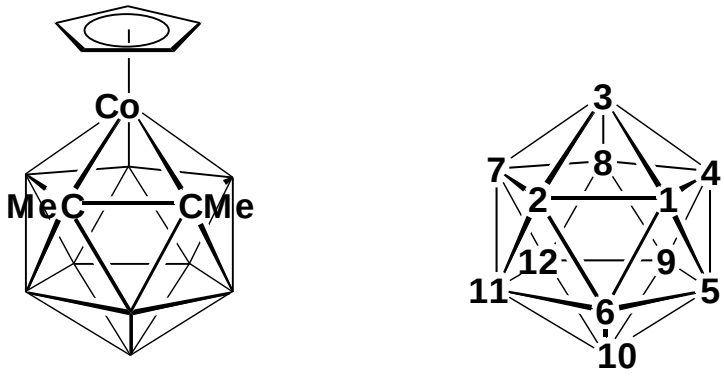

Figure 1.7.2 Structure of 1,2-Me_2-3-Cp-3,1,2-*closo*-$CoC_2B_9H_9$.

Twelve vertex metallacarboranes

Metallacarboranes can be considered as either molecules in which a metal replaces one of the boron vertices, or as a metal with a carborane ligand bound to it. The icosahedral metallacarboranes are generally made by decapitation of *closo*-$C_2B_{10}H_{12}$ to give a nido dianion, followed by metallation with an appropriate metal fragment (figure 1.7.3).[26]

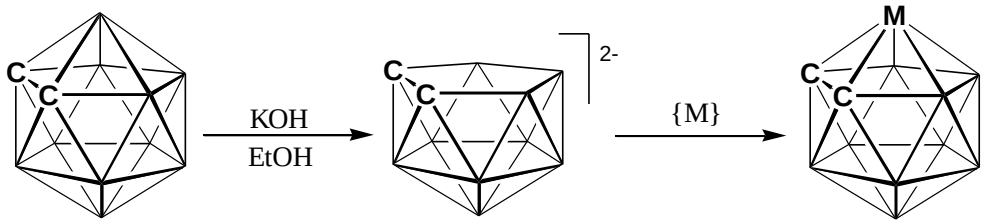

Figure 1.7.3 Decapitation of 1,2-*closo*-$C_2B_{10}H_{12}$ to give [7,8-*nido*-$C_2B_9H_{11}]^{2-}$, followed by metallation to give a 3,1,2-*closo*-$MC_2B_9H_{11}$ metallacarborane.

Bimetallic[46a] and trimetallic[46b] twelve vertex metallacarboranes are also known, as are icosahedral metallacarboranes with one[46c] or three[46d] cage carbon atoms, and non-icosahedral metallacarboranes with four[46e] or five[46f] carbon atoms. The metal fragment coordinating to the open face of a carborane can also be {M(carborane)}, giving a sandwich compound analogous to ferrocene. The first reported metallacarborane was a compound of this nature.[26]

PSEP theory broadly applies to the metallacarboranes, but there are examples of non-Wadian metallacarboranes. Some of these species are observed because large exo-polyhedral ligands inhibit formation of the predicted geometry (e.g. 1,2-Ph_2-3-(η-C_6H_6)-3,1,2-$RuC_2B_9H_9$[47] (figure 1.7.4), where the C-C connectivity length has been elongated to give effectively an open square face - such a compound is designated as pseudocloso), or because a metal fragment which is not isoelectronic with {BH} is present in the cluster (e.g. 3-Cp-3,1,2-$FeC_2B_9H_{11}$[48] which is one electron short of having the requisite n + 1 PSEPs for the observed icosahedral structure).

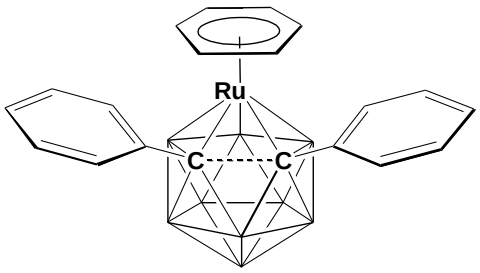

Figure 1.7.4 Structure of 1,2-Ph_2-3-(η-C_6H_6)-3,1,2-*pseudocloso*-$RuC_2B_9H_9$.

While the icosahedron is the dominant shape for twelve vertex closo clusters, some exception do exist. For example 1,2-Ph_2-5-(η-C_7H_7)-5,1,2-*closo*-$MoC_2B_9H_9$,[49a] has a non-icosahedral structure and is thought to be a metallacarborane isomerisation intermediate.

The most common twelve vertex mono-metallacarboranes have a 3,1,2- architecture, but nine isomers of the MC_2B_9 isomers are possible, with examples of each being reported, but not necessarily characterised by *X*-ray crystallography in every case.[6]

In addition to the decapitation/metallation approach, there also exist some direct nucleophilic insertion reactions to make icosahedral metallacarboranes.[50] This is when an appropriate metal fragment is inserted directly into a closo subicosahedral cage.

Thirteen vertex metallacarboranes

Thirteen vertex metallacarboranes were first made by reduction of a 1,2-*closo*-C_2B_{10} carborane with an alkali metal in THF, to give the [7,9-*nido*-C_2B_{10}]$^{2-}$ species, followed by the addition of an {M}$^{2+}$ metal salt to complete a thirteen vertex 4,1,6- docosahedron.[33,51] 1,12-*closo*-C_2B_{10} carboranes can also be reduced (Na/liq. NH_3), to give the [7,10-*nido*-C_2B_{10}]$^{2-}$ species which can then be metallated to give a 4,1,10- docosahedron.[52] Tethered 1,2-*closo*-C_2B_{10} carboranes can be reduced (to the [7,8-*nido*-C_2B_{10}]$^{2-}$ species) followed by metallation to give 4,1,2- tethered docosahedral (if Ni or Pt used) or henicosahedral compounds (if Co or Ru used).[53] Additionally non-tethered henicosahedral compounds of the type 1,2-Me_2-4-(L)-4,1,2-$MC_2B_{10}H_{12}$ can be prepared if a removable silane tether is used.[54]

In all known docosahedral monometalladicarboranes the metal atom and a BH vertex occupy the two degree six vertices, and a CR vertex occupies the degree four vertex. The other CR will occupy a variety of degree five sites, giving rise to different possible isomers (figure 1.7.5) of the type 4,1,X-*closo*-MC_2B_{10}, where X is the position of the degree five carbon atom within the cage.

Only the 4,1,2-, 4,1,6- and 4,1,10- isomers can be made directly, the 4,1,8- isomer is accessed by thermal isomerisation from the 4,1,6- isomer[33,55a,b], and the 4,1,12- isomer is accessed by thermal isomerisation from the 4,1,8- or the 4,1,10- isomer[56,52] (figure 1.7.5). The 1,2-Me_2-4-(L)-4,1,2-$MC_2B_{10}H_{12}$ (4,1,2-) compounds do not isomerise to the 4,1,6- isomers upon heating. While the isomerisation of the 4,1,6- isomer to the 4,1,8- isomer then the 4,1,12- isomer proceeds relatively easily for 4-(η-C_5H_5)-4,1,6-*closo*-$CoC_2B_{10}H_{12}$,[33,55a] it requires more forcing conditions for 4-(arene)-*closo*-4,1,6-$RuC_2B_{10}H_{12}$.[55b]

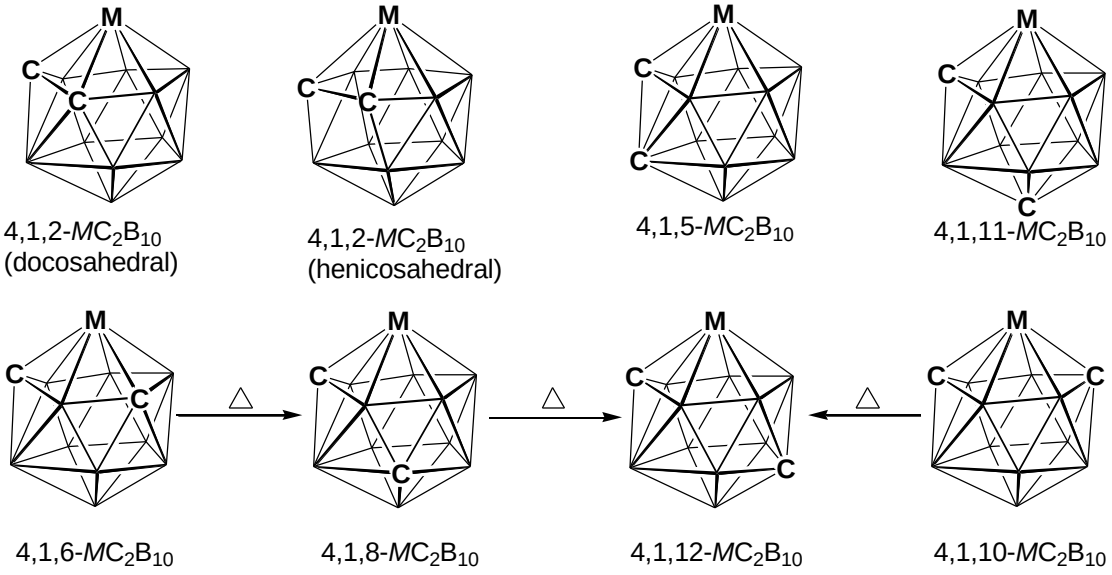

Figure 1.7.5 Different possible isomers of 4,1,X-*closo*-MC_2B_{10} (X = 2, 5, 6, 8, 10, 11, 12) and their thermal isomerisations.

The isomers of 4,1,X-*closo*-$MC_2B_{10}H_{12}$ become more stable the further apart the carbon atoms are,[56] with the 4,1,12- isomer being the most stable. The 4,1,11- isomer has been observed in trace amounts when 1,12-Ph_2-1,12-*closo*-$C_2B_{10}H_{10}$ is reduced and then capitated with Ru(*p*-cymene),[27b] but the 4,1,5- isomer has never been observed.

4,1,6- isomers are fluxional in solution at room temperature. This cage fluxionality takes the form of a double DSD process,[56] whereby the degree four carbon vertex becomes degree five and the degree five carbon vertex becomes degree four (rapid exchange), leading to C_s symmetry and a single carbon environment (and consequently a single CH resonance in the ^{1}H NMR spectrum) on the NMR timescale (figure 1.7.6). This double DSD mechanism is observed in most 4,1,6- metallacarboranes but not in 1,6-Me_2-1,6-*closo*-$C_2B_{11}H_{11}$.[40]

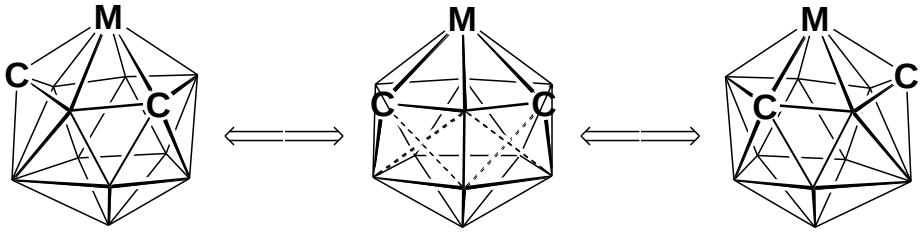

Figure 1.7.6 Double DSD mechanism leading to equivalent cage carbon atoms on NMR timescale.

Thirteen vertex tri- and tetra- carbon metallacarboranes,[46e,57a,b,c] sandwich metallacarboranes,[56] bimetallic[57d] and trimetallic[57e] metallacarboranes all exist, with the degree six boron vertex being replaced by a metal in going from the monometallic to the tri/bimetallic species.

In addition to the reduction-metallation approach, there also exist a limited number of examples of direct nucleophilic/electrophilic insertion reactions[14a,58a,b] to make supraicosahedral metallacarboranes (discussed further in chapter five).

Fourteen vertex metallacarboranes

Fourteen vertex metallacarboranes are generally of the type $M_2C_2B_{10}$ or MC_2B_{11}. The former compounds are made by the reduction metallation of thirteen vertex 4,1,8- or 4,1,12-cobalta/ruthenacarboranes.[59] Both thirteen vertex compounds give a fourteen vertex bicapped hexagonal antiprismatic structure upon reduction/metallation, but the 4,1,8- compounds give the 1,14,2,9- isomer, while the 4,1,12- compounds give the 1,14,2,10- isomer (figure 1.7.7 (a)). In both these isomers the metal atoms occupy the two degree six vertices. Recently fourteen vertex bicapped hexagonal antiprismatic bimetallacarboranes with one of the metal atoms at a degree six vertex and one of the metal atoms at a degree five vertex (e.g. figure 1.7.7 (b)) have been synthesised by a direct electrophilic insertion into a mono-metallated thirteen vertex anionic metallacarborane.[58b]

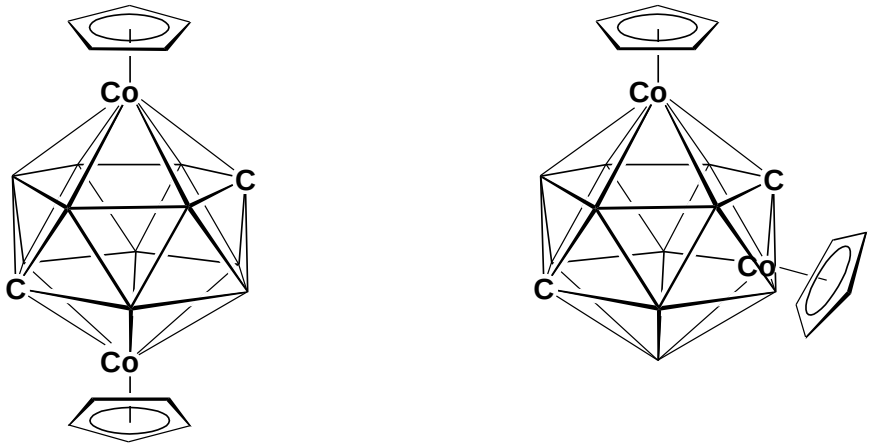

(a) (b)

Figure 1.7.7 Structures of (a) 1,14-(η-C_5H_5)$_2$-1,14,2,10-*closo*-$Co_2C_2B_{10}H_{12}$ and (b) 1,13-(η-C_5H_5)$_2$-1,13,2,10-*closo*-$Co_2C_2B_{10}H_{12}$.

The MC_2B_{11} compounds all have a bicapped hexagonal antiprismatic structure and are made by reduction metallation of a thirteen vertex carborane, which is usually tethered.[37,60] There is one example[40] of an untethered carborane being used, leading to a metallacarborane with the metal occupying a degree six vertex. If a reduced tethered carborane is metallated with a nickel diphosphine fragment the metal occupies a degree five vertex in the resulting metallacarborane,[37] whereas when a ruthenium arene fragment is used the metal occupies a degree six vertex - presumably first forming an intermediate with the metal in a degree five site which then undergoes cage rearrangement.[60] Two isomers are formed when {Ru(arene)} is used as the metal fragment (figure 1.7.8).

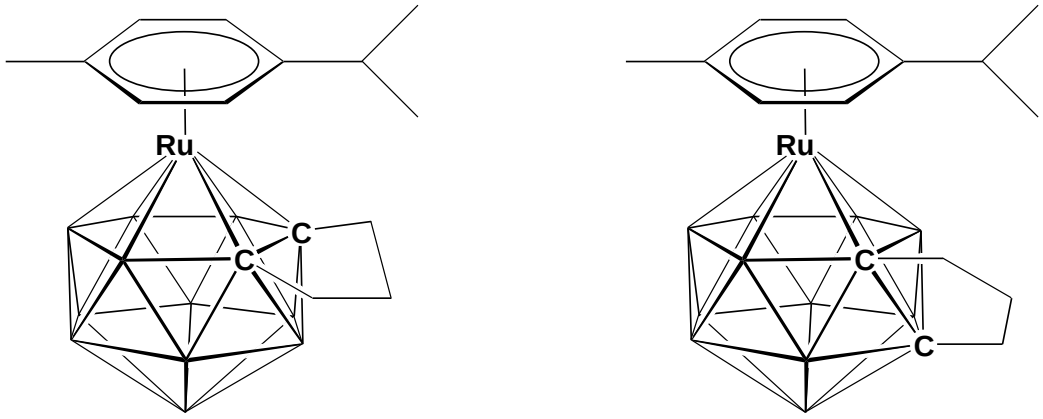

(a) (b)

Figure 1.7.8 Structures of (a) 1-(*p*-cymene)-2,3-μ-$(CH_2)_3$-1,2,3-*closo*-$RuC_2B_{11}H_{11}$ and (b) 1-(*p*-cymene)-2,8-μ-$(CH_2)_3$-1,2,8-*closo*-$RuC_2B_{11}H_{11}$.

The only other known fourteen vertex metallacarboranes are $(Et_4C_4B_8H_8)Co_2$[57c] and $(Cp)_2Fe_2(CH_3)_4C_4B_8H_8$.[57b] No structure has been reported for the cobaltacarboarne, but ^{11}B 2D (COSY) NMR analysis has led to the proposal of a structure consisting of two fourteen vertex bicapped hexagonal antiprisms fused at a Co-Co edge. The ferracarborane has three isomers which have open faced, low-symmetry structures which rearrange to give bicapped hexagonal antiprismatic structures upon heating. The tetracarbon ferracarboranes are discussed in more detail in chapter five.

Fifteen and sixteen vertex metallaheteroboranes

Only two fifteen vertex metallacarboranes are currently known. The first one reported (1-(*p*-cymene)-8,14-μ-$(CH_2)_3$-1,8,14-*closo*-$RuC_2B_{12}H_{12}$, figure 1.7.9 (a)) was made by the heating of 1-(*p*-cymene)-2,8-μ-1,2,8-$(CH_2)_3$-*closo*-$RuC_2B_{11}H_{11}$ in refluxing toluene, and is formed by the incorporation of a {BH} fragment into the cage.[60] This fragment must come from the decomposition of another fourteen vertex cage, but the exact mechanism by which one cage is degraded and another expanded is not known.

The fourteen vertex carborane 1,2-μ-$(CH_2)_3$-1,2-*closo*-$C_2B_{12}H_{12}$ can be reduced with sodium and metallated with {Ru(*p*-cymene)} to give 1-(*p*-cymene)-2,13-μ-$(CH_2)_3$-1,2,13-*closo*-$RuC_2B_{12}H_{12}$, the second reported fifteen vertex metallacarborane[61] and an isomer of 1-(*p*-cymene)-8,14-μ-$(CH_2)_3$-1,8,14-*closo*-$RuC_2B_{12}H_{12}$ (figure 1.7.9 (b)). The reduction/metallation of fourteen vertex carboranes with different/no tethers has not been reported.

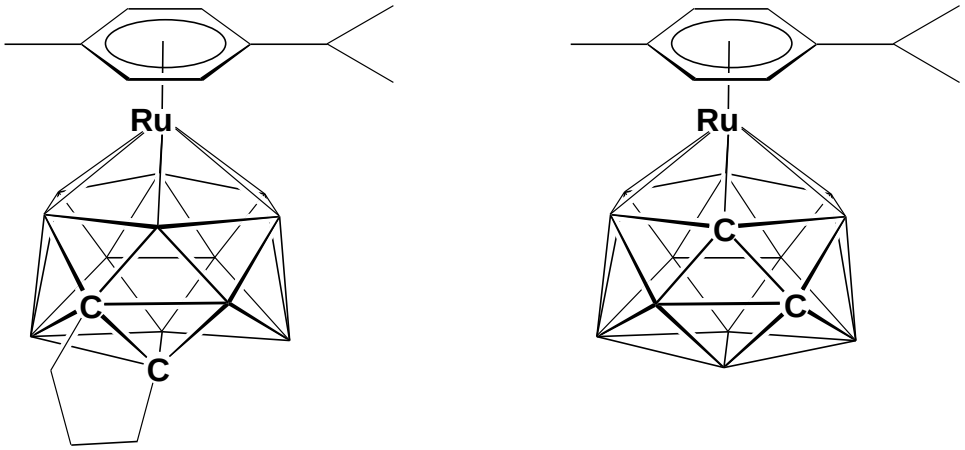

(a) (b)

Figure 1.7.9 Structures of (a) 1-(*p*-cymene)-8,14-μ-$(CH_2)_3$-1,8,14-*closo*-$RuC_2B_{12}H_{12}$ and (b) 1-(*p*-cymene)-2,3-μ-$(CH_2)_3$-1,2,3-*closo*-$RuC_2B_{12}H_{12}$ (tether not shown for clarity).

In addition to the two known fifteen vertex metallacarboranes, there exists a fifteen vertex metallaborane, $(Cp^*Rh)_2B_{13}H_{13}$ (figure 1.7.10 (a)) and a sixteen vertex metallaborane, $(Cp^*Rh)_3B_{12}H_{12}Rh\{Cp^*RhB_4H_9\}$ (figure 1.7.10 (b)). These metallaboranes are made by reaction of $(Cp^*RhCl_2)_2$ with $LiBH_4$ followed by thermolysis with excess BH_3·thf.[43]

The three fifteen vertex compounds all have a roughly hexacosahedral cage structure (as predicted[31b] for $[B_{15}H_{15}]^{2-}$), although 1-(*p*-cymene)-8,14-μ-$(CH_2)_3$-1,8,14-*closo*-$RuC_2B_{12}H_{12}$ has one connectivity missing to give an open quadrilateral face (making it a pentacosahedron). $(Cp^*Rh)_2B_{13}H_{13}$ is not dianionic, and so is classed as hypercloso.

The sixteen vertex metallaborane has an icosioctahedral structure (not the structure predicted[31b] for $[B_{16}H_{16}]^{2-}$). One of the rhodium vertices is not coordinated to an exo-polyhedral Cp* ligand, but rather to a small metallaborane fragment.

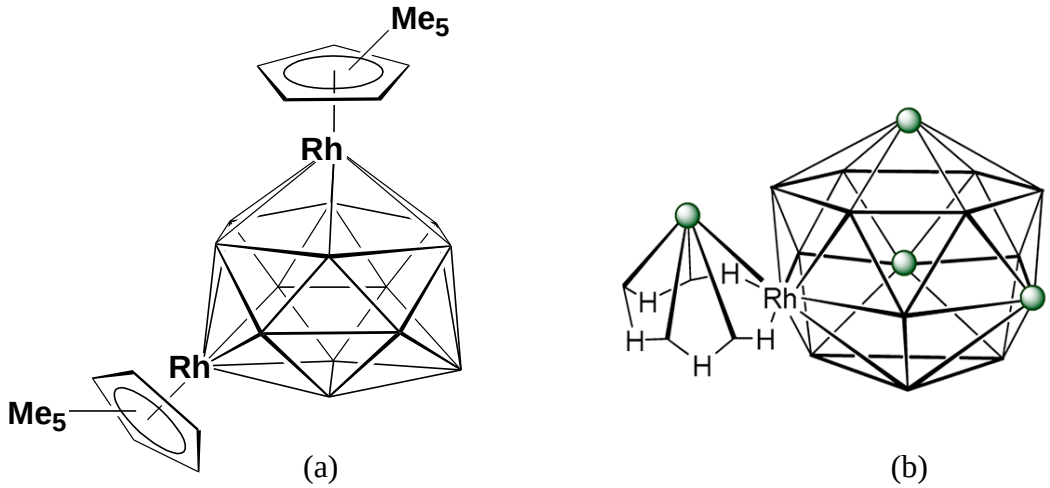

(a) (b)

Figure 1.7.10 Structure of (a) $(Cp^*Rh)_2B_{13}H_{13}$ and (b) cage structure of $(Cp^*Rh)_3B_{12}H_{12}Rh\{Cp^*RhB_4H_9\}$ (blue circles denote Rh atoms).

Other metallacarboranes

Metallacarboranes containing f-block elements are not as common as those containing d-block elements, but examples of the former containing many of the lanthanides/actinides (lanthanides more so) have been synthesised.[6,62] These examples include MC_2B_9[63a] and MC_2B_{10}[63b] (M = f-block element) compounds, bent sandwich compounds[64a] and compounds formed as the result of cage reduction by a lanthanide metal, followed by metallation of the resulting nido species with the oxidised metal.[64b]

Many of the f-block metallacarboranes display structures whereby a metal is bonded to the open face of one carborane and the exo-polyhedral ligands of another metallacarborane. The f-block metallacarboranes also include compounds containing η^7-C_2B_{10} carborane ligands,[65] the seven-membered coordinated face presumably stabilised by the diffuse orbitals of the metal. The η^7-C_2B_{10} ligand has a boat like structure and is described as an arachno $[C_2B_{10}]^{4-}$ ligand. The [*nido*-$C_2B_{10}]^{2-}$ species which is formed upon reduction is initially metallated, then the metallacarborane accepts two more electrons to give the unusual arachno carborane ligand.

Another area of current interest is biscarborane chemistry, which involves using two carborane cages which are joined by one of the cage carbon atoms in each cage[66] (figure 1.7.11 (a)). These compounds can be decapitated/reduced and then metallated on one or both cages to give metallacarboranes with a pendant carborane cage, or linked metallacarboranes[67a,b] (figure 1.7.11 (b)). Recent work has shown that the biscarboranes have properties not seen for the mono-carborane species, such as the ability to cleave aromatic bonds during reduction/metallation.[68]

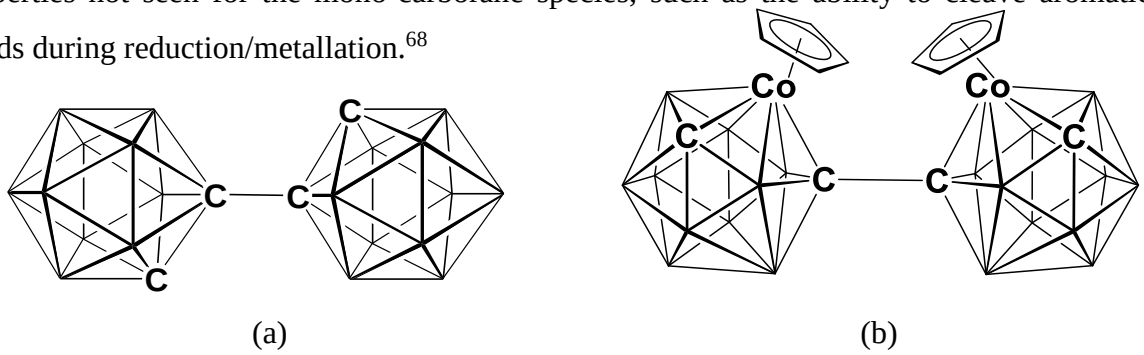

(a) (b)

Figure 1.7.11 Structure of (a) 1,1′-bis(*o*-carborane) and (b) 1-(1′-4′-Cp-4′,1′,6′-*closo*-$CoC_2B_{10}H_{11}$)-4-Cp-4,1,6-*closo*-$CoC_2B_{10}H_{11}$.

1.8 Orbital interactions between a metal fragment and a carborane cage

The interaction of an $\{ML_3\}$ d^8 metal fragment with a 7,8-*nido*-$C_2B_9H_{11}$ carborane operates primarily through three orbital interactions[69a,b,c] (figure 1.8.1). One of these interactions is between a hybrid s-z orbital of a_1 symmetry on the metal (the LUMO, viewing the metal and carborane fragments as neutral) and a carborane orbital of a′ (σ-interaction). The other two interactions are between a degenerate (e symmetry) pair of orbitals on the metal (both d-p hybrid orbitals) and two carborane orbitals, one of a′ and one of a″ symmetry (π-interactions). In this approach whereby the two fragments are treated as neutral, the carborane is an LX_2, Π_2' ligand which is participating in σ-donation, π-donation and π-acceptance with the metal.

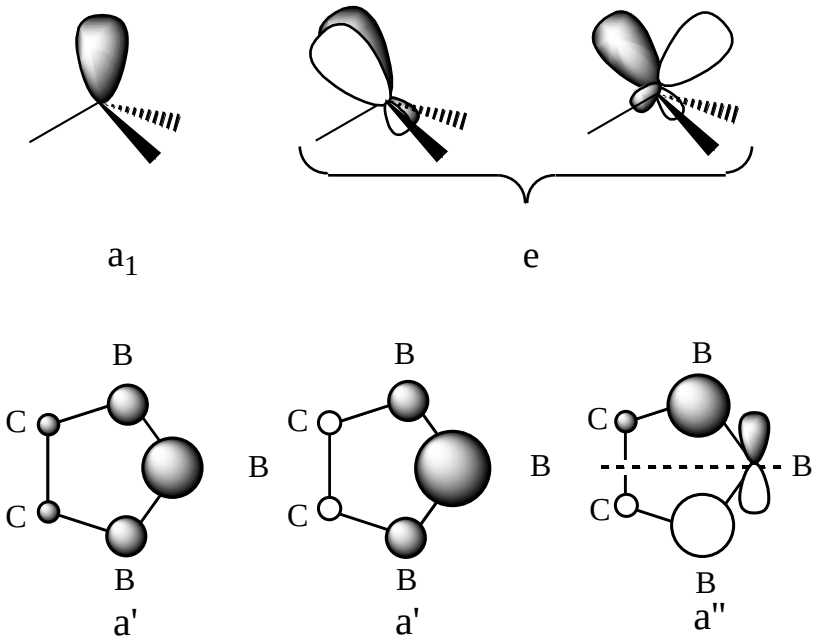

Figure 1.8.1 (top) $\{ML_3\}$ d^8 metal orbitals and (bottom) 7,8-*nido*-$C_2B_9H_{11}$ carborane orbitals primarily involved in metal-cage interaction.

For d^8 MCp/M(C_6R_6) the two metal d-p hybrid orbitals will again be degenerate, but for the d^8 ML_2L' (C_s symmetry)/MLL′L″ (C_1 symmetry) fragments the loss of symmetry renders the orbitals of e symmetry non-degenerate. Whether or not one of the metal orbitals will consequently have a better energy match with one of the carborane orbitals than if the degeneracy had not been lost is not easily determined.

Similar interactions take place in $MCB_{10}H_{11}$, 2,1,7-$MC_2B_9H_{11}$, $MXB_{10}H_{10}$ (X ≠ C) and sub/supraicosahedral metallacarboranes, although the energies/symmetry of the carborane orbitals will be slightly different.[69b,70]

If the metal fragment is d^6 {ML_4} or {d^{10}} ML_2, the metal-cage orbitals interactions are a σ-interaction and two π-interactions (as for a d^8 ML_3/ML_2L' fragment). However for an ML_2 fragment one of the π-interactions is four electron destabilising, while the other is a two electron bonding interaction.[69a,c,71] An ML_2 compound will adopt an exo-polyhedral ligand orientation (which will vary depending on what the carborane ligand is) which minimises this destabilising interaction, and maximises the bonding interaction.[69b,71] For a 3,1,2-metallacarborane the exo-polyhedral ligand orientation will usually be that seen in figure 1.8.2 (or close to this orientation - perturbations could be attributable to avoidance of eclipsing interactions, crystallographic packing forces or unusual exo-polyhedral ligand properties).

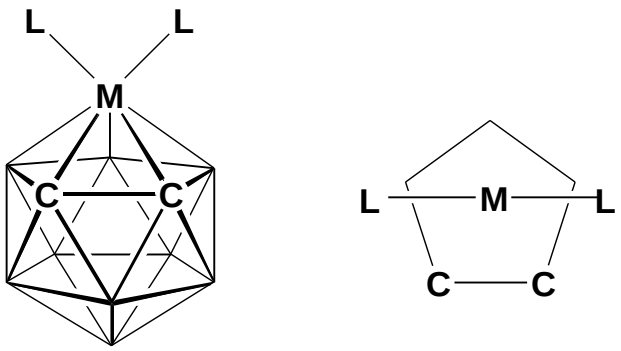

Figure 1.8.2 Exo-polyhedral ligand orientation observed for the majority of 3,3-L_2-3,1,2-$MC_2B_9H_{11}$ metallacarboranes.

The exo-polyhedral ligand orientation of sandwich compounds (i.e. the exo-polyhedral ligand is another carborane) appears to depend on the d-electron count of the metal, with metals which are d^6 or less having cisoid conformations, metals which are d^7 having transoid conformations, and metals which are d^8 or more having slipped transoid conformations.[20a,72,6] These three conformations are shown in figure 1.8.3. The change from cisoid to transoid to slipped transoid conformation as the metal d-electron count increases presumably occurs to minimise antibonding interactions. The orientation of one cage relative to the other also appears to sometimes be dependent on cage to counter-ion/solvent intermolecular interactions.[73]

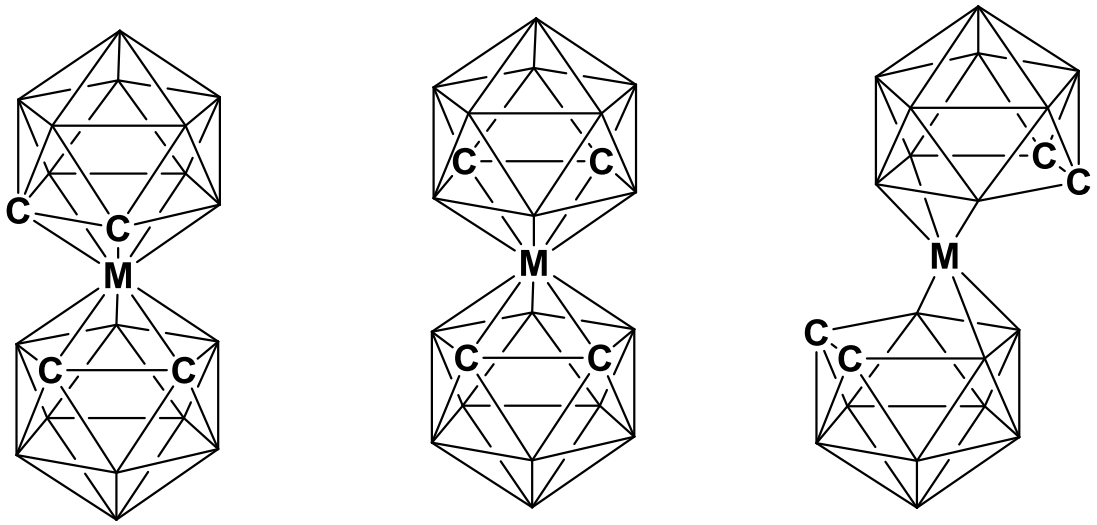

(a) (b) (c)

Figure 1.8.3 (a) Cisoid (≤ d^6), (b) transoid (d^7), and (c) slipped transoid (≥ d^8) conformations of 3,1,2- sandwich compounds.

1.9 The trans influence

The trans influence is a phenomenon which has been described as the ability of a ligand L to weaken (and lengthen) the bond trans to L in preference to the bonds cis to L.[74] The first studies of the trans influence were made by comparing the bond lengths in square planar, usually platinum, species.[75] Other methods of determining trans influences include IR and NMR spectroscopic measurements and computational studies.[75,76a,b,c] It has been suggested that the trans influence is electronic in origin, in that two ligands are forced to compete for the same metal orbital(s), resulting in a relative weakening of one of the metal-ligand bonds.[77]

Ligands which are strong σ-donors (e.g. H^-/CH_3^-) tend to have strong trans influences. The quantity $S^2/\Delta E$ has been proposed[78] as a qualitative measure of the trans influence of a ligand based on its σ-donation to a metal centre. According to this quantity the trans influence of a ligand should be proportional to the square of the orbital overlap integral divided by the difference in energy between the interacting orbitals in an M-L bond. This quantity predicts high trans influences for ligands with low electronegativity and orbitals suitably matched to overlap with a transition metal - i.e. ligands capable of forming highly covalent M-L bonds.

The equation $S^2/\Delta E$ predicts higher trans influences for ligands with π-acceptor abilities, such as CO and C_2H_4, than those observed in square planar complexes. One theory put forward to explain this is that π-acceptor ligands remove excess charge from the metal, and in doing so reduces repulsive interactions between the excess charge and the trans ligand,[78,79] while ligands with π-donor abilities (e.g. oxide and nitride, which tend to have high trans influences) increase the charge on the metal. However work on octahedral complexes has shown that a ligands π-acidity is not necessarily inversely proportional to its trans influence.[80]

There may also be a steric component to the trans influence in complexes which form short M-L bonds, as electrostatic repulsion between the M-L bond and the $M\text{-}L_{cis}$ bonds forces the $M\text{-}L_{cis}$ bonds towards the $M\text{-}L_{trans}$ bonds, lengthening the latter.[81]

The trans influence has been described[80,82a,b] as a mutual influence, in that the properties of the influencing and influenced ligands determine the degree of $M\text{-}L_{trans\ bond}$ lengthening. For example NO^+ shows a negligible trans influence when trans to a σ-donor, a moderate trans

influence when trans to a π-acceptor and an inverse trans influence when trans to a π-donor.[80] The type of metal, d-electron count and metal oxidation state also play an important role in the magnitude of the trans influence.

The trans influence should not be confused with the trans effect which is defined as the ability of a ligand to increase the rate of substitution of a ligand trans to itself.[83] The trans influence is a thermodynamic phenomenon, relating only to the degree of trans bond lengthening in the ground state, whereas the trans effect is a kinetic phenomenon. Weakening of the M-L_{trans} bond by a strongly trans influencing ligand will increase the rate of substitution of L_{trans}, but trans influencing ligands with strong π-acceptor abilities will stabilise the resulting transition state increasing the rate of substitution of L_{trans}.

It has been found that in some main group metal complexes the cis influence is comparable to the trans influence.[74b] This has been rationalised by arguing that the magnitude of the cis influence relative to the trans influence is related to which orbitals on the metal are interacting with the trans influencing ligand. The following situations have been proposed: 1) A comparable cis and trans influence implies that the M-L bond contains mostly metal s-orbital character; 2) The absence of a cis influence implies that the M-L bond contains mostly metal p-orbital character; 3) If the M-L bond contains mostly metal d-orbital character and relatively little metal s-orbital character then the cis influence is small compared to the trans influence and their relative magnitudes may depend on electron configuration.

Any attempt to create a universal trans influence series is unlikely to be successful, as relative trans influences vary depending on the nature of the complexes being used to measure trans bond weakening.

1.10 Research objectives

The aim of the work described in chapter two was to synthesise supraicosahedral metallacarboranes with indenyl exo-polyhedral ligands which could be used to probe the cage to metal bonding, something which had been previously explored in icosahedral metallacarboranes. Different isomers of $(C_9H_7)CoC_2B_{10}$ were synthesised and then studied by *X*-ray crystallography to determine the orientation of the indenyl ligand.

In chapter three different isomers of $(C_{10}H_8)RuC_2B_{10}H_{12}$ are synthesised and the orientation of the naphthalene ligand studied by *X*-ray crystallography. The $(C_9H_7)CoC_2B_{10}$ compounds have a five-membered ring (indenyl) above a six-membered ring (open face of the carborane). Naphthalene was substituted for indenyl in order to avoid the partially eclipsing/partially staggering interaction observed in the indenyl compounds and see whether this would have any significant effect on the orientations of the exo-polyhedral ligand.

While chapters two and three were designed to look at strong cage-to-metal bonding trans to weak exo-polyhedral ligand-to-metal bonding, the intention of chapter four was to look at weak cage-to-metal bonding trans to strong exo-polyhedral ligand-to-metal bonding. This was done by examining the orientation of exo-polyhedral ligands in *X*-ray crystal structures found during a database search.

Chapter five investigates whether metal fragments can be inserted directly into anionic supraicosahedral metallacarboranes (direct electrophilic insertion). This method of cage expansion has been observed before for twelve vertex anionic metallacarboranes, giving thirteen vertex species. The work described in chapter five used anionic thirteen and fourteen vertex metallacarboranes to determine whether these compounds can undergo polyhedral expansion via direct electrophilic insertion.

1.11 References

1.1 J. Daintith, *Dictionary of Chemistry 3rd Ed*, Oxford University Press, 1996.

1.2 H.W. Smith and W.N. Lipscomb, *J. Chim. Phys*., 1949, **46**, 268.

1.3 W.C. Price, *J. Chem. Phys*., 1948, **16**, 894.

1.4 H.C. Longuet-Higgins and M.de.V. Roberts, *Proc. Roy. Soc*., 1954, **A224**, 336; H.C. Longuet-Higgins and M.de.V. Roberts, *Proc. Roy. Soc*., 1955, **A230**, 110.

1.5 A.R. Pitochelli and M.F. Hawthorne, *J. Am. Chem. Soc.*, 1960, **82**, 3228.

1.6 R.N. Grimes, *Carboranes 2nd Ed*, Academic Press, Oxford, 2011.

1.7 (a) L.F Tietze, U. Griesbach, I. Schuberth, U. Bothe, A. Marra and A. Dondoni, *Chem. Eur. J.*, 2003, **9**, 1296.
(b) M.S Delaney, C.B. Knobler and M.F. Hawthorne, *Inorg. Chem.*, 1981, **20**, 1341.
(c) Q. Zhou, Z. Mao, L. Ni and J. Chen, *J. Appl. Polym. Sci.*, 2007, **104**, 2498.

1.8 W.N. Lipscomb, *Boron Hydrides*, W.A. Benjamin Inc., New York, 1963; I.R. Epstein and W.N. Lipscomb, *Inorg Chem*., 1971, **10**, 1921.

1.9 K. Wade, *Adv. Inorg. Chem. Radiochem*., 1976, **18**, 1; K. Wade, *J. Chem. Soc. D*, 1971, 792; D.M.P. Mingos, *Acc. Chem. Res*., 1984, **17**, 311.

1.10 R.E. Williams, *Inorg. Chem*., 1971, **10**, 210; R.E. Williams, *Adv. Inorg. Chem. Radiochem*., 1976, **18**, 66.

1.11 (a) F.L. Hirchfield, K. Eriks, R.E. Dickerson, E.L. Lippert Jr and W.N. Lipscomb, *J. Chem. Phys*., 1958, **28**, 56.
(b) C.E. Nordman and W.N. Lipscomb, *J. Am. Chem. Soc*., 1953, **75**, 4116.
(c) R.B. King, *Inorg. Chem*., 2001, **40**, 6369.

1.12 P.W. Fowler, *Polyhedron*, 1985, **4**, 2051.

1.13 M.E. O'Neill and K. Wade, *Polyhedron*, 1984, **3**, 199.

1.14 (a) A.R. Kudinov, D.S. Perekalin, S.S. Rynin, K.A. Lyssenko, G.V. Grintselev-Knyazev and P.V. Petrovskii, *Angew. Chem., Int. Ed.*, 2002, **41**, 4112.
(b) C.G. Salentine and M.F. Hawthorne, *Inorg. Chem.*, 1978, **17**, 1948.

1.15 For example: P.G. Simpson and W.N. Lipscomb, *J. Chem. Soc.*, 1963, **85**, 1879; J. Bould, W. Clegg, J.D. Kennedy and S.J. Teat, *Acta. Crystallogr., Sect. C: Cryst. Struct. Commun.*,, 2001, **57**, 779; J.H. Enemark, L.B. Friedman and W.N. Lipscomb, *Inorg. Chem.*, 1966, **5**, 2165.

1.16 L.B. Friedman, R.D. Dobrott and W.N. Lipscomb, *J. Am. Chem. Soc.*, 1963, **85**, 3505.

1.17 E.D. Jemmis, M.M. Balakrishnarajan and P.D. Pancharatna, *J. Am. Chem. Soc.*, 2001, **123**, 4313; E.D. Jemmis, M.M. Balakrishnarajan and P.D. Pancharatna, *Chem. Rev.*, 2002, **102**, 93.

1.18 (a) B. Siegel and J.I. Mack, *J. Chem. Educ.*, 1957, **34**, 317.
(b) E. Muetterties, *Boron Hydride Chemistry*, Academic Press Inc., 1975.

1.19 (a) A. Franken, B.T. King, J. Rudolph, P. Rao, B.C. Noll, and J. Michl, *Collect. Czech. Chem. Commun.*, 2001, **66**, 1238.
(b) W.M. Maxwell, V.R. Miller and R.N. Grimes, *J. Am. Chem. Soc*., 1974, **96**, 7116; W.M. Maxwell, V.R. Miller and R.N. Grimes, *Inorg. Chem.*, 1976, **15**, 1343.

1.20 (a) T.E. Paxon, M.K. Kaloustian, G.M. Tom, R.J. Wiersema and M.F. Hawthorne, *J. Am. Chem. Soc.*, 1972, **94**, 4882
(b) H.D. Smith, T.A. Knowles and H. Schroeder, *Inorg. Chem*., 1965, **4**, 107.

1.21 (a) T.L. Heying, J.W. Ager Jnr, S.L. Clark, D.J. Mangold, H.L. Goldstein, M.L. Hillman, R.J. Polak and J.W. Szymanski, *Inorg. Chem*., 1963, **2**, 1089.
(b) Y. Li, P.J. Carroll and L.G. Sneddon, *Inorg. Chem.*, 2008, **47**, 9193.
(c) R.L. Ernest, W. Quintana, R. Rosen, P.J. Carroll and L.G. Sneddon, *Organometallics*, 1987, **12**, 2711.

1.22 Y. Wang, B. Quillian, P. Wei, C.S. Wannere, Y. Xie, R.B. King, H.F. Schaefer III, P.v.R. Schleyer and G.H. Robinson, *J. Am. Chem. Soc.*, 2007, **129**, 12412.

1.23 H. Braunschweig, R.D. Dewhurst, K. Hammond, J. Mies, K. Radacki and A. Vargas, *Science*, 2012, **336**, 1420.

1.24 E.D. Jemmis, *J. Am. Chem. Soc*., 1982, **104**, 7017.

1.25 R.A. Wiesboeck, and M.F. Hawthorne, *J. Am. Chem. Soc*., 1964, **86**, 1642; P.M. Garrett, F.N. Tebbe and M.F. Hawthorne, *J. Am. Chem. Soc*., 1964, **86**, 5016.

1.26 M.F. Hawthorne, D.C. Young and P.A. Wegner, *J. Am. Chem. Soc*., 1965, **87**, 1818.

1.27 (a) S. Papetti and T.L. Heying, *J. Am. Chem. Soc.*, 1964, **86**, 2295.
(b) S. Zlatogorsky, M.J. Edie, D. Ellis, S. Erhardt, M.E. Lopez, S.A. Macgregor, G.M. Rosair and A.J. Welch, *Angew. Chem. Int. Ed*., 2007, **46**, 6706.

1.28 (a) W.N. Lipscomb, *Science*, 1966, **153**, 373.
(b) D.J. Wales, *J. Am. Chem. Soc*., 1993, **115**, 1557.

1.29 H.D. Kaesz, R. Bau, H.A. Beall and W.N. Libscomb, *J. Am. Chem. Soc.*, 1967, **89**, 4219.

1.30 C.A. Brown and M.L. McKee, *J. Mol. Model*., 2006, **12**, 653.

1.31 (a) L.D. Brown and W.N. Lipscomb, *Inorg. Chem*., 1977, **16**, 2989.

(b) P.v.R. Schleyer, K. Najafian and A.M. Mebel, *Inorg. Chem.*, 1998, **37**, 6765.

1.32 For example: D.M.P. Mingos and D.J. Wales, *Introduction to Cluster Chemistry*, Prentice Hall, Englewood Cliffs, NJ, 1990; M.L. McKee, *Inorg. Chem.*, 2002, **41**, 1299; E.D. Jemmis and P.v.R. Schleyer, *J. Am. Chem. Soc.*, 1982, **104**, 4781.

1.33 G.B. Dunks, M. M. McKown, M. F. Hawthorne, *J. Am. Chem. Soc*., 1971, **93**, 2541.

1.34 B.W. Hutton, F. MacIntosh, D. Ellis, F. Herisse, S.A. Macgregor, D. McKay, V. Petrie-Armstrong, G.M. Rosair, D.S. Perekalin, H. Tricas and A.J. Welch, *Chem. Commun.*, 2008, **42**, 5345.

1.35 R.N. Leyden and M.F. Hawthorne, *Inorg. Chem.*, 1975, **14**, 2018.

1.36 A. Burke, D. Ellis, B.T. Giles, S.A. Macgregor, G.M. Rosair and A.J. Welch, *Angew. Chem. Int. Ed*., 2003, **42**, 225.

1.37 L. Deng, H-S. Chan and Z. Xie, *J. Am. Chem. Soc.*, 2006, **128**, 5219.

1.38 D. McKay, 2008, Heriot-Watt University, Unpublished results.

1.39 L. Deng, H.-S. Chan and Z. Xie, *Angew. Chem. Int. Ed*., 2005, **44**, 2128.

1.40 J. Zhang, L. Deng, H.-S. Chan and Z. Xie, *J. Am. Chem. Soc.*, 2007, **129**, 18.

1.41 J. Zhang, F. Zheng and Z. Xie, *Organometallics*, 2013, **32**, 7399.

1.42 (a) R.W. Chapman, J.G. Kester, K. Folting, W.E. Streib and L.J. Todd, *Inorg. Chem.*, 1992, **31**, 979.

(b) S.A. Jasper Jnr, J.C. Huffman and L.J. Todd, *Inorg. Chem.*, 1998, **37**, 6060.

(c) M.J. Manning, C.B. Knobler and M.F. Hawthorne, *J. Am. Chem. Soc.*, 1988, **110** 4458.

1.43 D.K. Roy, S.K. Bose, R.S. Anju, B. Mondal, V. Ramkumar and S. Ghosh, *Angew. Chem. Int. Ed.*, 2013, **52**, 3222; D.K. Roy, B. Mondal, P. Shankhari, R.S. Anju, K. Geetharani, S.M. Mobin and S. Ghosh, *Inorg. Chem.*, 2013, **52**, 6705.

1.44 M. Elian, M.M.L. Chen, D.M.P. Mingos and R. Hoffmann, *Inorg. Chem.*, 1976, **15**, 1148; R. Hoffmann, *Angew. Chem. Int. Ed.*, 1982, **21**, 711.

1.45 (a) A.J. Welch, *J. Chem. Soc., Dalton Trans.*, 1975, 2270; M. Green, J.L. Spencer and F.G.A. Stone, *J. Chem. Soc., Dalton Trans.*, 1979, 1679.

(b) M. Green, J.A.K. Howard, J.L. Spencer and F.G.A. Stone, *J. Chem. Soc., Dalton Trans.*, 1975, 2275; G.K. Barker, M. Green, F.G.A. Stone, A.J. Welch, T.P. Onak and G. Siwapanyoyos, *J. Chem. Soc., Dalton Trans.*, 1979, 1687.

1.46 (a) M. Green, J.L. Spencer, F.G.A Stone and A.J. Welch, *J. Chem. Soc. Dalton Trans.*, 1975, 179; D.E. Kadlecek, A.M. Shedlow, S.O. Kang, P.J. Carroll and L.G. Sneddon, *J. Am. Chem. Soc.*, 2003, **125**, 212.

(b) W.J. Evans and M.F. Hawthorne, *J. Chem. Soc. Chem. Commun.* 1973, 706; S. Du, B.E. Hodson, P. Lei, T.D. McGrath and F.G.A Stone, *Inorg. Chem.*, 2007, **46**, 6613.

(c) R.R. Rietz, D.F. Dustin and M.F. Hawthorne, *Inorg. Chem.*, 1974, **13**, 1580; W.H. Knoth, *Inorg. Chem.*, 1971, **10**, 598.

(d) B. Štíbr, *J. Organomet. Chem.*, 2005, **690**, 2694.

(e) W.M. Maxwell, R.F. Bryan and R.N. Grimes, *J. Am. Chem. Soc.*, 1977, **99**, 4008.

(f) B.A. Barnum, P.J. Carroll, and L.G. Sneddon, *Organometallics*, 1995, **14**, 4463.

1.47 P.T. Brain, M. Bühl, J. Cowie, Z.G. Lewis and A.J. Welch, *J. Chem. Soc., Dalton Trans.,* 1996, *231*.

1.48 M.F. Hawthorne and T.D. Andrews, *J. Chem. Soc., Chem. Commun.,* 1965, 443; A. Zalkin, D.H. Templeton and T.E. Hopkins, *J. Am. Chem. Soc*., 1965, **87**, 3988.

1.49 (a) S. Dunn, G.M. Rosair, Rh.Ll. Thomas, A.S. Weller and A.J. Welch, *Angew. Chem. Int. Ed*., 1997, **36**, 645.

(b) R.D. McIntosh, D. Ellis, B.T. Giles, S.A. Macgregor, G.M. Rosair and A.J. Welch, *Inorg. Chim. Acta*, 2006, **359**, 3745.

1.50 For example: W.E. Carroll, M. Green, F.G.A Stone and A.J. Welch, *J. Chem. Soc., Dalton Trans.*, 1975, 2263; T.D. McGrath, A. Franken, J.A. Kautz and F.G.A. Stone, *Inorg. Chem.*, 2005, **44**, 8135; M.P. Garcia, M. Green, F.G.A. Stone, R.G. Somerville and A.J. Welch, *J. Chem. Soc., Chem. Commun.*, 1981, 871.

1.51 M.R. Churchill and B.G. DeBoer, *J. Chem. Soc., Chem. Commun.*, 1972, 1326.

1.52 D. Ellis, M.E. Lopez, R. McIntosh, G.M. Rosair, A.J. Welch and R. Quenardelle, *Chem. Commun.*, 2005, 1348.

1.53 R. McIntosh, D. Ellis, J. Gil-Lostes, K.J. Dalby, G.M. Rosair and A.J. Welch, *Dalton Trans*., 2005, **10**, 1842.

1.54 A. McAnaw, M.E. Lopez, G. Scott, D. Ellis, D. McKay, G.M. Rosair and A.J. Welch, *Dalton Trans.*, 2012, **41**, 10957.

1.55 (a) A. Burke, R. McIntosh, D. Ellis, G.M. Rosair and A.J. Welch, *Collect. Czech. Chem. Commun.*, 2002, **67**, 991.

(b) G. Scott, D. Ellis, G.M. Rosair and A.J. Welch *J. Organomet. Chem.*, 2012, **721**, 78.

1.56 D.F. Dustin, G.B. Dunks and M.F. Hawthorne, *J. Am. Chem. Soc*., 1973, **95**, 1109.

1.57 (a) B. Grüner, B. Štíbr, R. Kivekäs, R. Sillanpää, P. Stopka, F. Teixidor and C. Viňas, *Chem. Eur. J.*, 2003, **9**, 6115.; B. Grüner, L. Mikulasek, I. Cisařová and B. Štíbr. *J. Organomet. Chem.*, 2005, **690**, 2853.

(b) W.M. Maxwell, R. Weiss, E. Sinn and R.N. Grimes, *J. Am. Chem. Soc.*, 1977, **99**, 4016.

(c) Z-T. Wang, E. Sinn and R.N. Grimes, *Inorg. Chem.*, 1985, **24**, 826.

(d) M.E. Lopez, M.J. Edie, D. Ellis, A. Horneber, S.A. Macgregor, G.M. Rosair and A.J. Welch, *Chem, Commun.*, 2007, 2243; D.F. Dustin and M.F. Hawthorne, *J. Am. Chem. Soc.*, 1974, **96**, 3462.

(e) B.A. Barnum, P.J. Carroll and L.G. Sneddon, *Inorg. Chem.*, 1997, **36**, 1327.

1.58 (a) G.K. Barker, M.P. Garcia, M. Green, F.G.A. Stone and A.J. Welch, *J. Chem. Soc., Chem. Commun.*, 1983, 137.

(b) A. McAnaw, M.E. Lopez, D. Ellis, G.M. Rosair and A.J. Welch, *Dalton Trans.*, 2014, **43**, 5095.

1.59 W.J. Evans and M.F. Hawthorne, *J. Chem. Soc., Chem. Commun.*, 1974, 38; D. Ellis, M.E. Lopez, R. McIntosh, G.M. Rosair and A.J. Welch, *Chem. Commun.*, 2005, 1917; A. McAnaw, M.E. Lopez, D. Ellis, G.M. Rosair and A.J. Welch, *Dalton Trans.*, 2013, **42**, 671.

1.60 R.D. McIntosh, D. Ellis, G.M. Rosair and A.J. Welch, *Angew. Chem. Int. Ed.*, 2006, **45**, 4313.

1.61 L. Deng, J. Zhang, H-S. Chan and Z. Xie, *Angew. Chem. Int. Ed.*, 2006, **45**, 4309.

1.62 Z. Xie, *Coord. Chem. Rev.*, 2002, **231**, 23.

1.63 (a) K.F. Shaw, B.D. Reid and A.J. Welch, *J. Organomet. Chem.*, 1994, **482**, 207; D. Rabinovich, C.M. Haswell, B.L. Scott, R.L. Miller, J.B. Nielsen and K.D. Abney, *Inorg. Chem.*, 1996, **35**, 1425.

(b) R. Khattar, M.J. Manning, C.B. Knobler, S.E. Johnson and M.F. Hawthorne, *Inorg. Chem.*, 1992, **31**, 268; Z. Xie, S. Wang, Z. Zhou, F. Xue and T.C.W. Mak, *Organometallics*, 1998, **17**, 489.

1.64 (a) Z. Xie, Z. Liu, K-Y. Chiu, F. Xue and T.C.W. Mak, *Organometallics*, 1997, **16** 2460; D. Rabinovich, R.M. Chamberlin, B.L. Scott, J.B. Nielsen and K.D. Abney, *Inorg. Chem.*, 1997, **36**, 4216.

(b) Z. Xie, S. Wang, Z. Zhou and T.C.W. Mak, *Organometallics*, 1998, **17**, 1907.

1.65 Z. Xie, C. Yan, Q. Yang and T.C.W. Mak, *Angew. Chem. Int. Ed.*, 1999, **38**, 1761; Z. Xie, K. Chui, Q. Yang, and T.C.W. Mak, *Organometallics*, 1999, **18**, 3947.

1.66 J.A. Dupont and M.F. Hawthorne, *J. Am. Chem. Soc.*, 1964, **86**, 1643.

1.67 (a) G. Sivasubramaniam, 2011, Heriot-Watt University, Unpublished results.
(b) D. Ellis, G.M. Rosair and A.J. Welch *Chem. Commun.*, 2010, **46**, 7394.

1.68 D. Ellis, D. McKay, S.A. Macgregor, G.M. Rosair and A.J. Welch, *Angew. Chem. Int. Ed.*, 2010, **49**, 4943.

1.69 (a) T.A. Albright, J.K. Burdett and M-H. Whangbo, *Orbitals Interactions in Chemistry*, Wiley, 1985.
(b) D.M.P. Mingos, M.I. Forsyth and A.J. Welch, *J. Chem. Soc., Dalton. Trans.*, 1978, 1363.
(c) D.M.P. Mingos, *J. Chem. Soc., Dalton. Trans.*, 1977, 602.

1.70 K.J. Dalby, D. Ellis, S. Erhardt, R.D. McIntosh, S.A. Macgregor, K. Rae, G.M. Rosair, V. Settels, A.J. Welch, B.E. Hodson, T.D. McGrath and F.G.A. Stone, *J. Am. Chem. Soc.*, 2007, **129**, 3302.

1.71 P.D. Abram, D. McKay, D. Ellis, S.A. Macgregor, G.M. Rosair and A.J. Welch, *Dalton Trans.*, 2010, **39**, 2412.

1.72 M.F. Hawthorne and G.B. Dunks, *Science*, 1972, **178**, 462; D.M.P. Mingos, M.I. Forsyth and A.J. Welch, *J. Chem. Soc. Chem. Commun.*, 1977, 605.

1.73 D. Ellis, R.D. McIntosh, S. Esquirolea, C. Viňas, G.M. Rosair, F. Teixidor and A.J. Welch, *Dalton Trans.*, 2008, 1009.

1.74 (a) A. Pidcock, R.E. Richards and L.M. Venanzi, *J. Chem. Soc. A***,** 1966, 1707.
(b) K.M. Anderson and A.G. Orpen, *Chem. Commun.*, 2001, 2862.

1.75 F.R. Hartley, *Chem. Soc. Rev.*, 1973, **2**, 163; T.G. Appleton, H.C. Clark and L.E. Manzer, *Coord. Chem. Rev.*, 1973, **10**, 335.

1.76 (a) D.M. Adams J. Chatt, J. Gerratt and A.D. Westland, *J. Chem. Soc. A*, 1964, 734.
(b) M.H. Chisholm, H.C. Clark, L.E. Manzer and J.B. Stothers, *J. Am. Chem. Soc*., 1972, **94**, 5087.
(c) A.E. Anastasi and R.J. Deeth, *J. Chem. Theory Comput.*, 2009, **5**, 2339.

1.77 N. Kaltsoyannis and P. Mountford, *J. Chem. Soc*., *Dalton Trans*., 1999, 781.

1.78 R. Mason, R. McWeeny and A.D.C. Towl, *Discuss. Faraday Soc.*, 1969, **47**, 20; R. Mason and A.D.C. Towl, *J. Chem. Soc. (A), Inorg. Phys. Theor*., 1970, 1601.

1.79 L.J. Manojlović-Muir and K.W. Muir, *Inorg. Chim. Acta*, 1974, **10**, 47.

1.80 B.J. Coe and S. Glenwright, *Coord. Chem. Rev.*, 2000, **203**, 5.

1.81 P.D. Lyne and D.M.P. Mingos, *J. Chem. Soc., Dalton Trans.*, 1995, 1635.

1.82 (a) P.K. Sajith and C.H. Suresh, *Dalton Trans.*, 2010, **39**, 815.

(b) J.K. Burdett and T.A. Albright, *Inorg. Chem.*, 1979, **18**, 2112.

1.83 R.H. Crabtree, *The Organometallic Chemistry of the Transition Metals 4th Ed*, Wiley-Interscience, New Jersey, 2005; F. Basolo and R.G. Pearson, *Prog. Inorg. Chem.*, 1962, **4**, 381.

Chapter 2

Indenyl Cobaltacarboranes

2.1 Introduction

The indenyl ligand (C_9H_7) bonds to metals via the five-membered ring, but unlike in analogous Cp (Cp = η-C_5H_5) compounds it shows a greater tendency towards η^3 as opposed to η^5 bonding.[1] This slippage towards η^3 bonding is manifested in a selective lengthening of the bridging carbon atoms to metal bonds and is known as the structural indenyl effect (figure 2.1.1).

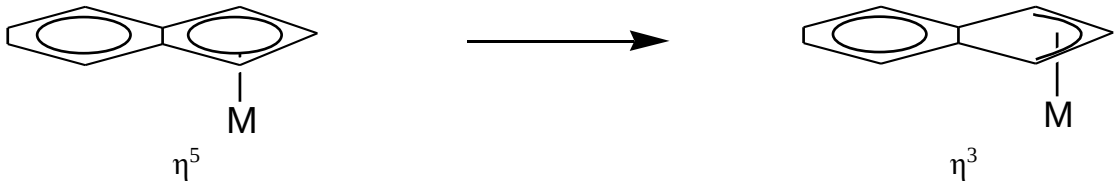

Figure 2.1.1 Indenyl ligand slipping from η^5 to η^3 bonding.

It is also the basis of the kinetic indenyl effect,[2] in which indenyl compounds have a faster rate of ligand substitution than their Cp analogues. This slippage occurs because the bound five-membered ring and the free six-membered ring share the bridging carbon atom's p_π orbitals, with the slipping facilitating the recovery of some of the resonance energy in the six-membered ring.[3]

Previous work has shown that in twelve vertex icosahedral indenyl cobaltacarboranes, the bridging carbon atoms of the indenyl ligand are orientated trans to the cage boron atoms, as opposed to the cage carbon atoms.[4] The preferred orientation in 3-(η-C_9H_7)-3,1,2-*closo*-$CoC_2B_9H_{11}$ (**I**) is one which is cisoid with respect to the metal-bound five-membered ring of the indenyl and the top pentagonal belt of the cage - presumably to avoid eclipsing interactions between the two rings (figure 2.1.2 (a)). A similar cisoid orientation was also found in 1-Ph-3-(η-C_9Me_7)-3,1,2-*closo*-$RhC_2B_9H_{10}$ and 1,2-Ph_2-3-(η-C_9Me_7)-3,1,2-*psuedocloso*-$RhC_2B_9H_9$.[5] It was found that the presence of bulky -CH_2OCH_3 groups on the cage carbon atoms in 1,2-$(CH_2OCH_3)_2$-3-(η-C_9H_7)-3,1,2-*closo*-$CoC_2B_9H_9$ caused the indenyl

ligand to adopt an orientation where one of the bridging carbon atoms is trans to a cage boron atom, whilst the other is almost trans to a cage carbon atom[6] (figure 2.1.2 (b)).

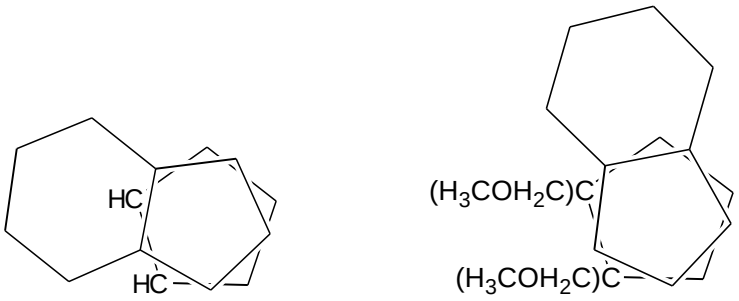

(a) (b)

Figure 2.1.2 (a) Orientation of indenyl with respect to open face of carborane ligand and (b) orientation of indenyl with respect to open face of ether-substituted carborane ligand.

The cage boron atoms have a stronger trans influence than the cage carbon atoms, causing the bonds trans to the cage boron atoms to be weakened relative to the bonds trans to the cage carbon atoms. The indenyl ligand bridging carbon atoms prefer to be trans to cage boron atoms (as opposed to cage carbon atoms) as this allows maximum lengthening/weakening of the bridging carbon atoms to metal bonding - thus increasing the aromaticity of the six-membered ring. The reason that the cage boron atoms have a greater trans influence than the cage carbon atoms[7a] is that boron is less electronegative than carbon, and so the FMOs of the nido ligand are localised on the former[7b] (figure 2.1.3).

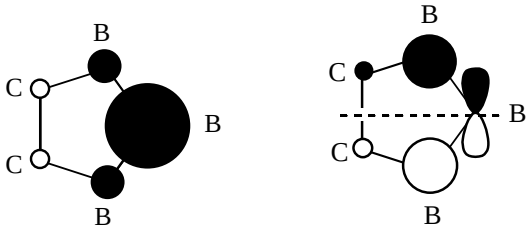

(a) (b)

Figure 2.1.3 (a) HOMO and (b) LUMO of [7,8-*nido*-$C_2B_9H_{11}$]$^{2-}$.

We decided to investigate whether similar orientational preferences would be found in thirteen vertex (η-C_9H_7)CoC_2B_{10} species and so synthesised two supraicosahedral indenyl cobaltacarboranes by the reduction of icosahedral carboranes followed by metallation with {(C_9H_7)Co}$^{2+}$. These compounds were then isomerised giving, in total, four isomers of the

supraicosahedral species 4-(η-C_9H_7)-4,1,X-*closo*-$CoC_2B_{10}H_{12}$ where X = 6,8,10 and 12 (compounds **1**, **3**, **7** and **5**). Similar reactions afforded three isomers of the dimethyl analogues 1,X-Me_2-4-(η-C_9H_7)-4,1,X-*closo*-$CoC_2B_{10}H_{10}$ where X = 6,8 and 12 (compounds **2**, **4**, and **6**). A fourteen vertex bi-metallic species (**8**) was also synthesised from reduction/metallation of **5**.

All compounds were characterised by CHN microanalysis, ^{11}B and ^{1}H NMR spectroscopy and mass spectrometry (except **3** and **8** which were not characterised by CHN), and then studied by *X*-ray crystallography (except for **3** which could not be persuaded to crystallise) in order to determine the orientation of the indenyl ligand relative to the six-membered face of the carborane moiety.

The compounds described in this chapter were made in a similar way to the known (CpCo)C_2B_{10} and (Cp*Co)C_2B_{10} compounds,[8a,b,c,d,e] with the C_5R_5 (R = H, Me) species providing a good spectroscopic and structural comparison (with respect to the cage) to the indenyl cobaltacarboranes.

2.2 Synthesis of 4-(η-C_9H_7)-4,1,6-*closo*-$CoC_2B_{10}H_{12}$ (1)

Reduction of 1,2-*closo*-$C_2B_{10}H_{12}$ with Na in THF results in [7,9-*nido*-$C_2B_{10}H_{12}]^{2-}$. To this was added $CoCl_2$ and Li[C_9H_7] in THF (generated from C_9H_8 and *n*-BuLi in THF) to give a brown solution which was stirred overnight. Upon aerial oxidation and chromatography brown **1** is isolated in 47.3% yield.

The MS of **1** contains an envelope centred on *m/z* 317 (M^+) (M_w **1** = 318.19 g/mol), and the elemental analysis is in good agreement with that expected for $C_{11}H_{19}B_{10}Co$.

Compound **1** shows one broad peak of integral two at 3.70 ppm in the ^1H NMR spectrum corresponding to the two cage CHs. This is consistent with C_s symmetry, which is the result of a fluxional double DSD process which renders both CHs equivalent on the NMR timescale[9] (figure 2.2.1).

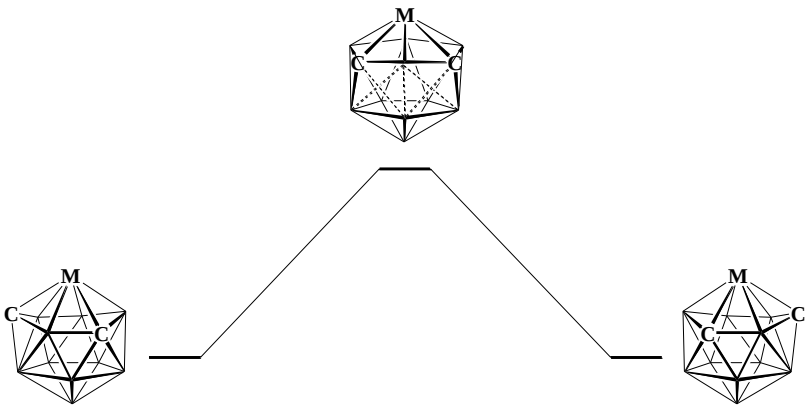

Figure 2.2.1 Double DSD mechanism leading to equivalent cage carbon atoms on NMR timescale.

The relevant indenyl peaks are observed as a triplet at 5.60 ppm corresponding to the unique proton of the indenyl five-membered ring and a doublet at 5.90 ppm corresponding to the other two protons on the indenyl five-membered ring. The four protons on the six-membered ring appear as multiplets at 7.60 and 7.70 ppm, but it is not easily possible to tell which peaks belong to the proton pairs H_A and H_B in figure 2.2.2.

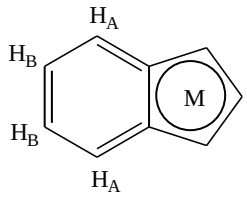

Figure 2.2.2 Metal bound indenyl ligand with labelled protons on six-membered ring.

The ^{11}B NMR spectrum consists of six peaks in a 1:2:1:3:2:1 ratio between -16.9 and 14.5 ppm. Seven peaks (three integral 2 and four integral 1) would be expected considering the C_s symmetry, suggesting that the peak of integral three is a 2 + 1 coincidence.

Both the ^{1}H and ^{11}B NMR spectra are consistent with C_s symmetry, which implies indenyl rotation (or at least substantial libration) about the centre of the five-membered ring at room temperature in solution. The only other explanation is that in going from the solid state temperature (100K) to room temperature the indenyl ligand has adopted an orientation whereby it sits across the time-averaged mirror plane. This seems unlikely given that other more bulky groups such as C_5Me_5[8a] are known to rotate at room temperature. The cage C_s symmetry (or time-averaged C_s symmetry) giving rise to the chemical equivalence of protons related by the indenyl ligand's mirror plane is found in all of the 4,1,6- and 4,1,10- ^{1}H NMR spectra described in this chapter.

Crystals of **1** were grown by diffusion of diethyl ether and a THF solution of **1** at -30 ^{o}C. Analysis by *X*-ray diffraction shows **1** to be the expected 4-(η-C_9H_7)-4,1,6-*closo*-$CoC_2B_{10}H_{12}$ (figure 2.2.3).

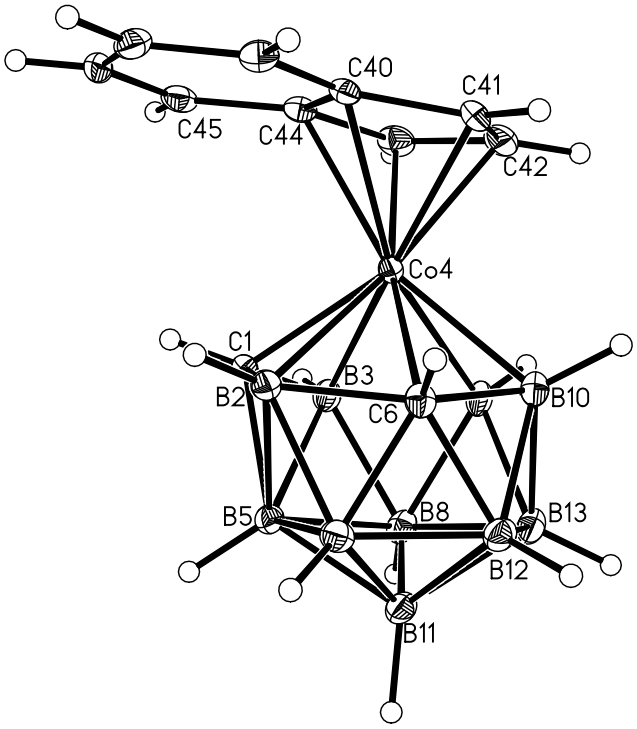

Figure 2.2.3 Molecular structure of 4-(η-C_9H_7)-4,1,6-*closo*-$CoC_2B_{10}H_{12}$ **(1)**.

The fluxionality observed in solution at room temperature is frozen out in the crystal structure giving the cage in **1** a docosahedral structure of C_1 symmetry. The cage structure of **1** is comparable to that of 4-Cp-4,1,6-*closo*-$CoC_2B_{10}H_{12}$[8e] and 4-Cp*-4,1,6-*closo*-$CoC_2B_{10}H_{12}$[8a] (Cp* = C_5Me_5), with degree four vertex 1 and degree five vertex 6 both occupied by carbon atoms, degree six vertex 4 occupied by cobalt, degree six vertex 5 occupied by boron and all other vertices (all degree five) occupied by boron.

The Co4-C1 distance is the shortest cage to metal connectivity (2.0175(15) Å compared to 2.1249(17) Å for the next shortest metal to cage connectivity) and the B-B connectivities B2-B5 and B3-B5 are characteristically long compared to the other B-B connectivities (B2-B5 = 2.035(2) Å, B3-B5 = 2.026(2) Å compared to 1.915(2) Å for the next longest B-B connectivity). Both of these features are generally characteristic of docosahedral structures and are encountered in most of the examples of this cage architecture reported in this chapter. The Co4-C distances to the bridging carbon atoms of the indenyl ligand are longer than the Co4-C distances to the non-bridging carbon atoms (2.1469(14) Å for Co4-C44 and 2.1642(15) Å for Co4-C40, compared to 2.0527(16) Å, 2.0228(16) Å and 2.0342(15) Å for Co4-C41, Co4-C42 and Co4-C43, respectively).

2.3 Synthesis of 1,6-Me_2-4-(η-C_9H_7)-4,1,6-*closo*-$CoC_2B_{10}H_{10}$ (2)

Compound **2** is made in the same way as **1**, but using 1,2-Me_2-1,2-*closo*-$C_2B_{10}H_{10}$ instead of 1,2-*closo*-$C_2B_{10}H_{12}$ giving, after chromatography, brown **2** in 33.8% yield.

The ^{11}B NMR spectrum of **2** consists of seven peaks in a 1:2:1:1:2:2:1 ratio between -12.1 and 15.1 ppm as would be expected considering the C_s symmetry.

The ^{1}H NMR spectrum shows one sharp singlet of integral six at 2.15 ppm corresponding to the two methyl groups on the cage carbon atoms - a single peak being observed due to the same fluxional double DSD process occurring in **1**. The relevant indenyl peaks are observed as a triplet at 5.75 ppm corresponding to the unique proton of the indenyl five-membered ring and a doublet at 5.80 ppm corresponding to the other two protons on the indenyl five-membered ring. The four protons on the six-membered ring appear as multiplets at 7.60 and 7.80 ppm.

The MS of **2** contains an envelope centred on *m/z* 346 (M^+) (M_w **2** = 346.24 g/mol), and the elemental analysis is in good agreement with that expected for $C_{13}H_{23}B_{10}Co$.

Crystals of **2** were grown by diffusion of 40-60 petroleum ether and a DCM solution of **2** at -30 ^oC. Analysis by *X*-ray diffraction shows **2** to be the expected 1,6-Me_2-4-(η-C_9H_7)-4,1,6-*closo*-$CoC_2B_{10}H_{10}$ (figure 2.3.1).

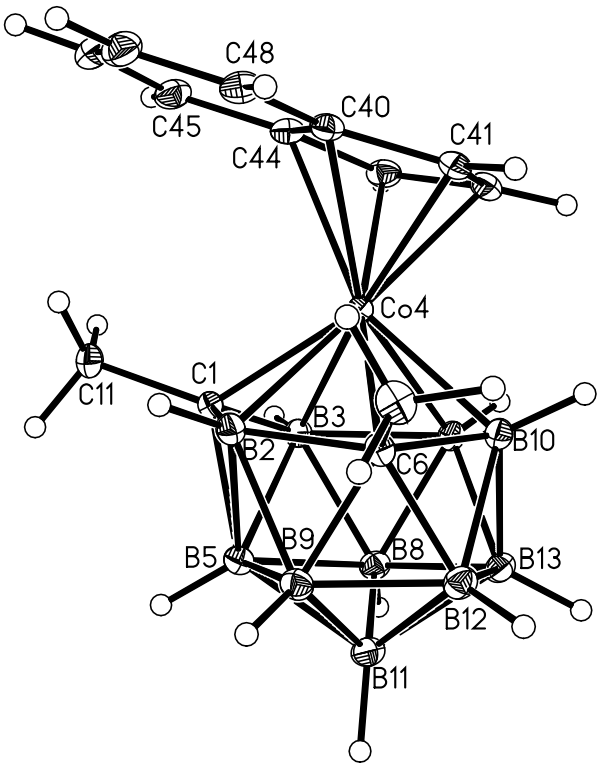

Figure 2.3.1 Molecular structure of 1,6-Me_2-4-(η-C_9H_7)-4,1,6-*closo*-$CoC_2B_{10}H_{10}$ **(2)**.

As in **1**, a docosahedral structure of C_1 symmetry is observed in **2** . The cage structure of **2** is similar to **1** and its Cp/Cp* analogues, but finds a more direct comparison in the structure of 1,6-Me_2-4-Cp-4,1,6-*closo*-$CoC_2B_{10}H_{12}$.[8c] All of the cage vertices in **2** are occupied by the same atoms as in **1**, and all are of the same conectivity.

As in **1**, the Co4-C distances to the bridging carbon atoms of the indenyl ligand are longer than the Co4-C distances to the non-bridging carbon atoms (2.2046(11) Å for Co4-C44 and 2.1777(10) Å for Co4-C40, compared to 2.0418(10) Å, 2.0234(10) Å and 2.0452(11) Å for Co4-C41, Co4-C42 and Co4-C43, respectively). The difference between the Co4-C distances to the bridging carbon atoms and the Co4-C distances to the non-bridging carbon atoms is slightly more pronounced in **2** than in **1**. The reason for this is the significant bending of the indenyl ligand away from co-planarity with the lower pentagonal ring of the cage in **2** compared to **1** which will be discussed in section 2.12.

2.4 Synthesis of 4-(η-C_9H_7)-4,1,8-*closo*-$CoC_2B_{10}H_{12}$ (3)

Overnight heating of **1** in refluxing THF followed by chromatography gave bronze **3** in 73.6% yield. Small amounts of the 4,1,6- and 4,1,12- isomers were also recovered.

Compound **3** shows two broad peaks each of integral one at 2.50 and 3.75 ppm in the ^{1}H NMR spectrum corresponding to the two cage CHs. The relevant indenyl peaks are observed as an apparent triplet at 5.10 ppm corresponding to the unique proton of the indenyl five-membered ring and multiplets at 5.80 and 5.86 ppm corresponding to the other two protons on the indenyl five-membered ring. The four protons on the six-membered ring appear as multiplets at 7.50 and 7.60 ppm.

The ^{11}B NMR spectrum consists of ten peaks all of integral one between -12.5 and 22.6 ppm. Both the ^{1}H and ^{11}B NMR spectra are consistent with C_1 symmetry, the time-averaged C_s symmetry being lost upon isomerisation of 4,1,6- to 4,1,8-. The result of this is that, despite any indenyl ligand rotation/libration, all of the protons on the indenyl ligand become inequivalent in the ^{1}H NMR spectrum (with any overlap being coincident) and the single cage CH peak seen in **1** (or CMe peak in **2**) becomes two distinct peaks separated by 1.25 ppm. All of the boron atoms become inequivalent - leading to the observed ten peaks in the ^{11}B NMR spectrum. Another feature of the ^{11}B NMR spectrum is the peak at 22.6 ppm, which is relatively upfield compared to the 4,1,X- X= 6, 10, 12 isomers, and is characteristic of the 4,1,8- isomer.

Unfortunately *X*-ray quality crystals of **3** could not be obtained despite trying several different solvent combinations, however the NMR spectra and mass spectrum (envelope centred on *m/z* 317 (M^+) (M_w **3** = 318.19 g/mol)) indicate that the 4,1,8- isomer has been formed.

The fact that **3** did not crystallise made it impossible to study the indenyl orientation in this compound, frustrating attempts to compare the orienations in all of the available isomers. Others within the group[10] managed to synthesise and obtain a crystal structure for 8-Me-4-(η-C_9H_7)-4,1,8-*closo*-$CoC_2B_{10}H_{11}$ by first making 6-Me-4-(η-C_9H_7)-4,1,6-*closo*-$CoC_2B_{10}H_{11}$ and then isomerising it to the Me-4,1,8- isomer. The Me-4,1,8- isomer provides a good approximation of **3** to study the indenyl orientaion, as the methyl group is

in the lower belt of the cage and should not have any significant steric interaction with the indenyl ligand - leaving only an electronic difference between the two compounds.

2.5 Synthesis of 1,8-Me_2-4-(η-C_9H_7)-4,1,8-*closo*-$CoC_2B_{10}H_{10}$ (4)

Overnight heating of **2** in refluxing THF followed by chromatography gave orange **4** in 66.5% yield. A small amount of the Me_2-4,1,12- isomer was also recovered.

The MS of **4** contains an envelope centred on *m/z* 346 (M^+) (M_w **4** = 346.24 g/mol), and the elemental analysis is in good agreement with that expected for $C_{13}H_{23}B_{10}Co$.

Compound **4** shows two sharp peaks each of integral three at 1.75 and 2.60 ppm in the ^1H NMR spectrum, corresponding to the two methyl groups on the cage carbon atoms. The relevant indenyl peaks are observed as an apparent triplet at 5.25 ppm corresponding to the unique proton of the indenyl five-membered ring and multiplets at 5.60 and 5.65 ppm corresponding to the other two protons on the indenyl five-membered ring. The four protons on the six-membered ring appear as multiplets at 7.50 and 7.60 ppm.

The ^{11}B NMR spectrum consists of ten peaks all of integral one between -13.2 and 21.2 ppm. As in **3** both the ^1H and ^{11}B NMR spectra are consistent with the C_1 symmetry of a 4,1,8-structure with the inequivalent cage methyl peaks having a separation of 0.85 ppm. The relatively high field boron peak is also present (21.2 ppm).

Crystals of **4** were grown by diffusion of 40-60 petroleum ether and a DCM solution of **4** at -30 ^oC. Analysis by *X*-ray diffraction shows **4** to be the expected 1,8-Me_2-4-(η-C_9H_7)-4,1,8-*closo*-$CoC_2B_{10}H_{10}$ (figure 2.5.1).

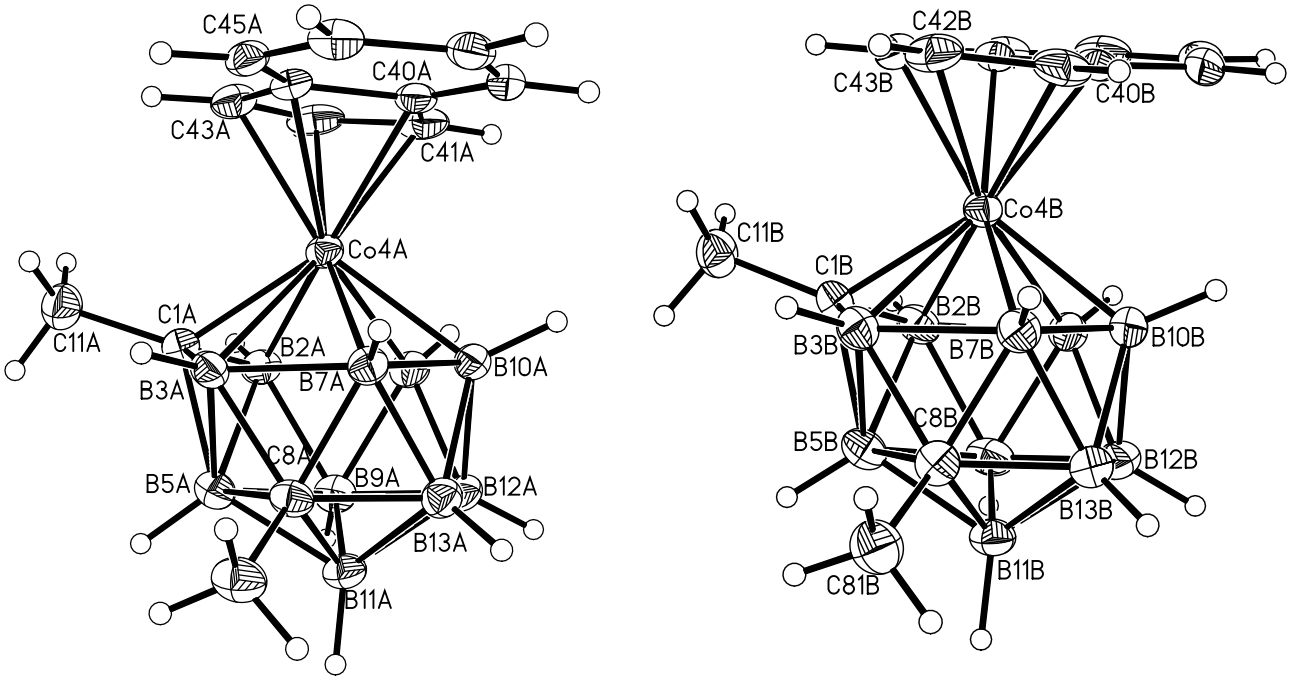

Figure 2.5.1 Molecular structures of 1,8-Me_2-4-(η-C_9H_7)-4,1,8-*closo*-$CoC_2B_{10}H_{10}$ **(4)**.

The crystal structure of **4** contains two crystallographically independent molecules - **4A** and **4B** - in the asymmetric unit, both of which have different indenyl orientations. Both molecules share the same docosahedral architecture (and C_1 symmetry) as **2**, however the result of thermal isomerisation can be seen as one of the CMe groups has migrated from the upper hexagonal belt to the lower pentagonal belt. All of the other vertices retain the same atoms and conectivities as in **2**. Whilst the cage structure of **4** is similar to that of 4-Cp-4,1,8-*closo*-$CoC_2B_{10}H_{12}$ and 4-Cp*-4,1,8-*closo*-$CoC_2B_{10}H_{12}$,[8a] both these structures suffer from cage disorder. However 1,8-Me_2-4-Cp-4,1,8-*closo*-$CoC_2B_{10}H_{10}$[8c] is known (the cage C positions are unambigous due to the presence of the methyl groups) and its structure is more directly comparable to that of **4A** and **4B**.

For **4A** the Co4-C distances to the bridging carbon atoms of the indenyl ligand are 2.146(2) Å for Co4-C44 and 2.137(2) Å for Co4-C40, compared to 2.038(2) Å, 2.052(2) Å and 2.070(2) Å for Co4-C41, Co4-C42 and Co4-C43 respectively.

For **4B** the Co4-C distances to the bridging carbon atoms of the indenyl ligand are 2.157(2) Å for Co4-C44 and 2.143(2) Å for Co4-C40, compared to 2.033(2) Å, 2.057(2) Å and 2.081(2) Å for Co4-C41, Co4-C42 and Co4-C43, respectively.

2.6 Synthesis of 4-(η-C_9H_7)-4,1,12-*closo*-$CoC_2B_{10}H_{12}$ (5)

Overnight heating of **7** (see section 2.8) in refluxing THF followed by chromatography gave brown **5** in 91.2% yield.

The ^{11}B NMR spectrum of **5** consists of nine peaks in a 1:1:1:1:1:2:1:1:1 ratio between -17.3 and 8.8 ppm. Asymmetric **5** would be predicted to have ten inequivalent peaks in the ^{11}B NMR spectrum, suggesting that the peak of integral two is a 1 + 1 coincidence.

The ^{1}H NMR spectrum shows two broad peaks each of integral one at 3.15 ppm and 3.70 ppm corresponding to the two cage CHs. The relevant indenyl peaks are observed as an apparent triplet at 5.15 ppm corresponding to the unique proton of the indenyl five-membered ring and multiplets at 5.76 and 5.86 ppm corresponding to the other two protons on the indenyl five-membered ring. The four protons on the six-membered ring appear as multiplets at 7.45 and 7.55 ppm. Both the ^{1}H and ^{11}B NMR spectra are consistent with C_1 symmetry as in **3**, with the cage CH peaks separated by 0.55 ppm.

Analysis by mass spectrometry showed an envelope centred on *m/z* 317 (M^+) (M_w **5** = 318.19 g/mol), and the elemental analysis is in good agreement with that expected for $C_{11}H_{19}B_{10}Co$.

Crystals of **5** were grown by diffusion of 40-60 petroleum ether and a DCM solution of **5** at -30 ºC. Analysis by *X*-ray diffraction shows **5** to be the expected 4-(η-C_9H_7)-4,1,12-*closo*-$CoC_2B_{10}H_{12}$ (figure 2.6.1).

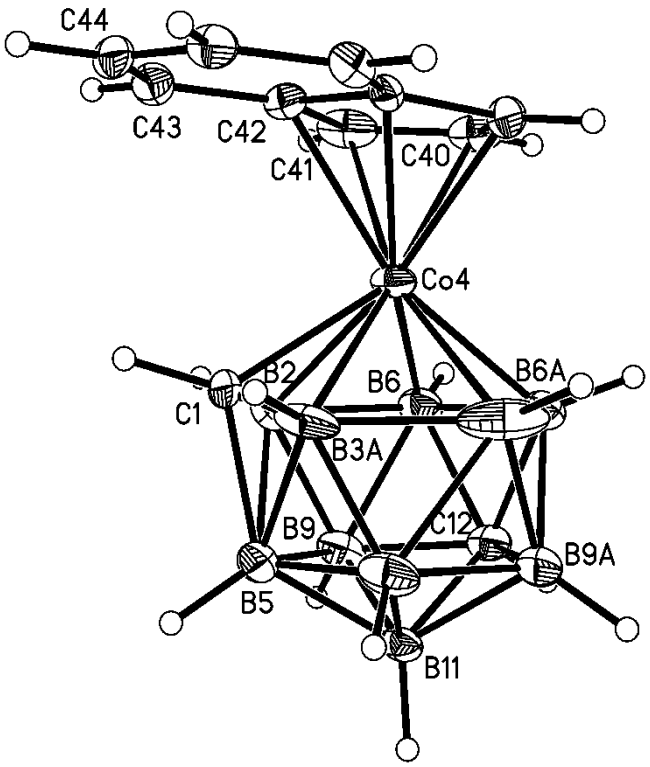

Figure 2.6.1 Molecular structure of 4-(η-C_9H_7)-4,1,12-*closo*-$CoC_2B_{10}H_{12}$ **(5)**.

The molecule found in the crystal stucture of **5** is disordered across a mirror plane which passes through Co4, B11 and C12. C1 and B3 sit across the mirror plane and are assigned occupancies of 0.5. In figure 2.6.1 B3 and C1A have been omitted for clarity. As with the crystal structures of the 4,1,6- and 4,1,8- compounds, C_1 symmetry is observed in the structure with the omitted atoms, which is shown in figure 2.6.1. This cage structure is similar to that found in the Cp/Cp* analogues,[8a] however, both these compounds suffer from some form of disorder - the Cp analogue having disorder in the lower belt, and the Cp* one containing ghost atoms. Isomerisation from the 4,1,10- isomer has clearly taken place, with the degree five carbon migrating from the ten position of the upper hexagonal belt to the twelve position of the lower pentagonal belt.

The Co4-C distances to the bridging carbon atoms of the indenyl ligand are 2.141(4) Å for Co4-C40, compared to 2.048(5) Å and 2.028(7) Å for Co4-C41 and Co4-C42 respectively, (because of the mirror symmetry the Co4-C bonds to C44 and C43 are the same length as those to C40 and C41, respectively).

2.7 Synthesis of 1,12-Me_2-4-(η-C_9H_7)-4,1,12-*closo*-$CoC_2B_{10}H_{10}$ (6)

Overnight heating of **4** in refluxing toluene followed by chromatography gave brown **6** in 74.7% yield. A small amount of the unchanged Me_2-4,1,8- isomer was also recovered.

Compound **6** shows two sharp peaks each of integral three at 1.72 and 2.38 ppm in the ^1H NMR spectrum corresponding to the two methyl groups on the cage carbon atoms. The relevant indenyl peaks are observed as an apparent triplet at 5.31 ppm corresponding to the unique proton of the indenyl five-membered ring and multiplets at 5.55 and 5.64 ppm corresponding to the other two protons on the indenyl five-membered ring. The four protons on the six-membered ring appear as a multiplet at 7.55 ppm.

The ^{11}B NMR spectrum consists of nine peaks in a 1:1:1:1:1:1:1:1:2 ratio between -14.4 and 10.2 ppm (peak of integral 2 is presumably a 1 + 1 coincidence). Both the ^1H and ^{11}B NMR spectra are consistent with the C_1 symmetry of a 4,1,12- structure, with the inequivalent cage methyl peaks having a separation of 0.66 ppm.

Both MS and CHN were consistent with **6**, an envelope centred on *m/z* 346 (M^+) being observed in the former.

Crystals of **6** were grown by diffusion of 40-60 petroleum ether and a DCM solution of **6** at -30 ^oC. Analysis by *X*-ray diffraction shows **6** to be the expected 1,12-Me_2-4-(η-C_9H_7)-4,1,12-*closo*-$CoC_2B_{10}H_{10}$ (figure 2.7.1).

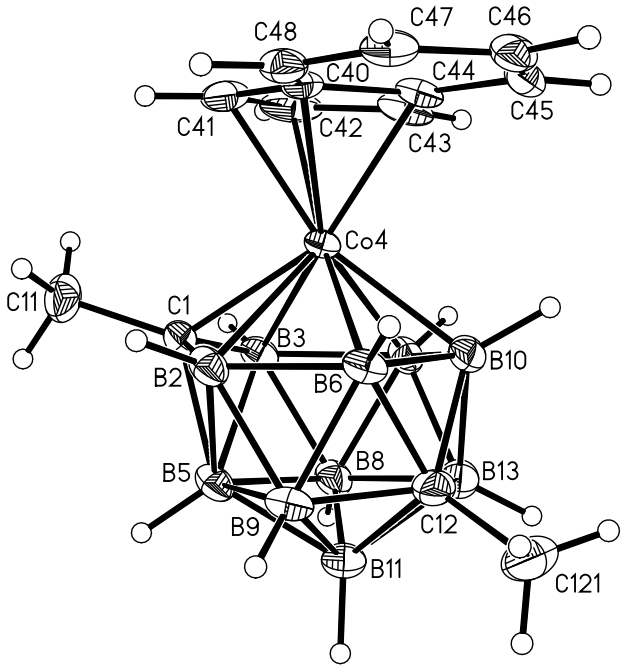

Figure 2.7.1 Molecular structure of 1,12-Me_2-4-(η-C_9H_7)-4,1,12-*closo*-$CoC_2B_{10}H_{10}$ **(6)**.

Unlike in the crystal structure of **5**, the molecule **6** does not sit on a mirror plane. The docosahedral architecture found in **4** is retained, but as in **5** the result of thermal isomerisation can be seen as one of the cage carbon atoms has migrated from the eight position of the lower pentagonal belt to the twelve position. All of the other vertices in **6** retain the same atoms and conectivities as in **4**. The cage structure is comparable to the known 1,12-Me_2-4-Cp-4,1,12-*closo*-$CoC_2B_{10}H_{10}$,[8c] and is free of the disorder associated with the 4,1,12- Cp/Cp* species.[8a]

The Co4-C distances to the bridging carbon atoms of the indenyl ligand are 2.138(2) Å for Co4-C44 and 2.139(2) Å for Co4-C40, compared to 2.058(2) Å, 2.042(2) Å and 2.052(2) Å for Co4-C41, Co4-C42 and Co4-C43, respectively.

2.8 Synthesis of 4-(η-C_9H_7)-4,1,10-*closo*-$CoC_2B_{10}H_{12}$ (7)

Reduction of 1,12-*closo*-$C_2B_{10}H_{12}$ with Na in liquid ammonia results in [7,10-*nido*-$C_2B_{10}H_{12}]^{2-}$. Following removal of ammonia and addition of THF, $CoCl_2$ and Li[C_9H_7] in THF (generated from C_9H_8 and *n*-BuLi in THF) were added to give a brown solution which was stirred overnight. Upon aerial oxidation and chromatography brown **7** is isolated in 47.5% yield.

The MS of **7** contains an envelope centred on *m/z* 317 (M^+) (M_w **7** = 318.19 g/mol), and the elemental analysis is in good agreement with that expected for $C_{11}H_{19}B_{10}Co$.

Compound **7** shows two broad peaks each of integral one at 1.90 and 5.05 ppm in the ^1H NMR spectrum corresponding to the two cage CHs. The expected 4,1,10- structure is expected to have C_s symmetry on the NMR timescale, with the mirror plane running through C1, M4, C10 and B11, giving inequivalent cage CHs. The relevant indenyl peaks are observed as a triplet at 5.65 ppm corresponding to the unique proton of the indenyl five-membered ring and a doublet at 5.80 ppm corresponding to the other two protons on the indenyl five-membered ring. The four protons on the six-membered ring appear as multiplets at 7.50 and 7.70 ppm.

The ^{11}B NMR spectrum consists of five peaks in a 2:2:1:3:2 ratio between -12.8 and 4.9 ppm. Six peaks (four integral 2 and two integral 1) would be expected considering the C_s symmetry, suggesting that the peak of integral three is a 2 + 1 coincidence.

Crystals of **7** were grown by diffusion of 40-60 petroleum ether and a DCM solution of **7** at -30 ^oC. Analysis by *X*-ray diffraction shows **7** to be the expected 4-(η-C_9H_7)-4,1,10-*closo*-$CoC_2B_{10}H_{12}$ (figure 2.8.1).

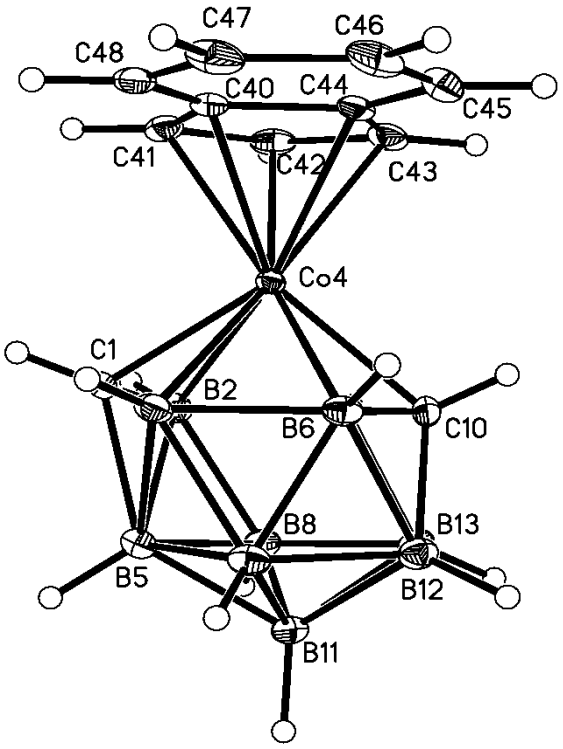

Figure 2.8.1 Molecular structure of 4-(η-C_9H_7)-4,1,10-*closo*-$CoC_2B_{10}H_{12}$ **(7)**.

Compound **7** crystallises with one molecule of DCM per molecule of cobaltacarborane (omitted from figure 2.8.1 for clarity), and unlike in **1** (where the fluxionality and resulting C_s symmetry is frozen out leaving a cage structure of C_1 symmetry), the cage structure in **7** retains effecive C_s symmetry upon crystallisation. The cage structure of **7** is similar to that of its Cp analogue,[8b] with the fact that the C10 position is unique meaning that it can be assigned unambigously.

The Co4-C distances to the bridging carbon atoms of the indenyl ligand are 2.1596(17) Å for Co4-C44 and 2.1328(17) Å for Co4-C40, compared to 2.0470(18) Å, 2.0555(18) Å and 2.0642(18) Å for Co4-C41, Co4-C42 and Co4-C43, respectively.

2.9 Synthesis of 1,14-(η-C_9H_7)$_2$-1,14,2,10-*closo*-$Co_2C_2B_{10}H_{12}$ (8)

Reduction of **5** with Na in THF results in [1-(η-C_9H_7)-1,2,10-*nido*-$CoC_2B_{10}H_{12}]^{2-}$. To this was added $CoCl_2$ and Li[C_9H_7] in THF (generated from C_9H_8 and *n*-BuLi in THF) to give a brown solution which was stirred overnight. Upon aerial oxidation and chromatography dark blue **8** is isolated in 2% yield.

Compound **8** shows one broad peak of integral two at 0.94 ppm in the ^{1}H NMR spectrum corresponding to the two cage CHs. The 1,14,2,10- structure is expected to have C_2 symmetry on the NMR timescale, rendering the cage CHs and indenyl ligands equivalent. The relevant indenyl peaks are observed as an apparent triplet at 5.65 ppm corresponding to the two unique protons of the indenyl five-membered rings and a doublet at 5.80 ppm corresponding to the other four protons on the indenyl five-membered rings. The eight protons on the six-membered rings appear as multiplets at 7.50 and 7.70 ppm.

The ^{11}B NMR spectrum consists of the expected five peaks in a 2:2:2:2:2 ratio between -18.7 and 6.2 ppm. Both the ^{1}H and ^{11}B NMR spectra are consistent with C_2 symmetry, which implies both indenyl rings are rotating (or at least substantially librating) about the centre of the five-membered ring at room temperature.

As for the molecules with cage C_s symmetry, the cage C_2 symmetry of **8** gives rise to the chemical equivalence of protons related by the indenyl ligand's mirror plane in the ^{1}H NMR spectrum.

The MS of **8** contains an envelope centred on *m/z* 493 (M^+) (M_w **8** = 492.27 g/mol).

Reduction/metallation of thirteen vertex 4,1,12- isomers gives fourteen vertex 1,14,2,10- isomers while reduction of thirteen vertex 4,1,8- isomers gives 1,14,2,9- isomers.[11] However as both of these compounds have C_2 symmetry (as would a 1,14,2,8- isomer), they are not distinguishable by NMR spectroscopy, necessitating crystallographic study to unambiguously tell which isomer has been formed.

Crystals of **8** were grown by diffusion of 40-60 petroleum ether and a DCM solution of **8** at -30 ^{o}C. Analysis by *X*-ray diffraction shows **8** to be the expected 1,14-(η-C_9H_7)$_2$-1,14,2,10-*closo*-$Co_2C_2B_{10}H_{12}$ (figure 2.9.1).

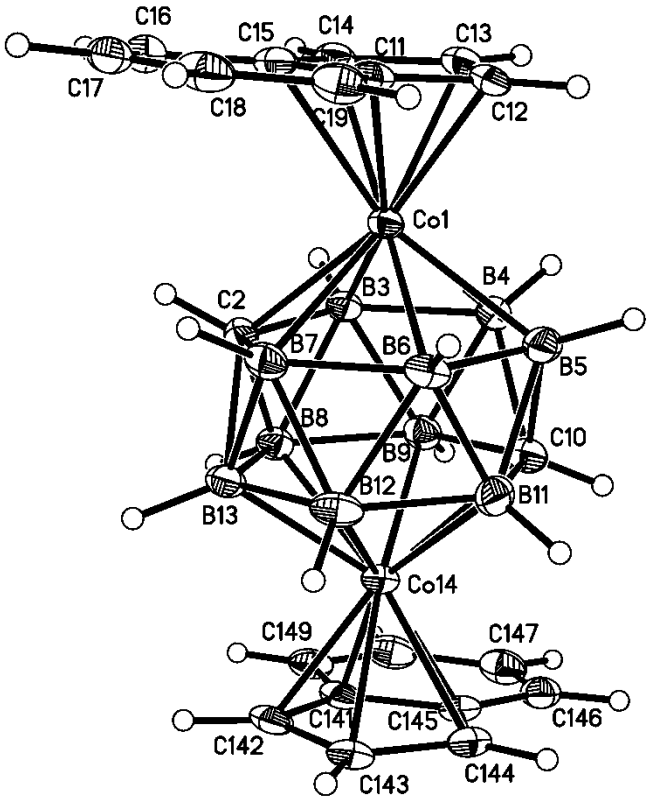

Figure 2.9.1 Molecular structure of 1,14-(η-C_9H_7)$_2$-1,14,2,10-*closo*-$Co_2C_2B_{10}H_{12}$ **(8)**.

The crystal structure shows that **8** has bicapped hexagonal anti-prismatic structure, an architecture which has been found in other fourteen vertex metallacarboranes.[12] This structure has two hexagonal faces capped by degree six vertices, while all of the other vertices are degree five. One of the cage CHs is disordered over two sites at vertices 10 and 11, and site occupancy factors were refined and converged at 0.61(2)C and 0.39(2)B for postion 10 and complementary occupations at vertex 11. Since the structure is 1,14,2,10- and the two metals are the same, the cage portion of the molecule has effective C_2 symmetry (or at least it would if one of the cage carbon atoms was not disordered over two sites).

The cage structure of **8** is similar to that found in the 1,14,2,10- Cp and Me_2-1,14,2,10-Cp analogues, the former of which also showed C/B disorder.[13] The lengths of the six

connectivities in the belt containing C1 support the C assignment, as the two B-C connectivities are about 0.1 Å shorter than the other four (B-B) connectivities.

The Co-C distances to the bridging carbon atoms of the indenyl ligand bound to Co1 are 2.140(2) Å for Co1-C11 and 2.162(2) Å for Co1-C15, compared to 2.041(2) Å, 2.055(2) Å and 2.074(2) Å for Co1-C12, Co1-C13 and Co1-C14 respectively. The Co-C distances to the bridging carbon atoms of the indenyl ligand bound to Co14 are 2.145(2) Å for Co14-C145 and 2.125(2) Å for Co14-C141, compared to 2.054(2) Å, 2.061(2) Å and 2.072(2) Å for Co14-C142, Co14-C143 and Co14-C144 respectively.

2.10 Comparison of ^{11}B NMR spectroscopic shifts

Table 2.10.1 presents the average ^{11}B NMR spectroscopic shifts (<δ^{11}B>) for all of the thirteen vertex compounds made and compares them to the values for the Cp/Cp* and dimethyl (with respect to the cage) Cp compounds[8a,b,c,d] (where available). Also given in the table are the average ^{11}B NMR spectroscopic shifts for the twelve and fourteen vertex indenyl cobaltacarboranes (and twelve[14a,b,8a] and fourteen[13] vertex Cp/Cp* and dimethyl (with respect to the cage) Cp compounds where available).

Table 2.10.1 Average ^{11}B NMR shifts (<δ^{11}B>) in ppm of various compounds.

	L = Cp, R = H	L = Cp*, R = H	L = Cp, R = Me	L = η-C_9H_7, R = H	L = η-C_9H_7, R = Me
1,2-R_2-3-L-3,1,2-*closo*-$CoC_2B_9H_9$	-7.3	-5.1	-15.5	-6.7	
1,6-R_2-4-L-4,1,6-*closo*-$CoC_2B_{10}H_{10}$	0.2	-1.3	-1.2	-3.4	-1.2
1,8-R_2-4-L-4,1,8-*closo*-$CoC_2B_{10}H_{10}$	3.6	2.5	2.1	0.1	2.7
1,10-R_2-4-L-4,1,10-*closo*-$CoC_2B_{10}H_{10}$	-4.1				-4.5
1,12-R_2-4-L-4,1,12-*closo*-$CoC_2B_{10}H_{10}$	-1.4	-2.5	-2.2	-3.8	-1.4
2,10-R_2-1,14-L_2-1,14,2,10-*closo*-$Co_2C_2B_{10}H_{10}$	-14.3		-9.4	-12.9	
2,9-R_2-1,14-L_2-1,14,2,9-*closo*-$Co_2C_2B_{10}H_{10}$	-13.4		-8.5	-12.1	

= Twelve vertex

= Thirteen vertex

= Fourteen vertex

Within the thirteen vertex compounds, the 4,1,8- isomers have the farthest downfield <δ^{11}B> value for a given exo-polyhedal ligand, followed by the 4,1,6- isomers and then the 4,1,12-isomers. Only the Cp and indenyl 4,1,10- isomers are known, and they both have the farthest upfield <δ^{11}B> value for these two exo-polyhedral ligands.

It is difficult to draw any definitive conclusions on how electron-donating/withdrawing the different exo-polyhedral ligands are, and the effect of dimethylation based on the average ^{11}B NMR shift, as the values for the different isomers/number of vertices show conflicting trends.

For example $<\delta^{11}B>$ values for the twelve vertex compounds and the two fourteen vertex compounds move downfield when going from Cp to indenyl, but for the thirteen vertex compounds $<\delta^{11}B>$ values move upfield. For the twelve vertex compounds the $<\delta^{11}B>$ value for the Cp* ligand is downfield of the Cp and indenyl $<\delta^{11}B>$ values, whilst for the thirteen vertex compounds the $<\delta^{11}B>$ value for the Cp* ligand lies in between the Cp and indenyl $<\delta^{11}B>$ values. Neither of these trends can be rationalised by arguing that the more electron-donating the exo-polyhedral ligand is, the more it will cause shielding and a consequent shift upfield of the $<\delta^{11}B>$ values. If this were the case the $<\delta^{11}B>$ value for the Cp* ligand (the most electron donating ligand, followed by Cp, and then indenyl) should be the most upfield for the twelve and thirteen vertex compounds, and the $<\delta^{11}B>$ value for Cp should be farther upfield than the $<\delta^{11}B>$ value for indenyl for the thirteen vertex compounds.

Another inconsistency is that for the thirteen vertex compounds, when going from Cp to indenyl the $<\delta^{11}B>$ values move upfield, but when going from dimethyl (with respect to the cage) Cp to dimethyl (with respect to the cage) indenyl the $<\delta^{11}B>$ values move downfield.

Finally, upon dimethylation, $<\delta^{11}B>$ values for the twelve vertex and the thirteen vertex Cp compounds move upfield, whilst for the fourteen vertex Cp compounds and the thirteen vertex indenyl compounds the $<\delta^{11}B>$ value moves downfield upon dimethylation. Clearly the exo-polyhedral ligand's/dimethylation's effect on the $<\delta^{11}B>$ value cannot easily be explained by simple electron donating/withdrawing arguments.

2.11 Discussion

In addition to the compounds described in sections 2.2-2.9, a further four related compounds were made by others within the group.[10] Reduction/metallation of 1-Me-1,2-*closo*-$C_2B_{10}H_{11}$ gave the monomethyl Me-4,1,6- Co/indenyl compound, which was then heated to give the Me-4,1,8- isomer. The methylene tethered $(CH_2)_3$-4,1,2- compound was made by reduction/metallation of 1,2-μ-$(CH_2)_3$-1,2-*closo*-$C_2B_{10}H_{10}$,[15] and the dimethyl Me_2-4,1,2- was made by reduction/metallation of 1,2-μ-$(CH_2SiMe_2CH_2)$-1,2-*closo*-$C_2B_{10}H_{10}$ followed by chromatography on silica to remove the silane tether.[16]

The structures of 8-Me-4-(η-C_9H_7)-4,1,8-*closo*-$CoC_2B_{10}H_{11}$ (**II**), 1,2-Me_2-4-(η-C_9H_7)-4,1,2-*closo*-$CoC_2B_{10}H_{10}$ (**III**) and 1,2-$(CH_2)_3$-4-(η-C_9H_7)-4,1,2-*closo*-$CoC_2B_{10}H_{10}$ (**IV**) are shown in figure 2.11.1 and 2.11.2.

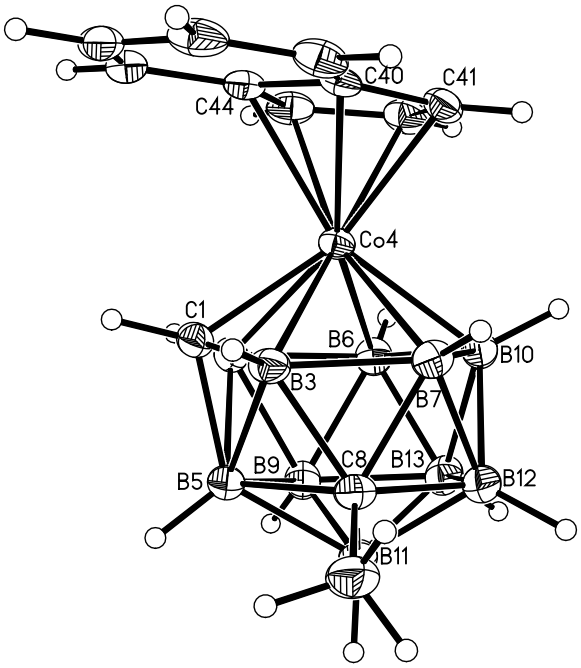

Figure 2.11.1 Molecular structure of 8-Me-4-(η-C_9H_7)-4,1,8-*closo*-$CoC_2B_{10}H_{11}$ (**II**).

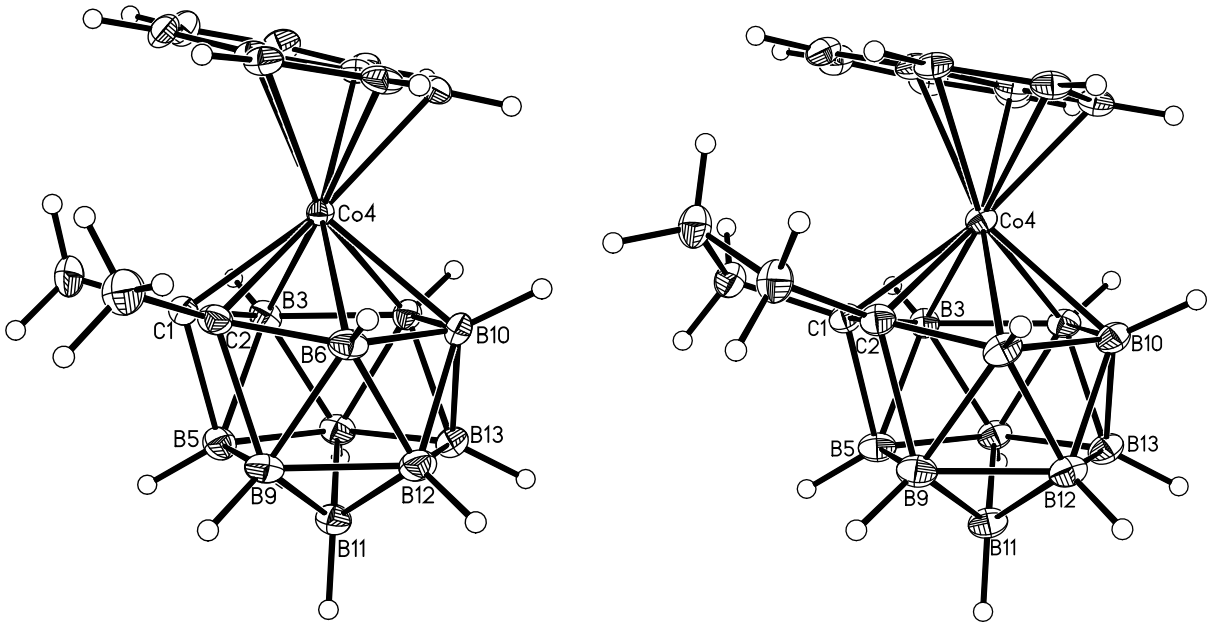

Figure 2.11.2 Molecular structures of (left) 1,2-Me_2-4-(η-C_9H_7)-4,1,2-*closo*-$CoC_2B_{10}H_{10}$ (**III**) and (right) 1,2-$(CH_2)_3$-4-(η-C_9H_7)-4,1,2-*closo*-$CoC_2B_{10}H_{10}$ (**IV**).

Compound **I** has a docosahedral structure, while **III** and **IV** are henicosahedral. This henicosahedral structure for the latter two compounds is confirmed by calculating the 'percentage docosahedral character' (*x*), which is a measure of how far a structure lies between purely henicosahedral and purely docosahedral.[17] For **IV** and **III** the values of *x* are 24.1% and 4.5% - ie both mostly henicosahedral, but the latter more so. In contrast, for **II** *x* = 79.4% - ie mostly docosahedral.

Table 2.11.1 summarizes some key structural parameters of the compounds **1**, **2**, **4A**, **4B**, **5**, **6**, **7**, **II**, **III** and **IV**, and table 2.11.2 key structural parameters of compound **8**.

Table 2.11.1 Selected molecular dimensions (Å, º) in compounds **1**, **2**, **4A**, **4B**, **5**, **6**, **7**, **II**, **III** and **IV**.

	1	**2**	**4A**	**4B**	**5**	**6**	**7**	**II**	**III**	**IV**
Co4-C1	2.0175(15)	2.0458(10)	2.049(2)	2.041(2)	2.090(10)	2.0500(19)	2.0392(18)	2.0169(19)	2.0762(19)	2.090(2)
Co4-X2	2.1828(17)	2.1886(12)	2.192(3)	2.216(3)	2.179(7)	2.202(2)	2.217(2)	2.201(2)	2.0686(19)	2.044(2)
Co4-Y6[a]	2.1734(15)	2.2290(11)	2.167(3)	2.175(3)	2.119(5)	2.132(2)	2.163(2)	2.183(2)	2.191(2)	2.233(2)
Co4-Z10	2.1249(17)	2.1064(12)	2.156(3)	2.140(3)	2.119(5)[b]	2.128(2)	2.1023(17)	2.135(2)	2.183(2)	2.173(2)
Co4-B7	2.1795(17)	2.1528(12)	2.133(3)	2.132(3)	2.179(7)[c]	2.189(2)	2.142(2)	2.152(2)	2.183(2)	2.156(2)
Co4-B3	2.2365(18)	2.2438(12)	2.193(3)	2.183(3)	2.178(11)	2.196(2)	2.201(2)	2.194(2)	2.172(2)	2.178(2)
Co4-C40	2.1642(15)	2.1777(10)	2.137(2)	2.143(2)	2.141(4)	2.1385(19)	2.1328(17)	2.1393(19)	2.1508(19)	2.134(2)
Co4-C41	2.0527(16)	2.0418(10)	2.038(2)	2.033(2)	2.048(5)	2.058(2)	2.0470(18)	2.0395(19)	2.034(2)	2.038(2)
Co4-C42	2.0228(16)	2.0234(10)	2.052(2)	2.057(2)	2.028(7)	2.043(2)	2.0555(18)	2.027(2)	2.0377(19)	2.052(2)
Co4-C43	2.0342(15)	2.0452(11)	2.070(2)	2.081(2)	2.048(5)[d]	2.051(2)	2.0642(18)	2.062(2)	2.0861(19)	2.0882(19)
Co4-C44	2.1469(14)	2.2046(11)	2.146(2)	2.157(2)	2.141(4)[e]	2.1392(19)	2.1596(17)	2.142(2)	2.1887(18)	2.168(2)
C40-C41	1.440(2)	1.4320(15)	1.441(3)	1.445(3)	1.440(6)	1.434(3)	1.446(3)	1.436(3)	1.440(3)	1.439(3)
C41-C42	1.422(2)	1.4226(15)	1.413(4)	1.403(4)	1.409(7)	1.417(3)	1.425(3)	1.426(3)	1.425(3)	1.426(3)
C42-C43	1.426(2)	1.4205(16)	1.417(3)	1.411(4)	1.409(7)[f]	1.418(3)	1.417(3)	1.412(3)	1.417(3)	1.416(3)
C43-C44	1.445(2)	1.4450(15)	1.429(3)	1.435(3)	1.440(6)[g]	1.439(3)	1.446(3)	1.436(3)	1.434(3)	1.437(3)
C44-C40	1.438(2)	1.4342(15)	1.436(3)	1.432(3)	1.452(9)	1.441(3)	1.436(2)	1.437(3)	1.445(3)	1.439(3)
τ[h]	36.1	36.2	-113.3	112.4	±39.3	123.2	95.0	-41.5	-84.8[j]	-79.7[j]
χ[i]	8.6	15.1	4.6	8.4	8.3	3.8	4.5	7.1	11.2	11.6

[a] For **1** and **2** X = Z = B and Y = C;
for **4**, **5**, **6** and **II** X = Y = Z = B;
for **7** X = Y = B and Z = C ;
for **III** and **IV** X = C and Y = Z = B.

[b] Co4-B10 = Co4-B6 by symmetry.

[c] Co4-B7 = Co4-B2 by symmetry.

[d] Co4-C43 = Co4-C41 by symmetry.

[e] Co4-C44 = Co4-C40 by symmetry.

[f] C42-C43 = C41-C42 by symmetry.

[g] C43-C44 = C40-C41 by symmetry.

[h] τ is the torsion angle A-B-Co4-C1
where A is the mid point of C40-C44
and B is the centroid of the C_5 ring.

[i] χ is the dihedral angle between C_5 and B5B9B12B13B8 least-squares planes.

[j] τ_2 is the torsion angle A-B-Co4-D
where A is the mid point of C40-C44,
B is the centroid of the C_5 ring,
and D is the mid point of C1-C2.

Table 2.11.2 Selected molecular dimensions (Å, º) in compound **8**.

	8 (face bound to Co1)
Co1-C2	2.160(2)
Co1-B3	2.162(2)
Co1-B4	2.155(3)
Co1-B5	2.170(2)
Co1-B6	2.162(2)
Co1-B7	2.160(2)
Co1-C11	2.140(2)
Co1-C12	2.041(2)
Co1-C13	2.055(2)
Co1-C14	2.074(2)
Co1-C15	2.162(2)
C11-C12	1.430(3)
C12-C13	1.423(3)
C13-C14	1.422(3)
C14-C15	1.436(3)
C15-C11	1.437(3)
τ_{C2}[a]	62.4

	8 (face bound to Co14)
Co14-B8	2.161(2)
Co14-B9	2.173(2)
Co14-B/C10	2.168(2)
Co14-B/C11	2.148(2)
Co14-B12	2.152(3)
Co14-B13	2.157(2)
Co14-C141	2.125(2)
Co14-C142	2.054(2)
Co14-C143	2.061(2)
Co14-C144	2.072(2)
Co14-C145	2.145(2)
C141-C142	1.429(3)
C142-C143	1.422(3)
C143-C144	1.412(3)
C144-C145	1.433(3)
C145-C141	1.446(3)
τ_{C10}[b]	-62.1

[a] τ_{C2} is defined as the torsion angle A-B-Co1-C2 where A is the mid point of C11-C15 and B is the centroid of the C_5 ring.

[b] τ_{C10} is defined as the torsion angle A-B-Co14-C/B10 where A is the mid point of C141-C145 and B is the centroid of the C_5 ring.

In all of the indenyl cobaltacarborane compounds, the Co-C40 and Co-C44 bond distances are longer than the Co-41, Co-C42 and Co-C43 bond lengths by about 0.04 - 0.16 Å, showing that the bridging carbon atoms of the indenyl ligand are less strongly bound to the metal than the other three carbon atoms in the indenyl five-membered ring.

As noted in section 2.2, the Co4-C1 connectivity is the shortest Co-cage connectivity in a docosahedral structure - as can be seen in table 2.11.1. Another characteristic of a docosahedral structure are the relatively long B2-B5 and B3-B5 distances, as can be seen in table 2.11.3 where these distances have been collated together with the next longest B-B distance. In all the docosahedral compounds studied in this chapter (except compound **5**) the B2-B5 and B3-B5 distances are the longest. For **5**, the crystallographic disorder makes measurement of these connectivities lengths somewhat unreliable.

Table 2.11.3 Lengths (Å) of connectivities B2-B5 and B3-B5 compared to next longest B-B connectivity in compounds **1**, **2**, **4A**, **4B**, **6**, **7** and **II**.

Compound	B2-B5	B3-B5	Next longest B-B connectivity
1	2.035(2)	2.026(2)	1.915(2)
2	2.0671(16)	1.9676(17)	1.8895(17)
4A	2.009(4)	1.969(4)	1.832(4)
4B	1.997(4)	1.965(4)	1.867(4)
6	1.999(3)	2.035(4)	1.901(3)
7	2.024(3)	2.029(3)	1.917(3)
II	2.038(3)	1.967(3)	1.880(3)

Examination of the C-C bond lengths in the non-bound six-membered ring of the indenyl ligand (table 2.11.4) shows a pattern of shorter bonds between C45-C46 and C47-C48 compared to the other four bonds. This is because coordination to the metal disrupts the aromaticity of the ligand, and consequently leads to localisation of four π-electrons in the non-bound ring into two essentially double bonds between C45-C46 and C47-C48. As shown in the table, a similar effect is seen in icosahedral **I**.

Table 2.11.4 Lengths of C-C bonds (Å) in unbound six-membered indenyl ring in all crystallographically studied compounds.

Compound	C40-C44	C44-C45	C45-C46	C46-C47	C47-C48	C48-C40
1	1.438(2)	1.425(2)	1.369(2)	1.425(2)	1.372(2)	1.428(2)
2	1.4342(15)	1.4152(16)	1.3709(16)	1.4232(17)	1.3663(17)	1.4229(15)
4A	1.436(3)	1.427(3)	1.359(3)	1.427(3)	1.353(4)	1.415(3)
4B	1.432(3)	1.413(3)	1.357(4)	1.422(4)	1.352(4)	1.419(4)
5[a]	1.452(9)	1.418(6)	1.363(6)	1.426(10)	1.363(6)	1.418(6)
6	1.441(3)	1.432(3)	1.360(3)	1.421(3)	1.365(3)	1.424(3)
7	1.436(2)	1.424(3)	1.369(3)	1.425(3)	1.364(3)	1.425(3)
8[b]	1.437(3)	1.429(3)	1.360(3)	1.429(3)	1.366(3)	1.425(3)
8[c]	1.446(3)	1.416(3)	1.362(3)	1.436(3)	1.360(3)	1.436(3)
II	1.437(3)	1.426(3)	1.358(4)	1.428(3)	1.357(3)	1.428(3)
III	1.445(3)	1.427(3)	1.360(3)	1.428(3)	1.356(3)	1.427(3)
IV	1.439(3)	1.421(3)	1.364(3)	1.427(3)	1.356(3)	1.423(3)
I[d]	1.4365(20)	1.4248(22)	1.3568(24)	1.4237(25)	1.3562(22)	1.4261(20)

[a] For **5**, C44-C45 = C48-C40 and C45-C46 = C47-C48 by symmetry.

[b] For indenyl bound to Co1, C40 = C15, C44 = C11, C45 = C19, C46 = C18, C47 = C17, C48 = C16

[c] For indenyl bound to Co14, C40 = C141, C44 = C145, C45 = C146, C46 = C147, C47 = C148, C48 = C149

[d] For **I**, C40 = C25, C44 = C24, C45 = C29, C46 = C28, C47 = C27, C48 = C26

2.12 Indenyl Orientations

One of the main reasons for synthesising this series of compounds was to probe the bonding between the cage and the metal fragment, specifically to see how the documented superior trans influence of the cage boron atoms over the cage carbon atoms would affect the indenyl ligand orientation. It was assumed that the bridging carbon atoms of the indenyl ligand would preferentially be oriented trans to the cage boron atoms in order to maximise the structural indenyl effect (as was the case in **I**), but we also sought to investigate whether the introduction of methyl groups would provide a steric interaction significant enough to change the orientation.

In the work done by Welch et al[4] on **I** the orientation of the indenyl ligands was probed using crystallographic data and a computational analysis at the EHMO level. Our work was supplemented with a DFT study[18] (performed by D. McKay at Heriot-Watt University) using {Fe(naph)} (naph = naphthalene = $C_{10}H_8$) as the metal fragment instead of {Co(indenyl)} to avoid any complications arising from having a five-membered ring (the metal bound indenyl ring) and a six-membered ring (the metal bound face of the cage) which must sometimes be staggered and sometimes eclipsed.

In order to define the indenyl orientation for the docosahedral structures we use τ, the torsion angle A-B-Co4-C1, where A is the midpoint of the C40-C44 bond, and B is the centroid of the indenyl C_5 ring. The value of τ would be about +60° if A is orientated above B2 and about -60° if A is orientated above B3. The Fe(naph) model would be expected to have energy minima at τ = 0°, 60°, 120°, 180°, 240° and 300°, corresponding to staggered conformations, and this is borne out in the calculated results. Figure 2.12.1 shows the indenyl orientations of the various compounds.

In **1** it is found that the τ value is 36° which puts C40/C44 roughly trans to the B7-B10 connectivity. It was expected that C40/C44 would be trans to B3, B7 or B10 or the connectivities between these atoms (as opposed to B2 which is sandwiched between two carbon atoms), although the exact orientation could not easily have been predicted based purely on trans influence arguments. Figure 2.12.2 shows the calculated energy profile for rotation of the naphthalene ligand about 360° in 4-(η-$C_{10}H_8$)-4,1,6-*closo*-$FeC_2B_{10}H_{12}$.

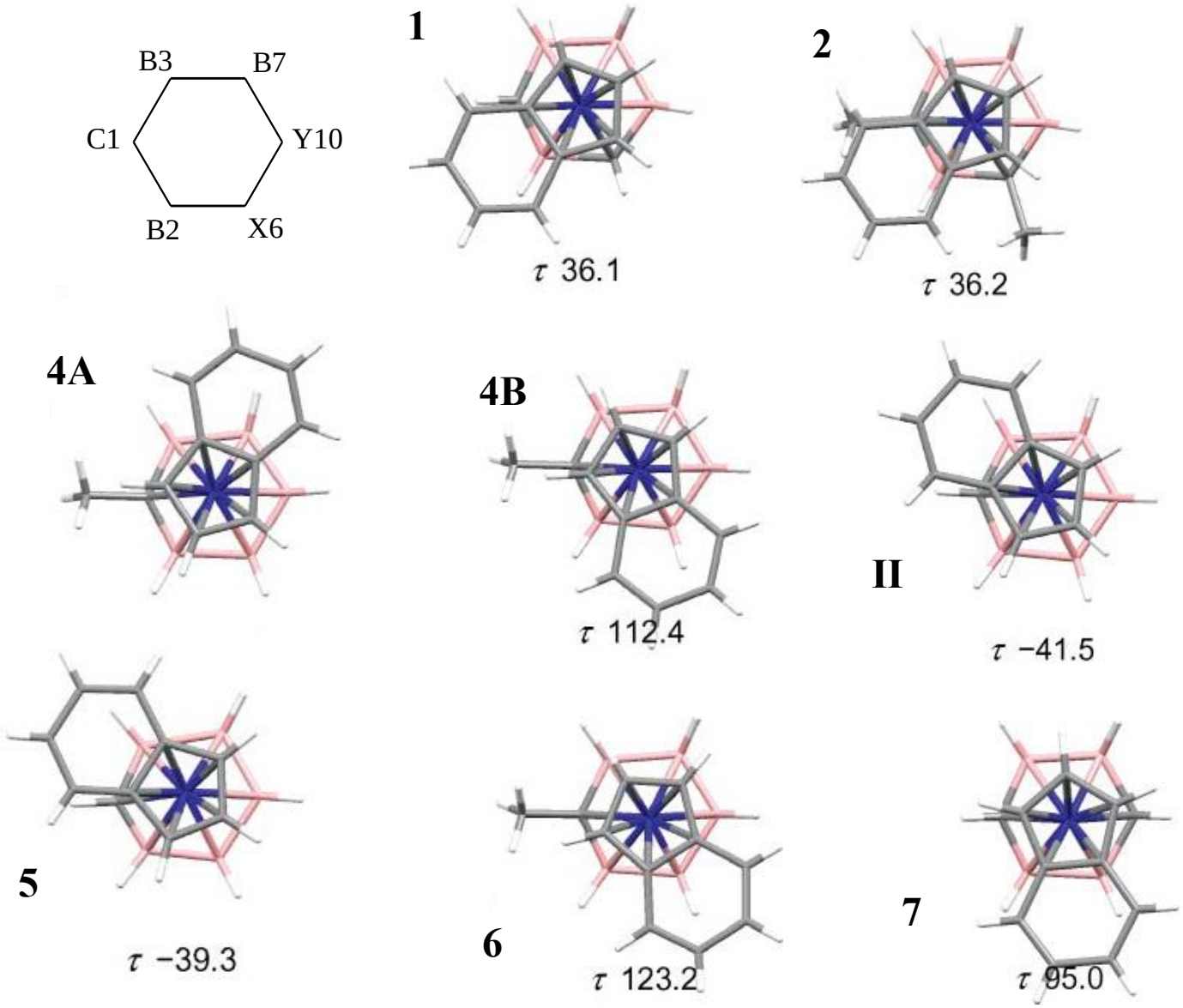

Figure 2.12.1 The indenyl orientation in compounds **1**, **2**, **4**, **5**, **6**, **7** and **II** viewed perpendicular to the C_5 indenyl ring and projected onto a common view of the C1B2C6Y10B7B3 carborane ligand face (for **1** and **2** X = C, Y = B; for **4**, **5**, **6** and **II** X = Y = B; for **7** X = B, Y = C).

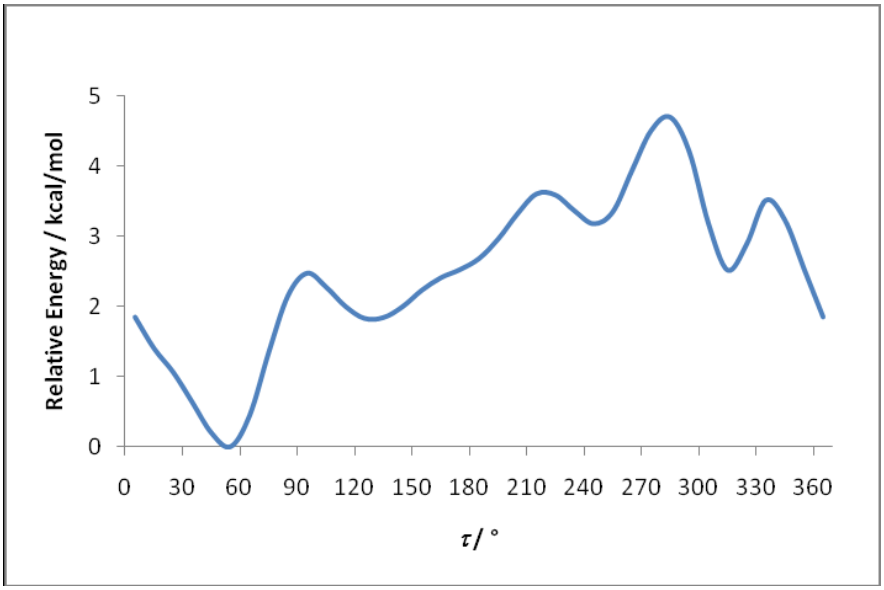

Figure 2.12.2 Relative energy (kcal mol^{-1}) versus τ (°) for naphthalene rotation in the model compound 4-(η-$C_{10}H_8$)-4,1,6-*closo*-$FeC_2B_{10}H_{12}$.

The τ value corresponding to the lowest calculated energy conformation for 4-(η-$C_{10}H_8$)-4,1,6-*closo*-$FeC_2B_{10}H_{12}$ is about 54°, which is moderately in agreement with the observed value for **1**. The 4,1,6- naphthalene orientation calculated to have the highest energy is the one at about τ = -77°, presumably because in this conformation the naphthalene bridging carbon atoms are mostly trans to a cage carbon atom.

For **2**, the dimethyl analogue of **1**, the τ value is found to be 36.2°, ie almost identical to that observed in **1**. The indenyl ligand is in a position whereby the six-membered ring is above the cage methyl groups, with the steric interaction causing a significant tilting of the indenyl ligand away from the cage compared to that seen in **1**. This tilting is measured by χ which is defined as the dihedral angle between the C40C41C42C43C44 and B5B9B12B13B8 least-squares planes; for **1** χ is 8.6°, while for **2** it is 15.1°. This tilting of the indenyl ligand is clearly favourable to the compromise which would involve indenyl rotation to a τ value whereby the steric interaction would be relieved, but C40/C44 would be trans to part of the C1-B2-C6 portion of the metal bound face. The steric interaction is well illustrated in figure 2.12.3.

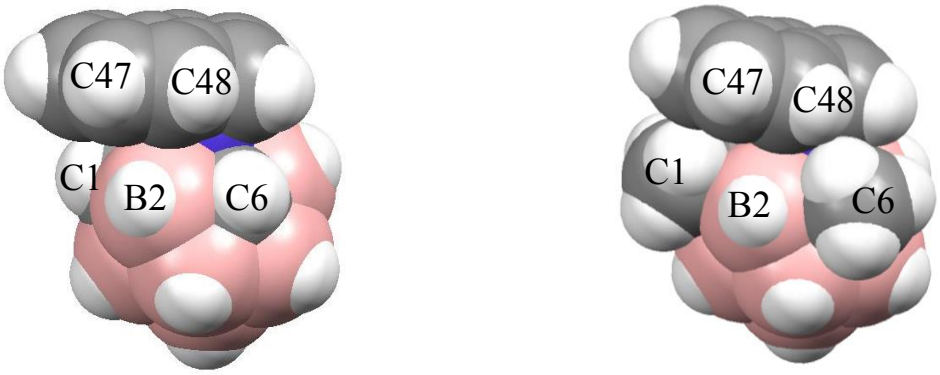

Figure 2.11.3 (left) Space filling views of 4-(η-C_9H_7)-4,1,6-*closo*-$CoC_2B_{10}H_{12}$ **1** and (right) 1,6-Me_2-4-(η-C_9H_7)-4,1,6-*closo*-$CoC_2B_{10}H_{12}$ **2**.

Ideally we would have been able to obtain the τ value for **3**, but as noted previously (section 2.4) this compound could not be persuaded to crystallise. As an alternative, the structure of **II** was determined and the indenyl orientation studied. While this compound is electronically and sterically different to **3**, the fact that the methyl group is on the lower pentagonal belt of the cage means that any steric interaction between the indenyl ligand and the methyl group is minimised, making **II** the best available alternative to **3**. The τ value in **II** is -41.5°, compared to a calculated lowest energy conformation at about τ = 43° for 4-(η-$C_{10}H_8$)-4,1,8-*closo*-$FeC_2B_{10}H_{12}$ (figure 2.12.4).

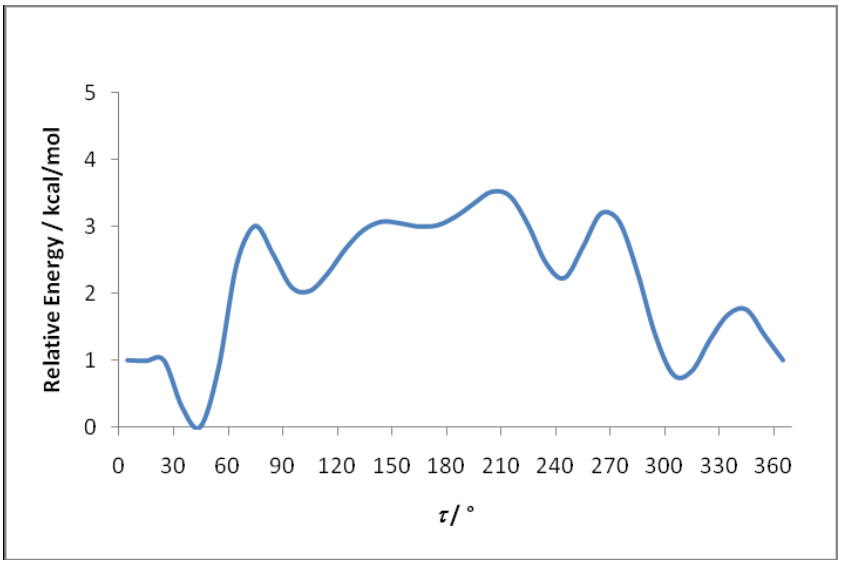

Figure 2.12.4 Relative energy (kcal mol^{-1}) versus τ (°) for naphthalene rotation in the model compound 4-(η-$C_{10}H_8$)-4,1,8-*closo*-$FeC_2B_{10}H_{12}$.

The orientation observed in **II** roughly corresponds to the second lowest energy conformation in the calculated energy profile which is at about τ = 309° (-51°). The difference between the

calculated lowest energy conformation and the observed conformation is only 0.8 kcal mol^{-1} which is within the range of crystal packing forces.[19]

The crystal structure of **4** has two molecules in the asymmetric fraction of the unit cell **4A** and **4B**; **4A** has a τ value of -113.3° whilst **4B** has a τ value of 112.4°. These two values roughly represent the calculated third and fourth lowest energy conformations and are presumably adopted instead of lower energy conformations to relieve the steric interaction with the C1 methyl group. The calculated energy between these two conformations is very small (~0.2 kcal mol^{-1}) which explains why two conformations of the same structure are seen within the same asymmetric unit.

Because of the disorder in **5,** τ can be either 39.3° or -39.3°. τ = -39.3° is moderately close to one of the two nearly identical lowest energy conformations (τ ≈ -23°) found for 4-(η-$C_{10}H_8$)-4,1,12-*closo*-$FeC_2B_{10}H_{12}$ (the other one being at about τ = -131°), (figure 2.12.5), while τ = 39.3 is moderately close to a second lowest energy conformation at τ ≈ 22°.

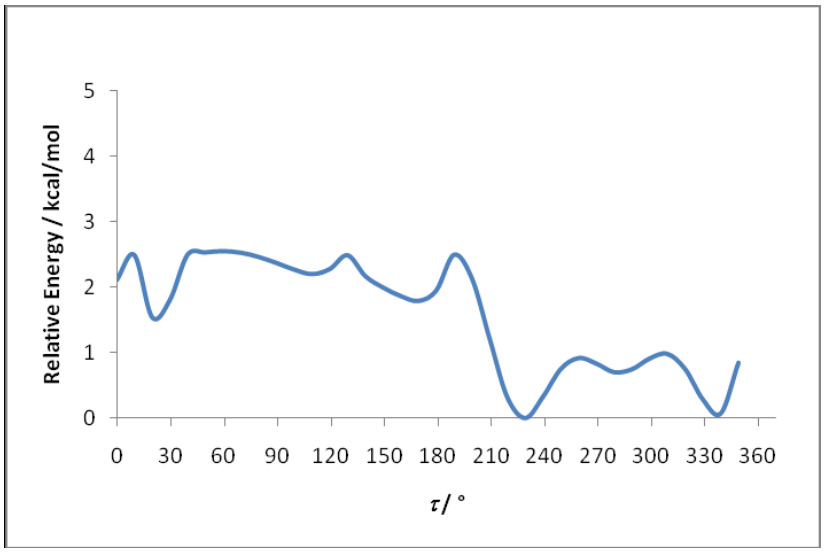

Figure 2.12.5 Relative energy (kcal mol^{-1}) versus τ (°) for naphthalene rotation in the model compound 4-(η-$C_{10}H_8$)-4,1,12-*closo*-$FeC_2B_{10}H_{12}$.

For **6** the τ value is 123.2° (which is close to a broad minimum at ~ τ =109° - the least stable minima on the energy profile), showing that the interaction of the methyl group with the indenyl ligand is significant enough to cause rotation away from a lower energy conformation. Why the indenyl ligand in **6** does not adopt an orientation of about τ = -123.2°, which is almost one of the two nearly identical lowest energy conformations found for 4-(η-

$C_{10}H_8$)-4,1,12-*closo*-$FeC_2B_{10}H_{12}$, (this would involve the indenyl ligand being reflected across a plane comprising C1-Co4-B10-B-11) is not known. A possible explanation is that, as in the case of **4A** and **4B**, the energy between the conformations at $\tau \approx 123.2^o$ and -123.2^o is small enough to be overcome by crystal packing effects,[19] but only the orientation at $\tau \approx 123.2^o$ is observed in the crystal structure.

The τ value for **7** is 95^o which has C40/C44 trans to B3 and B7. The calculated energy profile for 4-(η-$C_{10}H_8$)-4,1,10-*closo*-$FeC_2B_{10}H_{12}$ is particularly shallow and dominated by energy minima for the staggered conformations and energy maxima for the eclipsed conformations (figure 2.12.6).

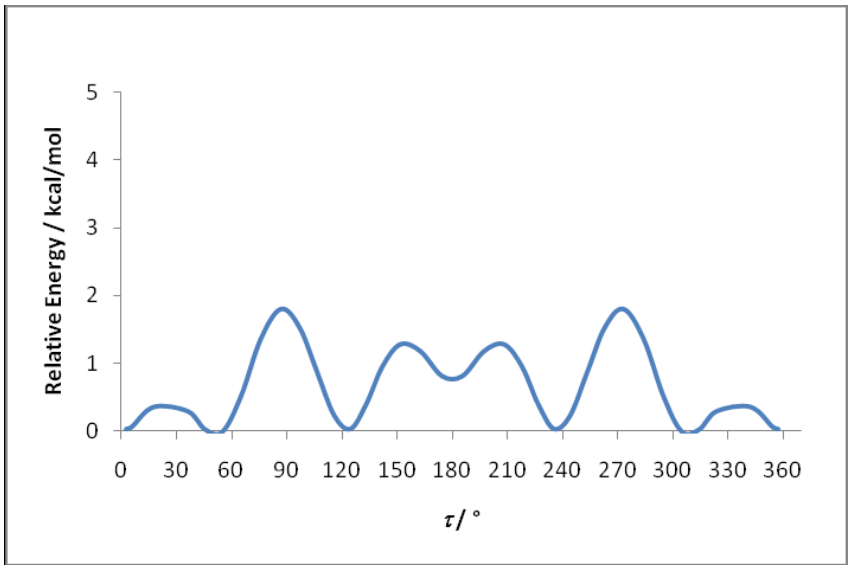

Figure 2.12.6 Relative energy (kcal mol^{-1}) versus τ (^{o}) for naphthalene rotation in the model compound 4-(η-$C_{10}H_8$)-4,1,10-*closo*-$FeC_2B_{10}H_{12}$.

It is therefore not all that helpful to use this profile to justify the τ value in **7**, which is actually close to an energy maximum as this would represent a roughly eclipsed conformation of 4-(η-$C_{10}H_8$)-4,1,10-*closo*-$FeC_2B_{10}H_{12}$.

For the henicosahedral compounds **III** and **IV** the torsion angle, τ_2, is defined as A-B-Co4-D, where A and B are as before, and D is the midpoint of the C1-C2 connectivity. The model compound used to calculate the rotation energy profile was 4-(η-$C_{10}H_8$)-4,1,2-*closo*-$FeC_2B_{10}H_{12}$. While this energy profile would be expected to show natural minima at $\tau = 30^o$, 90^o, 150^o, 210^o, 270^o and 330^o (these τ values representing staggered conformations) the

calculated energy profile does not contain the two minima at 30° or 330°, but does show the lowest energy conformation corresponding to τ = 0° (or 360°), (figure 2.12.7).

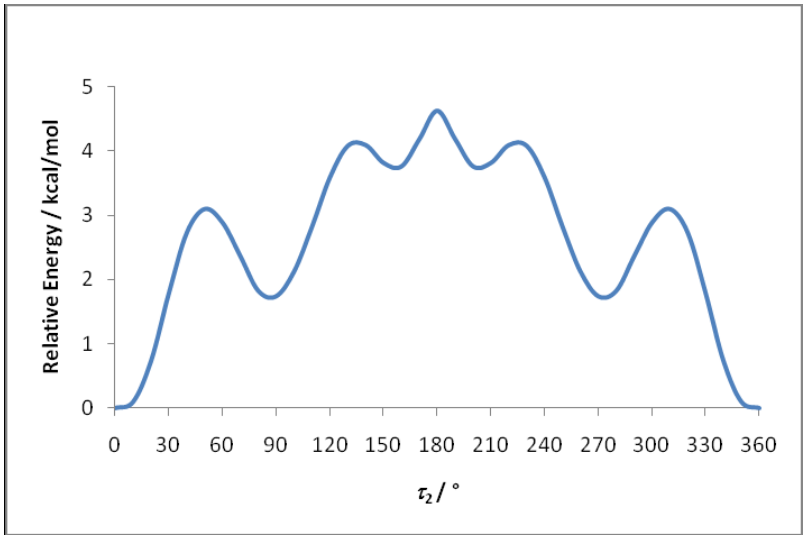

Figure 2.12.7 Relative energy (kcal mol^{-1}) versus τ (°) for naphthalene rotation in the model compound 4-(η-$C_{10}H_8$)-4,1,2-*closo*-$FeC_2B_{10}H_{12}$.

A possible explanation for this is that at τ = 0° C40/C44 are in an idealised position trans to B7 and B10, and that this electronic effect dominates the steric effect (staggered vs eclipsed) and moves the lowest energy conformation to τ = 0° instead of 30°/330°. The τ values for **III** and **IV** are -84.4° and -79.7° respectively (figure 2.12.8), both of which correspond roughly with the second lowest energy conformation at τ = 270°.

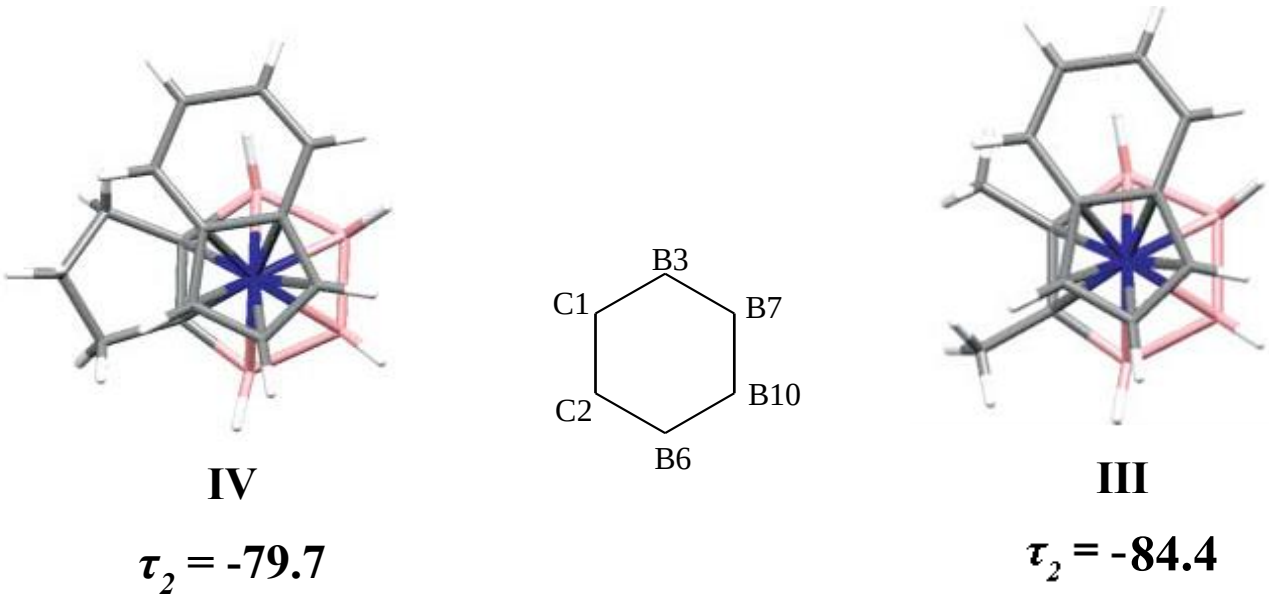

Figure 2.12.8 The indenyl orientation in compounds **III** and **IV** viewed perpendicular to the C_5 indenyl ring and projected onto a common view of the C1C2B6B10B7B3 carborane ligand face.

If the indenyl ligand were rotated any more clockwise (in figure 2.12.8) then C40/C44 would be trans to cage carbon atoms, whereas if it were rotated any more anticlockwise then there would be a significant steric interaction between the indenyl ligand and the methyl groups/methylene tether. The observed orientations are presumably a compromise between these two energetically unfavourable situations, with the steric interaction relieved somewhat by a tilting of the indenyl ligand in both **III** and **IV** (χ = 11.2° for **III** and 11.6° for **IV**, both these χ angles being exceeded only by that in **2**).

For compound **8** there are two τ values: τ_{C2} is defined (as before) as the torsion angle A-B-Co4-C2 and has a value of 62.4° and τ_{C10} is defined as the torsion angle A-B-Co4-C10 (C10 having the major C component of the two sites (vertices 10 and 11) over which one of the carbons is disordered) and has a value of -62.1° (see figure 2.12.9). No Fe(naph) model was used to give a rotation energy profile for the fourteen vertex compound, however the observed τ values are moderately comparable to those found for **II**, **5**, and both of the indenyl ligands in 1,14-(η-C_9H_7)$_2$-1,14,2,9-*closo*-$Co_2C_2B_{10}H_{12}$ (τ_{C2} = -39.4° and τ_{C10} = 55.1°), all of which also have an indenyl ligand above a CB_5 face.

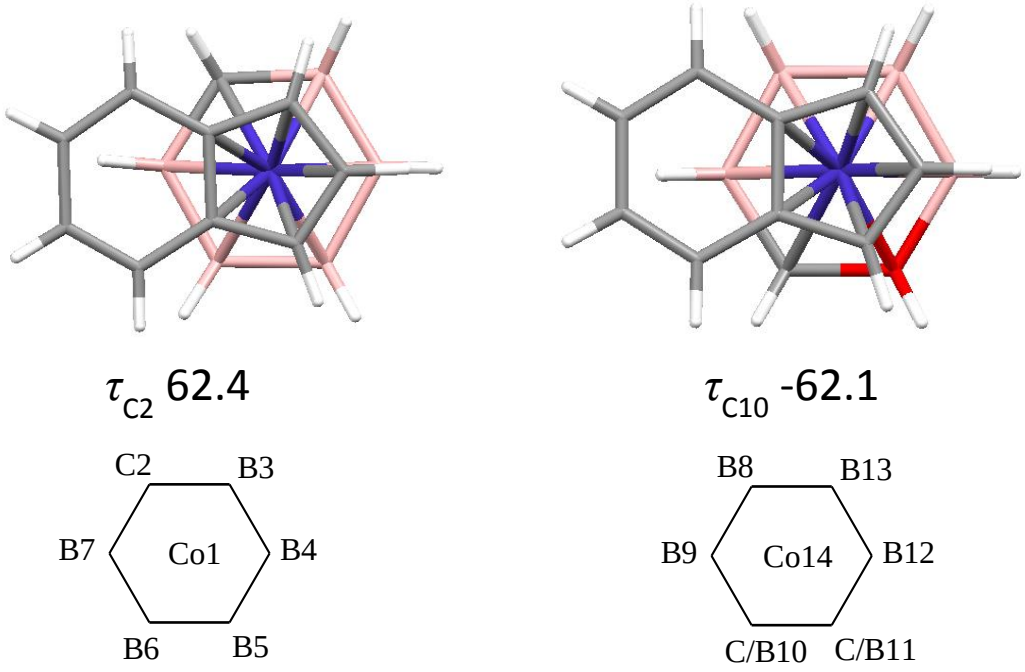

Figure 2.12.9 The indenyl orientation in compound **8** viewed perpendicular to (left) the C_5 indenyl ring bound to Co1 and projected onto a common view of the C2B3B4B5B6B7 carborane ligand face and (right) the C_5 indenyl ring bound to Co14 and projected onto a common view of the B8B9B/C10B/C11B12B13 carborane ligand face.

2.13 Summary

A series of thirteen vertex and one fourteen vertex indenyl cobaltacarboranes were synthesised and characterised. Reduction/metallation of 1,2-*closo*-$C_2B_{10}H_{12}$ and 1,2-Me_2-1,2-*closo*-$C_2B_{10}H_{10}$ gave metallacarboranes of 4,1,6- structure (**1** and **2**), which were isomerised to 4,1,8- (**3** and **4**) and 4,1,12- (**6**) isomers. Reduction/metallation of 1,12-*closo*-$C_2B_{10}H_{12}$ gave a metallacarborane of 4,1,10- structure (**7**), which was isomerised to the 4,1,12- isomer (**5**). Reduction metallation of the 4,1,12- compound gave a bimetallic compound of 1,14,2,10- structure (**8**).

The *X*-ray structures show similarities to those of their Cp/Cp* analogues with respect to the cage portion of the molecules. Compounds **4** and **6** are also free of disorder, which complicated the structural refinement of the 4,1,8- and 4,1,12- Cp/Cp* compounds. The *X*-ray structures also clearly demonstrate the structural indenyl effect, with all the indenyl ligands studied showing longer metal to bridging carbon bonds than metal to non-bridging carbon bonds.

Upon methylation of the 4,1,6- cage, the indenyl ligand becomes inclined away from lying parallel to the lower pentagonal belt of the cage in an effort to avoid steric interaction with the methyl groups. Upon methylation of the 4,1,8-/4,1,12- cage, the indenyl ligand rotates round to avoid the steric interaction. This difference between the 4,1,6- and 4,1,8-/4,1,12- isomers is due to the prescence of a second carbon atom in the top belt of the 4,1,6- isomer. Indenyl rotation, upon methylation, in the 4,1,6- isomer would leave the indenyl bridging carbon atoms (at least partially) trans to the C1B2C6 region, which is electronically unfavourable as this section of the carborane face has the weakest trans influence.

The potential energy profiles for rotation of the naphthalene ligand about the metal-cage axis in the compounds 4-(η-$C_{10}H_8$)-4,1,X-*closo*-$FeC_2B_{10}H_{12}$ (X = 6, 8, 10 and 12) were plotted by DFT calculations and then compared to the observed orientation of the indenyl ligands in the compounds synthesised. The observed τ values mostly only fitted moderately well with the calculated τ values, with a possible explanation of the discrepancies being a combination of the differences between the model iron naphthalene compounds (six-membered ring rotating about a six-membered ring) and the cobalt indenyl compounds (five-membered ring rotating about a six-membered ring and a different metal), and the relatively shallow calculated

potential energy profiles, parts of which have energy differences in the range of crystallographic packing forces.

The Me_2-4,1,10- compound was not synthesised, but it seems likely that the orientation of the indenyl ligand would very similar to that observed in **7**, as this orientation avoids the steric interaction of the indenyl ligand with either of the cage methyl groups.

The dimethyl analogue of the fourteen vertex compound (Me_2-1,14,2,10-) was also not synthesised, but it is suggested that the indenyl orientation would be $\tau = \pm$ 110-125º as this is the value range observed in **4**/**6** which would be similar to Me_2-1,14,2,10-, all compounds having a $MeCB_5$ belt bound to the metal.

Further work in this area could be to try and synthesise and obtain the crystal structure of 4-(η-C_9H_7)-4,1,6-*closo*-$NiC_2B_{10}H_{12}$ (3-(η-C_5H_5)-3,1,2-*closo*-$NiC_2B_9H_{11}$ has been reported,[20] although the crystal structure has not). This paramagnetic compound would have nineteen electrons associated with the nickel, and it would be interesting to see whether the increased electron density would lead to greater slippage of the indenyl ligand compared to the cobaltacarboranes.

2.14 References

2.1 For example: J.H. Burns and P.G. Laubereau, *Inorg. Chem.*, 1971, **10**, 2789; S. R.Allen, P.K. Baker, S.G. Barnes, M. Green, L. Trollope, L.M. Muir and K. Muir, *J. Chem. Soc., Dalton Trans.*, 1981, 873; Y.N. Al-Obaidi, M. Green, N.D. White, J.M. Bassett and A.J. Welch, *J. Chem. Soc., Chem. Commun.*, 1981, 494; S.R. Allen, P.K.Baker, S.G. Barnes, M. Bottrill, M. Green, A.G. Orpen, I.D. Williams and A.J. Welch, *J. Chem. Soc., Dalton Trans.*, 1983, 927.

2.2 (a) A.J. Hart-Davis and R.J. Mawby, *J. Chem. Soc. A*, 1969, 2403.
(b) F. Basolo, *Coord. Chem. Rev.*, 1982, **43**, 7.
(c) M.J. Calhorda, *Chem.-Eur. J.*, 2002, **8**, 868.

2.3 J.W. Faller, R.H. Crabtree and A. Habih, *Organometallics*, 1985, **4**, 929.

2.4 D.E. Smith and A.J. Welch, *Organometallics*, 1986, **5**, 760.

2.5 U. Grädler, A.S. Weller, A.J. Welch and D. Reed, *J. Chem. Soc., Dalton Trans.*, 1996, 335.

2.6 Z.G. Lewis, D. Reed and A.J. Welch, *J. Chem. Soc., Dalton Trans.*, 1992, 731.

2.7 (a) G.K. Barker, M.P. Garcia, M. Green, G.N. Pain, F.G.A. Stone, S.K.R. Jones and A.J. Welch, *J. Chem. Soc., Chem. Commun.*, 1981, 652.
(b) D.M.P. Mingos, *J. Chem. Soc., Dalton Trans.*, 1977, 602; D.M.P. Mingos, M.I. Forsyth and A.J. Welch, *J. Chem. Soc., Dalton Trans.*, 1978, 1363.

2.8 (a) A. Burke, R. McIntosh, D. Ellis, G.M. Rosair and A.J. Welch, *Collect. Czech. Chem. Commun.*, 2002, **67**, 991.
(b) D. Ellis, M.E. Lopez, R. McIntosh, G.M. Rosair, A.J. Welch and R. Quenardelle, *Chem, Commun.*, 2005, 1348.
(c) A. McAnaw, M.E. Lopez, G. Scott, D. Ellis, D. McKay, G.M. Rosair and A.J. Welch, *Dalton Trans.*, 2012, **41**, 10957.
(d) G.B. Dunks, M.M. McKown, M.F. Hawthorne, *J. Am. Chem. Soc.*, 1971, **93**, 2541.
(e) M.R. Churchill and B.G. Deboer, *Inorg. Chem.*, 1974, **13**, 1411.

2.9 D.F. Dustin, G.B. Dunks and M.F. Hawthorne, *J. Am. Chem. Soc.*, 1973, **95**, 1109.

2.10 G. Scott, A. McAnaw, D. McKay, A.S.F. Boyd, D. Ellis, G.M. Rosair, S.A. Macgregor, A.J. Welch, F. Laschi, F. Rossi and P. Zanello, *Dalton Trans.*, 2010, **39**, 5286.

2.11 W.J. Evans and M.F. Hawthorne, *J. Chem. Soc., Chem. Commun.*, 1974, 38.

2.12 For example: D. Ellis, M.E. Lopez, R. McIntosh, G.M. Rosair and A.J. Welch, *Chem. Commun.*, 2005, 1917; L. Deng, J. Zhang, H.S. Chan and Z. Xie, *Angew. Chem. Int. Ed.*, 2006, **45**, 4309; references 2.11 and 2.13.

2.13 A. McAnaw, M.E. Lopez, D. Ellis, G.M. Rosair and A.J. Welch, *Dalton Trans.*, 2013, **42**, 671.

2.14 (a) X.L.R. Fontaine, N.N. Greenwood, J.D. Kennedy, K. Nestor and M. Thornton-Pett, *J. Chem. Soc., Dalton Trans.*, 1990, 681.
(b) M.K. Kaloustian, R.J. Wiersema and M.F. Hawthorne, *J. Am. Chem. Soc.*, 1972, **94**, 6679.

2.15 A. Burke, D. Ellis, B.T. Giles, S.A. Macgregor, G.M. Rosair and A.J. Welch, *Angew. Chem. Int. Ed.*, 2003, **42**, 225.

2.16 J. Zhang, L. Deng, H. –S. Chan and Z. Xie, *J. Am. Chem. Soc.*, 2007, **129**, 18.

2.17 P.D. Abram, D. McKay, D. Ellis, S.A. Macgregor, G.M. Rosair and A.J. Welch, *Dalton Trans.*, 2010, **39**, 2412.

2.18 For details of calculations see chapter six.

2.19 J. Giacovazzo, H.L. Monaco, D. Viterbo, F. Scordari, G. Gilli, G. Zanotti and M. Catti, *Fundamentals of Crystallography*, Oxford University Press, 1992; R.P.A. Bettens, D. Dakternieks, A. Duthie, F.S. Kuanab and E.R.T. Tiekink, *CrystEngComm*, 2009, **11**, 1362; P. Dauber and A.T. Hagler, *Acc. Chem. Res.*, 1980, **13**, 105; D. O'Connell, T.R. Spalding, G. Ferguson, J.F. Gallagher and J.D. Kennedy, *J. Organomet. Chem.*, 1995, **503**, C12.

2.20 R.J. Wilson, L.F. Warren and M.F. Hawthorne, *J. Am. Chem. Soc.*, 1969, **91**, 758.

Chapter 3
Naphthalene Ruthenacarboranes

3.1 Introduction

For the indenyl cobaltacarboranes described in the previous chapter a consequence of having the five-membered ring of the indenyl ligand over the six-membered ring of the carborane is that there will always be some parts of the molecule where the overall conformation is staggered and others where it is eclipsed, somewhat compromising attempts to find an optimal orientation based solely on the relative trans influences of the atoms bound to the metal.

Thirteen vertex naphthalene metallacarboranes would have a six-membered ring above a six-membered ring, eliminating this problem of partial eclipsing/staggering, whilst still showing selective lengthening of the bridging carbon atoms to metal bonds - the structural naphthalene effect.[1]

The only reports of naphthalene metallacarboranes in the literature are those of subicosahedral/icosahedral compounds. An icosahedral naphthalene ferracarborane was made by the direct insertion of [Fe(1,5-C_8H_{12})(η-C_5H_5)] into 2,3-$Me_2C_2B_9H_9$ in the presence of naphthalene,[2] however this approach was unsuccessful for the preparation of supraicosahedral species. The only other known naphthalene metallacarboranes are 2-(η-$C_{10}H_8$)-2,1-*closo*-$CoCB_{10}H_{11}$[3] (which was made by reacting [2-(η-C_5H_5)-2,1-*closo*-$CoCB_{10}H_{11}$]$^-$ with sodium naphthalenide, then [C_5H_5]$^-$ and $NiBr_2$) and (η-$C_{10}H_8$)Fe($Et_2C_2B_4H_4$) which was made two ways, firstly from the reaction of (η^6-C_8H_{10})Fe($Et_2C_2B_4H_4$) with naphthalene at 200 ^oC,[4] and secondly from the reaction of [*nido*-($Et_2C_2B_4H_5$)]$^-$ with $Li_2[C_{10}H_8]$ and $FeCl_2$ in THF.[5] It was thought that perhaps the second of these reactions could be used with [7,9-*nido*-7,9-$C_2B_{10}H_{12}$]$^{2-}$ instead of [*nido*-($Et_2C_2B_4H_5$)]$^-$, but unfortunately it did not yield a naphthalene ferracarborane (see 3.9/3.13).

Bis-arene iron cations of the type [Fe(arene)$_2$]$^{2+}$ (where arene = mesitylene, benzene or hexamethylbenzene) have successfully been reacted with [*nido*-$C_2B_{10}H_{12}$]$^{2-}$ anions to give (arene)Fe$C_2B_{10}H_{12}$ compounds,[6a,b] but unfortunately the [Fe(η-$C_{10}H_8$)$_2$][PF_6]$_2$ compound

could not be synthesised. Since it did not seem possible to make supraicosahedral naphthalene metallacarboranes using iron as the metal, it was decided instead to try using ruthenium.

The established route to making an (arene)$RuC_2B_{10}H_{12}$ species is to react reduced carborane with $[RuCl_2(arene)]_2$[7] (figure 3.1.1).

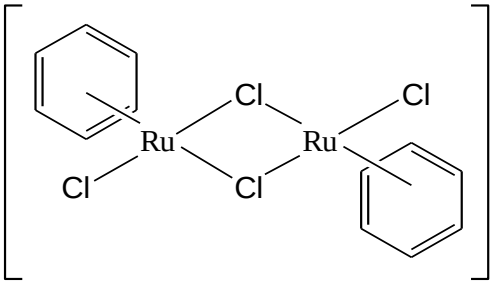

Figure 3.1.1 $[RuCl_2(\eta\text{-}C_6H_6)]_2$ dimer.

The dimer is formed by adding $RuCl_3 \cdot nH_2O$ to the appropriate cyclohexadiene in refluxing ethanol.[8] However, when this reaction was carried out using 1,2-dihydronaphthalene as the cyclohexadiene in an attempt to make $[RuCl_2(naphthalene)]_2$, only naphthalene and dihydronaphthalene could be detected in the product. This suggests that the dihydronaphthalene is being reduced, but that the coordination to the ruthenium is not favourable. It is expected that the presence of electron withdrawing groups on the arene will decrease its ability to bind to transition metals. This may explain why one ring of the naphthalene ligand - with the electron withdrawing other ring fused to it - fails to form the $[RuCl_2(naphthalene)]_2$ dimer.

Since the established route to (arene)$RuC_2B_{10}H_{12}$ species could not be followed, an alternative was proposed whereby $[RuCl_2(COD)]_x$ (COD = cyclo-octa-1,5-diene) is reacted with reduced carborane in the presence of an excess of naphthalene (figure 3.1.2).

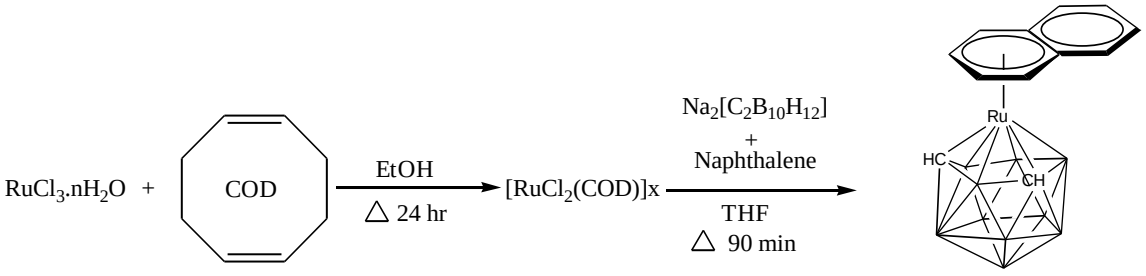

Figure 3.1.2 Synthesis of 4-(η-$C_{10}H_8$)-4,1,6-$RuC_2B_{10}H_{12}$.

The reasoning behind this reaction was that if the nido fragment was capitated with a {Ru(COD)} fragment, the resulting carborane would be unstable - as the metal only has sixteen electrons associated with it - and the COD would be replaced by naphthalene to give a stable eighteen electron count.

Before attempting to use this procedure to make a thirteen vertex metallacarborane, the procedure was first tested using [7,8-*nido*-7,8-$C_2B_9H_{11}]^{2-}$ as the *nido*-carborane (to establish the optimal experimental conditions) yielding 3-(η-$C_{10}H_8$)-3,1,2-*closo*-$RuC_2B_9H_{11}$ (**9**) as the product. This method (and subsequent isomerisations) was then used to make the docosahedral species 4-(η-$C_{10}H_8$)-4,1,X-*closo*-$RuC_2B_{10}H_{12}$ where X = 6,8,10 and 12 (compounds **11**, **12**, **13** and **14**). Two unexpected compounds bearing EtPh and cyclooctatriene exo-polyhedral ligands were also isolated (compounds **10** and **15**)

Attempts to make the naphthalene ferracarboranes were unsuccessful, with the closest compound we could make being 4-(η-$C_{10}H_{12}$)-4,1,6-*closo*-$FeC_2B_{10}H_{12}$ (**16**), where the non-bound naphthalene ring has been reduced.

All compounds were characterised by CHN microanalysis, ^{11}B and ^{1}H NMR spectroscopy and mass spectrometry (except **16** which was not characterised by CHN). In addition to this all compounds were studied by *X*-ray crystallography, although the structural studies on the thirteen vertex naphthalene ruthenacarboranes are generally not as precise as those of the indenyl cobaltacarboranes, the former typically having larger e.s.d.s on bond lengths and angles.

While the method of preparing the naphthalene ruthenacarboranes described in this chapter is different to the conventional method of using a $[RuCl_2(arene)]_2$ reagent, the products of the two reactions are similar (particularly with respect to the cage). This allows the known (arene)RuC_2B_9 [2,9a,b,c] and (arene)RuC_2B_{10} [7,10a,b] compounds to be compared to the naphthalene ruthenacarboranes.

3.2 Synthesis of 3-(η-$C_{10}H_8$)-3,1,2-*closo*-$RuC_2B_9H_{11}$ (9)

Li_2[7,8-*nido*-$C_2B_9H_{11}$] (from *n*-BuLi deprotonated NEt_3H[7,8-*nido*-$C_2B_9H_{12}$]), excess naphthalene and $[RuCl_2(COD)]_x$ were heated to reflux for 90 minutes. Upon chromatography yellow **9** is isolated in 10.6% yield.

The MS of **9** contains an envelope centred on *m/z* 361 (M^+) (M_w **9** = 361.58 g mol^{-1}), and the elemental analysis is in good agreement with that expected for $C_{12}H_{19}B_9Ru$.

Compound **9** shows one broad singlet of integral two at 2.95 ppm in the ^1H NMR spectrum corresponding to the two equivalent cage CHs. The relevant naphthalene peaks are observed as two doublets of doublets at 6.35 and 6.75 ppm and an apparent singlet at 7.55 ppm. The peak at 7.55 ppm is presumably from the four protons on the free ring while the peaks at 6.35 and 6.75 ppm are from the four protons on the coordinated ring, as protons on transition metal bound rings tend to be moved upfield. It is not easily possible to tell which of the two upfield peaks correspond to the protons pairs H_A and H_B in figure 3.2.1.

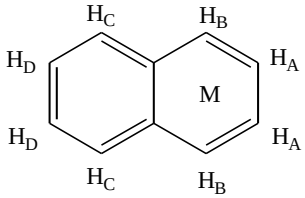

Figure 3.2.1 Metal bound naphthalene ligand with labelled protons.

The ^{11}B NMR spectrum consists of six peaks in a 1:1:2:2:2:1 ratio between -24.5 and 2.0 ppm as would be expected considering the C_s symmetry. Both the ^1H and ^{11}B NMR spectra are consistent with C_s symmetry and naphthalene rotation (or at least substantial libration) about the centre of the bound ring at room temperature. As noted in chapter two, the cage C_s symmetry of **9** gives rise to the chemical equivalence of protons related by the naphthalene ligand's mirror plane in the ^1H NMR spectrum. This is seen in the ^1H NMR spectra of all the compounds with cage C_s symmetry (3,1,2- and 4,1,10-) and all the 4,1,6- compounds (time-averaged cage C_s symmetry) described in this chapter.

Crystals of **9** were grown by diffusion of 40-60 petroleum ether and a DCM solution of **9** at -30 °C. Analysis by *X*-ray diffraction shows **9** to be the expected 3-(η-$C_{10}H_8$)-3,1,2-*closo*-$RuC_2B_9H_{11}$ (figure 3.2.2).

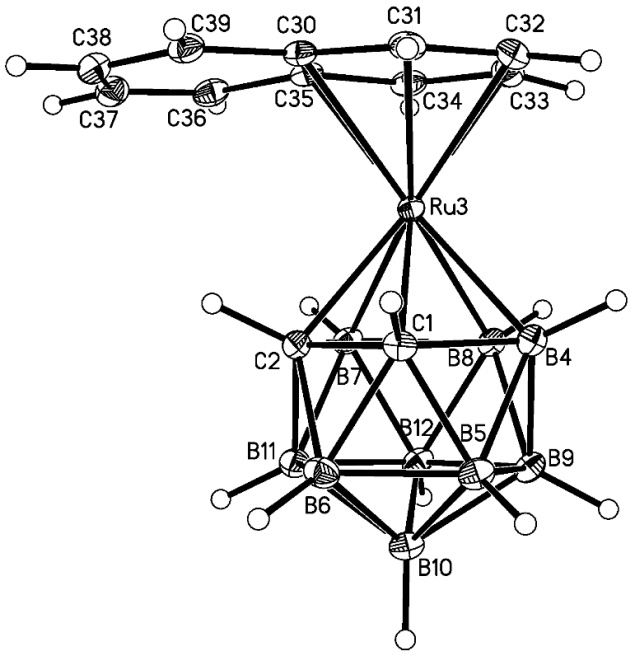

Figure 3.2.2 Molecular structure of 3-(η-$C_{10}H_8$)-3,1,2-*closo*-$RuC_2B_9H_{11}$ **(9)**.

Compound **9** has an icosahedral structure with effective cage C_s symmetry, C atoms at the one and two positions, and the Ru atom at the three position. The cage structure of **9** is similar to that observed in 3-(η-C_6R_6)-3,1,2-*closo*-$RuC_2B_9H_{11}$[9a,b] (R = H, Me) and 3-(*p*-cymene)-3,1,2-*closo*-$RuC_2B_9H_{11}$[9c]. The C1-C2 connectivity is the shortest of the five connectivities in the top pentagonal belt (1.6343(19) Å compared to 1.725(2) Å for next longest connectivity) which helped to assign the cage carbon atoms (the positions of the cage carbon atoms was confirmed using the vertex to centroid distance method).[11] As in chapter two the relative lengths of the ruthenium to naphthalene bonds are indicative of the strength of these bonds, however now there are four metal to non-bridging carbon atom distances to consider instead of three.

The Ru3-C distances to the bridging carbon atoms of the naphthalene ligand are longer than the Ru3-C distances to the non-bridging carbon atoms (2.2696(13) Å for Ru3-C35 and 2.3033(13) Å for Ru3-C30, compared to 2.2395(14) Å, 2.2217(14) Å, 2.2060(14) Å and 2.2038(14) Å for Ru3-C31, Ru3-C32, Ru3-C33 and Ru3-C34 respectively).

The Ru-C bonds Ru3-C32 (2.2217(14) Å) and Ru3-C31 (2.2395(14) Å) are longer than their respective counterparts, Ru3-C33 (2.2060(14) Å) and Ru3-C34 (2.2038(14) Å). The reason for this is that C33 and C34 are trans to the cage carbon atoms, while C31 and C32

are trans to cage boron atoms - which have a greater trans influence than the cage carbon atoms. This phenomenon of M-C bond lengths within the same η-ligand being different depending on whether they are trans to the cage carbon or cage boron atoms is explored further in chapter four.

3.3 Synthesis of 3-(η-EtPh)-3,1,2-*closo*-$RuC_2B_9H_{11}$ (10)

$Tl[TlC_2B_9H_{11}]$, excess naphthalene and $[RuCl_2(COD)]_x$ were stirred overnight in DCM, then heated to reflux for 2 hrs. The DCM was then removed *in vacuo* and THF added. The mixture was then heated to reflux for 6 hrs. Upon chromatography yellow **10** is isolated in 9.51% yield. A small amount of **9** was also present at a nearly identical R_f as **10**.

Compound **10** shows one broad singlet of integral two at 3.85 ppm in the ^1H NMR spectrum corresponding to the two equivalent cage CHs. The aromatic protons are observed as a single multiplet of integral five at 5.95 ppm, while the ethyl CH_2 group appears as a quartet of integral two at 2.60 ppm, and the ethyl CH_3 group as a triplet of integral three at 1.25 ppm.

The ^{11}B NMR spectrum consists of six peaks in a 1:1:2:2:2:1 ratio between -24.0 and 1.9 ppm, and the MS shows an envelope centred on *m/z* 339 (M^+) (M_w **10** = 339.57 g mol^{-1}).

Despite multiple preparative TLCs, **10** could not be completely separated from **9**, which is also formed during this reaction. As a consequence of this the peaks in the ^{11}B NMR spectrum are quite broad, presumably through the multiple overlap of resonances from two very similar species. In the ^1H NMR spectrum the peaks in the NMR spectrum of **9** are clearly visible, albeit in smaller amount than the peaks corresponding to **10**. The MS contains, together with the major peak at *m*/*z* 339, a smaller peak at *m*/*z* 361 (M_w **9** = 361.58 g mol^{-1}) and the CHN is consistent with the presence of a small amount of **9** (higher percentage carbon and lower percentage hydrogen than expected - $C_{12}H_{19}B_9Ru$ requires C 35.4 H 6.23. Found for **10**: C 36.6 H 5.87%).

Crystals of **10** were grown by diffusion of 40-60 petroleum ether and a DCM solution of **10**/**9** at -30 ºC, with **10** crystallising preferentially. Analysis by *X*-ray diffraction shows **10** to be 3-(η-EtPh)-3,1,2-*closo*-$RuC_2B_9H_{11}$ (figure 3.3.1).

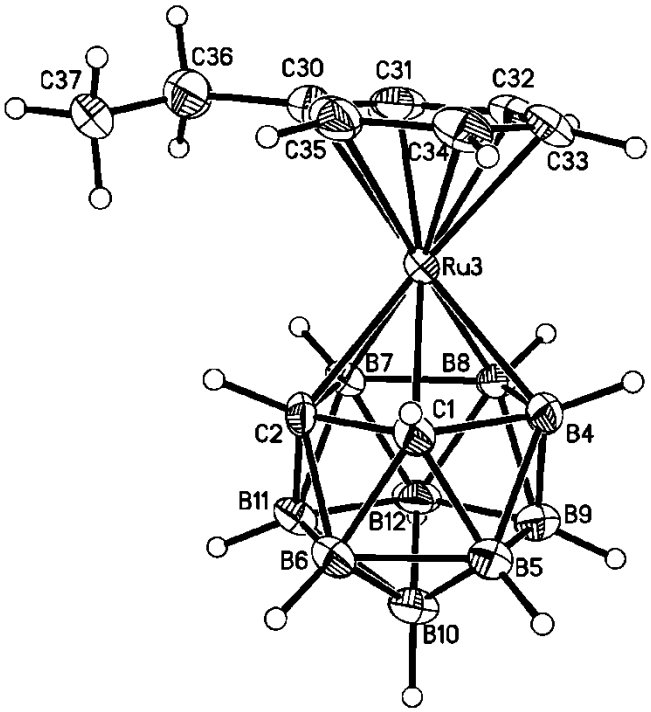

Figure 3.3.1 Molecular structure of 3-(η-EtPh)-3,1,2-*closo*-$RuC_2B_9H_{11}$ **(10)**.

The structure of the cage in **10** is very simlilar to that observed in **9**. As in **9** the C-C connectivity is the shortest in the upper pentagonal belt (1.636(5) Å compared to 1.720(6) Å for next longest connectivity).

The isolation of **10** was clearly unexpected, and is discussed later (section 3.13).

3.4 Synthesis of 4-(η-$C_{10}H_8$)-4,1,6-*closo*-$RuC_2B_{10}H_{12}$ (11)

Reduction of 1,2-*closo*-$C_2B_{10}H_{12}$ with Na in THF results in [7,9-*nido*-$C_2B_{10}H_{12}]^{2-}$. To this was added $[RuCl_2(COD)]_x$ and an excess amount of naphthalene and the mixture heated to reflux for 90 minutes. Upon chromatography yellow **11** is isolated in 9.0% yield.

The ^{11}B NMR spectrum of **11** consists of seven peaks in a 1:1:2:1:2:2:1 ratio between -23.4 and 9.1 ppm as would be expected considering the time-averaged C_s symmetry.

The ^1H NMR spectrum shows one broad singlet of integral two at 3.55 ppm corresponding to the two cage CHs - a single peak being observed presumably due to the same fluxional double DSD process occurring in compounds **1** and **2** (see section 2.2/2.3). The relevant naphthalene peaks are observed as doublets of doublets at 6.20, 6.35, 7.60 and 7.80 ppm. As for **9**, it is not easily possible to tell which of the two upfield peaks correspond to the proton pairs H_A and H_B, nor which of the two downfield peaks correspond to the proton pairs H_C and H_D in figure 3.2.1.

The MS of **11** contains an envelope centred on *m/z* 374 (M^+) (M_w **11** = 373.38 g mol^{-1}), and the elemental analysis is in good agreement with that expected for $C_{12}H_{20}B_{10}Ru$.

Crystals of **11** were grown by diffusion of 40-60 petroleum ether and a THF solution of **11** at -30 ^oC. Analysis by *X*-ray diffraction shows **11** to be the expected 4-(η-$C_{10}H_8$)-4,1,6-*closo*-$RuC_2B_{10}H_{12}$ (figure 3.4.1).

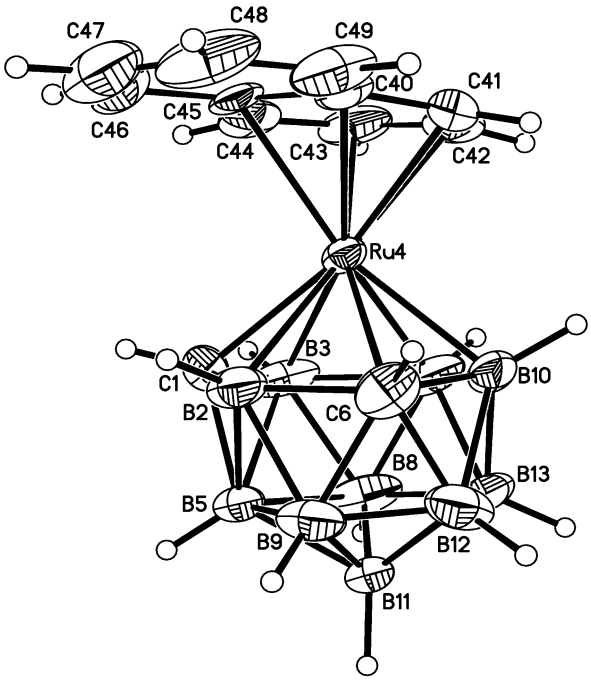

Figure 3.4.1 Molecular structure of 4-(η-$C_{10}H_8$)-4,1,6-*closo*-$RuC_2B_{10}H_{12}$ **(11)**.

Compound **11** co-crystallises with one molecule of partially disordered THF of solvation (omitted from figure 3.4.1 for clarity), and has a docosahedral structure as in the majority of the compounds in chapter two. The cage structure of **11** stands comparison with that of 4-(*p*-cymene)-4,1,6-*closo*-$RuC_2B_{10}H_{12}$,[7] and shows the same characteristic docosahedral features mentioned in chapter two, specifically Ru4-C1 is the shortest M-cage connectivity, and B2-B5 and B3-B5 are the longest of the B-B conectivities.

The Ru4-C distances to the bridging carbon atoms of the naphthalene ligand are 2.303(4) Å for Ru4-C45 and 2.331(5) Å for Ru4-C40, compared to 2.214(5) Å, 2.203(5) Å, 2.215(5) Å and 2.206(4) Å for Ru4-C41, Ru4-C42, Ru4-C43 and Ru4-C44, respectively.

3.5 Synthesis of 4-(η-$C_{10}H_8$)-4,1,8-*closo*-$RuC_2B_{10}H_{12}$ (12)

Overnight heating of **11** in refluxing toluene followed by chromatography gave yellow **12** in 33.3% yield. Small amounts of the 4,1,6- isomer were also recovered.

Compound **12** shows two broad peaks each of integral one at 2.10 and 3.18 ppm in the ^1H NMR spectrum corresponding to the two cage CHs. The relevant naphthalene peaks are observed as apparent triplets at 6.08 and 6.15 ppm corresponding to the protons H_B and H_C, and doublets at 6.56 and 6.57 ppm corresponding to the protons H_A and H_D in figure 3.5.1 (it is impossible to easily tell which doublet/apparent triplet belongs to which of the four proton though). The four protons on the non-metal bound ring appear as multiplets at 7.55-7.65 and 7.70-7.72 ppm.

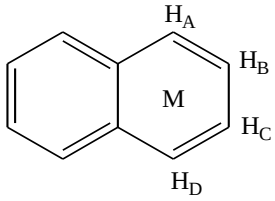

Figure 3.5.1 Metal bound naphthalene ligand with labelled protons.

The ^{11}B NMR spectrum consists of ten peaks all of integral one between -19.4 and 15.7 ppm. Both the ^1H and ^{11}B NMR spectra are consistent with C_1 symmetry, the C_s symmetry being lost upon isomerisation of 4,1,6- to 4,1,8-, as noted in chapter two. The result of this is that the protons on the naphthalene ligands become inequivalent in the ^1H NMR spectrum, and the cage CHs becomes two distinct peaks separated by 1.08 ppm.

In the mass spectrum of **12** there is an envelope centred on *m/z* 374 (M^+) (M_w **12** = 373.38 g mol^{-1}), and the elemental analysis is in good agreement with that expected for $C_{12}H_{20}B_{10}Ru$.

Crystals of **12** were grown by solvent diffusion of 40-60 petroleum ether and a DCM solution of **12** at -30 ^oC. Analysis by *X*-ray diffraction shows **12** to be the expected 4-(η-$C_{10}H_8$)-4,1,8-*closo*-$RuC_2B_{10}H_{12}$ (figure 3.5.2).

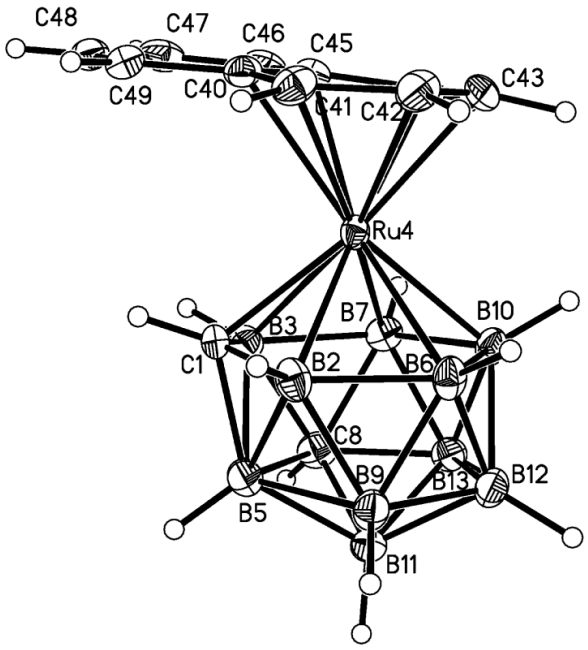

Figure 3.5.2 Molecular structure of 4-(η-$C_{10}H_8$)-4,1,8-*closo*-$RuC_2B_{10}H_{12}$ **(12)**.

Compound **12** is only the second 4-(arene)-4,1,8-*closo*-RuC_2B_{10} compound to be synthesised, the first being 1,8-Ph_2-4-(*p*-cymene)-4,1,8-*closo*-$RuC_2B_{10}H_{10}$.[10b] Both molecules have a similar cage structure which also resembles those of the two crystallographically independent molecules of 1,8-Me_2-4-(η-C_9H_7)-4,1,8-*closo*-$CoC_2B_{10}H_{12}$.

The Ru4-C distances to the bridging carbon atoms of the naphthalene ligand are 2.324(3) Å for Ru4-C45 and 2.330(3) Å for Ru4-C40, compared to 2.235(3) Å, 2.250(3) Å, 2.232(3) Å and 2.212(3) Å for Ru4-C41, Ru4-C42, Ru4-C43 and Ru4-C44, respectively.

3.6 Synthesis of 4-(η-$C_{10}H_8$)-4,1,10-*closo*-$RuC_2B_{10}H_{12}$ (13)

Reduction of 1,12-*closo*-$C_2B_{10}H_{12}$ with Na in liquid ammonia results in [7,10-*nido*-$C_2B_{10}H_{12}]^{2-}$. Following removal of ammonia and addition of THF, $[RuCl_2(COD)]_x$ and an excess amount of naphthalene were added and the mixture heated to reflux for 90 minutes. Upon chromatography yellow **13** is isolated in 3% yield.

Compound **13** shows two broad peaks each of integral one at 1.30 and 4.05 ppm in the ^1H NMR spectrum corresponding to the two cage CHs. The relevant naphthalene peaks are observed as doublets of doublets at 6.10 and 6.40 ppm (proton pairs H_A and H_B in figure 3.2.1) and doublets of doublets at 7.45 and 7.65 ppm (protons on the unbound ring).

The ^{11}B NMR spectrum consists of five peaks in a 2:2:2:2:2 ratio between -12.8 and 4.9 ppm, with one of the peaks a 1 + 1 coincidence.

An envelope centred on *m/z* 374 (M^+) (M_w **13** = 373.38 g mol^{-1}) is observed in the MS of **13**, and the elemental analysis is in good agreement with that expected for $C_{12}H_{20}B_{10}Ru$.

Crystals of **13** were grown by diffusion of 40-60 petroleum ether and a DCM solution of **13** at -30 ^oC. Analysis by *X*-ray diffraction shows **13** to be the expected 4-(η-$C_{10}H_8$)-4,1,10-*closo*-$RuC_2B_{10}H_{12}$ (figure 3.6.1).

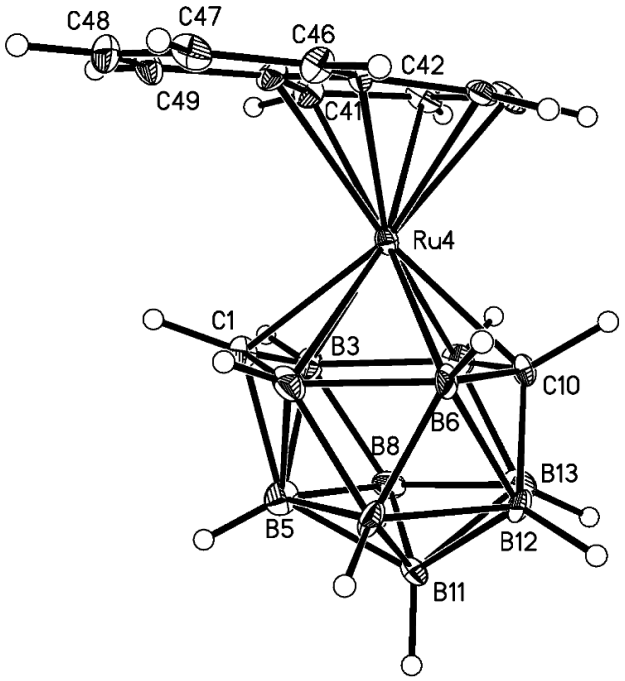

Figure 3.6.1 Molecular structure of 4-(η-$C_{10}H_8$)-4,1,10-*closo*-$RuC_2B_{10}H_{12}$ **(13)**.

The structure of **13** was solved as a three component twin, and shows the same effective C_s cage symmetry and cage structure as that found in **7**, and the known 4,1,10- Ru(arene) compounds[10a] 4-(*p*-cymene)-4,1,10-*closo*-$RuC_2B_{10}H_{12}$, 4-(η-C_6H_6)-4,1,10-*closo*-$RuC_2B_{10}H_{12}$ and 4-(η-C_6Me_6)-4,1,10-*closo*-$RuC_2B_{10}H_{12}$.

The Ru4-C distances to the bridging carbon atoms of the naphthalene ligand are 2.319(8) Å for Ru4-C45 and 2.327(8) Å for Ru4-C40, compared to 2.231(8) Å, 2.248(8) Å, 2.227(8) Å and 2.207(8) Å for Ru4-C41, Ru4-C42, Ru4-C43 and Ru4-C44, respectively.

3.7 Synthesis of 4-(η-$C_{10}H_8$)-4,1,12-$RuC_2B_{10}H_{12}$ (14)

Overnight heating of **13** in refluxing toluene followed by chromatography gave yellow **14** in 80.0% yield.

The ^{11}B NMR spectrum of **14** consists of seven peaks in a 1:2:1:1:1:2:2: ratio between -22.7 and 3.4 ppm, with the peaks of integral two being 1 + 1 coincidences.

The MS of **14** contains an envelope centred on *m/z* 374 (M^+) (M_w **14** = 373.38 g mol^{-1}), and the elemental analysis is in good agreement with that expected for $C_{12}H_{20}B_{10}Ru$.

The ^1H NMR spectrum shows two broad peaks each of integral one at 3.00 and 3.20 ppm corresponding to the two cage CHs. The relevant naphthalene peaks are observed as apparent triplets at 5.95 and 6.10 ppm corresponding to the protons H_B and H_C and doublets at 6.48 and 6.50 ppm corresponding to the protons H_A and H_D (figure 3.5.1). The four protons on the non-metal bound ring appear as multiplets at 7.50-7.60 and 7.60-7.70 ppm.

Crystals of **14** were grown by diffusion of 40-60 petroleum ether and a DCM solution of **14** at -30 °C. Analysis by *X*-ray diffraction shows **14** to be the expected 4-(η-$C_{10}H_8$)-4,1,12-*closo*-$RuC_2B_{10}H_{12}$ (figure 3.7.1).

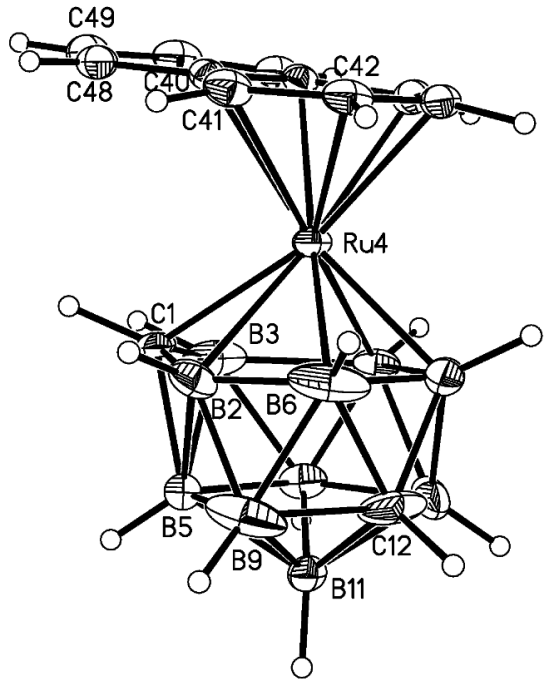

Figure 3.7.1 Molecular structure of 4-(η-$C_{10}H_8$)-4,1,12-$RuC_2B_{10}H_{12}$ **(14)**.

The structure of **14** contains disorder arising from crystallographically-imposed mirror symmetry. Unlike in **5** (see section 2.6) where vertices 1 and 3 sit across a mirror plane that goes through vertices 4, 11 and 12 and is perpendicular to the C40-C44 bond, the mirror plane in **14** goes through vertices 3, 4, 12 and 11 and is perpendicular to the C40-C45 bond. The best model of the disorder (shown in figure 3.7.1) is that whereby the cage of a single molecule is composed of B3, Ru4, C12, C1, B2, B7A, B11, B6 & B6A, B5 & B5A and B9 & B9A (where A represents a reflected atom). H3 lies off the mirror plane and the best interpretation of the disorder is that H3A is associated with the previously identified atom list. With respect to normal docosahedral numbering, B6A is B10, B5A is B8, B9A is B13 and B7A is B7. Figure 3.7.2 shows the grown asymmetric unit of **14** and **5** for comparison of the mirror planes in the two molecules.

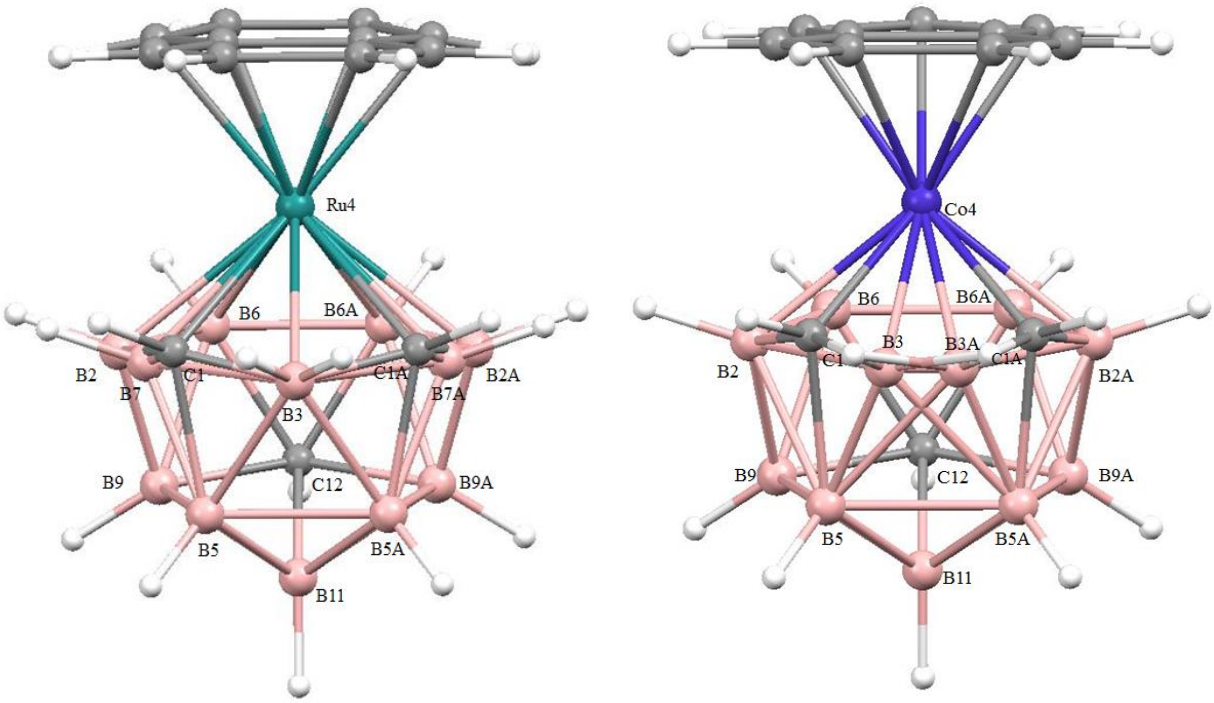

(a) (b)

Figure 3.7.2 (a) Grown asymmetric unit of **14** and (b) grown asymmetric unit of **5**.

The Ru4-C distances to the bridging carbon atoms of the naphthalene ligand are 2.327(5) Å for Ru4-C40, compared to 2.226(5) Å and 2.229(5) Å for Ru4-C41 and Ru4-C42, respectively (because of the mirror symmetry the Ru4-C bonds to C45, C44 and C43 are the same length as those to C40, C41 and C42, respectively).

3.8 Synthesis of 4-(η^6-C_8H_{10})-4,1,6-*closo*-$RuC_2B_{10}H_{12}$ (15)

Reduction of 1,2-*closo*-$C_2B_{10}H_{12}$ with Na and a catalytic amount of naphthalene in THF results in [7,9-*nido*-$C_2B_{10}H_{12}]^{2-}$. To this was added half an equivalent of $[RuCl_2(COD)]_x$ and the mixture stirred overnight. THF was removed *in vacuo*, then ethanol added, followed by an ethanol solution of [BTMA]Cl (the relevance of this step is explained in 3.13) to give a brown precipitate. The precipitate and the ethanol solution were recombined and the ethanol removed by rotary evaporation, leaving a brown solid. Upon chromatography yellow **15** is isolated in 4.10% yield.

Compound **15** shows one broad singlet of integral two at 4.20 ppm in the ^1H NMR spectrum corresponding to the two cage CHs. The four cyclooctatriene CH_2 protons are observed as a broad multiplet and an apparent broad singlet at 2.25 and 1.33 ppm respectively, while the six CH protons appear as three multiplets at 5.60, 5.70 and 6.25 ppm, with each multiplet corresponding to two protons. The ^1H NMR spectrum is similar to that observed for (η^6-C_8H_{10})Fe(2,3-$Et_2C_2B_4H_4$),[12] which also has a cyclooctatriene exo-polyhedral ligand.

The ^{11}B NMR spectrum consists of seven peaks in a 1:1:2:2:1:2:1 ratio between -21.7 and 9.4 ppm as would be expected considering the C_s symmetry. As in **11**, both the ^1H and ^{11}B NMR spectra are consistent with time-averaged C_s symmetry, and the ^{11}B NMR spectrum is similar to that observed in **11**, except that one of the peaks of integral two has swapped relative positions with one of the peaks of integral one.

An envelope centred on *m/z* 346 (M_w **15** = 351.37 g mol^{-1}) is observed in the MS of **15** and the elemental analysis is in good agreement with that expected for $C_{10}H_{22}B_{10}Ru$.

Crystals of **15** were grown by diffusion of 40-60 petroleum ether and a THF solution of **15** at -30 ^oC. Analysis by *X*-ray diffraction shows **15** to be 4-(η^6-C_8H_{10})-4,1,6-*closo*-$RuC_2B_{10}H_{12}$ (figure 3.8.1).

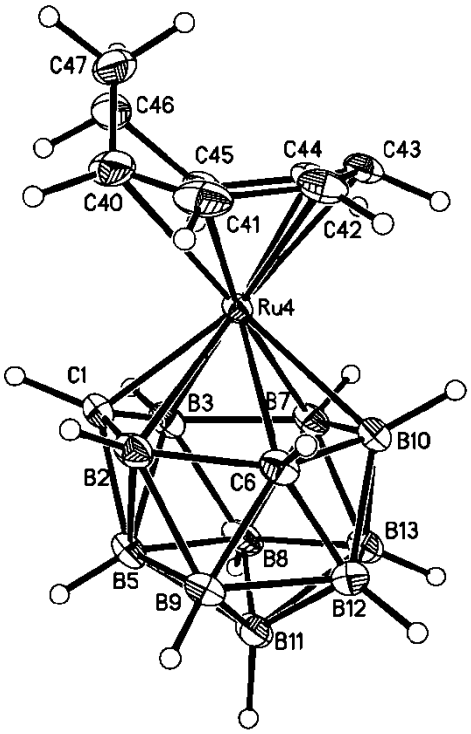

Figure 3.8.1 Molecular structure of 4-(η^6-C_8H_{10})-4,1,6-*closo*-$RuC_2B_{10}H_{12}$ **(15)**.

The structure of the cage in **15** is very similar to that of **11**, and the exopolyhedral bound cyclooctatriene ligand is similar to that observed in (η^6-C_8H_{10})Fe($Et_2C_2B_4H_4$). Four of the five CH-CH bonds of the cyclooctatriene ligand are all roughly the same length (~ 1.43 Å), indicating significant conjugation. The CH-CH bonds are all shorter than the CH-CH_2 and CH_2-CH_2 bonds (~ 1.51 Å) as would be expected in going from conjugated to single bonds.

3.9 Synthesis of 4-(η-$C_{10}H_{12}$)-4,1,6-*closo*-$FeC_2B_{10}H_{12}$ (16)

Reaction of [7,9-*nido*-$C_2B_{10}H_{12}]^{2-}$ with $Li_2[C_{10}H_8]$ and $FeCl_2$ in THF followed by chromatography gave pink **16** in 2.17% yield.

The MS of **16** contains an envelope centred on *m/z* 332 (M^+) (M_w **16** = 332.16 g mol^{-1}).

Compound **16** shows one broad singlet of integral two at 2.25 ppm in the ^1H NMR spectrum corresponding to the two cage CHs. The four $C_{10}H_{12}$ CH protons appear as two multiplets, each of integral two, at 5.70 and 5.90 ppm. The eight CH_2 protons appear as four multiplets, each of integral two at 2.95, 2.50, 2.10 and 1.75 ppm. It is not easily possible to tell which of the two downfield peaks correspond to the proton pairs H_A and H_B, and which of the four upfield peaks correspond to the proton pairs H_C, H_D, H_E and H_F in figure 3.9.1.

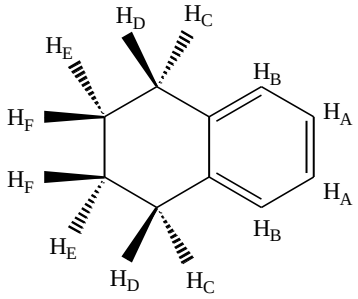

Figure 3.9.1 Tetrahydronaphthalene ligand with labelled protons.

The ^{11}B NMR spectrum consists of seven peaks in a 1:1:2:2:1:2:1: ratio between 11.2 and -20.5 ppm. The ^1H NMR spectrum of **16** is similar to that observed in (η-$C_{10}H_{12}$)$Fe(Et_2C_2B_4H_4)$,[4] while the ^{11}B NMR spectrum is similar to that observed in 4-(η-$C_6Me_3H_3$)-4,1,6-*closo*-$FeC_2B_{10}H_{12}$.[6a]

Crystals of **16** were grown by solvent diffusion of 40-60 petroleum ether and a DCM solution of **16** at -30 ^oC. Analysis by *X*-ray diffraction shows **16** to be 4-(η-$C_{10}H_{12}$)-4,1,6-*closo*-$FeC_2B_{10}H_{12}$ (figure 3.9.2).

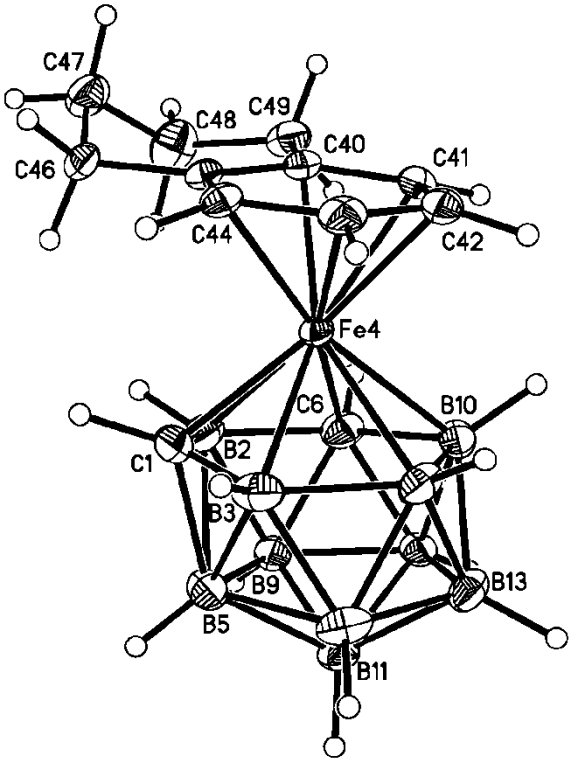

Figure 3.9.2 Molecular structure of 4-(η-$C_{10}H_{12}$)-4,1,6-*closo*-$FeC_2B_{10}H_{12}$ **(16)**.

Compound **16** crystallises with one molecule of DCM per molecule of ferracarborane (omitted from figure 3.9.2 for clarity), and the structure shows how the un-bound ring has reduced, as evidenced by its non-planarity compared to those in **9** and **11-14**. The unbound ring adopts a half-chair conformation, as neccesitated by the sp^2 nature of C40 and C45. The structure of the cage in **16** is similar to that in 4-(η-$C_6H_3Me_3$)-4,1,6-*closo*-$FeC_2B_{10}H_{12}$.

3.10 Comparison of ^{11}B NMR spectroscopic shifts

Table 3.10 presents the average ^{11}B NMR spectroscopic shifts ($<\delta^{11}B>$) for the ruthenium compounds[2,9,b,c,7,10a,b] and compares them to the values of other known arene ruthenium compounds. The list is less complete than the corresponding one for cobalt Cp/Cp*/indenyl compounds particularly with respect to other 4,1,8- arene ruthenacarboranes. Apart from **12**, the only other known 4,1,8- arene ruthenacarboranes is diphenylated at the cage carbon atoms and so not really comparable to **12** with respect to ^{11}B NMR spectra.

Table 3.10 Average ^{11}B NMR shifts ($<\delta^{11}B>$) in ppm of various compounds.

Compound	Average ^{11}B chemical shift ($<\delta^{11}B>$)(ppm)
4-(*p*-cymene)-4,1,6-*closo*-$RuC_2B_{10}H_{12}$	-5.2
4-(*p*-cymene)-4,1,10-*closo*-$RuC_2B_{10}H_{12}$	-9.6
4-(η-C_6H_6)-4,1,10-*closo*-$RuC_2B_{10}H_{12}$	-10.4
4-(η-C_6Me_6)-4,1,10-*closo*-$RuC_2B_{10}H_{12}$	-9.5
4-(*p*-cymene)-4,1,12-*closo*-$RuC_2B_{10}H_{12}$	-10.0
11 (4,1,6-)	-7.7
12 (4,1,8-)	-4.8
13 (4,1,10-)	-8.9
14 (4,1,12-)	-9.3
15 (4,1,6-)	-6.9
9 (3,1,2-)	-10.3
10 (3,1,2-)	-10.3
3-(η-C_6H_6)-3,1,2-*closo*-$RuC_2B_9H_{11}$	-10.1
3-(*p*-cymene)-3,1,2-*closo*-$RuC_2B_9H_{11}$	-9.6
3-(η-C_6Me_6)-3,1,2-*closo*-$RuC_2B_9H_{11}$	-10.2

= Thirteen vertex

= Twelve vertex

As with the cobalt compounds, the 4,1,8- isomer has the farthest downfield $<\delta^{11}B>$ value, followed by the 4,1,6- isomer. However, for both the naphthalene and *p*-cymene compounds the $<\delta^{11}B>$ value for the 4,1,10 isomer is downfield of that for the 4,1,12- isomer, which is the reverse of that found in the cobalt compounds.

The $<\delta^{11}B>$ values for all of the arene ruthenium twelve vertex compounds are very similar and show less variation (0.7 ppm) than the three twelve vertex cobalt compounds (2.2 ppm) from section 2.10. All of the $<\delta^{11}B>$ values for the ruthenium compounds are upfield of the

$<\delta^{11}B>$ values found for comparable cobalt compounds, reflecting the lower oxidation state of the former metal.

Like the various cobalt compounds studied in chapter two, there are no obvious conclusions which can be made on the effect of the exo-polyhedral ligands on the $<\delta^{11}B>$ values based on simple electron donating/withdrawing arguments.

3.11 Discussion

Tables 3.11.1 and 3.11.2 summarizes some key structural parameters of compounds **9**–**16**.

Table 3.11.1 Selected molecular dimensions (Å, º) in thirteen vertex compounds **11–16**.

	11	**12**	**13**	**14**	**15**[a]	**16**[b]
Ru4-C1	2.144(5)	2.121(3)	2.129(8)	2.190(10)	2.1469(17)	2.042(3)
Ru4-B2	2.297(6)	2.297(3)	2.324(9)	2.362(15)	2.3208(18)	2.213(3)
Ru4-X6[c]	2.254(5)	2.275(3)	2.259(9)	2.188(7)	2.3286(17)	2.187(3)
Ru4-Y10	2.230(5)	2.244(3)	2.197(8)	2.188(7)[d]	2.257(2)	2.160(3)
Ru4-B7	2.266(6)	2.252(3)	2.240(9)	2.209(13)	2.2962(19)	2.216(3)
Ru4-B3	2.286(6)	2.291(3)	2.288(10)	2.292(9)	2.380(2)	2.236(3)
Ru4-C40	2.331(5)	2.330(3)	2.327(8)	2.327(5)	2.4273(19)	2.184(3)
Ru4-C41	2.214(5)	2.235(3)	2.231(8)	2.226(5)	2.2528(18)	2.108(3)
Ru4-C42	2.203(5)	2.250(3)	2.248(8)	2.229(5)	2.2356(18)	2.096(3)
Ru4-C43	2.215(5)	2.232(3)	2.227(8)	2.229(5)[e]	2.2664(17)	2.108(3)
Ru4-C44	2.206(4)	2.212(3)	2.207(8)	2.226(5)[f]	2.2035(16)	2.114(3)
Ru4-C45	2.303(4)	2.324(3)	2.319(8)	2.327(5)[g]	2.2310(18)	2.181(3)
C40-C41	1.414(7)	1.437(4)	1.433(13)	1.429(7)	1.386(3)	1.420(3)
C41-C42	1.391(8)	1.402(4)	1.440(12)	1.403(7)	1.436(3)	1.405(4)
C42-C43	1.375(8)	1.402(4)	1.397(11)	1.412(11)	1.435(2)	1.401(4)
C43-C44	1.400(8)	1,408(4)	1.420(12)	1.403(7)[h]	1.433(3)	1.403(4)
C44-C45	1.432(7)	1.436(4)	1.423(12)	1.429(7)[i]	1.431(3)	1.414(4)
C45-C40	1.437(7)	1.434(4)	1.449(11)	1.441(9)	N/A	1.417(4)
τ[j]	67.7	-48.1	47.2	±45.9	N/A	N/A
χ[k]	7.0	4.1	6.0	7.0	N/A	5.1

[a] For **15** the three additional C-C cyclooctatriene bond lengths are C45-C46 = 1.515(3) Å, C46-C47 = 1.517(3) Å and C40-C47 = 1.513(3) Å.

[b] For **16** the metal is Fe, not Ru.

[c] For **11** and **16** X = C, Y = B; for **12** and **14** X = Y = B; for **13** X = B, Y = C.

[d] Ru4-B10 = Ru4-B6 by symmetry.

[e] Ru4-C43 = Ru4-C42 by symmetry.

[f] Ru4-C44 = Ru4-C41 by symmetry.

[g] Ru4-C45 = Ru4-C40 by symmetry.

[h] C43-C44 = C41-C42 by symmetry.

[i] C44-C45 = C40-C41 by symmetry.

[j] τ is the torsion angle A-B-Ru4-C1 where A is the midpoint of C40-C44 and B is the centroid of the metal bound C_6 ring.

[k] χ is the dihedral angle between the metal bound C_6 ring and B5B9B12B13B8 least-squares planes.

Table 3.11.2 Selected molecular dimensions (Å, º) in twelve vertex compounds **9** and **10**.

	9	**10**
Ru3-C1	2.1700(13)	2.176(4)
Ru3-C2	2.1517(13)	2.195(4)
Ru3-B4	2.3040(15)	2.201(4)
Ru3-B7	2.2039(15)	2.210(4)
Ru3-B8	2.2217(15)	2.221(4)
Ru3-C30	2.3033(13)	2.265(4)
Ru3-C31	2.2395(14)	2.226(4)
Ru3-C32	2.2217(14)	2.206(4)
Ru3-C33	2.2060(14)	2.209(4)
Ru3-C34	2.2038(14)	2.224(4)
Ru3-C35	2.2696(13)	2.256(4)
C30-C31	1.432(2)	1.401(7)
C31-C32	1.410(2)	1.406(6)
C32-C33	1.418(2)	1.407(6)
C33-C34	1.411(2)	1.399(6)
C34-C35	1.434(2)	1.440(7)
C35-C30	1.4408(19)	1.435(7)
τ^a	47.9	N/A
χ^b	1.0	3.1

[a] τ is the torsion angle A-B-Ru4-C where A is the midpoint of C40-C44, B is the centroid of the C_5 ring and C is the midpoint of C1-C2.

[b] χ is the dihedral angle between C_5 and B5B6B9B11B12 least-squares planes.

The bound naphthalene ligands - as for the bound indenyl ligand - show longer bridging carbon atoms to metal bonds relative to the non-bridging carbon atoms to metal bonds. In all the naphthalene compounds the Ru-C40 and Ru-C45 bond distances are longer than the Ru-41, Ru-C42, Ru-C43 and Ru-C44 bond lengths by about 0.03 - 0.13 Å.

The bridging carbon atoms to metal bonds of **16** are also longer than the non-bridging carbon atoms to metal bonds, although this is probably just a result of a steric interaction between the cage and the reduced non-bound ring of the naphthalene which is no longer planar. Examination[13] of other compounds with metal bound tetrahydronaphthalene or tetrahydroindenyl ligands shows no clear pattern of bridging carbon atoms to metal bonds being longer than non-bridging carbon atoms to metal bonds, whereas the indenyl cobaltacarboranes/naphthalene ruthenacarboranes clearly do show this pattern.

As in chapter two, an examination of the lengths of the B-B connectivities in the thirteen vertex species reveals B2-B5 and B3-B5 to be significantly longer than the other B-B connectivities, as can be seen in table 3.11.3. For **14**, the crystallographic disorder makes measurement of these connectivities lengths somewhat unreliable, as was the case for compound **5**.

Table 3.11.3 Lengths (Å) of connectivities B2-B5 and B3-B5 compared to next longest B-B connectivity in compounds **11**-**13**, **15** and **16**.

Compound	B2-B5	B3-B5	Next longest B-B connectivity
11	2.067(9)	2.025(9)	1.916(10)
12	2.014(5)	1.996(4)	1.884(4)
13	2.003(13)	2.024(14)	1.917(14)
15	2.061(3)	1.994(3)	1.906(3)
16	2.049(5)	1.990(5)	1.902(5)

Coordination of the naphthalene ligand causes a localisation of four π-electrons in the non-bound ring into two essentially double bonds between C45-C46 and C47-C48, as seen by the relatively shorter distances of these two bonds in table 3.11.4.

Table 3.11.4 Lengths of C-C bonds (Å) in unbound six-membered naphthalene ring in all crystallographically studied naphthalene compounds.

Compound	C40-C45	C45-C46	C46-C47	C47-C48	C48-C49	C49-C40
9[a]	1.4408(19)	1.439(2)	1.360(2)	1.427(2)	1.360(2)	1.4356(19)
11	1.437(7)	1.421(7)	1.294(9)	1.400(9)	1.392(9)	1.441(7)
12	1.434(4)	1.430(4)	1.355(4)	1.418(4)	1.355(4)	1.429(4)
13	1.449(11)	1.432(12)	1.335(11)	1.418(13)	1.369(12)	1.437(12)
14[b]	1.441(9)	1.426(7)	1.354(7)	1.413(11)	1.354(7)	1.426(7)

[a] For **9**, C40 and C45-49 = C30 and C35-39 respectively.

[b] For **14**, C45-C46 = C49-C40 and C46-C47 = C48-C49 by symmetry.

3.12 Naphthalene Orientations

In chapter two the crystallographically determined indenyl orientations in cobaltacarboranes were compared to the DFT calculated naphthalene orientations in ferracarboranes. As noted, comparison of these two results is compromised somewhat by the fact that the indenyl ligand in a thirteen vertex indenyl metallacarborane is a five-membered ring over a six-membered face, while the naphthalene ligand in a thirteen vertex metallacarborane is a six-membered ring over a six-membered face. The observed orientations in the naphthalene ruthenacarboranes should be more comparable with the computed orientations in the naphthalene ferracarboranes, although there is still a difference in the metal used. As in chapter two, the naphthalene orientation is defined by τ which is the torsion angle A-B-Ru-C1, where A is the midpoint of the C40-C45 bond, and B is the centroid of the naphthalene metal bound C_6 ring. Figure 3.12.1 shows the measured naphthalene orientations in the various compounds.

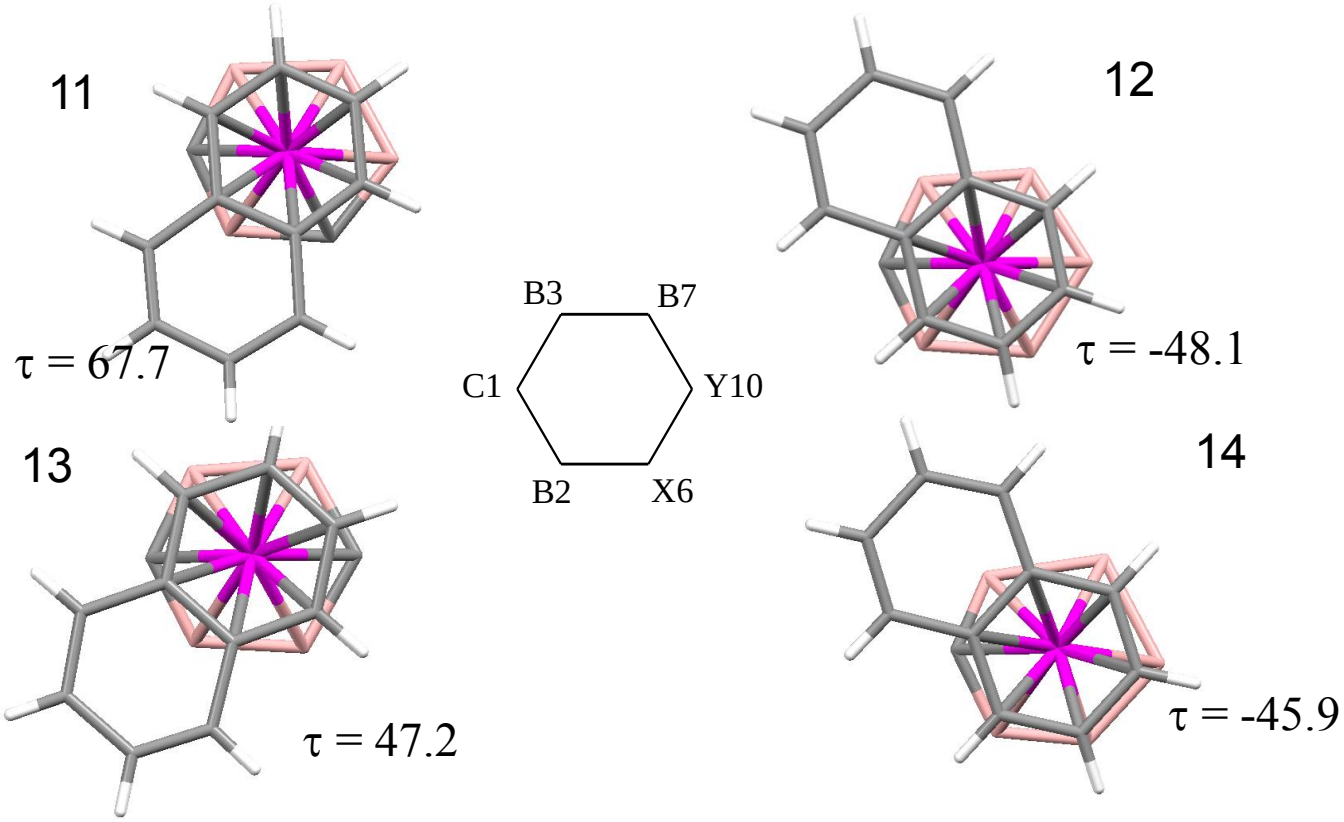

Figure 3.12.1 The naphthalene orientations in compounds **11**-**14** viewed perpendicular to the metal bound C_6 indenyl ring and projected onto a common view of the C1B2C6Y10B7B3 carborane ligand face (for **11** X = C, Y = B; for **12** and **14** X = Y = B; for **13** X = B, Y = C).

The τ value for **11** is 67.7°, representing a staggered conformation of naphthalene/carborane faces (for energy profiles see figures 2.12.2 and 2.12.4 - 2.12.6 from chapter two). The τ value corresponding to the lowest energy conformation for 4-(η-$C_{10}H_8$)-4,1,6-*closo*-$FeC_2B_{10}H_{12}$ is about 54°, which is moderately in agreement with the observed value for **11**.

The τ value for **12** is -48.1° which is in good agreement with the second lowest energy conformation of 4-(η-$C_{10}H_8$)-4,1,8-*closo*-$FeC_2B_{10}H_{12}$ at $\tau \approx -51°$. The lowest and second lowest energy conformations are only separated by ~ 0.8 $kcal^{-1}$ which is within the range of crystallographic packing forces. The orientation corresponding to the second lowest energy conformation was also observed in compound **II** (section 2.12).

The naphthalene orientation observed in **13** is a staggered one which serves to place C40/C45 roughly trans to B7. The τ value for **13** is 47.2°, which fits well with the second of three equally stable energy minima of 4-(η-$C_{10}H_8$)-4,1,10-*closo*-$FeC_2B_{10}H_{12}$ at about $\tau = 0°$, 50° and 120° (although as noted in 2.12 the energy profile is relatively shallow and dominated by energy minima for the staggered conformations and energy maxima for the eclipsed conformations).

The crystallographic disorder present in **14** means that the τ value can be descrided as either 45.9° or -45.9°. The lowest energy conformations in 4-(η-$C_{10}H_8$)-4,1,12-*closo*-$FeC_2B_{10}H_{12}$ are at roughly $\tau = -131°$ and $\tau = -23°$, and the second lowest energy conformation is at roughly $\tau = 22°$. The disorder in **14** means that there is a mixture of staggering and eclipsing between the naphthalene ligand and the cage. This makes comparison of the observed structure with that of 4-(η-$C_{10}H_8$)-4,1,12-*closo*-$FeC_2B_{10}H_{12}$ difficult with any real confidence beyond noting that the τ values of 45.9° and -45.9° are moderately close to the minima at roughly $\tau = 20°$ and -20° respectively.

Compounds **1** and **11** (4,1,6-) have τ values separated by 31.6°, quite distinct from one another, but both moderately close to the calculated lowest energy conformation. Compounds **II** and **12** (Me-4,1,8-/4,1,8-) have τ values in good agreement with each other, differing by only 6.6° and both being in good agreement with the calculated second lowest energy conformation.

Compounds **7** and **13** (4,1,10-) have very distinct τ values from one another, being separated by 47.8°. A possible explanation for this is that the indenyl ligand is not as likely to adopt a staggered conformation, (as seen by the naphthalene ligand) as regardless of the orientation there will be some degree of eclipsing. The disorder present in **5** and **14** (4,1,12-) makes comparison of their τ values difficult, although the magnitude of the two values is similar (±39.3 for **5** vs ±45.9 for **14**).

The τ value for twelve vertex **9** (see figure 3.12.2) of 47.9° (τ is defined as the torsion angle A-B-Ru3-D, where A and B are defined as above and D is the centroid of the C1-C2 connectivity), is comparable to the τ value found for 3-(η-C_9H_7)-3,1,2-*closo*-$CoC_2B_9H_{11}$ (τ = 28.4°) and (η-$C_{10}H_8$)Fe($Et_2C_2B_4H_4$) (τ = 43.7°).

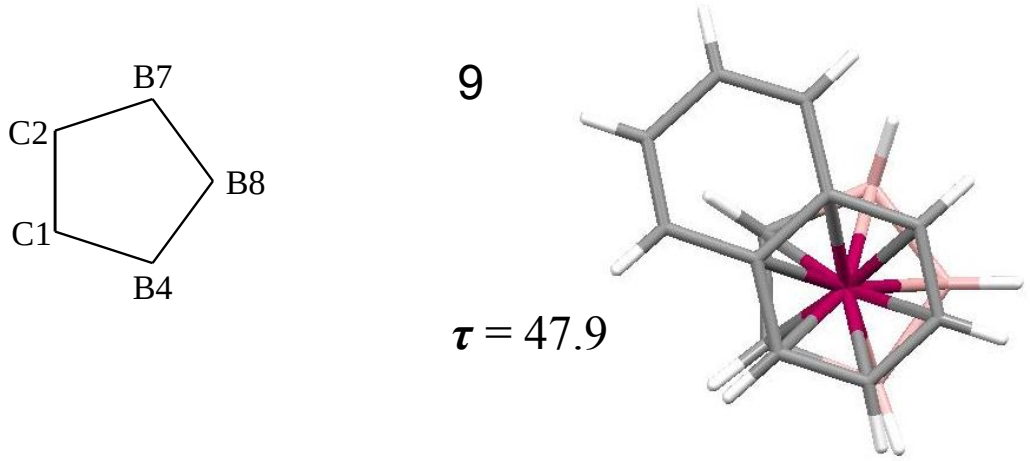

Figure 3.12.2 The naphthalene orientation in compound **9** viewed perpendicular to the metal bound C_6 indenyl ring and projected onto a common view of the C1C2B7B8B4 carborane ligand face.

The greater similarity between the iron and the ruthenium compounds than between the ruthenium and the cobalt compounds is possibly because **9** and (η-$C_{10}H_8$)Fe($Et_2C_2B_4H_4$) have a six-membered ring over a five-membered face, while 3-(η-C_9H_7)-3,1,2-*closo*-$CoC_2B_9H_{11}$ has a five-membered ring over a five-membered face.

3.13 Discussion of unexpected compounds

The isolation of **10** was unexpected, as it was assumed that only **9** would be formed in the reaction. It is not clear whether the EtPh group is formed from the cyclooctadiene (COD) ligand or the naphthalene (figure 3.13.1).

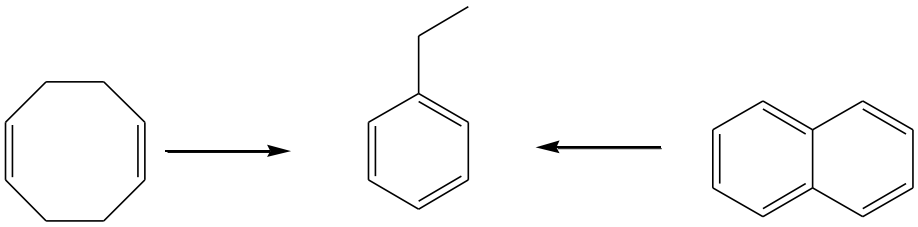

Figure 3.13.1 Alternative sources of EtPh.

The former case would involve cleavage of a single C-C bond then the reformation of a single C-C bond accompanyed by oxidation of a C-C bond. It might be thought that the latter case would involve cleavage of two aromatic C-C bonds, but it is possible that the cleavage occurs after the naphthalene becomes bound to the metal. As seen in table 3.11.5, metal coordination causes a degree of localisation of the π-electron density into C36-C37 and C38-39, leaving C35-36 and C37-38 (the bonds that would need to be cleaved to give EtPh) essentially single bonds.

A previous example of a ruthenacarborane cleaving the bonds in an aromatic ring is seen in the reaction of reduced 1,1′-bis(*o*-carborane) with $[RuCl_2(p\text{-cymene})]_2$, which led to cleavage of one of the *p*-cymene groups instead of formation of the expected $((arene)Ru)_2$bis-carborane.[14]

In order to establish which ring (COD or naphthalene) is the source of the EtPh, the reaction would need to be repeated with a labelled naphthalene ligand such as dimethyl naphthalene, or in the absence of naphthalene. The fact that no EtPh was observed during the reaction using $Li_2[7,8\text{-}nido\text{-}C_2B_9H_{11}]$, but that it was the major product in the reaction using $Tl[TlC_2B_9H_{11}]$, suggests that the carborane source is also an important factor in the reaction. There were no supraicosahedral EtPh species observed during the reduction/metallation of $C_2B_{10}H_{12}$, where $Na_2[7,9\text{-}nido\text{-}C_2B_{10}H_{12}]^{2-}$ is the carborane source, and the dithallium salt of this compound is not known.

The reaction affording **15** was performed in an attempt to make [4,4′-Ru-(1,6-*closo*-$C_2B_{10}H_{12})_2]^{2-}$ (figure 3.13.2), as it was suspected that this sandwich compound may have been being formed in competition with 4-(η-$C_{10}H_8$)-4,1,6-*closo*-$RuC_2B_{10}H_{12}$ during the reaction with excess naphthalene and one equivalent of $[RuCl_2(COD)]_x$.

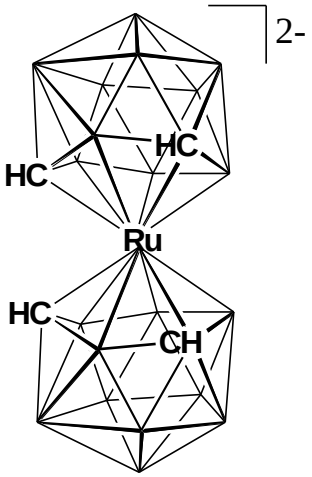

Figure 3.13.2 Proposed structure of [4,4′-Ru-(1,6-*closo*-$C_2B_{10}H_{12})_2]^{2-}$

It was thought that this would proceed by a second reduced carborane, rather than naphthalene, displacing the COD ligand, thus perhaps explaining the low yields of **11** and **13**. We hoped that using no excess naphthalene and only half an equivalent of $[RuCl_2(COD)]_x$ would lead to only the sandwich compound being formed. Upon attempting to precipitate the sandwich compound from ethanol using [BTMA]Cl or NEt_4Cl, it was established that the precipitate did not contain any of the desired [4,4′-Ru-(1,6-*closo*-$C_2B_{10}H_{12})_2]^{2-}$ anion. The precipiate and the filtrate were combined, then the solvent removed under vacuum and the resulting brown solid subjected to chromatography, ultimately yielding **15**.

Oxidation of the COD ligand has occurred instead of coordination of a second carborane ligand, presumably meaning that formation of [4,4′-Ru-(1,6-*closo*-$C_2B_{10}H_{12})_2]^{2-}$ is somewhat unfavourable. Exactly how this oxidation has taken place is not known. There are some COT ferracarborane compounds known (such as (η^6-C_8H_{10})Fe(2,3-$Et_2C_2B_4H_4$)[12] and (η^6-C_8H_{10})Fe(2,3-$Et_2C_2B_4H_3$-5-Br)),[15] however **15** is believed to be the first example of a COT ruthenacarborane, and it is also the first supraicosahedral compound to contain this exo-polyhedral ligand.

The procedure to make **16** was similar to that used to make (η-$C_{10}H_8$)Fe($Et_2C_2B_4H_4$) (see 3.1), only using [7,9-*nido*-$C_2B_{10}H_{12}]^{2-}$ as the carborane source instead of *nido*-$[Et_2C_2B_4H_5]^-$. When the larger carborane is used the naphthalene is reduced to tetrahydronaphthalene during the reaction. This also occurs in the reaction between (η-C_8H_{10})Fe($Et_2C_2B_4H_4$), naphthalene, Al and $AlCl_3$ in methanol/water, giving (η-$C_{10}H_{12}$)Fe($Et_2C_2B_4H_4$) as the product[4] (see figure 3.13.3).

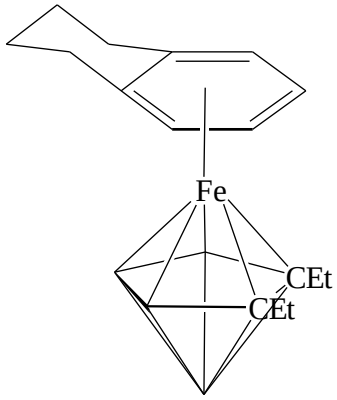

Figure 3.13.3 Structure of (η-$C_{10}H_{12}$)Fe($Et_2C_2B_4H_4$)

The reaction yielding **16** was retried with *nido*-$[C_2B_{10}H_{13}]^-$ as the carborane source, but this only led to smaller amounts of **16** being formed than when the dianion was used. The fact that [7,9-*nido*-$C_2B_{10}H_{12}]^{2-}$ proceeds to the tetrahydronaphthalene product while *nido*-$[Et_2C_2B_4H_5]^-$ proceeds to the naphthalene product under the same reaction conditions is possibly due to the increased reducing potential of the larger *nido*-carborane. The reaction to make (η-$C_{10}H_8$)Fe($Et_2C_2B_4H_4$) from (η-C_8H_{10})Fe($Et_2C_2B_4H_4$) and naphthalene at 200°C was not attempted with 4-(η-C_8H_{10})-4,1,6-*closo*-$FeC_2B_{10}H_{12}$ as it was anticipated that this compound would only be able to be synthesised in a low yield, if at all.

3.14 Summary

One twelve and four thirteen vertex naphthalene ruthenacarboranes were synthesised and characterised. Metallation of $[C_2B_9H_{11}]^{2-}$ gave **9** when the dilithium salt was used, and **9** and **10** when the dithallium salt was used. Reduction/metallation of 1,2-*closo*-$C_2B_{10}H_{12}$ gave the 4,1,6- compounds **11** and **15**, the former of which was isomerised to the 4,1,8- isomer (**12**). Reduction/metallation of 1,12-*closo*-$C_2B_{10}H_{12}$ gave the 4,1,10- compound (**13**), which was isomerised to the 4,1,12- isomer (**14**). A thirteen vertex tetrahydronaphthalene ferracarborane (**16**) was also prepared in low yield by the metallation of reduced *o*-carborane with $Li_2[C_{10}H_8]/FeCl_2$.

The *X*-ray structures of **11**, **13** and **14** show similarities to those of the *p*-cymene/C_6R_6 (R = H, Me) analogues with respect to the cage portion of the molecules and, as in chapter two, all the naphthalene compounds studied clearly demonstrate the structural naphthalene effect.

Compound **12** is only the second 4,1,8- thirteen vertex metallacarborane reported which does not have Co as the metal, the first being 1,8-Ph_2-4-(*p*-cymene)-4,1,8-*closo*-$RuC_2B_{10}H_{10}$, which was made by the thermolysis of 1,6-Ph_2-4-(*p*-cymene)-4,1,6-*closo*-$RuC_2B_{10}H_{10}$ at 180^{o}C.[10b] (The same work reports that 4-(*p*-cymene)-4,1,6-*closo*-$RuC_2B_{10}H_{12}$ also undergoes isomerisation to the 4,1,8- isomer at 180^{o}C (but not in refluxing toluene), but the structure of the 4,1,8- compound is yet to be published). An explanation for the fact that the 4,1,6- naphthalene compound isomerises at a lower temperature may be that the cage is less electron rich than the cage in the *p*-cymene analogue, as there is a degree of slippage of the naphthalene ligand from η^6 to η^4 (thus making it more similar to a 4,1,6- cobaltacarborane cage, which readily undergoes isomerisation).

As with the indenyl compounds in chapter two, the naphthalene orientations in the thirteen vertex ruthenacarboranes were compared to the DFT calculated potential energy profiles for rotation of the naphthalene ligand about the metal-cage axis in the compounds 4-(η-$C_{10}H_8$)-4,1,X-*closo*-$FeC_2B_{10}H_{12}$ (X = 6, 8, 10 and 12). The observed τ values again mostly fitted only moderately well with the calculated τ values, with the possible reasons for the discrepancies being related to those given in section 2.13, although perhaps with more emphasis on the shallowness of the potential energy profiles, as the synthesised and

model compounds are more similar (both have a six-membered ring above a six membered ring, but the metal is still different).

Upon dimethylation the τ values of the ruthenium naphthalene compounds would likely change in a similar way to those of the indenyl cobalt compounds, with the naphthalene ligand either inclining or rotating away from a steric interaction with the methyl groups.

Compound **10** is the first example of a metallacarborane containing an exo-polyhedral EtPh ligand, and demonstates the catalytic potential of metallacarboranes, as the EtPh ligand must come from either re-arrangement of COT or abstraction of a C-C unit from naphthalene.

The exo-polyhedral ligands in compounds **15** and **16** have been reported before in the metallacarborane literature, however these compounds are the first supraicosahedral examples to have their respective exo-polyhedral ligands.

3.15 References

3.1 For example: M. Crocker, M. Green, J.A.K. Howard, N.C. Norman and D.M. Thomas, *J. Chem. Soc., Dalton Trans.*, 1990, 2299; N.P. Do Thi, S. Spichiger, P. Paglia, G. Bernardinelli, E.P. Kundig and P.L. Timms, *Helv. Chim. Acta*, 1992, **75**, 2593; H. Kubo, M. Hirano and S. Komiya, *J. Organomet. Chem.*, 1998, **556**, 89; G. Zhu, K. E. Janak, J. S. Figueroa and G. Parkin, *J. Am. Chem. Soc.*, 2006, **128**, 5452; M. Kaftory, *Acta Crystallogr., Sect. B: Struct. Crystallogr. Cryst. Chem.*, 1980, **36**, 2971; T.G. Gardner and G.S. Girolami, *Angew. Chem., Int. Ed.*, 1988, **27**, 1693; P.A. Wender and T.J. Williams, *Angew. Chem., Int. Ed.*, 2002, **41**, 4550.

3.2 M.P. Garcia, M. Green, F.G.A. Stone, R.G. Somerville, A.J. Welch, C.E. Briant, D.N. Cox and D.M.P. Mingos, *J. Chem. Soc., Dalton Trans.*, 1985, 2343.

3.3 C.G. Salentine and M.F. Hawthorne, *J. Am. Chem. Soc.*, 1975, **97**, 6382.

3.4 R.G. Swisher, E.Sinn and R.N. Grimes, *Organometallics*, 1985, **4**, 896.

3.5 J.T. Spencer and R.N. Grimes, *Organometallics*, 1987, **6**, 323.

3.6 (a) D. Ellis, unpublished results, Heriot-Watt University, 2009.

(b) B. Štíbr, M. Bakardjiev, J. Holub, A. Růžlčka and M. Kvíčalově, *Inorg. Chem.*, 2009, **48**, 10904.

3.7 A. Burke, D. Ellis, D. Ferrer, D.L. Ormsby, G.M. Rosair and A.J. Welch, *Dalton Trans*., 2005, 1716.

3.8 M.A. Bennett, T.N. Huang, T.W. Matheson and A.K. Smith, *Inorg. Synth.*, 1982, **21**, 74.

3.9 (a) J.G. Planas, C. Viñas, F. Teixidor, M.E. Light, M.B. Hursthouse and H.R. Ogilvie, *Eur. J. Inorg. Chem.*, 2005, 4193.

(b) M. Bown, X.L.R. Fontaine, N.N. Greenwood, J.D. Kennedy, J. Plešek, B. Štíbr and M. Thornton-Pett, *Acta. Crystallogr., Sect. C: Cryst. Struct. Commun.*, 1990, **46**, 995; M. Bown, J. Plešek, K. Baše, B. Štíbr, X.L.R. Fontaine, N.N. Greenwood and J.D. Kennedy, *Magn. Reson. Chem.*, 1989, **27**, 947.

(c) M.E. Lopez, M.J. Edie, D. Ellis, A. Horneber, S.A. Macgregor, G.M. Rosair and A.J. Welch, *Chem.Commun.*, 2007, 2243; J. Cowie, B.D. Reid, J.M.S. Watmough and A.J. Welch, *J. Organomet. Chem.*, 1994, **481**, 283.

3.10 (a) D. Ellis, M.E. Lopez, R. McIntosh, G.M. Rosair, A.J. Welch and R. Quenardelle, *Chem, Commun.*, 2005, 1348.

(b) S. Zlatagorsky, D. Ellis, G.M. Rosair and A.J. Welch, *Chem. Commun.*, 2007, 2178.

3.11 A. McAnaw, G. Scott, L. Elrick, G.M. Rosair and A.J. Welch, *Dalton Trans.*, 2013, **42**, 645.

3.12 R.B. Maynard, R.G. Swisher, R.N. Grimes, *Organometallics*, 1983, **2**, 500.

3.13 F.H. Allen, *Acta Crystallogr., Sect. B: Struct. Sci.*, 2002, **B58**, 380. For this study we used CSD Version 5.33 (November 2011).

3.14 D. Ellis, D. McKay, S.A. Macgregor, G.M. Rosair and A.J. Welch, *Angew. Chem. Int. Ed.*, 2010, **49**, 4943.

3.15 K.E. Stockman, D.L. Garrett and R.N. Grimes, *Organometallics*, 1995, **14**, 4661.

Chapter 4
Exo-Polyhedral Ligand Orientations

4.1 Introduction

In chapters two and three the relative weakness of the bridging carbon to metal bonds in indenyl and naphthalene ligands in metallacarboranes was measured by comparing the lengths of these bonds to the non-bridging carbon to metal bonds, and was maximised by the bridging carbons being trans to cage boron atoms. For metallacarboranes, the naphthalene/indenyl ligands will have longer bridging carbon to metal bonds (relative to non-bridging carbon to metal bonds) regardless of whether they are trans to cage boron or carbon atoms (the structural indenyl/naphthalene effect). However it seems likely that the atoms of an exo-polyhedral ligand which is a non-fused aromatic ring would show selective bond lengthening/shortening based exclusively on which part of the carborane cage they were trans to. It follows from this that identical ligands (as part of an Exo-Polyhedral Ligand (EPL) set (for example ML_3)) would have different metal to ligand bond lengths if one was trans to a cage boron atom and the other trans to a cage carbon atom.

Having established in the indenyl/naphthalene work that weak metal to exo-polyhedral ligand (M-EPL) bonding is compensated by strong metal to cage bonding, we wished to see whether strong M-EPL bonding would be compensated by weak metal to cage bonding. To probe this we initially looked at ML_2L' EPL sets and tried to rationalise the Exo-polyhedral Ligand Orientation (ELO) based on the relative trans influences[1a-i] of the ligands L/L′. It seems likely that the ligand or ligands with the stronger trans influence within the ML_2L' EPL set would be more likely to be trans to the part of the cage with the weakest trans influence (for example cage carbon over cage boron), while the ligand or ligands with the weaker trans influence would be more likely to be trans to the part of the cage with the strongest trans influence.

In order to probe the relative M-EPL bond lengths an initial search of the Cambridge Structural Database (CSD)[2] was carried out for 3-(X)-3,1,2-*closo*-$MC_2B_9H_{11}$ (X = Cp/Cp*/arene) and 3,3,3-$(L)_3$-3,1,2-*closo*-$MC_2B_9H_{11}$ compounds (table 4.1.1). This icosahedral 3,1,2- architecture was chosen as a starting point for several reasons: firstly it

represents the largest class of metallacarboranes, and consequently provides the greatest number of crystallographic data; secondly, the upper pentagonal belt gives a relatively weak cage to metal bonding section (the two carbon atoms) and a relatively strong cage to metal bonding section (the three boron atoms)[3], all of which are degree five vertices; lastly, the unsubstituted cage means that there is no significant steric interaction between the cage and the EPLs to compromise the significance of the M-EPL bond lengths/ELOs, or to change the trans influences of the cage atoms by disrupting them electronically. For example in the compound 1,2-(*o*-xylylene)-3,3-$(PPh_3)_2$-3-(H)-3,1,2-$RhC_2B_9H_9$ (CIDHAY) - shown in figure 4.1.1 - the ELO is presumably determined by a necessity to avoid the steric interaction between the bulky phosphine groups and the *o*-xylylene tether.

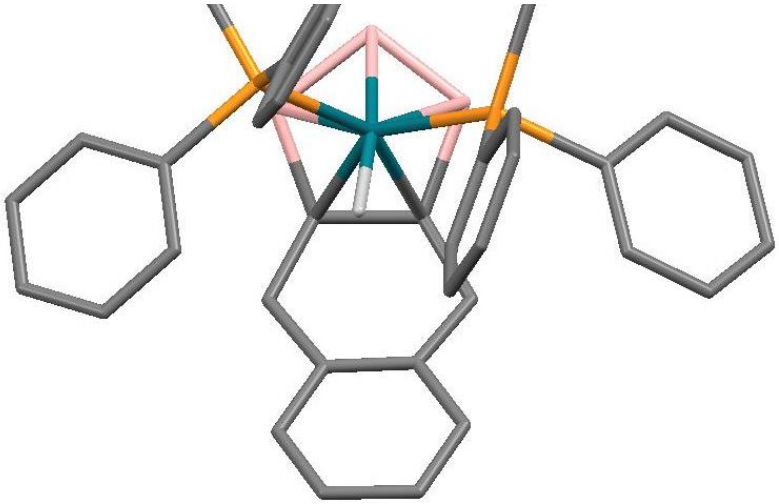

Figure 4.1.1 Structure of CIDHAY, 1,2-(*o*-xylylene)-3,3-$(PPh_3)_2$-3-(H)-3,1,2-$RhC_2B_9H_9$ (lower belt omitted for clarity).

In the absence of this tether the ELO would be predicted to be at ~180^o to the one shown in figure 4.1.1, with the hydride ligand trans to the carbon part of the cage (see section 4.6).

Only compounds with formally seventeen or eighteen electron count metals are included from the results of the database search in order to maintain consistency and so that the FMOs of the metal/cage interaction will be as similar as possible. Consequently, this necessitates a lack of consistency in the type of metal incorporated into the cage, the oxidation state of the metal and the overall charge of the molecule. This in turn makes comparing the ELOs of two compounds with different metals/oxidation states/charge less reliable than if the same variables were used. However it is necessary both to provide enough compounds for

comparisons to be made, and so that comparisons can be made between, for example, an EPL set with three L type ligands and an EPL set with two L and one X type ligand.

Ta/Nb compounds with π-donor EPLs which can complete an eighteen electron count for the metal are included in the results of the database search. All of these compounds are formally d^0 (see section 4.5) which does not make comparison to the other (formally) d^6/d^8 compounds ideal, but the ELOs/EPL bond lengths of these few (d^0) compounds can be compared to each other to identify any trends.

In order to probe the ELOs, a search was then carried out for other icosahedral and sub/supraicosahedral metallacarboranes, the details of which are listed in table 4.1.1. In compounds with two independent molecules in the asymmetric unit, each molecule is counted as one example.

Table 4.1.1 Results from CSD database search.

Type of compound	Number of examples in CSD	Section
3-R-3,1,2-*closo*-$MC_2B_9H_{11}$ (R = Cp/Cp*/arene)	13	**4.3**
3-R-3,1,2-*closo*-$MC_2B_9H_{11}$ (R = substituted arene/heterocyclic rings/four membered rings)	15	**4.4**
3,3,3-L_3-3,1,2-*closo*-$MC_2B_9H_{11}$	15	**4.5**
3,3-L_2-3-L′-3,1,2-*closo*-$MC_2B_9H_{11}$	42	**4.6**
3-L-3-L′-3-L″-3,1,2-*closo*-$MC_2B_9H_{11}$	7	**4.7**
2-(L_2L′/L_3)-2,1-*closo*-$MCB_{10}H_{11}$	6	**4.8**
2-(L_2L′/Cp/arene)-2,1-*closo*-$MXB_{10}H_{10}$ (X ≠ C)	11	**4.9**
3-(L_2L′$_2$/L_2L′L″/L_3L′)-3,1,2-*closo*-$MC_2B_9H_{11}$	8	**4.10**
2-(L_2L′/LL′L″/Cp/arene)-2,1,7-*closo*-$MC_2B_9H_{11}$	10	**4.11**
Subicosahedral	7	**4.12**
Supraicosahedral	8 + 3*	**4.13**

*Two bimetallic bicapped hexagonal antiprismatic fourteen vertex compounds were found, one which has one M/EPL set with an M-EPL bond trans to a cage carbon atom, and one which has two M/EPL sets with an M-EPL bond trans to a cage carbon atom.

Each class of compound is examined in turn, before a discussion of the limitations/potential applications of the work, and a look at the future of the ELO method. All structures were checked using the Vertex to Centroid Distance (VCD) method[4] to make sure that the cage carbon atom assignments were correct, and to assess whether any cage carbon atom disorder is present. In discussion of examples with incorrectly assigned cage carbon atoms (see appendix two for details), the cage carbon atoms referred to are the correctly (by VCD) assigned ones. Geometry measurements were performed using Mercury.[5]

The numbering scheme for each type of cage is illustrated in figure 4.1.2. All structures are discussed according to these numbering schemes, which are not necessarily those used in the original structures.

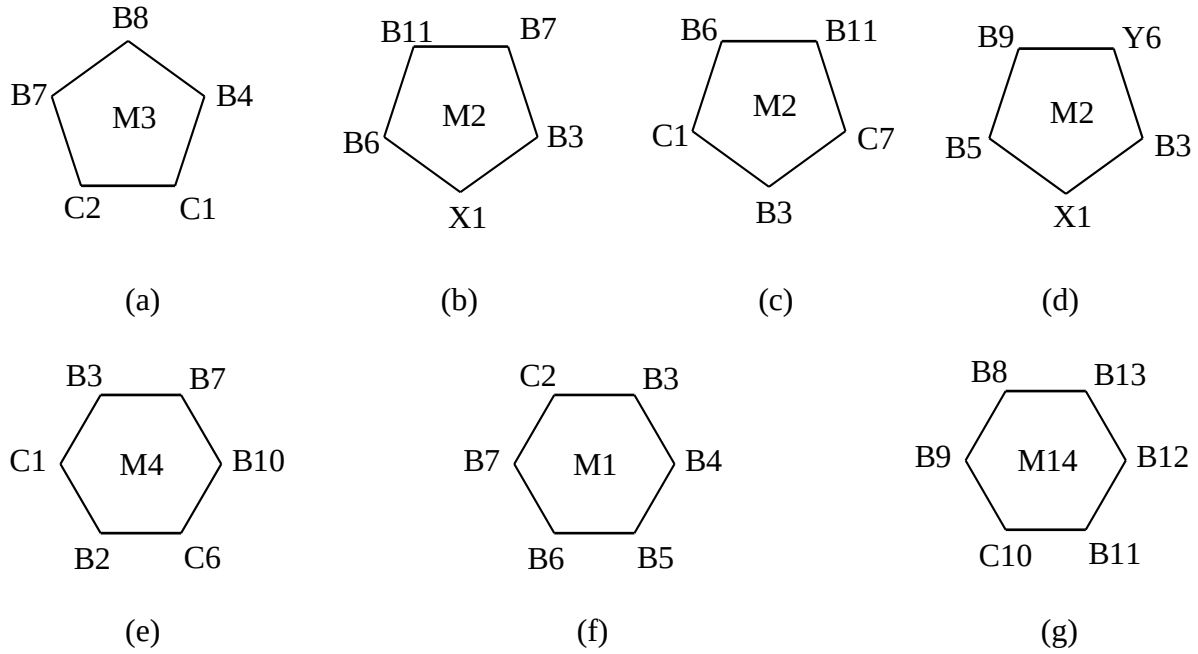

Figure 4.1.2 Numbering scheme for the following cage architectures: (a) 3,1,2-*closo*-$MC_2B_9H_{11}$; (b) 2,1,-*closo*-$MXB_{10}H_{10}$ (X = CH or heteroatom); (c) 2,1,7-*closo*-$MC_2B_9H_{11}$; (d) 2,1,6-$MC_2B_7H_9$ (X = C, Y = B) and 2,1-MXB_8H_8 (X = CH or heteroatom, Y = B); (e) 4,1,6-*closo*-$MC_2B_{10}H_{12}$; (f) 1,14,2,10-*closo*-$M_2C_2B_{10}H_{12}$, top face and (g) 1,14,2,10-*closo*-$M_2C_2B_{10}H_{12}$ bottom face.

In the figures which show a view looking down the M-Cb bond (Cb = centroid of C1C2B7B8B4 or equivalent upper face), the lower belt and antipodal boron of the cage are omitted for clarity. All hydrogen atoms (with the exception of hydride ligands), counter-ions and molecules of solvent have also been omitted from these figures for clarity, and many have been selectively cropped to show only the cage and M-EPL bonds. Formulae and

references for all compounds which are referred to by their CSD code can be found in appendix two.

Compounds HPRHCB and TPNRHB were resynthesised and recrystallised as the original structures were poor (see section 4.14) and our structures are referred to as compounds **V** and **VI** respectively. In addition to this, a structure was determined for the compound 3,3-$(PPh_3)_2$-3-(NO_3)-3,1,2-$RhC_2B_9H_{11}$ (compound **VII**), the synthesis[6] of which (but not the structure) has been reported from compound **VI**.

4.2 Analysis of metal to cage interaction

For d^8 ML_3/ML_2L' metal fragments the interaction of the hybrid s-z orbital with the a′ orbital (see section 1.8) of 7,8-*nido*-$C_2B_9H_{11}$ has no consequences for the orientation of the metal fragment, but the interaction of the degenerate e (ML_3)/a′, a″ (ML_2L') metal orbitals with the carborane orbitals of a′ and a″ symmetry means that one of the four orientations shown in figure 4.2.1 should be observed.

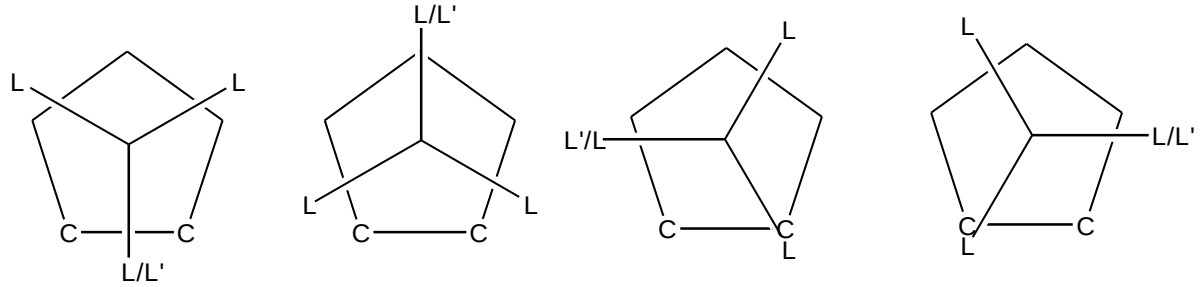

Figure 4.2.1 Theoretical orientations of ML_3/ML_2L' metal fragments above the open face of a 7,8-*nido*-$C_2B_9H_{11}$ carborane.

However, experimentally it is found that slight perturbations from these idealised orientations mean that effectively any orientation can be observed. It seems likely that steric interactions also play a significant role in the orientation of the metal fragment (particularly when the EPLs are bulky), with orientations which minimise eclipsing between the EPLs and the carborane being favoured.

Steric interactions between the EPLs themselves could also play a role in determining the ELO: In the discussion that follows, a ligand is described as being trans to a particular part of the cage only in terms of the torsion angle X-Cb-M-EPL (where X = a point on the upper belt of the cage and Cb = centroid of C1C2B7B8B4 (or the equivalent metal bound carborane face)). When this angle is ~ 180^o the EPL and X are described as being trans (when assigning an EPL as being trans to a cage atom or trans to a cage connectivity, the two torsion angles X-Cb-M-EPL (X = the centroid of the cage connectivity) and X-Cb-M-EPL (X = the cage atom) are compared, with the point on the cage with the angle closer to 180^o being defined as being trans to the EPL).

However, in some cases the angle X-M-EPL is significantly deviated from 180^o (figure 4.2.2), and so the ligand is not trans in all three dimensions. This is particularly prevalent in

the $L_2L'_2/L_2L'L''/L_3L'$ compounds, where there is an extra ligand in the EPL set. While this is then not strictly a trans influence, it is convenient to refer to it as such to aid comparison with other EPL set's ELOs, whilst fully acknowledging that the 'trans' influence may be operating through an orbital which is not directly trans to the influencing ligand.

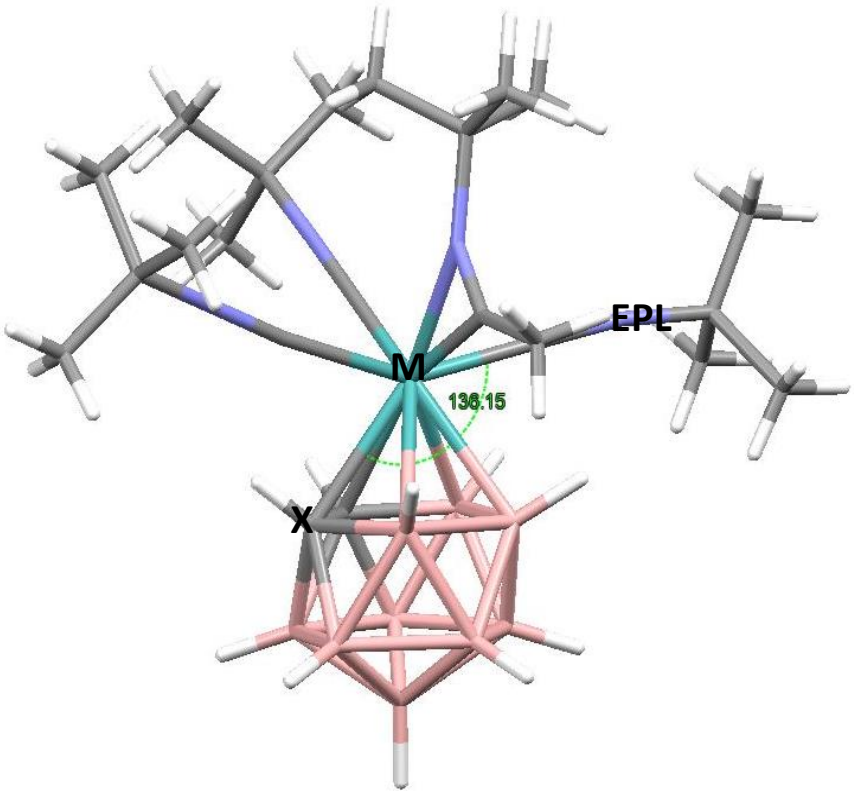

Figure 4.2.2 Structure of WELNEG, [3,3,3-(NC^{t}Bu)$_3$-3-(t-butyliminoethyl-C,N)-3,1,2-$MoC_2B_9H_{11}$][SO_3CF_3]. The angle X-M-EPL (where X = C1) is 136.15^o - significantly less than 180^o (i.e. perfectly trans).

The majority of the 3,1,2- ML_3/ML_2L' compounds discussed in this chapter have an orientation whereby one of the three ligands lies over the cage C-C connectivity and is trans to a boron atom/B-B connectivity. This ligand's M-EPL bond lies within the 'boundary' of the C-C connectivity when looking down the M-Cb axis (i.e. the torsion angle defined by Y-Cb-M-L_{EPL}, where Y = the centre of the C-C bond, does not exceed the angle Y-Cb-C_{cage}).

This approximate orientation is relatively staggered: as the ligand over the C-C connectivity is rotated round beyond the angle Y-Cb-C_{cage} the other two ligands are forced into eclipsing interactions with B8 and B4 or B7. However, this orientation is not exclusively observed in 3,1,2- compounds, as will be discussed in section 4.5, and for the compounds where the cage

does not have a 3,1,2- architecture the situation is more complicated due to non-adjacency of the cage carbon atoms/additional vertices in the open face.

As noted in section 1.8, the ELO of ML_2 compounds is different to that of ML_3/ML_2L' compounds because of a closed shell four electron destabilising interaction.[7] It is therefore not possible to rationalise the orientation based on any trans influence arguments, however in ML_2 compounds where the ligand is a four membered ring (three hits in the CSD), the M-EPL bond lengths of ring atoms trans to the carbon part of the cage can be compared to the M-EPL bond lengths of ring atoms trans to the boron part of the cage.

When ligands of differing trans influences are incorporated into the metal fragment, the components of the orbitals (which are available for bonding to the carborane) which lie trans to strongly trans influencing ligands will be less diffuse than the components of the orbitals which lies trans to weak trans influence ligands (figure 4.2.3). It is the matching of these orbitals with the carborane orbitals to optimise bonding, combined with a rotation away from optimal orbital overlap to minimise steric interactions between the EPLs/cage, which will ultimately determine the ELO.

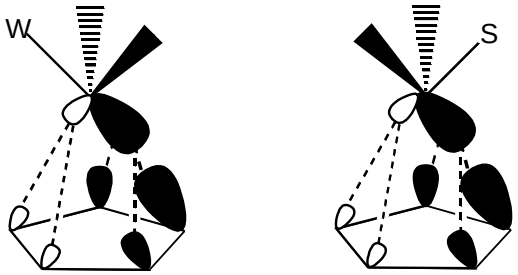

Figure 4.2.3 Pictorial comparison of component of orbital (a) trans to a weak (W) trans influence ligand and (b) trans to a strong (S) trans influence ligand, and their respective interactions with the HOMO of the 7,8-*nido*-$C_2B_9H_{11}$ carborane.

Another factor which may contribute to the ELO is the influence of Crystal Packing Forces (CPFs). The magnitude[8] of these effects can potentially exceed the barrier to rotation of the EPLs, particularly when the EPLs have a similar M-EPL bond strength. [9]

For the purposes of this chapter the ELO will be rationalised exclusively on the principle of trans influences, as the effects of CPFs/steric interactions are not immediately clear, other than to say that presumably EPL/cage eclipsing interactions will be avoided where possible.

4.3 3-R-3,1,2-*closo*-$MC_2B_9H_{11}$ (R = Cp/Cp*/arene)

Examination of this class of compounds shows that for twelve of the thirteen examples the M-EPL bond lengths trans to the carbon part of the cage are shorter than the M-EPL bond lengths trans to the boron part of the cage, though for many of the 3-R-3,1,2-*closo*-$MC_2B_9H_{11}$ (R = Cp/Cp*/arene**)** compounds the differences in bond length maybe negligible when the bond length e.s.d.s are taken into account (see section 4.15). Figure 4.3.1 (a) shows an example of a CoCp compound (DUBDIN01), and figure 4.3.1 (b) shows an example of a Rh(arene) compound (EQUIYAF), along with their respective M-EPL bond lengths.

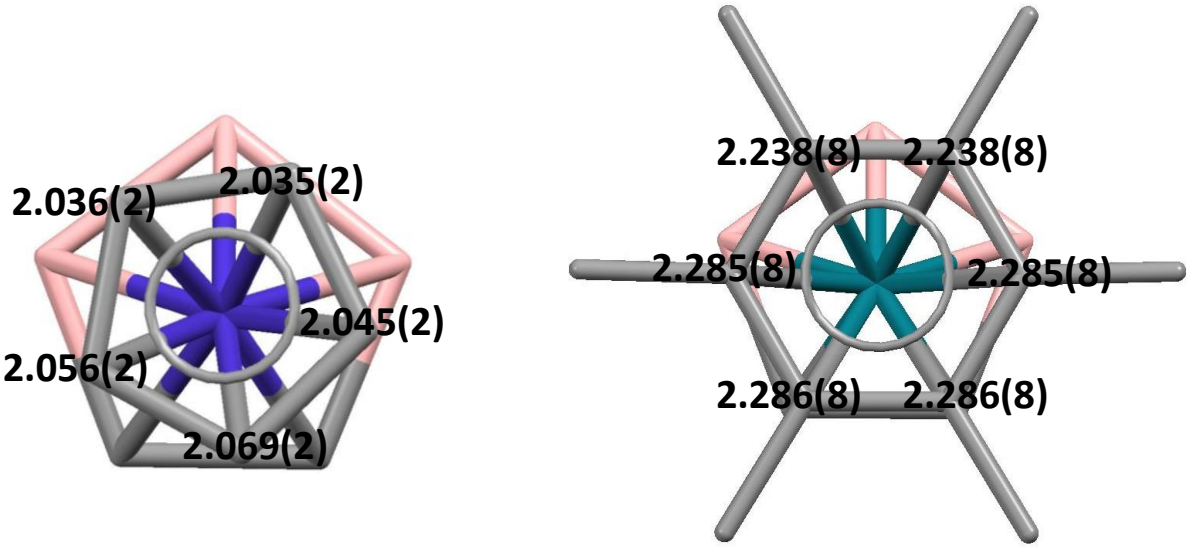

(a) (b)

Figure 4.3.1 Structure and M-EPL bond lengths (Å) of (a) DUBDIN01, 3-(η-C_5H_5)-3,1,2-$CoC_2B_9H_{11}$ and (b) EQUIYAF, [3-(η-C_6Me_6)-3,1,2-$RhC_2B_9H_{11}$][BF_4] (sits on a crystallographic mirror plane).

Seven out of the thirteen examples have crystallographically imposed mirror symmetry, however only one of these seven - LUKKUX, a CoCp* compound - has a mirror plane which goes through B10, M3 and C1, the rest having a mirror plane which goes through the mid-point of the C1-C2 bond, M3 and B10.

The structure which does not follow the trend of M-EPL trans to the boron part of the cage > M-EPL trans to the carbon part of the cage is LULHAB (figure 4.3.2). For this compound, which has disordered cage carbon atoms (C/B), the M-EPL bond trans to a C-B/B

connectivity is shorter (2.169(4) Å) than the two M-EPL bonds (2.177(4) and 2.178(4) Å) which both lie trans to a C-(C/B) connectivity, though the three bonds are all similar lengths.

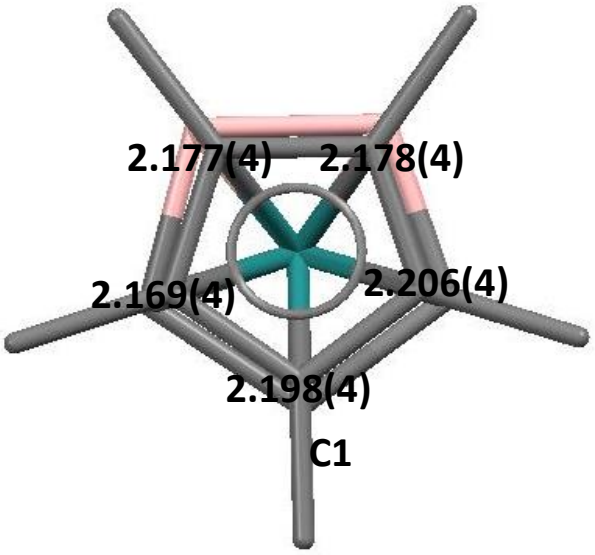

Figure 4.3.2 Structure and M-EPL bond lengths (Å) of LULHAB, $[N(PPh_3)_2][3\text{-}(\eta\text{-}C_5Me_5)\text{-}3,1,2\text{-}RuC_2B_9H_{11}]$.

4.4 3-R-3,1,2-*closo*-$MC_2B_9H_{11}$ (R = substituted arene/heterocyclic rings/four membered rings)

For the compounds with substituted arene EPLs, only the M-EPLs of equivalent ring atoms can be compared. For example figure 4.4.1 shows an Fe(toluene) compound FOTLEF, in which M-C3 can only be compared with M-C7, and M-C4 can only be compared with M-C6. M-C5 and M-C8 have no comparable atoms and so are not considered.

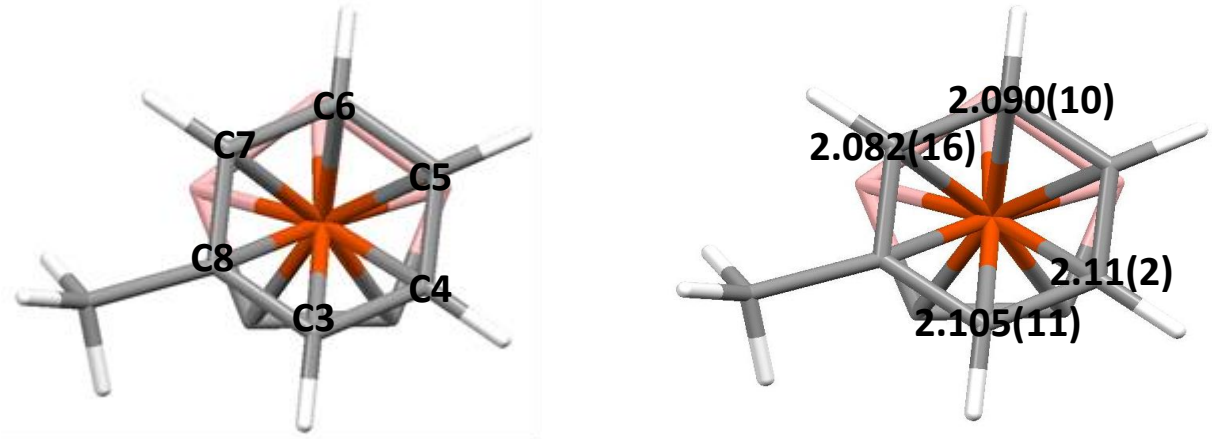

(a) (b)

Figure 4.4.1 (a) Structure with labels and (b) selected M-EPL bond lengths (Å) of FOTLEF, 3-(toluene)-3,1,2-$FeC_2B_9H_{11}$.

As can be seen from figure 4.4.1, the two M-EPL bonds which are trans to the carbon part of the cage (M-C6 is trans to the C-C connectivity, whilst M-C7 is trans to one of the cage carbon atoms) are shorter than the two M-EPL bonds which are trans to the boron part of the cage, though the bonds are all of similar lengths.

The M-EPL bond lengths trans to the carbon part of the cage are shorter than the M-EPL bond lengths trans to the boron part of the cage for eight out of the nine examples found of this class of compound. For the compound FOTLAB, one of the M-EPL bonds which is trans to a cage carbon atom is longer than an M-EPL bond which is trans to a cage boron atom, though the bonds are similar lengths.

Two of the compounds have a disordered cage carbon atom when checked by VCD (BEXLAR and BEXLAR01, both different crystal structures of 3-(mesitylene)-3,1,2-$FeC_2B_9H_{11}$), and the shortest M-EPL bonds are those that are trans to the definite cage carbon

atom and the two C/B disordered vertices (though for BEXLAR the M-CMe bonds are of similar length).

To these nine examples of substituted arenes can be added compounds **9** and **10** from chapter three, as they both display the lengthening of the M-EPL bonds which lie trans to the boron part of the cage relative to the M-EPL bonds which lie trans to the carbon part of the cage.

The exo-polyhedral aromatic rings up to this point have only included carbon atoms, however there are also several examples of compounds with heterocyclic EPLs.

Two such compounds are KAXGEV and KAXGIZ, which along with LOPFUS (see figure 4.4.2), are technically of the EPL type ML_2 (LOPFUS has a four-membered ring but is not heterocyclic). ML_2 compounds, as noted in section 4.2, tend to have a set orientation that for 3,1,2- compounds is that with the plane of the EPL set being parallel to the C-C connectivity, and the ligands being roughly trans to either B4 or B8. However, these compounds with tetramethylcyclobutane and four membered heterocycles as the EPLs allow the comparison of M-EPL bond distances, if care is taken only to compare equivalent atoms. In all three examples of this type of compound the (comparable) M-EPL distances were greater for the ligand atoms trans to the boron part of the cage than the ligand atoms trans to the carbon part of the cage (figure 4.4.2), though for KAXGEV the M-C^{t}Bu bonds are both similar lengths.

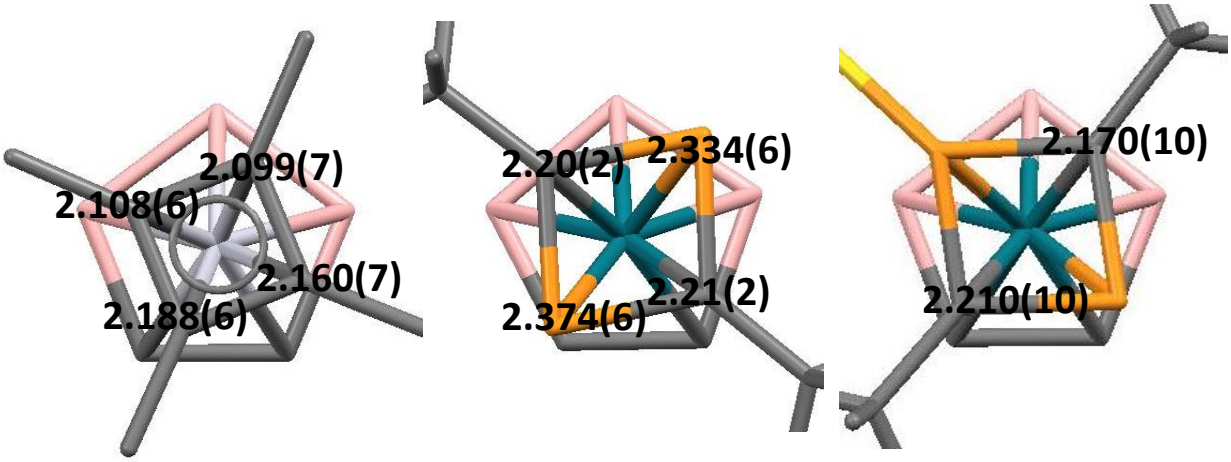

(a) (b) (c)

Figure 4.4.2 Structure and selected M-EPL bond lengths (Å) of (a) LOPFUS, 3-(η-C_4Me_4)-3,1,2-$PtC_2B_9H_{11}$, (b) KAXGEV, [NEt_4][3-(η-$P_2(C^tBu)_2$)-3,1,2-$RhC_2B_9H_{11}$] and (c) KAXGIZ, 3-(η-P(P(Au(PPh_3)))$(CtBu)_2$)-3,1,2-$RhC_2B_9H_{11}$.

Three examples were found which contain a single heteroatom in an exopolyhedral heterocycle, two containing pyrrole type rings (RADCUU and XOQDAI) and one containing a C_5H_5BMe ligand (OPIQOU). In these compounds the M-EPL bond lengths cannot really be compared as the comparable atoms lie almost across a mirror plane and so are trans to equivalent parts of the cage, but the heteroatoms/groups (N vs BMe) have opposite orientational preferences. The N ligands are orientated trans to the unique boron atom of the upper belt, while the BMe group is orientated trans to the C-C connectivity (figure 4.4.3).

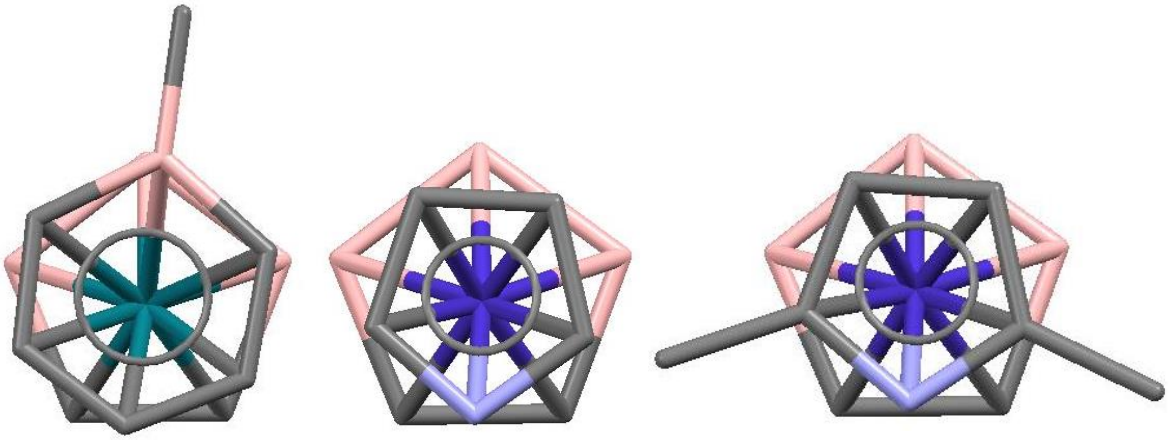

(a) (b) (c)

Figure 4.4.3 Structure of (a) OPIQOU, 3-(η-C_5H_5BMe)-3,1,2-$RhC_2B_9H_{11}$, (b) RADCUU, 3-(η-NC_4H_4)-3,1,2-$CoC_2B_9H_{11}$ and (c) XOQDAI, 3-(2,5-Dimethylpyrrolyl)-3,1,2-$CoC_2B_9H_{11}$.

Nitrogen is a more electronegative element than carbon, so presumably the nitrogen atom has the lowest trans influence of the heterocycle and is thus orientated trans to the boron part of the cage, whereas boron is a less electronegative element than carbon, so presumably the BMe group has the highest trans influence of the heterocycle and is thus orientated trans to the carbon part of the cage. This example is a good illustration of how the ELO is dependent on the relative trans influences of the exo-polyhedral ligands, and is further explored in section 4.6.

4.5 3,3,3-L_3-3,1,2-*closo*-$MC_2B_9H_{11}$

In the case where there are three identical ligands in the EPL set the ligands which are trans to the carbon part of the cage have shorter M-EPL bonds than the ligands which are trans to the boron part of the cage in thirteen out of the fifteen examples. Of the fifteen examples found, five of them are $M(CO)_3$ compounds, nine are species with π-donor ligands and group five metals, and the other one is a Rh(hydrogen tris(1-pyrazolyl)borate) species.

The metal tricarbonyls all adopt an orientation whereby one of the three ligands lies over the cage C-C connectivity and is trans to a boron atom/B-B connectivity. This carbonyl's M-CO bond lies within the 'boundary' of the C-C connectivity, as mentioned in section 4.2. This leaves one carbonyl group trans to a cage carbon atom and the other trans to a C-B connectivity (CSCREC, KISCEU and KOBLOC) or both carbonyl ligands trans to C-B connectivities (MOGSAC). Figure 4.5.1 shows both these approximate orientations.

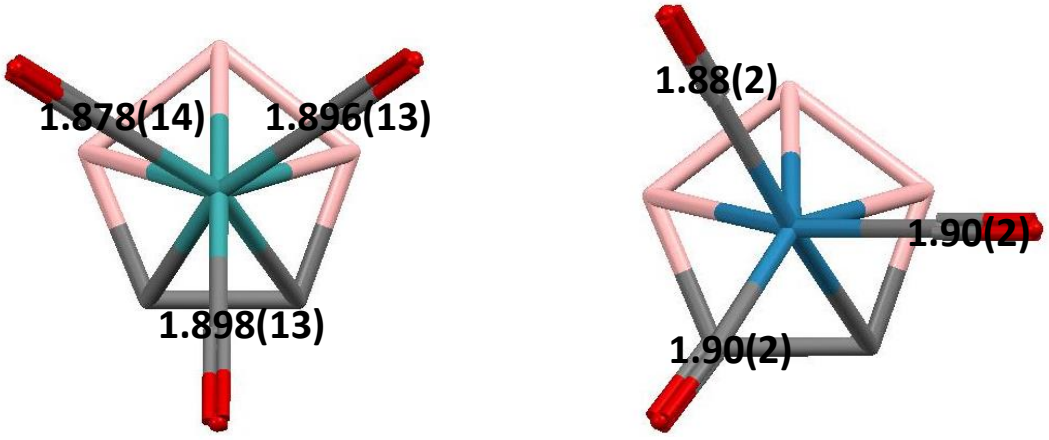

(a) (b)

Figure 4.5.1 Structure and M-EPL bond lengths (Å) of (a) MOGSAC, $[NEt_4][3,3,3\text{-}(CO)_3\text{-}3,1,2\text{-}TcC_2B_9H_{11}]$ and (b) CSCREC, $[Cs][3,3,3\text{-}(CO)_3\text{-}3,1,2\text{-}ReC_2B_9H_{11}]$.

For CSCREC, KISCEU and KOBLOC the M-EPL distances of the single carbonyl trans to a cage carbon atom, are shorter than the M-EPL distances of the carbonyls trans to the cage boron atoms or B-B/C-B connectivities. For MOGSAC the M-EPL distances of the two carbonyls trans to the C-B connectivities are shorter than the M-EPL distance of the carbonyl trans to the unique boron atom. However for KISCEU, KOBLOC, CSCREC and MOGSAC some of the $M\text{-}EPL_{trans\ C}$ bond lengths are very similar to the $M\text{-}EPL_{trans\ B}$ bond lengths. For the fifth example, HOSGIF, one of the cage carbon atoms is disordered over two sites (C/B).

The carbonyl which is trans to a C-(C/B) connectivity has the longest M-EPL bond of the three carbonyl groups (figure 4.4.3).

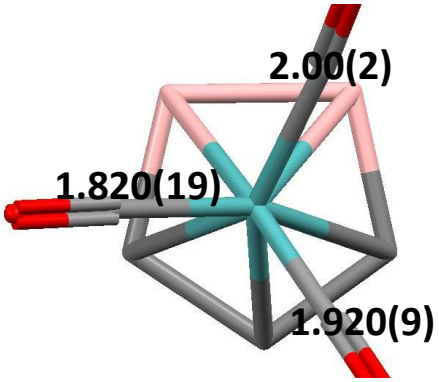

Figure 4.5.2 Structure and M-EPL bond lengths (Å) of HOSGIF, $[NMe_4]_2[3,3,3\text{-}(CO)_3\text{-}3,1,2\text{-}MoC_2B_9H_{11}]$.

For the eight π-donor ligands/group five metal d^0 compounds, two have an ELO similar to the tricarbonyl compounds, with one of the three ligands lying over the cage C-C connectivity. For one of these compounds (XAMPIK) the EPL (figure 4.5.3 (a)) which is closest to being trans to a cage carbon atom (but is in fact trans to a C-B connectivity) has the shortest M-EPL distance, while for the other compound (XAMPOQ) the EPL which is trans to a cage carbon atom has the longest M-EPL distance. The fact that there is no ligand directly trans to a cage carbon atom for XAMPIK makes comparison of these two compounds difficult, beyond saying that the M-EPL bond lengths observed in XAMPOQ do not seem to fit the general trend (of M-EPL bonds which are trans to the carbon part of the cage being shorter than M-EPL bonds which are trans to the boron part of the cage).

Five of the group five metal/π-donor compounds have an ELO where one of the EPLs is close to eclipsing B8 (the torsion angle B8-Cb-M-EPL does not exceed 11°) and there are no EPLs lying within the boundary of the cage C-C connectivity. For four of these molecules (LAQSOL/LAQSUR, two independent molecules per asymmetric unit in each) the EPLs are NR_2 three electron π-donors. The plane of the NR_2 ligand which is located over B8 is described[10] as being 'horizontal' with respect to the Cb-M axis (i.e. is perpendicular to it) and the other two ligands are described as being 'vertical' (parallel with Cb-M axis). The horizontal ligand is assumed to be best orientated for maximum π-donation[10], making it the strongest π-donor and consequently this leads to it being trans to the cage C-C connectivity and having the shortest M-EPL bond length of the ML_3 set in all four compounds (figure 4.5.3 (b)). This is supported by work which shows that the strongest π-donor tends to be

orientated trans to the cage carbon atoms or the C-C connectivity in (LL′L″)-3,1,2-*closo*-$MC_2B_9H_{11}$ (L, L′, L″ = potential π-donors) compounds.[11]

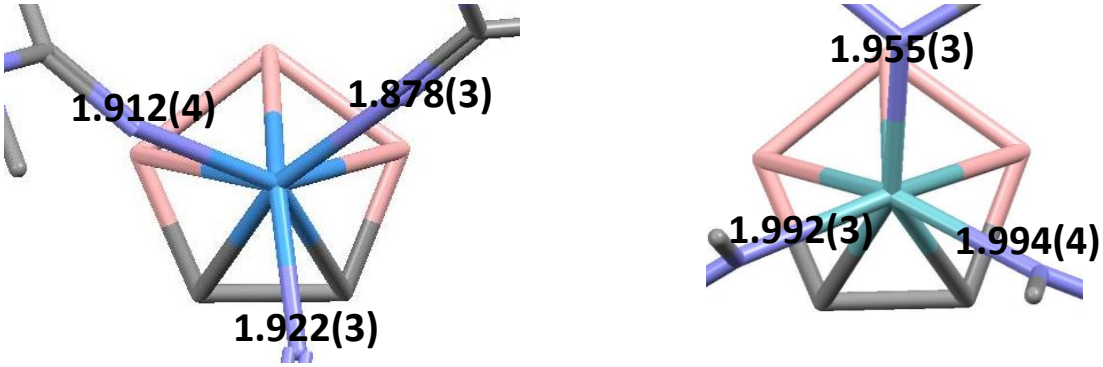

(a) (b)

Figure 4.5.3 Structure and M-EPL bond lengths (Å) of (a) XAMPIK, 3,3,3-(N,N-dimethylacetamidinato)$_3$-3,1,2-$TaC_2B_9H_{11}$ and (b) LAQSOL, 3,3,3-$(NMe_2)_3$-3,1,2-$NbC_2B_9H_{11}$ (one of two independent molecules in asymmetric unit shown).

The other compound with an EPL over B8 is VUPBAJ, where the EPLs are Cl (assumed to be acting as three electron π-donors). Obviously there can be no horizontal/vertical description of the EPLs here, but the Cl atom which is trans to the C-C connectivity has the shortest M-EPL bond, implying that it is in fact the strongest π-donor.

The final compound with a group five metal/π-donor ligands is XAMQAD, which has two independent molecules in the asymmetric unit, both of which have one of the two cage carbon atoms disordered over two sites (C/B). In one of the molecules the shortest M-EPL bond is trans to the cage carbon atom (the other two are trans to a (C/B)-B connectivity and a boron atom), while in the other molecule the shortest M-EPL bond is trans to a cage C-(C/B) connectivity, the second shortest M-EPL bond is trans to a cage C/B vertex and the longest M-EPL bond is trans to a B-B connectivity.

It is not immediately clear why some of the group five metal/π-donor compounds adopt an ELO with one of the EPLs above B8, while others adopt an ELO with one of the EPLs within the boundary of the C-C connectivity. All the ML_3 compounds with group five metals/π-donor EPLs except XAMPOQ follow the pattern of the EPL with the shortest M-EPL bond, which is presumably providing the strongest π-donation, being trans to the carbon part of the cage.

The only ML_3 compound found which has neither carbonyl nor π-donor ligands is SEZWUP. This compound has a tridentate hydrogen tris(1-pyrazolyl)borate EPL and one of the cage carbon atoms is either assigned incorrectly or disordered over two positions. The shortest M-EPL bond length is situated trans to the non-disordered cage carbon atom.

4.6 3,3-L_2-3-L′-3,1,2-*closo*-$MC_2B_9H_{11}$

Forty two examples of this class of compound were found. For thirty seven of them the M-EPL length of the identical ligand trans to the carbon part of the cage is shorter than the M-EPL bond length of the identical ligand trans to the boron part of the cage. The exceptions are KISBIX, HOHDIR, HOHDEN, HIPQII and ZEPYIC in which one of the M-EPL bonds trans to a C-B connectivity is shorter than the M-EPL bond which is directly trans to a cage carbon atom, although in four of the compounds (HIPQII being the exception) these two bond lengths are similar.

For the purposes of studying the ELO's of the 3,3-L_2-3-L′-3,1,2-*closo*-$MC_2B_9H_{11}$ compounds the trans influence being described is not the ability of the EPLs to lengthen the bonds trans to themselves (this value cannot be measured in any meaningful way), but the EPL's propensity for being trans to the carbon part of the cage at the expense of other ligands in the EPL set. This 'trans influence' is denoted in this chapter as the Rotational Trans Effect or RTE (a qualitative term) to distinguish it from the conventional trans influence.

It could be argued that one of the cage carbon to metal bonds will show selective lengthening if it has a strong trans influencing group trans to it. For cage carbon atoms trans to a very strongly σ-donating group such as hydride there does seem to be a trend of selective lengthening relative to the other M-C_{cage} bond. However this does not seem to be the case for other EPLs, where the M-C_{cage} bond trans to the strong trans influence ligand is as likely to be longer than the other M-C_{cage} bond as it is to be shorter. In addition to this, most of the structures found do not have two different EPLs directly trans to the two cage carbon atoms, so it is not really possible to use the lengths of the M-C_{cage} bonds to gauge the strengths of the M-EPL bonds, other than to note the effect of strongly σ-donating ligands.

The following conclusions can be drawn from studying the orientational preferences of the ML_2L' EPLs:

Halides are generally considered to have a weak trans influence,[1k,i] and based on the CSD search results they also have a weak RTE. In thirteen out of fourteen halide containing examples (including NITWOC (figure 4.6.1 (a))) the halide ligand is trans to the boron part

of the cage, leaving only one example - CAZDOW (the only dihalide example in the ML_2L' class of compounds) - where there is a halide trans to a cage carbon atom.

Both of the two examples containing hydride ligands (one of which is CEHCIB - shown in figure 4.6.1 (b)) are orientated with the hydride ligand trans to the cage carbon atoms or the C-C connectivity. Hydrides have a strong trans influence[1k,i] as they are strong σ-donors, and they also have a strong RTE.

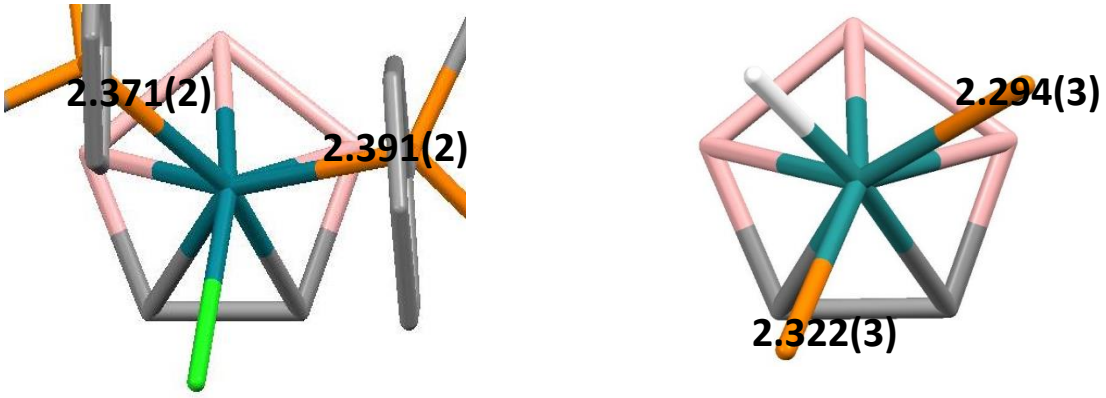

(a) (b)

Figure 4.6.1 Structure and selected M-EPL bond lengths (Å) of (a) NITWOC, 3,3-$(PPh_3)_2$-3-Cl-3,1,2-$RhC_2B_9H_{11}$ and (b) CEHCIB, $[NEt_4]$[3,3-$(PPh_3)_2$-3-H-3,1,2-$RuC_2B_9H_{11}$].

Carbonyls seem to have quite a strong RTE. In five out of six compounds with one carbonyl ligand, the carbonyl is trans to a carbon atom or the C-C connectivity. In eleven out of the twelve compounds (the exception being TAKCIR - see below) with two carbonyl ligands either both of the carbonyls are trans to C-B connectivities (two examples), or one is trans to a carbon atom and the other trans to a C-B connectivity (nine examples).

There are two examples of carbonyl containing EPL sets whereby the carbonyl ligand(s) are trans to the carbon part of the carborane at the expense of alkene/allyl ligands (HIZQIQ (figure 4.6.2 (a)) and TAKCOX), two examples where the carbonyl ligands are trans to the carbon part of the carborane at the expense of metal-methylidynyl ligands (HOHDEN and HOHDAJ), and one example where the carbonyls are trans to the carbon part of the carborane at the expense of a σ-bonded C ligand (HIZQOW (figure 4.6.2 (b))).

The compound TAKCIR has two carbonyl ligands and an $SnPh_3$ ligand as the EPL set, with the observed orientation being as shown in figure 4.6.2 (c). One of the carbonyl ligands is trans to a cage carbon atom, while the other is trans to the unique boron atom, leaving the $SnPh_3$ ligand trans to a C-B connectivity. This indicates that either CO has a stronger RTE than a strong σ-donating ligand like $SnPh_3$,[1b] or that the ELO of TAKCIR is dictated by factors such as steric effects or CPFs

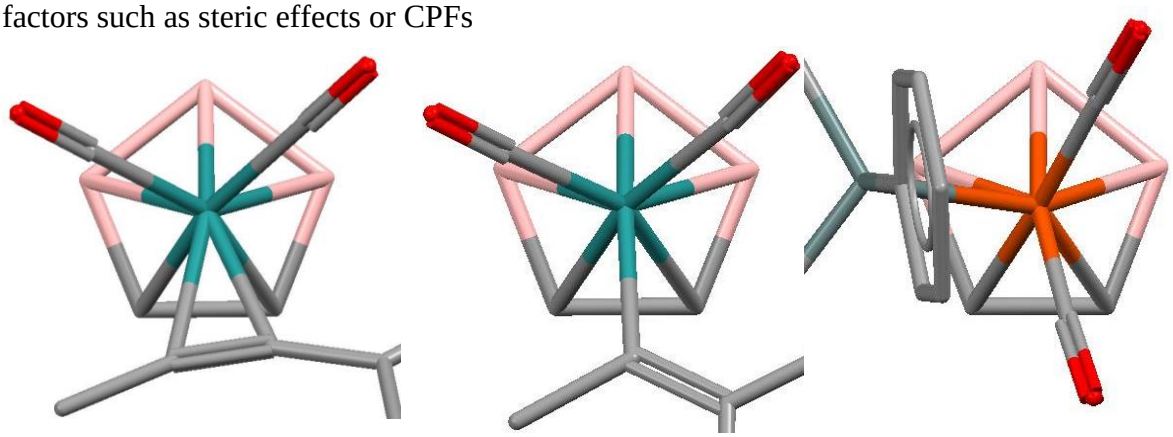

(a) (b) (c)

Figure 4.6.2 Structure of (a) HIZQIQ, 3,3-$(CO)_2$-3-(η^2-1-phenyl-prop-2-yne)-3,1,2-$RuC_2B_9H_{11}$, HIZQOW, (b) 3,3-$(CO)_2$-3-(1-phenyl-1-triethylphosphineprop-2-en-2-yl)-3,1,2-$RuC_2B_9H_{11}$, and (c) TAKCIR, [NEt_4][3,3-$(CO)_2$-3-($SnPh_3$)-3,1,2-$FeC_2B_9H_{11}$].

Carbonyls are conventionally thought to have a weak trans influence,[1g,i,j] which is at odds with their strong RTE, although the trans influence of carbonyls has historically been measured based on the length of M-X (usually Pt-Cl) bonds trans to carbonyl.[1d,g,h] Glenwright and Coe[1e] express the importance of the mutual nature of the trans influence, in that a given ligand's ability to cause trans lengthening is also dependent on the nature of the trans ligand (in this case a carborane).

The carbonyl ligand's strong RTE in metallacarboranes may be due to its π-acceptor abilities, however the exact interaction between the π-acceptor orbitals, the metal and the cage which leads to the strong RTE is not immediately clear. The carbonyl ligand illustrates the difference between RTE and conventional trans influences, and is important when considering potential applications of studying ELO. The main application proposed for ELO is to distinguish between cage boron and cage carbon atoms during crystallographic refinement (see section 4.15), and knowing a given ligands RTE relative to other ligands in the EPL set is necessary to achieve this.

Phosphine has a stronger RTE than halide (based on ten out of eleven examples containing halide and phosphine), as would be expected from trans influence arguments, but not as strong a trans influence as carbonyl. Evidence for this can be seen in the ELO of FIRHOD/TAKCOX (figure 4.6.2 (a) and (b)). In FIRHOD (EPLs = allyl and phosphine) the allyl group has the stronger RTE, as one of the carbons of the allyl group is trans to the carbon part of the cage at the expense of the phosphine. When the phosphine in FIRHOD is replaced with a carbonyl (TAKCOX, EPLs = allyl and carbonyl), the carbonyl ligand has the stronger RTE, as it is trans to the C-C connectivity (figure 4.6.3 (b)). If carbonyl has a stronger RTE than allyl, and allyl has a stronger RTE than phosphine, then it seems likely that carbonyl has a stronger RTE than phosphine.

Further evidence for carbonyl having a stronger RTE than phosphine are the compounds in which there are carbonyl and phosphine/phosphite ligands in the EPL set (BIHQUE (figure 4.6.3 (c)), KISBIX and KISBUJ). In these compounds the carbonyl ligand or ligands are trans to the carbon part of the cage at the expense of the phosphine/phosphite ligand(s).

Phosphines are generally better σ-donors and weaker π-acceptors than carbonyls, and are conventionally thought of as having quite a weak trans influence[1i,j], albeit slightly stronger than carbonyl.[1j] The fact that carbonyls have a stronger RTE than phosphines could support the idea that the better a ligands π-accepting abilities, the stronger its RTE.

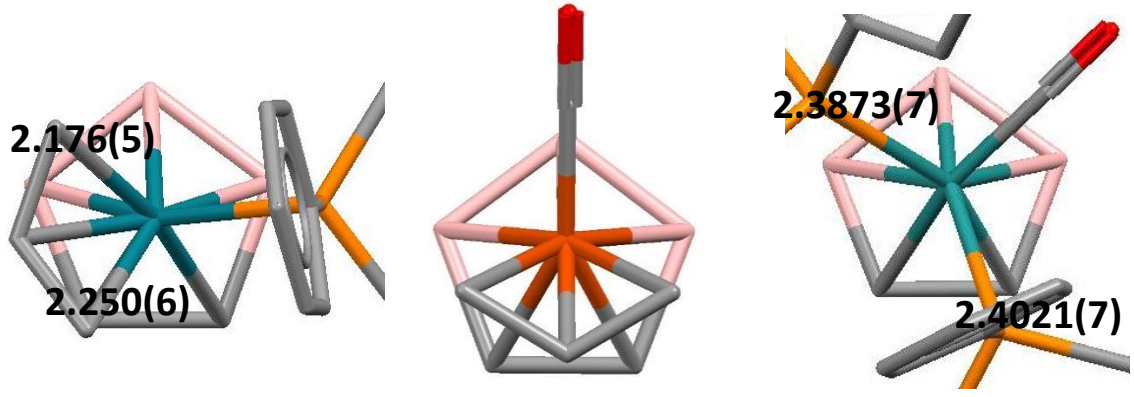

(a) (b) (c)

Figure 4.6.3 Structure and selected M-EPL bond lengths (Å) of (a) FIRHOD, 3-(η-allyl)-3-(PPh_3)-3,1,2-$RhC_2B_9H_{11}$, (b) TAKCOX, [$N(PPh_3)_2$][3-(η-allyl)-3-(CO)-3,1,2-$FeC_2B_9H_{11}$] (sits on a crystallographic mirror plane, one of two independent molecules in asymmetric unit shown) and (c) BIHQUE, 3,3-$(PPh_3)_2$-3-(CO)-3,1,2-$RuC_2B_9H_{11}$.

Both carbonyl and phosphine have a stronger RTE than acetonitrile (ZOTVIN and MEFNEQ) and the σ-bonded sulphur donors found during the CSD search (REQSIP and HOHDIR). However phosphine has a weaker RTE than the bidentate dithioformato found in VENBIZ, but a stronger RTE than the bidentate nitrato ligand found in **VI**. Unfortunately there are no carbonyl thioformato/nitrato compounds to compare to the phosphine ones.

The compound WURZUF (figure 4.6.4 (a)) has a phosphine and a bipy ligand as the EPL set, and the compound YEBHOD (figure 4.6.4 (b)) has a carbonyl and a bipy ligand as the EPL set. For YEBHOD, one of the nitrogen donors of the bipy ligand is trans to a C-B connectivity while the other is trans to a B-B connectivity and the carbonyl is trans to a C-B connectivity (the nitrogen donor of the bipy ligand is closer to being trans to a cage carbon atom than the carbonyl). For WURZUF, one of the nitrogen donors of the bipy ligand is trans to a cage carbon atom while the other is trans to a B-B connectivity and the phosphine is trans to a C-B connectivity. In these compounds bipy would appear to have a stronger RTE than carbonyl or phosphine, which would not be expected based on the relatively high electronegativity of the nitrogen donor and the moderate π-acceptor properties of bipy.[1a,j]

The compound YEBHUJ is similar to YEBHOD, except the bidentate EPL is TMEDA, which has no π-acceptor capabilities. In YEBHUJ the carbonyl EPL is directly trans to one of the cage carbon atoms (figure 4.6.4 (c)), indicating that in this compound the carbonyl has the stronger RTE. These compounds indicate that either bipy has a stronger RTE than carbonyl or that the ELO of YEBHOD is dictated by factors such as steric effects or CPFs. More compounds featuring bipy/phenathroline etc. would be helpful in determining relative RTEs.

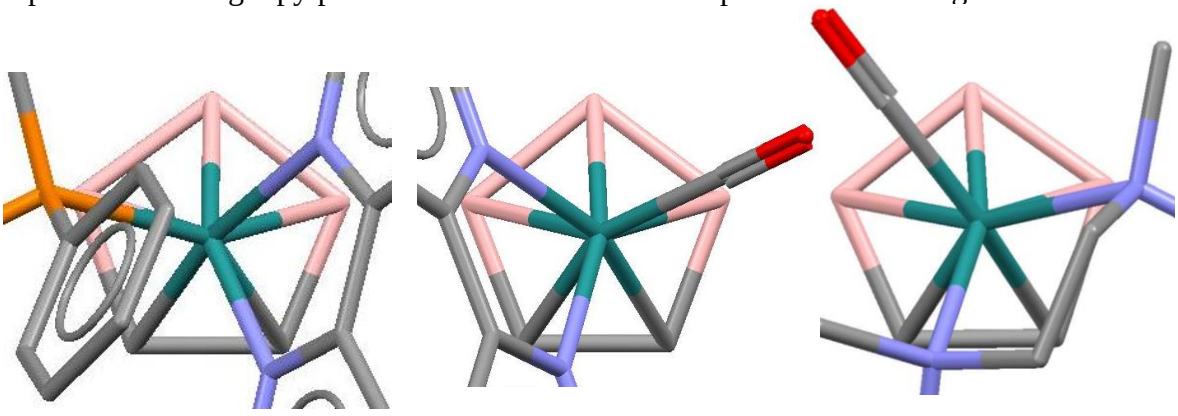

(a) (b) (c)

Figure 4.6.4 Structure of (a) WURZUF, 3-(PPh_3)-3-(bipy)-3,1,2-$RuC_2B_9H_{11}$, (b) YEBHOD, 3-(bipy)-3-(CO)-3,1,2-$RuC_2B_9H_{11}$ and (c) YEBHUJ, 3-(N,N,N′,N′-tetramethylethylenediamine)-3-(CO)-3,1,2-$RuC_2B_9H_{11}$.

The EPL ligands in the group five metal/π-donor ligand compounds TOJROZ and XODXAP (figure 4.6.5 (a) and (b)) adopt the orientation discussed in section 4.5 where one of the EPLs is roughly above the unique boron atom in the upper belt. In both compounds this EPL is one of the two identical ligands and forms the shorter of the two M-EPL$_{identical}$ bonds.

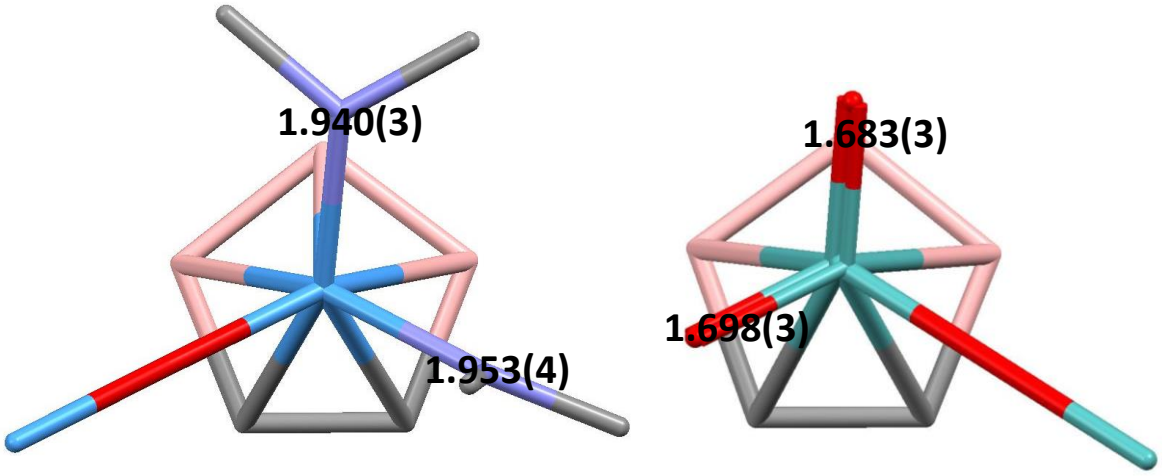

(a) (b)

Figure 4.6.5 Structure and selected M-EPL bond lengths (Å) of (a) XODXAP, 3-(μ^2-oxo)-(3,3-$(NMe_2)_2$-3,1,2-$TaC_2B_9H_{11})_2$ and (b) TOJROZ, [*p*-$(PPh_3CH_2)_2(C_6H_4)$][3-(μ^2-oxo)-(3,3-$(O)_2$-3,1,2-$MoC_2B_9H_{11})_2$] (only one cage of each shown for clarity).

Table 4.6.1 lists the torsion angle Y-Cb-M-L_{EPL} (where Y and Cb are defined as in section 4.2) for all three ligands in the EPL set for all forty two examples of 3,1,2- ML_2L' compounds. Ligand A is the EPL which lies to the left of the unique ligand when the unique ligand is positioned downward, and ligand B the one which lies to the right (figure 4.6.6). For compounds which are coordinated to the metal by a bond as opposed to a single atom, L_{EPL} is taken to be the midpoint of the bond.

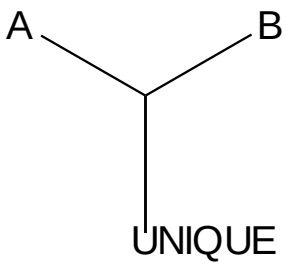

Figure 4.6.6 Labels used to designate each ligand within an ML_2L' EPL set in table 4.6.1.

Table 4.6.1 Torsion angles (θ,º) for all three ligands in 3,1,2- ML_2L' compounds.

CSD reference code or compound number	θ, unique ligand	θ, ligand A	θ, ligand B
BIHQUE	131.5	15.5	-118.3
CAZDOW	102.8	-18.6	-138.4
CEHCEX	-12.9	-127.2	99.5
CEHCIB	136.4	116.7	-24.8
HIZQUC cage 1	8.5	-113.6	127.4
cage 2	-11.5	-130.2	114.3
HIZQIQ	5.5	-117.4	130.9
HIZQOW	3.1	-114.9	128.7
V	-140.4	118.0	-26.9
KISBIX	-12.8	-133.5	113.1
KISBUJ*	144.5/-144.5	25.9/97.0	-25.9/-97.0
MEFNEQ	-6.2	-126.9	118.6
NITWOC	-12.4	-127.2	98.5
QAQQAB	-15.8	-137.5	99.6
QEXWEW	15.6	-114.4	132.9
REQSIP	-33.9	-141.4	87.3
TAKCIR	-99.0	149.3	16.1
TAKCOX* structure 1	180.0	53.4	-53.4
structure 2	180.0	58.0	-58.0
TELCIW	12.6	-98.3	127.6
VI structure 1	168.9	38.0	46.5
structure 2	174.3	46.5	36.0
TUBLUX	-15.5	-128.9	99.3
VENBIZ	1.6	-132.5	131.3
WURZUF	-104.6	131.6	25.37
YEBHOD	114.1	-17.5	-157.8
YEBHUJ	-142.8	98.1	-21.7
ZEPYIC	9.6	-111.9	132.7
BIHYOG	-150.0	91.0	-39.5
ZOTVOT	9.1	-107.6	127.9
FIRHOD	94.2	-34.5	-132.0
UZUYEU	-14.6	-138.5	101.0
ZOTVIN	-8.1	-125.5	108.7
SEMZIV	18.7	-95.2	143.3
TOJROZ cage 1	-56.5	-175.8	58.6
cage 2	56.5	-58.6	175.8
XODXAP cage 1	60.1	176.3	61.7
cage 2	61.9	173.7	60.7
HOHDEN	14.9	-123.3	129.1
HOHDIR	-14.5	-129.8	111.7
HOHDAJ structure 1	8.2	-129.0	127.7
structure 2	-35.2	-144.7	108.9
HIPQII	11.4	-102.9	131.6

*Sits on a crystallographic mirror plane.

If the magnitude of the torsion angle (for the unique ligand), θ, is plotted against itself as in figure 4.6.7, the resulting graph shows that θ for most of the unique ligands falls within a range of either ± 1.6-35.2 (twenty four examples) or ± 131.4-180.0 (ten examples).

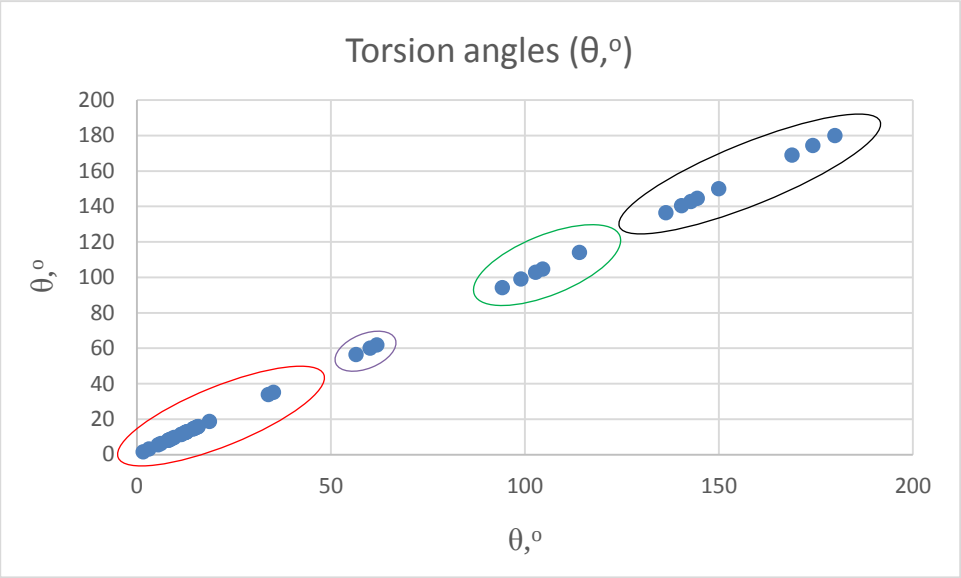

Figure 4.6.7 Plot of torsion angles of unique ligand (θ,°) for all ML_2L' compounds.

The compounds within the lower range of θ (circled in red) have the unique ligand situated within the boundary of the C-C connectivity and one of the identical ligands (or both in the case of VENBIZ) trans to the carbon part of the cage. For these compounds the identical ligands have a stronger RTE than the unique ligand - 'two strong, one weak'. The compounds within the higher range of θ (circled in black) have the unique ligand situated trans to the carbon part of the cage and one of the identical ligands is within the boundary of the C-C connectivity. For these compounds the unique ligand has a stronger RTE than the identical ligands - 'one strong, two weak'.

The compounds CAZDOW, TAKCIR, FIRHOD, WURZUF and YEBHOD have θ values of ±94.2-114.1 (circled in green), meaning that the unique ligand is neither trans to the carbon part of the cage or within the boundary of the C-C connectivity. These compounds are technically 'two strong and one weak', as the ligand which is trans to the carbon part of the cage is one of the two identical ligands. Four of the five compounds do not fit the general RTE trends that have been discussed above. More examples containing similar EPL sets to those present in CAZDOW, TAKCIR, FIRHOD, WURZUF and YEBHOD may be helpful in explaining why these five compounds do not fit the general RTE trends, and/or why they have a θ value outwith the majority of the other ML_2L' compounds.

The compounds TOJROZ and XODXAP have an ELO similar to LAQSOL/LAQSUR (one ligand roughly 180^{o} to the centre of the C-C connectivity) and so the θ values (circled in yellow) of the unique ligand (±56.5-61.2^{o}) is out with the three ranges discussed above.

4.7 3-L-3-L′-3-L′′-3,1,2-*closo*-$MC_2B_9H_{11}$

For the compounds where the EPL set comprises three unique ligands, five of the seven examples have a carbonyl ligand. The carbonyl ligand has the strongest RTE in three of the compounds (KISBOD, LOBSUQ and TAKCUD). In JEMDAG the carbonyl ligand and the gold based ligand are both trans to the cage carbon atoms (figure 4.7.1)).

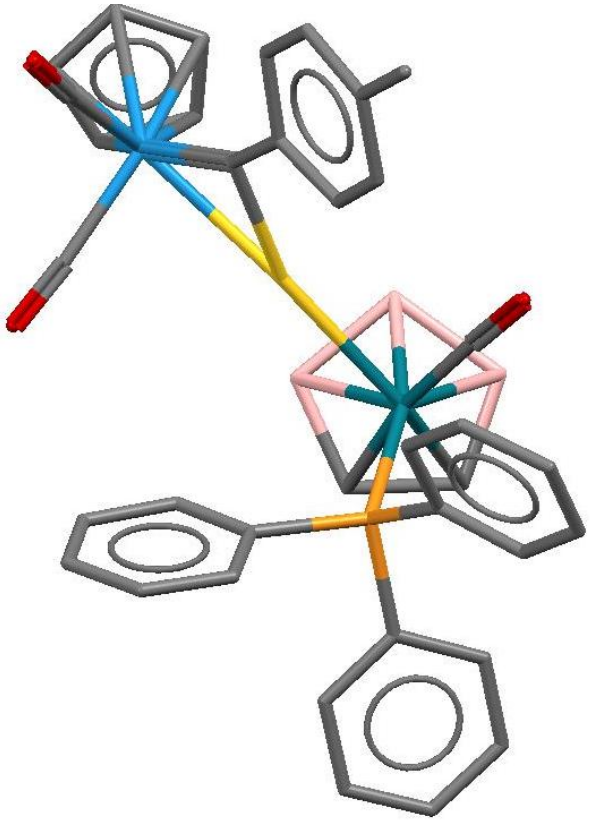

Figure 4.7.1 **S**tructure of JEMDAG, 3-(PPh_3)-3-(CO)-3-((η-C_5H_5)$(CO)_2$(μ^2-p-tolylmethylidyne)WAu)-3,1,2-$RhC_2B_9H_{11}$.

Transition metal ligands would be expected to be very strong σ-donors, explaining why in this compound the gold based ligand is trans to a cage carbon atom. The compound LIQDOC has the EPLs NO^+, CO and the carbene C(OMe)(tolyl), with the linear nitrosyl ligand being trans to one of the cage carbon atoms, while the carbonyl is trans to a C-B connectivity. Linear nitrosyl (NO^+) is a very strong π-acceptor, which supports the fact that ligands with strong π-accepting abilities appear to have strong RTE values (carbene is generally considered[1d,i] to be a weak π-acceptor relative to CO/NO^+).

The compound TAKCUD provides more evidence of the carbonyl ligands unexpectedly (based on its trans influence) strong RTE, as the ELO in this compound shows the carbonyl

ligand trans to the carbon part of the carborane despite the presence in the EPL set of an MeCO ligand (generally considered[1i,12] to have quite a strong trans influence through strong σ-donation).

There are two compounds (BOZMUY and DIKFUY) which have a phosphine ligand and a σ-bonded carbon atom. In BOZMUY the σ-bonded carbon atom is trans to the carbon part of the cage at the expense of the phosphine ligand, while in DIKFUY the σ-bonded carbon atom and the phosphine are both trans to the cage carbon atoms (figure 4.7.1), although the σ-bonded carbon atom and the phosphine in question are part of the same bidentate ligand.

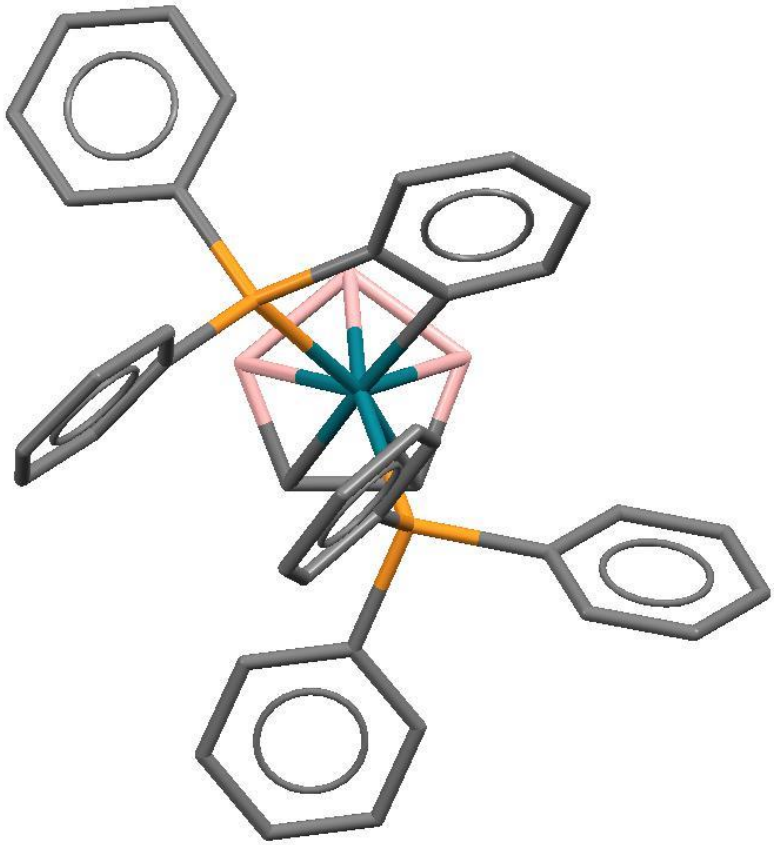

Figure 4.7.2 **S**tructure of DIKFUY, 3-(2-(diphenylphosphino)-phenyl-C^1,P)-3-(PPh_3)-3,1,2-$RhC_2B_9H_{11}$.

4.8 2-(L_2L'/L_3)-2,1-*closo*-$MCB_{10}H_{11}$

For all the previous compounds discussed the weakest bonding from the cage to the metal is via the C-C connectivity, but for the monocarborane compounds this region of relatively weak cage to metal bonding is only a single cage carbon atom.

Four of the examples found for this class of compound (RURZUZ (two independent molecules in asymmetric unit), RUSBIQ and RUSBAI) show a single (strong trans influence) hydride or HgR/AuR ligand lying trans to the cage carbon atom. The other ligands in the EPL sets were all PEt_3, showing that, as expected, the strongly σ-donating ligands have the stronger RTE (figure 4.8.1).

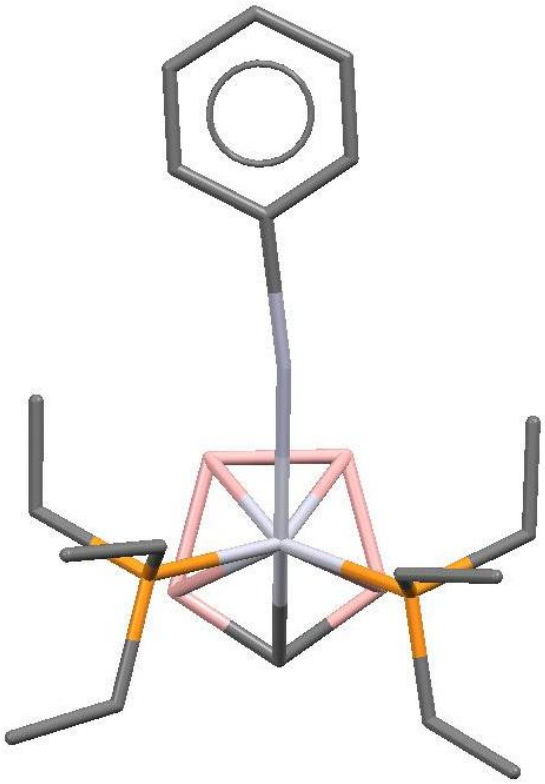

Figure 4.8.1 **S**tructure of RUSBIQ, 2,2-$(PEt_3)_2$-2-(Hg(Ph))-2,1-$PtCB_{10}H_{11}$

Of the other two compounds found, VABCOQ has a $(PPhMe_2)_2Cl$ EPL set, with one of the phosphines orientated trans to the cage carbon atom (figure 4.8.2). The M-EPL bond of the phosphine trans to the cage carbon atom is shorter than the M-EPL bond of the phosphine which is trans to a B-B connectivity.

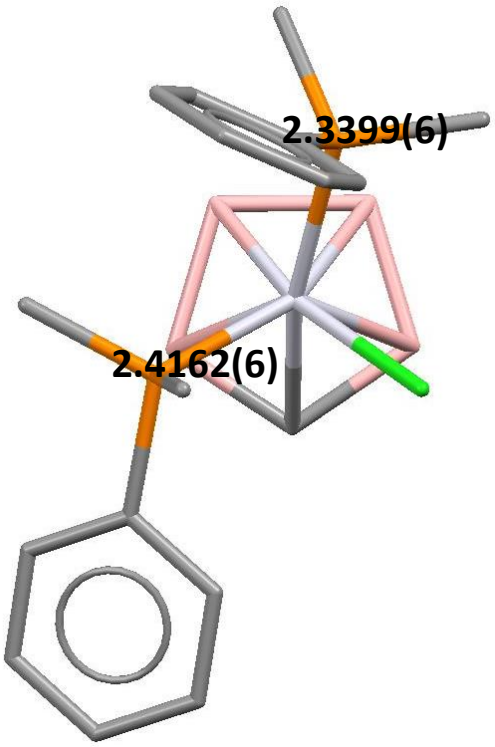

Figure 4.8.2 **S**tructure and selected M-EPL bond lengths (Å) of VABCOQ, 2,2-$(PPhMe_2)_2$-2-Cl-2,1-$PtCB_{10}H_{11}$

SEQQIO is a tricarbonyl compound, but the carbonyl ligand which is trans to the cage carbon atom has a longer M-EPL bond than one of the carbonyls which is trans to a B-B connectivity (figure 4.8.3), though the two bonds are similar lengths.

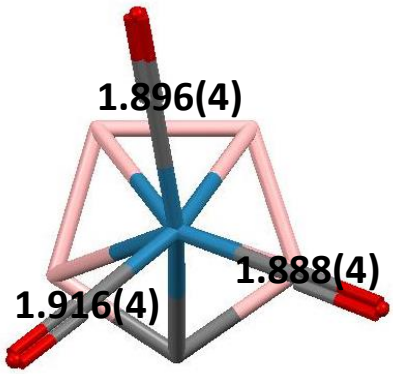

Figure 4.8.3 **S**tructure and M-EPL bond lengths (Å) of SEQQIO, $[N(CH_2Ph)Et_3]_2[2,2,2-(CO)_3-2,1-ReCB_{10}H_{11}]$.

4.9 2-(L_2L'/Cp/arene)-2,1-*closo*-$MXB_{10}H_{10}$ ($X \neq C$)

This class of compound has a heteroatom incorporated into the cage instead of carbon atoms. Previous work[13] on phosphaboranes has indicated that the phosphorous atoms in 3-(η-C_9H_7)-3,1,2-*closo*-$CoP_2B_9H_9$ have a lower trans influence than the cage boron atoms, as the indenyl ligand bridging carbon atoms are trans to the boron part of the cage.

The elements comprising all of the heteroatoms in this class of compound have higher electronegativity than boron, and so it is reasonable to assume that they will have a lower trans influence when incorporated into the cage. This is supported by the fact that in all six of the ML_2L'/heteroatom compounds found, the ligand with what would be predicted to be the strongest RTE (based on the observations of the previous sections) lies trans to the heteroatom. For example in GEXFEU and WIBSAB it is predicted that the CRS_2 group should have a stronger RTE than phosphine (based on the ELO of VENBIZ which has a similar EPL set), and it is one of the sulphur atoms of this group which is found to lie trans to the cage heteroatom in both compounds (figure 4.9.1). In both compounds the sulphur atom which is trans to the cage heteroatom forms a shorter M-EPL bond than the sulphur atom which is trans to the boron part of the cage.

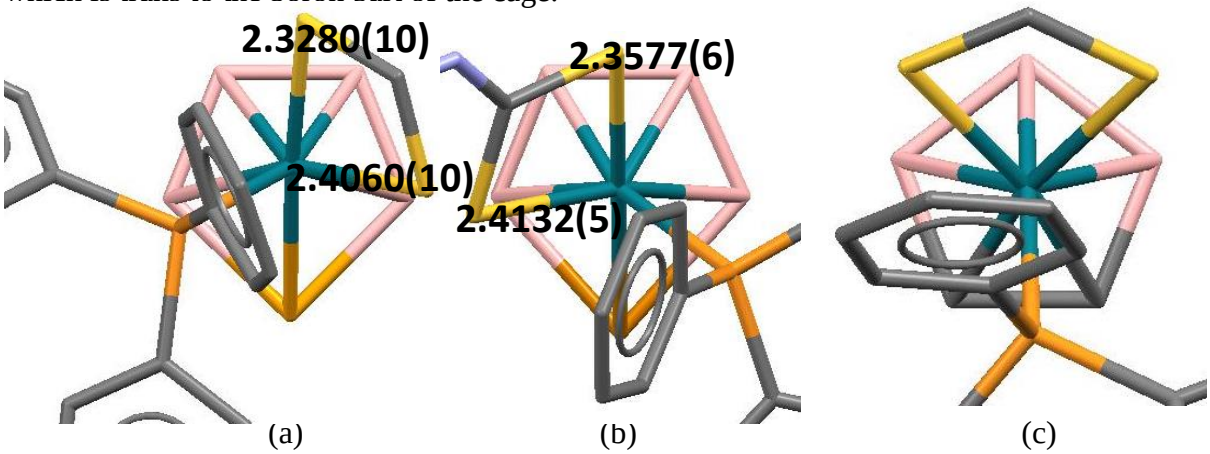

Figure 4.9.1 **S**tructure and selected M-EPL bond lengths (Å) of (a) GEXFEU, 2-(dithioformato-S,S′)-2-(PPh_3)-2,1-$RhSeB_{10}H_{10}$, (b) WIBSAB, 2-(N-phenyldithiocarbamato-S,S′)-2-(PPh_3)-2,1-$RhTeB_{10}H_{10}$ and (c) VENBIZ, 3-(dithioformato-S,S′)-3-(PPh_3)-3,1,2-$RhC_2B_9H_{11}$.

Similarly, KOJKUP and SABDAA have the same EPL set as HPRHCB (H and 2 x PPh_3), REQSOV has the same EPL set as REQSIP (figure 4.9.2), and CIVFUJ has a similar EPL set

to TUBLUX/ZOTVOT (Cl and 2 x phosphine). In all these examples the ligand with the strongest RTE in the 3,1,2 compounds is also trans to the heteroatom in the complementary 2,2-L_2-2-L′-2,1-*closo*-$MXB_{10}H_{10}$ (X ≠ C) compounds.

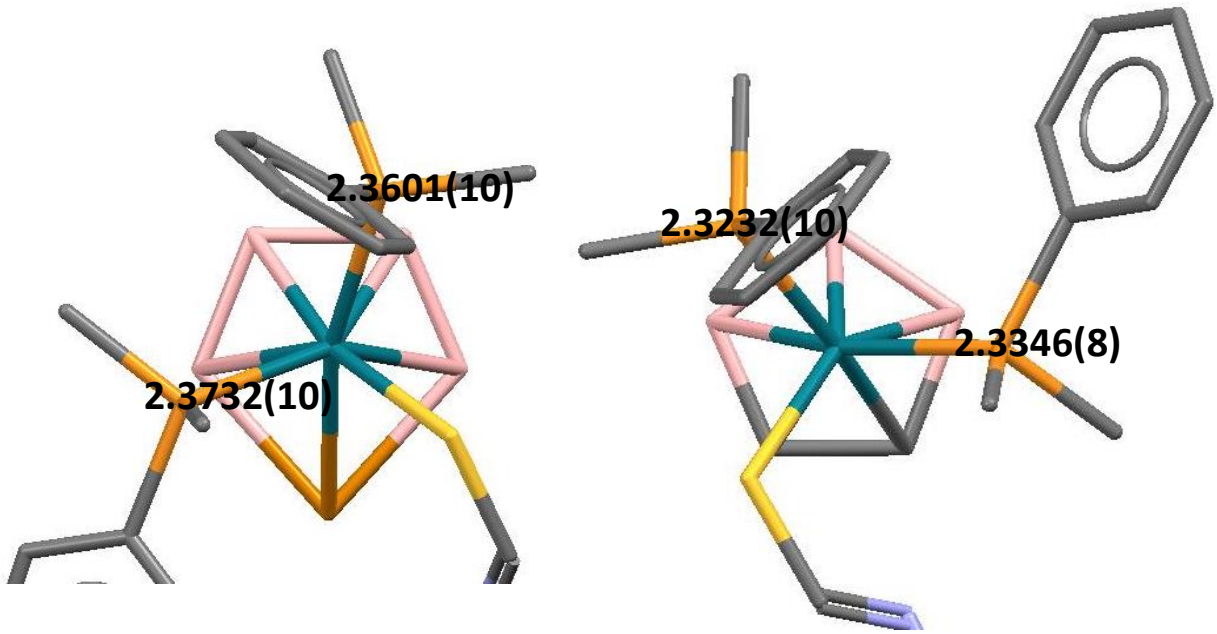

(a) (b)

Figure 4.9.2 **S**tructure and selected M-EPL bond lengths (Å) of (a) REQSOV, 2,2-$(PPhMe_2)_2$-2-(N-phenylthioformamido)-2,1-$RhTeB_{10}H_{10}$ and (b) REQSIP, 3,3-$(PPhMe_2)_2$-3-(N-phenylthioformamido)-3,1,2-$RhC_2B_9H_{11}$.

This provides good evidence both that the cage heteroatom has a weaker trans influence than the cage boron atoms, and that the relative RTE's of the EPL sets are consistent in going from 3,3-L_2-3-L′-3,1,2-*closo*-$MC_2B_9H_{11}$ to 2,2-L_2-2-L′-2,1-*closo*-$MXB_{10}H_{10}$ (X ≠ C) compounds.

There were also one M(Cp) compound (with two independent molecules in the asymmetric unit), two M(arene) compounds and one M(substituted arene) compound found during the CSD search. For four of these compounds the M-EPL bond which is trans to the cage heteroatom is shorter than the M-EPL bonds which are trans to the boron part of the cage. This again indicates that for these compounds the cage heteroatom has the weakest trans influence of the bonded heteroborane face. The other compound of this type, SEWVEV (figure 4.9.3), sits on a crystallographic mirror plane which includes the heteroatom and has the same metal/EPL as YOYHAV, but a different cage heteroatom (tellurium for SEWVEV and nitrogen for YOYHAV).

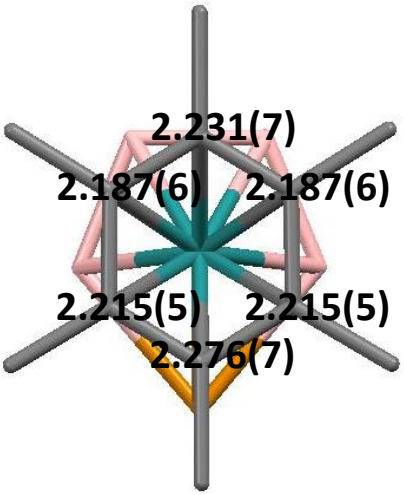

Figure 4.9.3 **S**tructure and M-EPL bond lengths (Å) of SEWVEV, 2-(η-C_6Me_6)-2,1-$RuTeB_{10}H_{10}$ (sits on a crystallographic mirror plane).

In SEWVEV, the M-EPL bond trans to the cage heteroatom is unexpectedly the second longest of the M-EPL bonds after the M-EPL bond which is trans to the unique boron atom of the bonded heteroborane face. This anomaly seems to be at odds with the fact that all the other compounds which have a tellurium cage heteroatom (REQSOV, SABDAA, WIBSAB and SEWVAR) suggest that tellurium has the weakest trans influence of the atoms in the open heteroborane face.

4.10 3-($L_2L'_2$/$L_2L'L''$/L_3L')-3,1,2-*closo*-$MC_2B_9H_{11}$

For this class of compounds there are four EPLs to consider instead of three. Four of the eight compounds found during the CSD search have two carbonyl ligands, and in all four compounds the two carbonyls are cis to each other and either have one carbonyl ligand trans to a cage carbon atom/the C-C connectivity (HOSGOL/HOSGUR), or both carbonyl ligands trans to the cage carbon atoms (TOJREP/FINWIJ). For HOSGOL, the carbonyl lying trans to the C1-C2 connectivity has a longer M-C bond than the carbonyl lying trans to the C1-B4 connectivity, but there appears to be cage carbon disorder associated with this structure, making B4 partially carbon (and C2 partially boron) (figure 4.10.1).

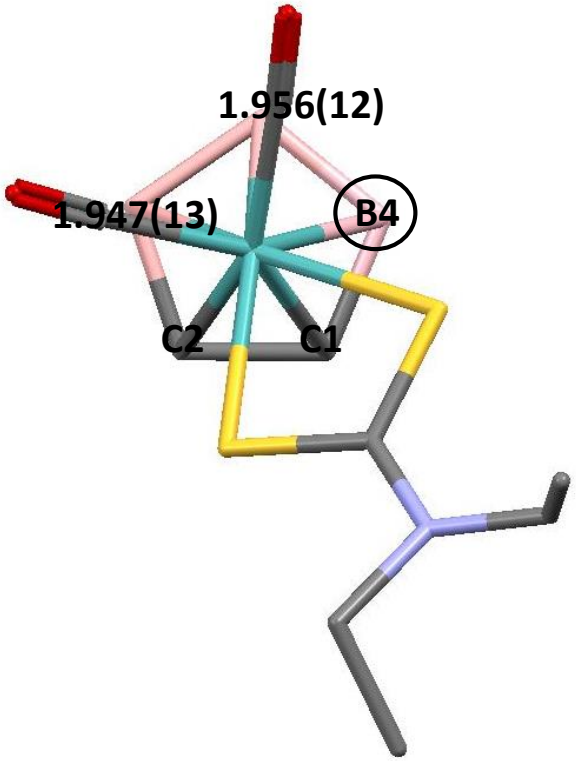

Figure 4.10.1 **S**tructure and selected M-EPL bond lengths (Å) of HOSGOL, $[N(PPh_3)_2][3,3\text{-}(CO)_2\text{-}3\text{-}(diethyldithiocarbamato\text{-}S,S')\text{-}3,1,2\text{-}MoC_2B_9H_{11}]$. B4 is circled as it is suspected that this atom is partially carbon.

Three of the remaining four compounds have hydride, chloride and two phosphines (or a bidentate phosphine) as the EPL set, and all three have the hydride ligand trans to the C-C connectivity. The other compound (WELNEG) has three NC^{t}Bu ligands and one π-bound ^{t}butyliminoethyl-C,N ligand as the EPL set. The ^{t}butyliminoethyl-C,N and one of the NC^{t}Bu ligands are both trans to cage carbon atoms. The NC^{t}Bu which is trans to the cage carbon

atom has a shorter M-EPL bond length than the other cis NC^{t}Bu which is trans to a cage boron atom, although the two bonds are of similar length. The structures of one of the phosphine/hydride compounds (QEXWAS) and WELNEG are shown in figure 4.10.2.

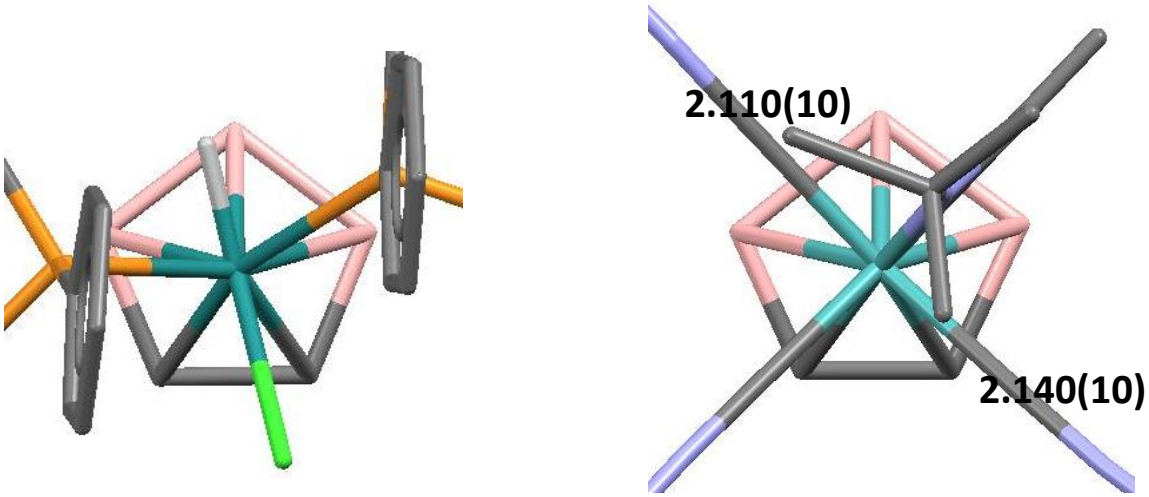

(a) (b)

Figure 4.10.2 **S**tructure and selected M-EPL bond lengths (Å) of (a) QEXWAS, 3,3-(PPh$_3$)-3-(H)-3-(Cl)-3,1,2-RuC$_2$B$_9$H$_{11}$ and (b) WELNEG, [3,3,3-(NC^{t}Bu)$_3$-3-(t-butyliminoethyl-C,N)-3,1,2-MoC$_2$B$_9$H$_{11}$][SO$_3$CF$_3$].

4.11 2-($L_2L'/LL'L''$/Cp/arene)-2,1,7-*closo*-$MC_2B_9H_{11}$

This class of compounds has two non-adjacent carbon atoms in the cage. Two of the ten structures - SEZXAW (two independent molecules in asymmetric unit) - are ML_3 species, with a tridentate hydrogen tris(1-pyrazolyl)borate ligand. For molecule one (figure 4.11.1 (a)), two of the nitrogen atom donor ligands are approximately trans to the two cage carbon atoms, and these two donor atoms form shorter M-EPL bonds than does the donor nitrogen atom which is trans to a B-B connectivity. For molecule two (figure 4.11.1 (b)) one of the cage carbon atoms is disordered over two sites. The M-EPL bonds trans to the cage carbon atom and one of the disordered carbon/boron vertex are shorter than the M-EPL bond trans to the B-(C/B) connectivity.

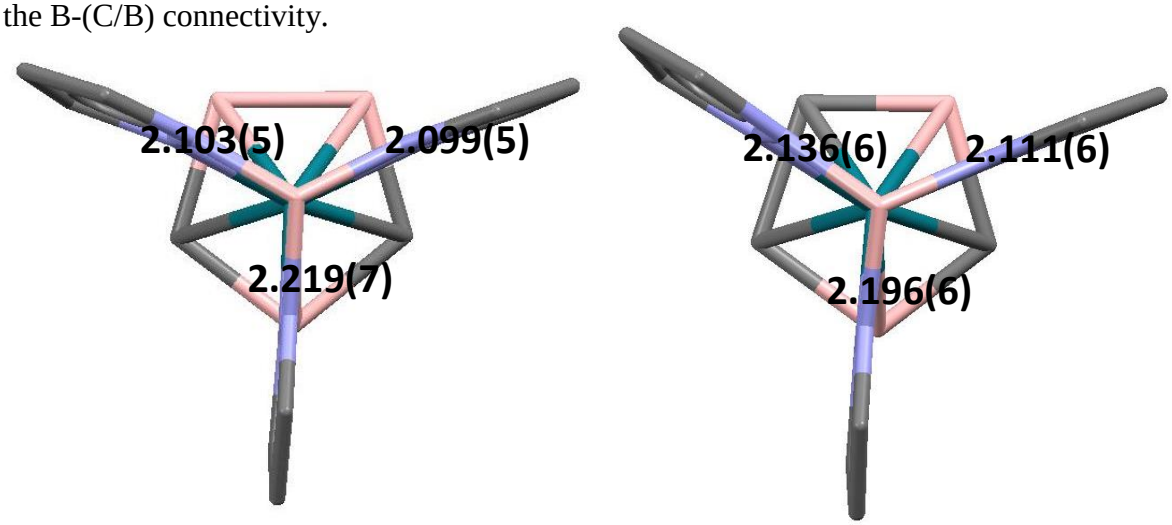

(a) (b)

Figure 4.11.1 Structures (two independent molecules in asymmetric unit) and M-EPL bond lengths (Å) of SEZXAW, 2-(Hydrogen tris(1-pyrazolyl)borate)-2,1,7-$RhC_2B_9H_{11}$. (a) Molecule one, (b) molecule two.

One of the compounds (BUVBUP, an $MLL'L''$ compound) has a σ-bonded carbon atom (part of a bidentate κ^2-(m-fluorobenzonitrile N-oxycarbonyl)) trans to one of the cage carbon atoms at the expense of a phosphine ligand. HABKIE (an ML_2L' compound with two molecules in the asymmetric unit) has one of the donor atoms of a dithioformato ligand trans to one of the cage carbon atoms, and a triphenylphosphine ligand trans to the other cage carbon atom.

One of the compounds (EDAGAS) is an $ML_2L'_2$ compound, with two hydride ligands and two phosphine ligands. Based on the strong RTE of the hydride ligand established in previous

sections, it would be predicted that one of the hydride ligands would be trans to a cage carbon atom, however this is not the case (figure 4.11.2). The angle made by the H-M-H bond is 153.4°, putting the hydrides more trans than cis to each other (the P-M-P angle is 104.0°). Trans hydrides have been found to give a particularly destabilising interaction in other (non-metallacarborane) compounds,[14] and could possibly be at least partly responsible for the unexpected ELO. Unfortunately the structure of the ruthenacarborane analogue of EDAGAS (which would have been helpful for comparison) in not available on the CSD.[15]

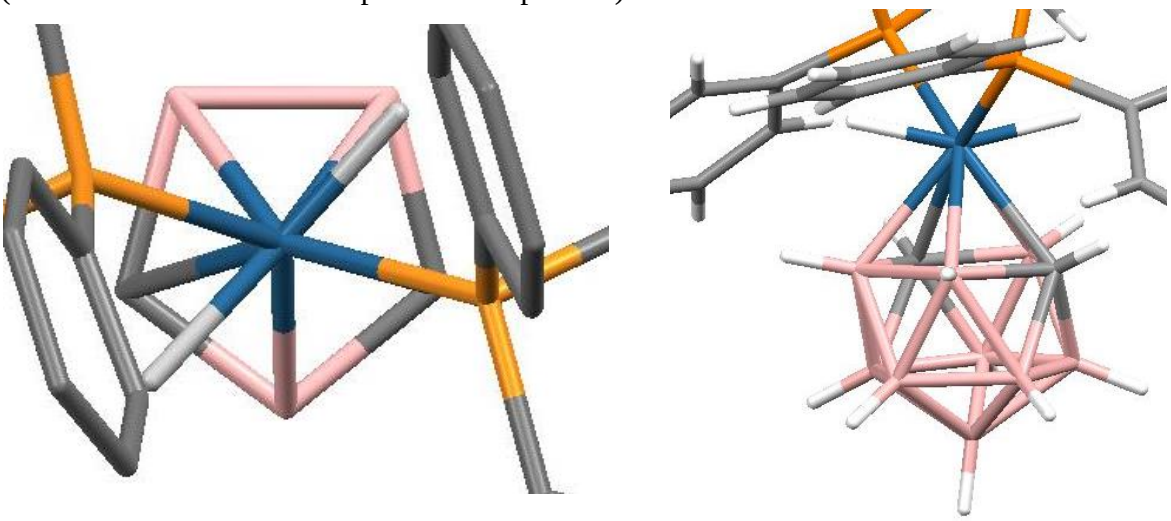

Figure 4.11.2 **S**tructure of EDAGAS, 2,2-$(PPh_3)_2$-2,2-$(H)_2$-2,1,7-$OsC_2B_9H_{11}$.

The remaining compounds are two substituted arene species, a pentamethylcyclopentadiene compound and a Cp compound. For equivalent atoms in the substituted arene compounds, the M-EPL bond lengths which are trans to the boron parts of the cage are all longer than the M-EPL bond lengths which are trans to cage carbon atoms. For the pentamethylcyclopentadiene compound (an ML_2 species) EZEZIS, the M-EPL bond trans which is to a cage carbon atom is shorter than the equivalent M-EPL bond which is trans to a boron atom.

The Cp compound (UJEYEO) has two independent molecules in the asymmetric unit. One of the molecules has a staggered conformation with respect to the EPL and the cage, rendering all of the CH units of the Cp ligand trans to a C-B or B-B connectivity, and so is not included in the results. The other molecule has an eclipsed conformation with respect to the cage, but does not fit the predicted pattern of M-EPL bonds trans to cage B > M-EPL bonds trans to cage C, as two of the M-EPL bonds that are trans to cage boron atoms are shorter than the two M-EPL bonds that are trans to cage carbon atoms, although all four bonds are of similar length.

4.12 Subicosahedral

Unfortunately most subicosahedral metallacarboranes found during a CSD search were substituted on the cage, causing the assignment of relative ligand RTEs to be compromised by potential steric interactions between the EPL set and the cage substituents. Only one unsubstituted subicosahedral compound with a bound carborane face containing topologically equivalent vertices was found during the CSD search. MOKHOJ, an $(L_2L'L'')MC_2B_4$ compound, has a hydride, a chloride and two triphenylphosphines as the EPL set (same EPL set as QEXWAS/TEXYUQ). The hydride is orientated trans to the C-C connectivity (figure 4.12.1) - as would be expected based on the ELO of QEXWAS/TEXYUQ, and the relative RTEs found for the ML_2L' compounds.

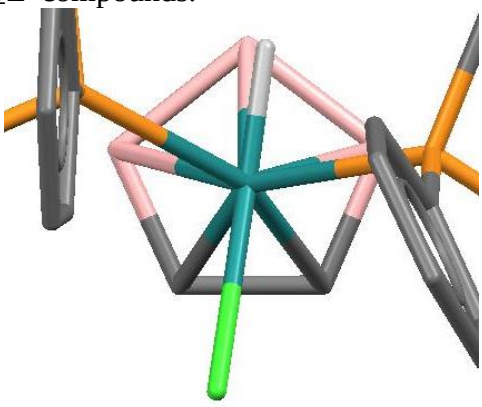

Figure 4.12.1 Structure of MOKHOJ, 1-H-1-Cl-1,1-$(PPh_3)_2$-1,2,3-$RuC_2B_4H_6$.

When a search was carried out for species with a bound carborane face containing topologically inequivalent vertices (8-11 vertex compounds), no usable eight or nine vertex compounds were found, and the only eleven vertex ones found had Cp/arene type ligands as the EPLs, none of which had M-EPL bonds directly trans to the cage heteroatoms. Six ten vertex compounds were found (one degree four and four degree five vertices in the metal bound face), and these compounds provide an insight into the relative M-EPL bond lengths/ELOs when the atoms of the bound carborane face are topologically inequivalent, something explored further in section 4.13.

One structure (OCEWUP) has a single degree four carbon atom in the metal bound carborane face and a tricarbonyl as the EPL set. One of the carbonyl ligands is trans to the cage carbon atom, and this has the shortest of the M-EPL bonds, although they are all similar lengths (figure 4.12.2).

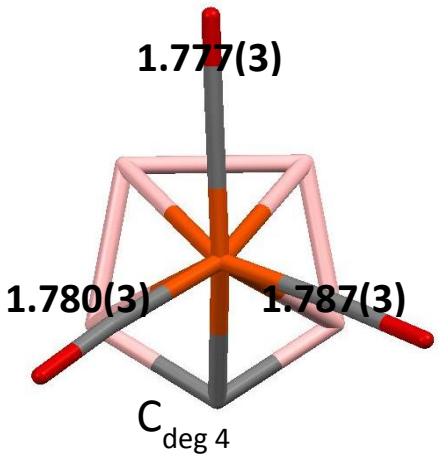

Figure 4.12.2 **S**tructure and M-EPL bond lengths (Å) of OCEWUP, $[N(PPh_3)_2][2,2,2\text{-}(CO)_3\text{-}2,1\text{-}FeCB_8H_9]$.

Three structures were found with a degree four and a degree five cage carbon atom in the metal bound carborane face, the three EPL sets being C_6Me_6 (GETMAT), $(PEt_3)_2H$ (HEPCOB) and Cp (ZOMTOK). For the Cp (figure 4.12.3 (a)) and the C_6Me_6 compounds, the M-EPL bond which is trans to the degree five cage carbon is the shortest of the M-EPL bonds, but the M-EPL bonds trans (or closest to being trans) to the degree four cage carbon are not the next shortest in either case, although some of the M-EPL bonds lengths are very similar. In HEPCOB, the EPL set is orientated with the hydride ligand trans to the degree five cage carbon (figure 4.12.3 (b)).

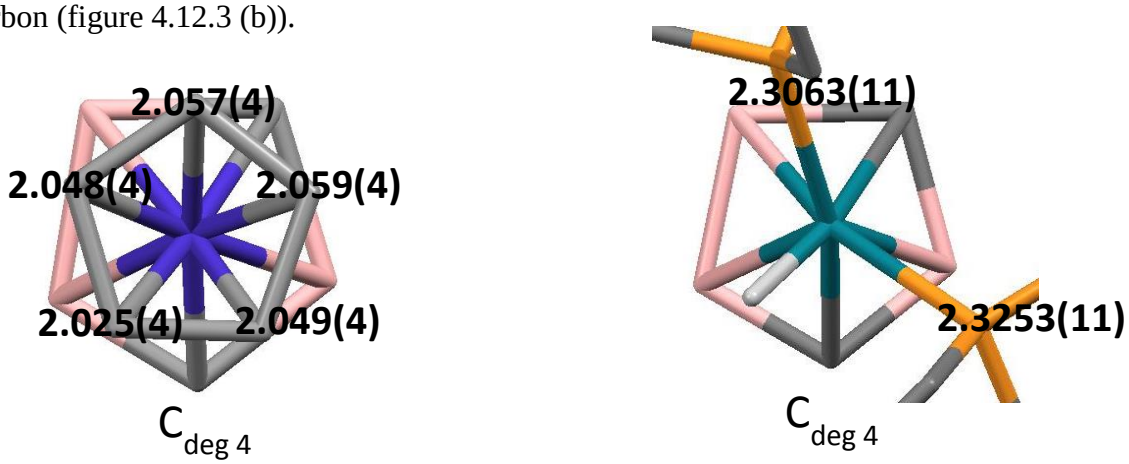

(a) (b)

Figure 4.12.3 **S**tructure and selected M-EPL bond lengths (Å) of (a) ZOMTOK, $2\text{-}(\eta\text{-}C_5H_5)\text{-}2,1,6\text{-}CoC_2B_7H_9$ and (b) HEPCOB, $2,2\text{-}(PEt_3)_2\text{-}2\text{-}(H)\text{-}2,1,6\text{-}RhC_2B_7H_9$.

Two structures were found with a degree four sulphur atom in the metal bound heteroborane face, one having a $(PMe_3)_2H$ EPL set (RARJUP), the other having a $(PPh_3)_2H$ EPL set

(XIDPEH). In both compounds the hydride ligand is trans to the degree four sulphur atom. The structures of RARJUP and XIDPEH are shown in figure 4.12.3.

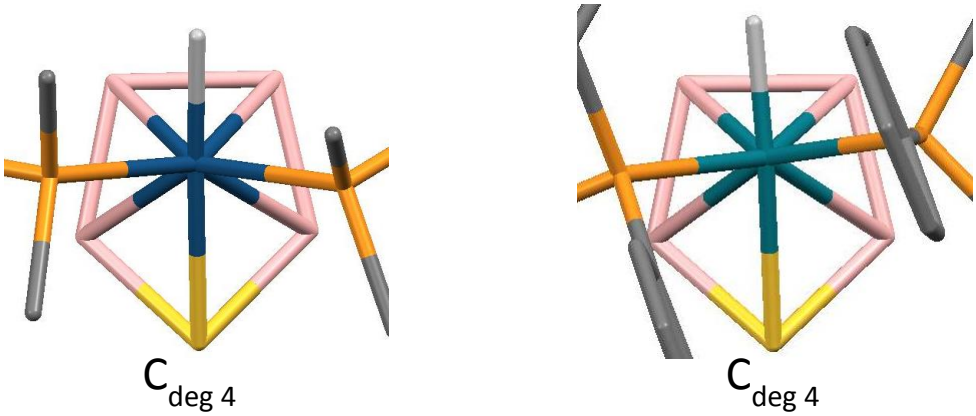

(a) (b)

Figure 4.12.3 **S**tructure of (a) RARJUP, 2,2-$(PMe_3)_2$-2-H-2,1-$IrSB_8H_8$ and (b) XIDPEH, 2,2-$(PPh_3)_2$-2-H-2,1-$RhSB_8H_8$.

The ELOs/relative bond lengths of the ten vertex compounds indicate that the degree five cage carbon forms the weakest cage to metal bonding, while the degree four cage carbon is either about the same as, or slightly weaker than a degree five boron in terms of the strength of M-cage bonding. That the degree five cage carbon is more weakly bound to the metal than the degree four cage carbon is an observation which has been made before,[16] and is thought to be a result of the former's greater involvement in bonding to neighbouring cage vertices making it less available for bonding to the metal atom. When a degree four sulphur atom is present in the cage, it appears to exhibit the weakest cage to metal bonding of the bound cage based on the ELO's of the metallathioboranes RARJUP and XIDPEH.

4.13 Supraicosahedral

The thirteen vertex docosahedron is less symmetrical than the icosahedron, and in a 4,1,6-thirteen vertex metallacarborane none of the atoms in the open face of the carborane are equivalent. Of the eight such structures found during the CSD search, two are ML_3 compounds, and there are one each of $ML_2L'_2$, Cp, Cp*, COD and *p*-cymene compounds, although this last one has two molecules in the asymmetric unit.

In the $ML_2L'_2$ compound (JACCOG), the EPL set is an allyl ligand and two carbonyls. As would be expected based on the ELO of TAKCOX (CO/allyl), one of the carbonyls is trans to the degree five carbon atom (C6), while the other carbonyl is trans to the C1-B2 connectivity and all the carbon atoms of the allyl ligand are trans to cage boron atoms/B-B connectivities (figure 4.13.1).

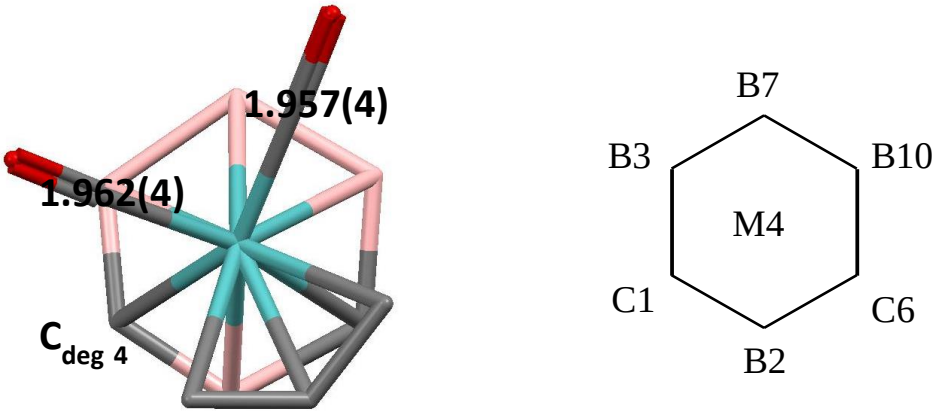

(a) (b)

Figure 4.13.1 (a) Structure and M-EPL bond lengths (Å) of JACCOG, $[N(CH_2Ph)Me_3][4,4-(CO)_2-4-(\eta\text{-allyl})-4,1,6-MoC_2B_{10}H_{12}]$ and (b) numbering scheme for 4,1,6-docosahedral metallacarborane.

The M-EPL bond trans to the C1-B2 connectivity is the shorter of the two, perhaps unexpectedly as the other carbonyl is trans to a cage carbon atom, although the two M-EPL bond lengths are very similar. There is no clear pattern throughout the few examples of 4,1,6-supraicosahedral structures which have been found to suggest that M-EPL bonds which are trans to B2 or B2-C connectivities are longer than M-EPL bonds which are trans to the cage carbon atoms, but it does seem that atoms trans to the C1B2C6 belt have a shorter M-EPL bond than atoms trans to the B3B7B10 belt.

An ML_2L' species - 4,4-$(PPh_3)_2$-4-H-4,1,6-*closo*-$RhC_2B_{10}H_{12}$ - is known from the literature,[17] but the crystal structure information has not been deposited with the CSD, and so commenting on the finer details of the ELO with any confidence is not possible.

Two of the carbonyls in the ML_3 compounds (KAPQAU and KAPQEY) are trans to the cage carbon atoms, and consequently have shorter M-EPL bonds than the third carbonyl which is trans to a B-B connectivity. The M-EPL bond trans to the degree five cage carbon is shorter than the M-EPL bond trans to the degree four cage carbon (figure 4.13.2) in KAPQAU and KAPQEY (although the difference in bond lengths is quite small in both). This could suggest that the degree four cage carbon is bonded more strongly to the metal than the degree five cage carbon, as found in the ten vertex metallacarboranes (section 4.12). While more supraicosahedral ML_3 structures are needed to confirm this observation, it is supported by previous work[16] on supraicosahedral bipy stannacarboranes which suggests that the degree four cage carbon is bonded more strongly to the metal than the degree five cage carbon in the 4,1,10- cage structure.

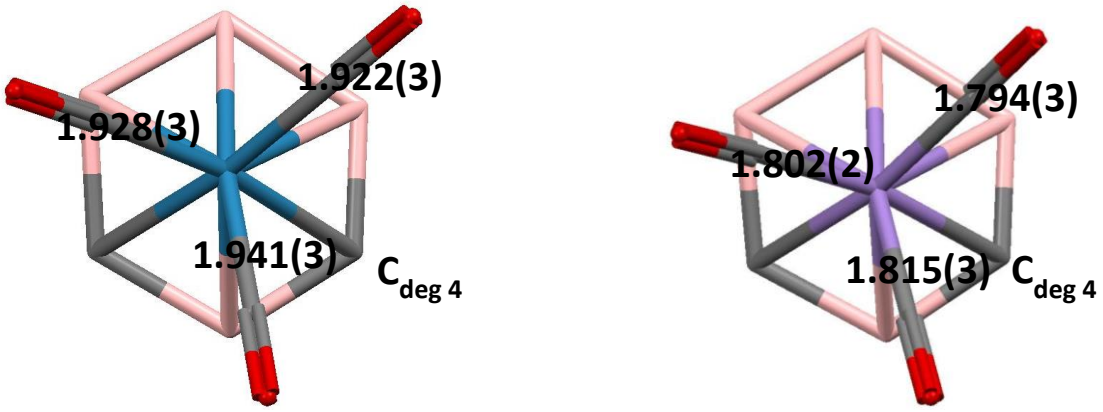

(a) (b)

Figure 4.13.2 **S**tructure and M-EPL bond lengths (Å) of (a) KAPQAU, $[N(PPh_3)_2][4,4,4\text{-}(CO)_3\text{-}4,1,6\text{-}ReC_2B_{10}H_{12}]$ and (b) KAPQEY, $[N(PPh_3)_2][4,4,4\text{-}(CO)_3\text{-}4,1,6\text{-}MnC_2B_{10}H_{12}]$.

Both the Cp (CPCOTB10) and Cp* (LUKKEH) ligands have very similar orientations above the carborane face in their respective compounds. In the Cp compound the M-EPL bond which is trans to B2 is the shortest, the M-EPL bond which is trans to C6 is the second shortest and the three M-EPL bonds which are trans to the B3B7B10 belt are the longest. In

the Cp* compound the M-EPL bond which is trans to C6 is the shortest and the M-EPL bond which is trans to the C1-B2 connectivity is the second shortest.

For the *p*-cymene compound (CANNOV01), one of the molecules (figure 4.13.3 (a)) has two non-equivalent EPL atoms trans to the C1B2C6 belt, and both these M-EPL bond lengths are shorter than their equivalent M-EPL bond lengths which are both trans to the B3B7B10 belt. For the second molecule (figure 4.13.3 (b)) the M-EPL bond lengths do not seem to follow the same trend as in the first molecule. The only M-EPL bond which lies trans to the C1B2C6 belt is longer than the equivalent M-EPL bond which lies trans to a the C6-B10 connectivity, although the difference in these bond lengths is small.

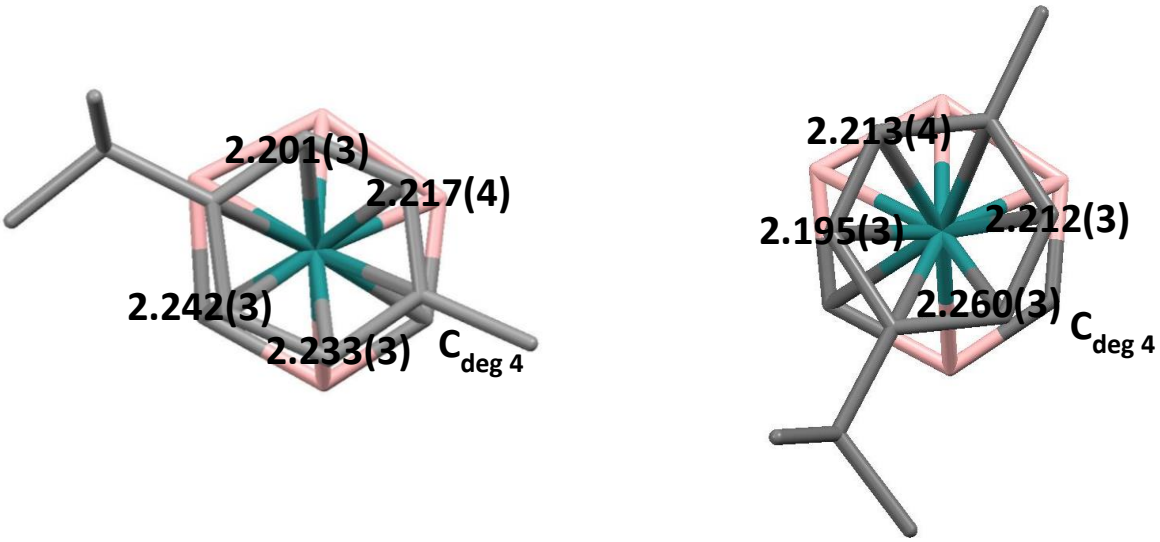

(a) (b)

Figure 4.13.3 Structures (two independent molecules in asymmetric unit) and M-EPL bond lengths (Å) of CANNOV01, 4-(*p*-cymene)-4,1,6-$RuC_2B_{10}H_{12}$. (a) Molecule one, (b) molecule two.

The COD ligand in YALZUH is orientated with two of the M-EPL bonds trans to the C1B2C6 belt, and these M-EPL bonds are shorter than the other two which are trans to the B3B7B10 belt.

Apart from JACCOG and 4,4-$(PPh_3)_2$-4-H-4,1,6-*closo*-$RhC_2B_{10}H_{12}$, there do not appear to be any supraicosahedral $ML_2L'_2$ or ML_2L' compounds in the literature which can be used to study the RTE in these types of compounds. The ELO of JACCOG does seem to obey the RTE orders established for icosahedral species, and for the other supraicosahedral species (apart from one of the molecules in CANNOV01) comparison of the M-EPL bond lengths

seems to suggest that M-EPL bonds which are trans to the C1B2C6 belt will be shorter than M-EPL bonds which are trans to the B3B7B10 belt in 4,1,6- compounds. However more supraicosahedral compounds need to be examined before it can be determined whether or not the ELO method is as applicable to these compounds as it appears to be to icosahedral compounds.

Two fourteen vertex compounds were found which were not substituted on the cage or had disorder in both carbon positions. These two compounds have a bicapped hexagonal antiprismatic 1,14,2,10- architecture, with the metal atoms occupying vertices 1 and 14. The first structure is XERBED, which has two CoCp groups (figure 4.13.4 (a) and (b)) and the second structure is XERBIH, which has a Ru(*p*-cymene) (which has no comparable carbon atom trans to the cage carbon atom) and a CoCp (figure 4.13.4 (c)). The carbon atom in the face bound to Co14 in XERBED is disordered over two adjacent sites. In all three Cp ligands the M-EPL bonds trans to the cage carbon atom/(C/B) disorder are shorter than the M-EPL bonds trans to the boron part of the cage (although for XERBIH and one of the molecules of XERBED the difference in length is small). This suggests that in these compounds the weakest cage to metal bonding is from the cage carbon atoms.

The icosahedral compound UJEYIS (two molecules in asymmetric unit) also has a single cage carbon atom in the metal bound face (figure 4.13.4 (d) and (e)), and a single cage carbon atom in the lower belt. The M-EPL bond trans to the cage carbon atom is shorter than the rest of the M-EPL bonds in both molecules (although in both molecules the difference in length of the M-EPL$_{\text{trans C}}$ bond and two or more of the M-EPL$_{\text{trans B}}$ bonds is small).

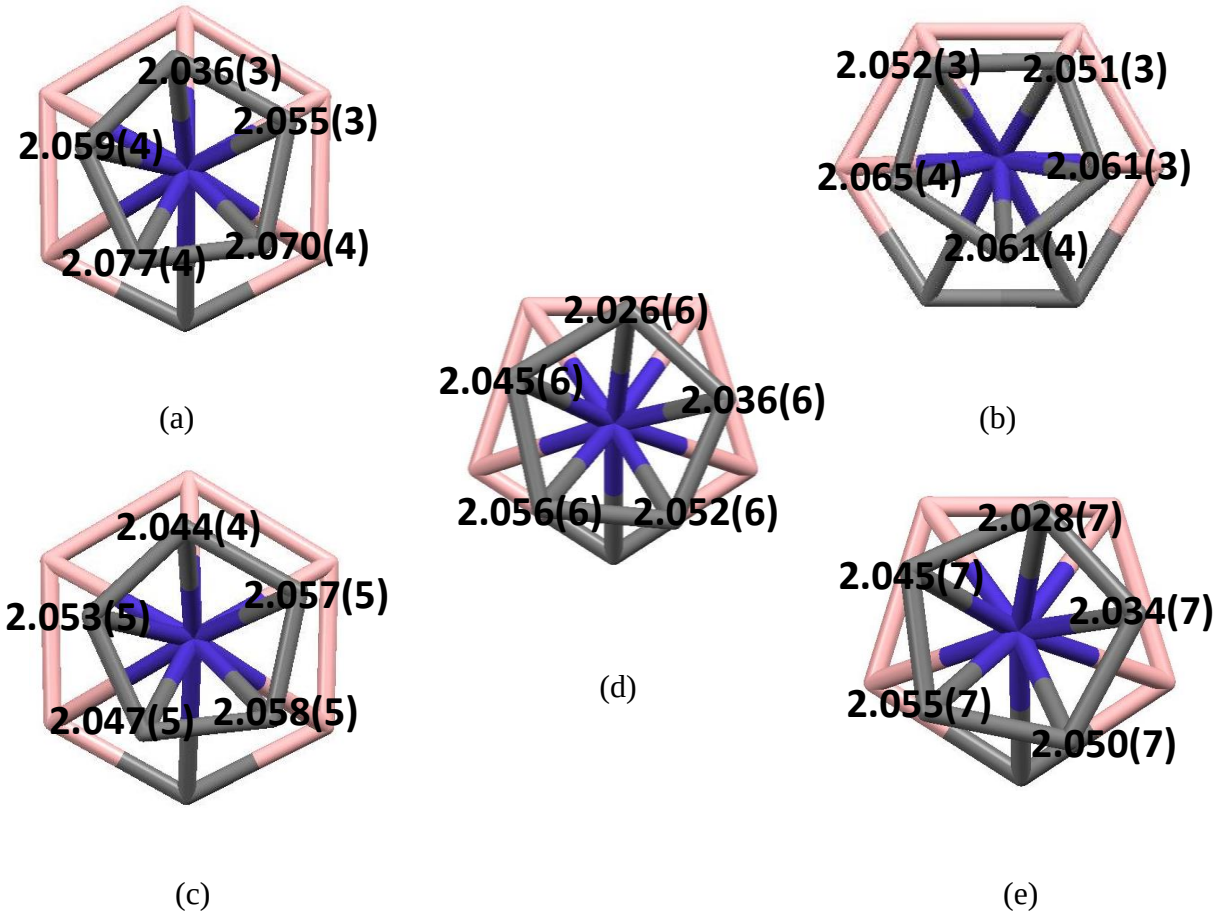

Figure 4.13.4 Structure and M-EPL bond lengths (Å) of (a) XERBED, 1,14-(η-C_5H_5)$_2$-1,14,2,10-$Co_2C_2B_{10}H_{12}$ - Co1 bound carborane face, (b) Co14 bound carborane face, (c) XERBIH, 1-(*p*-cymene)-14-(η-C_5H_5)-1,14,2,10-$RuCoC_2B_{10}H_{12}$ - Co bound carborane face and UJEYIS, 2-(η-C_5H_5)-2,1,12-$CoC_2B_9H_{11}$ (two independent molecules in asymmetric unit) (d) molecule one, (e) molecule two.

4.14 Resynthesised compounds

In the course of the CSD search, we encountered several compounds which had incorrectly assigned cage carbon/boron atoms or unidentified disorder. The details of these structures can be found in the notes in appendix two, but an example is detailed here to show how the ELO method has been used to identify an incorrectly refined structure. The compound TPNRHB is an ML_2L' 3,1,2- compound with the EPL set consisting of bidentate nitrato and a triphenylphosphine ligand. There are two independent molecules in the asymmetric unit of TPNRHB, and as can be seen in figure 4.14.1, the phosphine ligand in both molecules appears to be trans to a B-B connectivity, while one of the oxygen donors of the nitrato ligand is trans to the C-C connectivity.

(a) (b)

Figure 4.14.1 Structures (two independent molecules in asymmetric unit) of TPNRHB, 3-(κ^2-NO_3)-3-(PPh_3)-3,1,2-$RhC_2B_9H_{11}$. (a) Molecule one, (b) molecule two.

The phosphine ligand, based on its RTE in other structures, would be expected to be trans to the carbon part of the cage in this structure where the other ligand in the EPL set is nitrato, which would be expected to have a weak RTE (based primarily on the relative electronegativity of an oxygen donor vs a phosphorus donor). The vertex to adjacent vertex distances of the open face of the carborane are listed in table 4.14.1, and the vertex to centroid distances for the open face are listed in table 4.14.2.

Table 4.14.1 Selected molecular dimensions (Å, º) in TPNRHB (e.s.d.s on these distances estimated to be 0.02 Å).

Connectivity	Molecule one	Molecule two
C1-C2	1.87	1.90
C1-B4	1.78	1.65
B4-B8	1.59	1.85
B8-B7	1.65	1.72
B7-C2	1.83	1.82

Table 4.14.2 Selected vertex to centroid distances (Å) in TPNRHB (e.s.d.s on these distances estimated to be 0.02 Å).

	Molecule one	Molecule two
Vertex 1	1.76	1.71
Vertex 2	1.74	1.77
Vertex 4	1.55	1.63
Vertex 7	1.70	1.73
Vertex 8	1.52	1.63

For molecule one, the connectivity assigned as C-C is the longest in the open face of the carborane. The connectivity labelled as B4-B8 is the shortest, making it a more likely candidate for the C-C connectivity. This is supported by the VCDs, the shortest of which are to B4 and B8, and by the ELO which has the (presumably stronger RTE) phosphine trans to the B4-B8 connectivity. For molecule two, the connectivity lengths and the VCDs are somewhat at odds, the former suggesting C1-B4 is the real C-C connectivity and the latter suggesting B4-B8. Going by the VCD alone indicates that B4-B8 is the real C-C connectivity (although it could be that one of the cage carbon atoms is disordered over vertices 1 and 8), and this assignment is supported by the ELO which has the phosphine ligand trans to the B4-B8 connectivity.

While our confidence in the correct reassignment of the carbon atoms is high, the poor quality of the structure of TPNRHB (*R* factor = 12.3%) led us to resynthesise and recrystallise the compound to see if better quality data could be obtained. The synthesis[6] involves adding nitric acid to 3,3-$(PPh_3)_2$-3-H-3,1,2-$RhC_2B_9H_{11}$,[18] a structure which was

among the CSD search hits (HPRHCB) and which we also crystallised prior to use. Our sample of HPRHCB (**V**) crystallised in the space group *P*-1 (HPRHCB = $P2_1/n$) and with a molecule of DCM in the asymmetric unit. Our structure appears to be free of the disorder associated with HPRHCB (figure 4.14.2 (a)), the carbon atoms being assigned unambiguously by VCD, and the hydride ligand lying trans to C1 (figure 4.14.2 (b)).

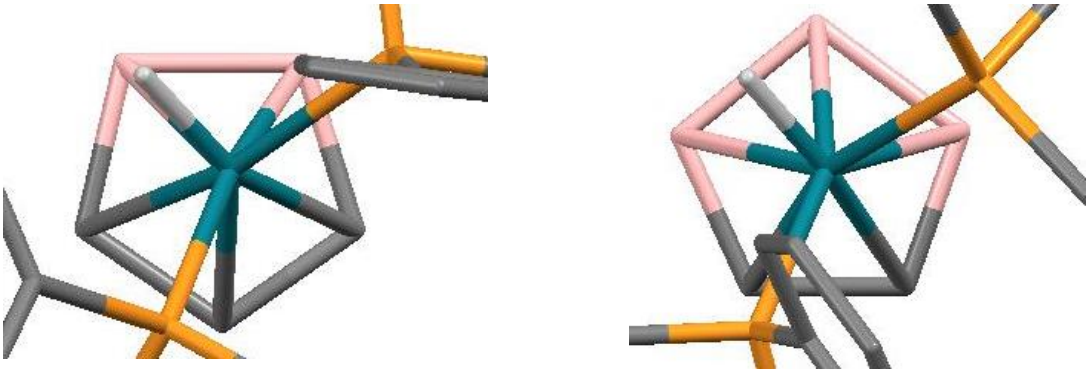

(a) (b)

Figure 4.14.2 Structure of (a) HPRHCB, and (b) compound **V**, both 3,3-$(PPh_3)_2$-3-H-3,1,2-$RhC_2B_9H_{11}$.

Our sample of TPNRHB (**VI**) crystallised in the space group *P*-1 (TPNRHB = *P*1) and has two molecules in the asymmetric unit (figure 4.14.3). Assignment of the carbon atoms in the cage was done by examination of connectivity lengths and VCD, confirming that the phosphine ligand does in fact lie trans to the C-C connectivity as was suspected in TPNRHB.

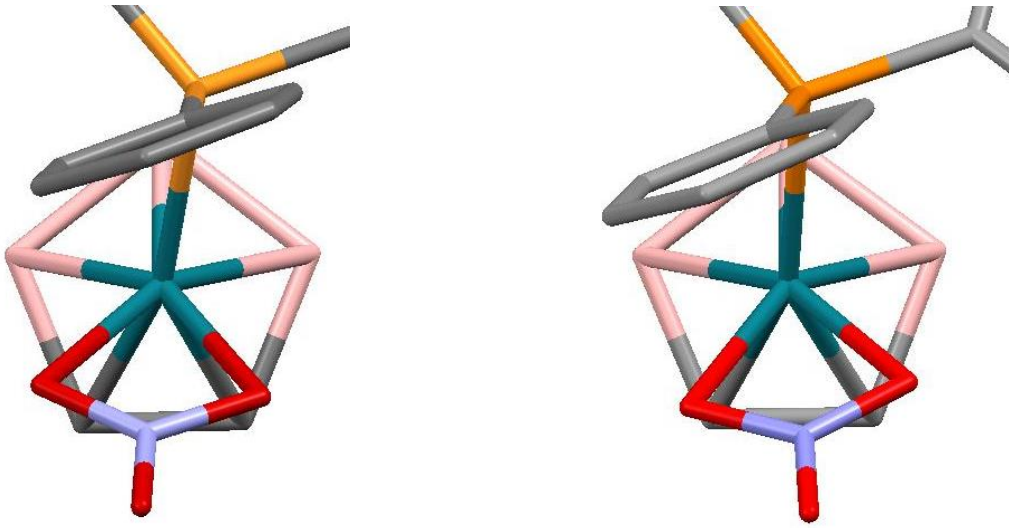

(a) (b)

Figure 4.14.3 Structures (two independent molecules in asymmetric unit) of compound **VI**, 3-(κ^2-NO_3)-3-(PPh_3)-3,1,2-$RhC_2B_9H_{11}$. (a) Molecule A, (b) molecule B.

In addition to the resynthesis and recrystallisation of HPRHCB and TPNRHB we also took the opportunity to resynthesise and crystallise the compound 3,3-$(PPh_3)_2$-3-(NO_3)-3,1,2-$RhC_2B_9H_{11}$ (**VII**).[6] The monodentate nitrate compound has previously been synthesised by addition of PPh_3 to **VI**, but the crystal structure had not yet been determined. Compound **VII** crystallises in the space group *P*-1 and the EPLs are orientated with both phosphines trans to a C-B connectivity (although one phosphine is closer to being trans to a cage carbon atom than the other), and the nitrate group trans to a B-B connectivity (figure 4.14.4). This orientation makes sense based on the RTE arguments previously established.

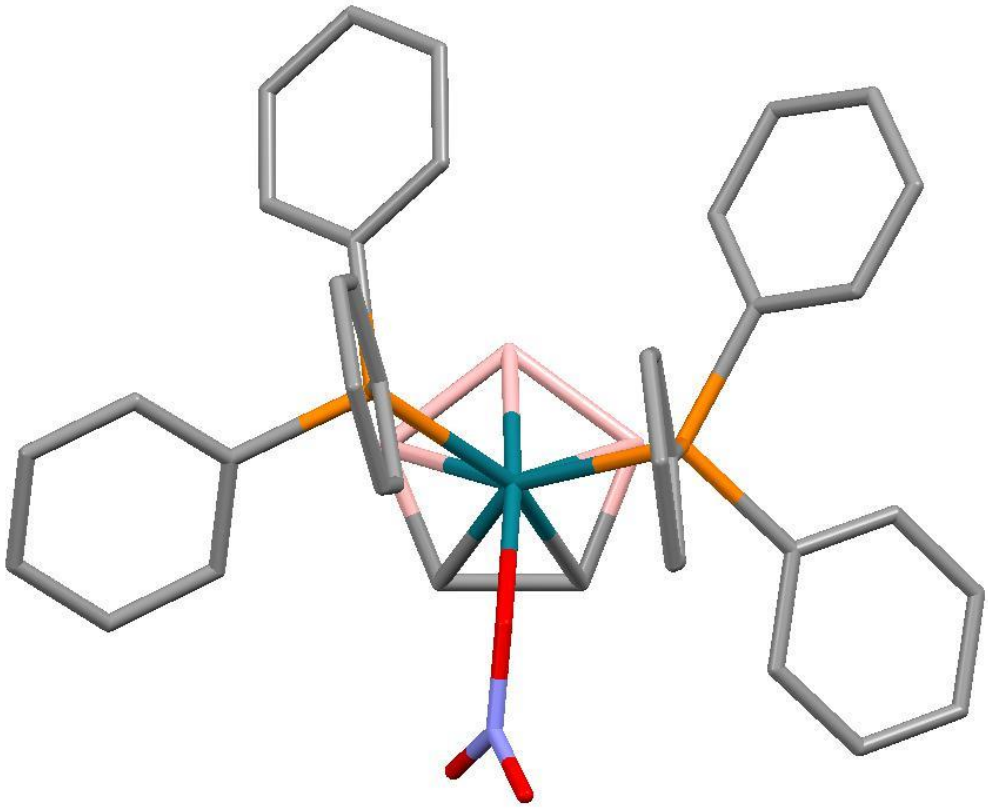

Figure 4.14.4 Structure of compound **VII**, 3,3-$(PPh_3)_2$-3-(NO_3)-3,1,2-$RhC_2B_9H_{11}$.

4.15 Summary

Limitations

The ELO method outlined in this chapter supports two key points: the first is that the M-EPL bond lengths trans to the boron part of the cage tend to be longer than M-EPL bonds which are trans to the carbon (or other heteroatom) part of the cage; and the second is that the RTE of a given ligand is relatively consistent across the range of structures studied. The ELO method is not perfect though, and all structures which have unexpected relative bond lengths or unexpected ELOs are noted in the relevant sections.

The reasons that some of the structures do not fit the trend is difficult so say with certainty, as there may be unconsidered steric or electronic effects operating within the molecule, or CPFs operating on an intermolecular level to give relative bond lengths/ELOs which would not have been predicted. This latter effect is unavoidable, but care must be taken when interpreting the ELOs of compounds with EPLs that are assumed to have similar RTEs, as the barrier to rotation may be less than the magnitude of the CPFs[9] (particularly if strong CPFs such as hydrogen bonding are possible). Clear enough trends seem to appear in the compounds studied to suggest that RTEs play a significant role in determining the ELOs in compounds with non-identical ligands in the EPL set.

The difference in M-EPL bond lengths between two identical EPLs which are trans to different parts of the cage (e.g. B vs C) is sometimes very small and may, in some compounds, be negligible when the reported bond length e.s.d.s are taken into consideration. Such compounds are listed in table 4.15.1, and the fact that the M-EPL bond lengths (of two identical EPLs which are trans to different parts of the cage) are very similar has been noted in sections 4.3 to 4.13 if the compound was discussed. For these cases more precise structural studies would be needed to confirm that the M-EPL bond length trans to the carbon part of the cage is indeed shorter than the M-EPL bond length trans to the boron part of the cage, although even then the difference may be very small.

Table 4.15.1 Compounds where difference in lengths of M-EPL bonds trans to B or B-B/C-B connectivity and M-EPL bonds trans to C or C-C connectivity may be negligible after taking bond length e.s.d.s into account.

CSD reference code	Lengths of M-EPL bonds (Å). Subscript con denotes a connectivity, Subscript ring denotes Cp/benzene or substituted derivative.
DEHFIF	C_{ring} trans to C-C_{con} = 2.191(3), C_{ring} trans to C-B_{con}= 2.196(3)
DUBDIN	C_{ring} trans to C = 2.030(5); 2.028(5), C_{ring} trans to B = 2.044(5)
KEJVEA	C_{ring} trans to C = 2.169(5), C_{ring} trans to B = 2.179(5)
KEJVIE	C_{ring} trans to C = 2.157(11); 2.162(11), C_{ring} trans to B = 2.196(11)
LUKKUX	C_{ring} trans to disordered C/B = 2.065(3), C_{ring} trans to B = 2.073(3)
VEMNIK	C_{ring} trans to C = 2.213(5), C_{ring} trans to C-B_{con} = 2.222(5)
JIMXUY	C_{ring} trans to C-C_{con} = 2.085(9), C_{ring} trans to C-B_{con}= 2.091(6), C_{ring} trans to B = 2.111(7); 2.112(8)
LULHAB	C_{ring} trans to disordered (C/B)-C_{con} = 2.178(4); 2.177(4), C_{ring} trans to disordered (C/B)-B_{con} = 2.169(4)
HUSKOW	C_{ring} trans to C = 2.124(3), C_{ring} trans to C-B_{con} = 2.125(3)
FOTLAB	CMe_{ring} trans to C = 2.132(9), CMe_{ring} trans to B-B_{con} = 2.130(9), CH_{ring} trans to C-C_{con} = 2.094(9), CH_{ring} trans to B = 2.113(9), CH_{ring} trans to C-B_{con} = 2.095(9), CH_{ring} trans to B = 2.127(9)
BEXLAR	CMe_{ring} trans to C = 2.125(9), CMe_{ring} trans to disordered (C/B)-B_{con} = 2.145(12), CMe_{ring} trans to B = 2.134(10), CH_{ring} trans to B-B_{con} = 2.140(12), CH_{ring} trans to disordered (C/B)-C_{con} = 2.103(14)
FOTLEF	C_{ring} trans to C-C_{con} = 2.082(16), C_{ring} trans to C-B_{con}= 2.090(10), C_{ring} trans to B = 2.11(2); 2.105(11)
HUSKUC	CMe_{ring} trans to C = 2.120(2), CMe_{ring} trans to B = 2.126(2)
KAXGEV	C_{ring} trans to C = 2.20(2), C_{ring} trans to C-B_{con} = 2.21(2)
TANTOR	C_{ring} trans to C = 2.098(10), C_{ring} trans to B = 2.118(10)
MOGSAC	CO trans to C-B_{con} = 1.896(13), CO trans to C-B_{con} = 1.878(14), CO trans to B = 1.898(13)
KOBLOC	CO trans to C = 1.84(3), CO trans to C-B_{con} = 1.88(3), CO trans to B-B_{con} = 1.87(3)
CSCREC	CO trans to C = 1.88(2), CO trans to B = 1.90(2), CO trans to B-B_{con} = 1.90(2)
KISCEU	CO trans to C = 1.777(9), CO trans to C-B_{con} = 1.792(9)
CEHCEX	P trans to C-B_{con} = 2.346(2), P trans to C = 2.344(2)
KISBIX	CO trans to C = 1.762(12), CO trans to C-B_{con} = 1.754(12)
ZEPYIC	CO trans to C = 1.902(5), CO trans to C-B_{con} = 1.890(6)
HOHDEN	CO trans to C = 1.890(6), CO trans to C-B_{con} = 1.872(6)
HOHDIR	CO trans to C = 1.885(4), CO trans to C-B_{con} = 1.869(4)
HOHDAJ	Molecule containing Ru2: CO trans to C = 1.88(2), CO trans to C-B_{con} = 1.91(2)
HIZQUC	Cage containing Ru1: CO trans to C = 1.880(7), CO trans to C-B_{con} = 1.886(7) Cage containing Ru2: CO trans to C = 1.884(6), CO trans to C-B_{con} = 1.889(7)
SEQQIO	CO trans to C = 1.896(4), CO trans to B-B_{con} = 1.888(4)
SEWVAR	Molecule containing Rh1: C_{ring} trans to Te = 2.199(10), C_{ring} trans to B = 2.204(10); 2.217(11); 2.221(10); 2.226(11) Molecule containing Rh2: C_{ring} trans to Te = 2.185(10), C_{ring} trans to B = 2.212(10); 2.215(11); 2.225(11)
SEWVEV	C_{ring} trans to Te = 2.231(7), C_{ring} trans to B-B_{con} = 2.215(5)

Table 4.15.1 continued

WELNEG	C trans to C = 2.110(10), C trans to B-B_{con} = 2.140(10)
UJEYEO	Molecule containing Co2: C_{ring} trans to C atoms = 2.025(15); 2.023(12), C_{ring} trans to B atoms = 2.011(14); 2.020(14); 2.039(12)
GETMAT	C_{ring} trans to deg5 C = 2.201(2), C_{ring} trans to deg4 C = 2.210(3), C_{ring} trans to B = 2.203(2), C_{ring} trans to B = 2.205(2)
KAPQAU	C_{ring} trans to deg4 C = 1.928(3), C_{ring} trans to deg5 C = 1.922(3)
KAPQEY	C_{ring} trans to deg4 C = 1.802(3), C_{ring} trans to deg5 C = 1.794(3)
JACCOG	CO trans to C = 1.962(4), CO trans to C-B_{con} = 1.957(4)
CANNOV01	C_{ring} trans to deg4 C-B_{con} = 2.013(4), C_{ring} trans to deg5 C-B_{con} = 2.012(3)
XERBED	Cp bonded to Co2: C_{ring} trans to disordered C/B = 2.052(3); 2.051(3), C_{ring} trans to B = 2.061(3), C_{ring} trans to B-B_{con}= 2.061(4); 2.065(4)
XERBIH (Cp)	C_{ring} trans to C = 2.044(4), C_{ring} trans to B-B_{con} = 2.047(5); 2.053(5); 2.057(4); C_{ring} trans to B = 2.057(4)
UJEYIS	Molecule containing Co2A: C_{ring} trans to C = 2.026(6), C_{ring} trans to B = 2.036(6); 2.045(6) Molecule containing Co2B: C_{ring} trans to C = 2.028(7), C_{ring} trans to B = 2.034(7); 2.045(7); 2.050(7); 2.055(7)

Conversely, some of the M-EPL bonds of identical EPLs which are trans to similar parts of the cage differ greatly (for example TOJREP (figure 4.15.1)). This is perhaps somewhat unexpected, but does not affect the RTEs, or the fact that for the majority of compounds the M-EPL bond lengths trans to the boron part of the cage are longer than M-EPL bonds which are trans to the carbon part of the cage.

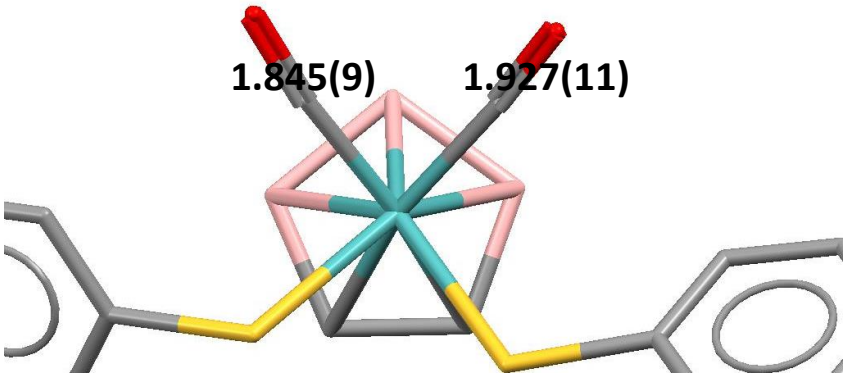

Figure 4.15.1 Structure and selected M-EPL bond lengths (Å) of TOJREP, $[NMe_4]_2[3,3\text{-}(CO)_2\text{-}3,3\text{-}(SPh)_2\text{-}3,1,2\text{-}MoC_2B_9H_{11}]$.

Applications

Despite the limitations outlined above, comparison of M-EPL bond lengths and ELOs seems to describe general patterns, which if used carefully and in conjunction with all the other available methods, could prove useful during crystallographic solution.

For example currently four different methods are generally used to help find the cage carbon atoms during crystallographic studies: Vertex to centroid distance (VCD); size of U_{iso} (a carbon vertex which has been wrongly assigned as boron will have a smaller U_{iso} value than if it had been correctly assigned); length of cage connectivity (for 3,1,2- compounds the C-C connectivity is usually the shortest in the open carborane face); B-H/C-H distances[19] (if the hydrogen is allowed to refine freely, C-H bonds tend to be shorter if the carbon atom has been refined as boron than if they are refined as carbon). In the future the ELO method will hopefully also be used to aid locating the cage carbon atoms (or heteroatoms).

If identical ligands are present in the EPL set then comparison of M-EPL bond lengths can be used to help determine where the cage carbon atoms/heteroatoms are, while if different ligands are present then using the RTEs established in section 4.6-4.13 can be used. It is difficult to give any definitive RTE series to be used as a reference because different metals are used throughout the structures found in the CSD searches, different phosphines are used and more EPL combinations would need to be examined to confirm a given ligand's position within the series. However, based on the information available from the CSD search, a very general RTE series would perhaps look as follows:

Transition metal based ligand, H > CO > R, S_2CR > PR_3 > Cl

Whilst the RTE and the trans influence are not the same as each other, the RTEs of metallaheteroboranes may provide complementary information about the strength of M-L bonding which could be useful in determining relative trans influences.

Future Work

While the number of compounds in the CSD has been enough to establish a pattern in the relative M-EPL bond lengths and the ELOs, the availability of more structures with both diverse EPL sets and families of similar EPL sets would help to determine the reliability of the ELO method, and to develop a more clearly defined RTE series (figure 4.15.2). For example: more structures which incorporate both a strong σ-donor ligand and a carbonyl ligand would hopefully show definitively which of these two types of ligands has the stronger RTE; a structure with a strong π-acceptor phosphine (e.g. PCl_3) and a weak π-acceptor phosphine (e.g. PMe_3) would potentially show whether stronger π-accepting ligands have a stronger RTE, as would more structures like LICDOQ where a ligand which is a stronger π-acceptor than carbonyl (e.g. NO or CS) is incorporated into an EPL set with carbonyl. As noted previously, care would need to be taken when interpreting the ELOs of these suggested compounds as the ELOs may be susceptible to the influence of CPFs if the EPLs have similar RTEs.

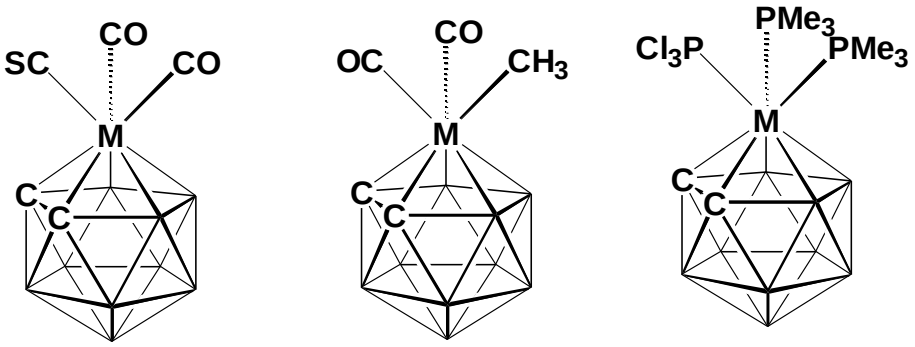

Figure 4.15.2 Examples of proposed compounds to help refine the RTE series (EPLs are randomly orientated).

For the majority of the 2,1- , 2,1,7- and sub/supraicosahedral metallacarboranes compounds found during the database search the RTEs and relative bond lengths seem to support the trends established for the 3,1,2- compounds. However the number of examples of 2,1-, 2,1,7- and sub/supraicosahedral metallacarboranes compounds found was lacking compared to the number of 3,1,2- compounds. More examples of these types of compounds would be needed to assess how well the ELO method works when the cage architecture is not 3,1,2-, and this would also help to further define an RTE series, and perhaps give information on the relative M-cage bond strengths of topologically inequivalent vertices.

For the 2,1- metallaheteroborane compounds (section 4.9) found, all the heteroatoms have a higher Pauling electronegativity than boron. If a heteroatom with a lower electronegativity than boron (for example Si, Ge or Sn) could be incorporated into a metallaheteroborane, then the EPLs with a strong trans influence/RTE would potentially be orientated trans to the cage boron atoms (or trans to the heteroatom in the case of indenyl/naphthalene). This is because the FMOs would presumably be more localised on the less electronegative heteroatom, giving the boron atoms a weaker trans influence than the heteroatom.

There were no eighteen electron compounds found which contained both π-donors and π-acceptors or exclusively σ-donors as EPLs. Such compounds would help to gauge the RTEs of π-donor ligands relative to the other two types of ligands. The only two compounds found which incorporate a π-donor and an exclusively σ-donating ligand in the EPL are two formally sixteen electron compounds of the type 3,3-$(NR_2)_2$-3-(NR_2H)-3,1,2-$MC_2B_9H_{11}$ (R = Me/Et, M = Ti, Zr),[20a,b] which show conflicting ELOs, with one having an amide EPL trans to a cage carbon atom, and the other having an amine ligand trans to the cage C-C connectivity.

In addition to the examination of further compounds, a computational study could be used to both predict the ELO of compounds and to analyse which steric and orbital interactions play the most important roles in determining the orientations.

4.16 References

4.1 (a) N. Kaltsoyannis and P. Mountford, *J. Chem. Soc., Dalton Trans.*, 1999, 781.
(b) J. Zhu, Z. Lin and T.B. Marder, *Inorg. Chem.*, 2005, **44**, 9384.
(c) K.M. Anderson and A.G. Orpen, *Chem. Commun.*, 2001, 2862.
(d) F.R. Hartley, *Chem. Soc. Rev.*, 1973, **2**, 163.
(e) P.D. Lynea and D.M.P. Mingos, *J. Chem. Soc., Dalton Trans*., 1995, 1635.
(f) R. Mason, R. McWeeny and A.D.C. Towl, *Discuss. Faraday Soc.*, 1969, **47**, 20.
(g) L.J. Manojlović-Muir, and K.W. Muir, *Inorg. Chim. Acta*, 1974, **10**, 47.
(h) T.G. Appleton, H.C. Clark, L.E. Manzer, *Coord. Chem. Rev.*, 1973, **10**, 335.
(i) B.J. Coe and S. Glenwright, *Coord. Chem. Rev.*, 2000, **203**, 5.
(j) R. Mason and A.D.C. Towl. *J. Chem. Soc. (A), Inorg. Phys. Theor.*, 1970, 1601.
(k) P.K. Sajith and C.H. Suresh, *Dalton Trans.*, 2010, **39**, 815.

4.2 F.H. Allen, *Acta Crystallogr., Sect. B: Struct. Sci.*, 2002, **B58**, 380. For this study we used CSD Version 5.33 (November 2011).

4.3 G.K. Barker, M.P. Garcia, M. Green, G.N. Pain, F.G.A. Stone, S.K.R. Jones and A.J. Welch, *J. Chem. Soc., Chem. Commun.*, 1981, 652.

4.4 A. McAnaw, G. Scott, L. Elrick, G.M. Rosair and A.J. Welch, *Dalton Trans.*, 2013, **42**, 645.

4.5 *Mercury*, version 3.3, Cambridge Crystallographic Data Centre, Cambridge, UK, 2006.

4.6 Z. Demidowicz, R.G. Teller and M.F. Hawthorne, *J. Chem. Soc., Chem. Commun.*, 1979, 831.

4.7 D.M.P. Mingos, *J. Chem. Soc., Dalton Trans*., 1977, 602.

4.8 J. Giacovazzo, H.L. Monaco, D. Viterbo, F. Scordari, G. Gilli, G. Zanotti and M. Catti, *Fundamentals of Crystallography*, Oxford University Press, 1992; R.P.A. Bettens, D. Dakternieks, A. Duthie, F.S. Kuanab and E.R.T. Tiekink, *CrystEngComm*, 2009, **11**, 1362; P. Dauber and A.T. Hagler, *Acc. Chem. Res.*, 1980, **13**, 105; D. O'Connell, T.R. Spalding, G. Ferguson, J.F. Gallagher and J.D. Kennedy, *J. Organomet. Chem.*, 1995, **503**, C12.

4.9 D. McKay, unpublished results, Heriot-Watt University, 2012.

4.10 A.S. Batsanov, A.V. Churakov, J.A.K. Howard, A.K. Hughes, A.L. Johnson, A.J. Kingsley, I.S. Neretin and K. Wade, *J. Chem. Soc., Dalton Trans.*, 1999, 3867.

4.11 A.S. Batsanov, A.E. Goeta, J.A.K. Howard, A.K. Hughes, A.L. Johnson and K. Wade, *J. Chem. Soc., Dalton Trans.*, 2001, 1210.

4.12 F.A. Cotton, B.A. Frenz and A. Shaver, *Inorg. Chim. Acta*, 1973, **7**, 161.

4.13 R. McLellan, unpublished results, Heriot-Watt University, 2009.

4.14 Z. Lin and M.B. Hall, *J. Am. Chem. Soc.*, 1992, **114**, 6102.

4.15 E.H.S. Wong and M.F. Hawthorne, *J. Chem. Soc., Chem. Commun.*, 1976, 257.

4.16 P.D. Abram, D. Ellis, G.M. Rosair and A.J. Welch, *Chem. Commun.*, 2009, 5403.

4.17 J.D. Hewes, C.B. Knobler and M.F. Hawthorne, *J. Chem. Soc., Chem. Commun.*, 1981, 206.

4.18 (a) T.E. Paxson and M.F. Hawthorne, *J. Am. Chem. Soc.*, 1974, **96**, 4674
(b) R.T. Baker, M.S. Delaney, R.E. King, C.B. Knobler, J.A. Long, T.B. Marder, T.E. Paxson, R.G. Teller and M.F. Hawthorne, *J. Am. Chem. Soc.*, 1984, **106**, 2965.

4.19 A. Burke, R. McIntosh, D. Ellis, G.M. Rosair and A.J. Welch, *Collect. Czech. Chem. Commun.*, 2002, **67**, 991; A. McAnaw, M.E. Lopez, D. Ellis, G.M. Rosair and A.J. Welch, *Dalton Trans.*, 2014, **43**, 5095.

4.20 (a) D.E. Bowen, R.F. Jordan and R.D. Rogers, *Organometallics*, 1995, **14,** 3630.
(b) G. Zi, H-W. Li and Z. Xie, *Organometallics*, 2002, **21,** 3850.

Chapter 5
Pentamethylcyclopentadienyl Ruthenacarboranes

5.1 Introduction

The most commonly used method of making supraicosahedral metallacarboranes is to reduce a dicarborane or a metallacarborane with an alkali metal, opening up the structure, and then add a suitable metal fragment to complete the polyhedron.[1] However, there is one example[2] in the literature of a reaction involving direct nucleophilic insertion of a metal fragment into a neutral closo carborane, and two examples[3,4] of reactions involving direct electrophilic insertion (DEI) of metal fragments into anionic closo metallacarboranes to give, in all three cases, supraicosahedral compounds. There are a number of examples of direct nucleophilic insertion into subicosahedral closo carboranes to give subicosahedral and icosahedral compounds[5] - however these particular reactions have proved unsuccessful in preparing supraicosahedral species.

The reaction[2] of 1-Me-1,2-$C_2B_{10}H_{11}$ with $Co(PEt_3)_4$ gives thirteen vertex 1-Me-4-(Et_3P)-$\mu_{4,6\text{-or-}7}$-$\{Co(PEt_3)_2$-μ-$(H)_2\}$-4,2,1-$CoC_2B_{10}H_{10}$. The formation of fourteen vertex $(CpCo)_2C_2B_{10}H_{12}$ compounds which have a degree five and a degree six cobalt is believed[3] to proceed via DEI of a $\{CpCo^+\}$ fragment into $[CpCoC_2B_{10}]^-$. Kudinov et al[4] have reported the reaction (figure 5.1.1) of $[RuClCp^*]_4$ (a source of $\{RuCp^{*+}\}$) with Tl[3-Cp*-3,1,2-*closo*-$RuC_2B_9H_{11}$] (this was made from reaction of $Tl[TlC_2B_9H_{11}]$ and $[RuClCp^*]_4$) to give the non-Wadian thirteen vertex bimetallic species 4,5-Cp^*_2-4,5,2,3-*closo*-$Ru_2C_2B_9H_{11}$ (compound **VIII**). The reaction can all be done in one step or the twelve vertex species can be isolated prior to the DEI. The reaction also proceeds when $[CpRu(MeCN)_3]PF_6$ is used for the DEI, giving 4-Cp*-5-Cp-4,5,2,3-*closo*-$Ru_2C_2B_9H_{11}$, albeit in lower yield than when $[RuClCp^*]_4$ is used.

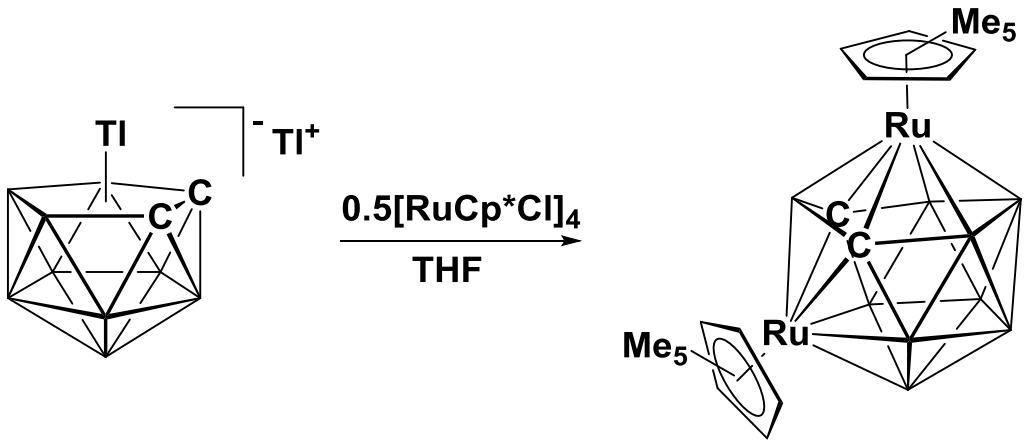

Figure 5.1.1 Reaction of $Tl[TlC_2B_9H_{11}]$ and $[RuClCp^*]_4$ to give 4,5-Cp^*_2-4,5,2,3-*closo*-$Ru_2C_2B_9H_{11}$ (**VIII**).

Compound **VIII** is non-Wadian as the RuCp* units only contribute one electron each to cluster bonding (instead of two electrons as Ru(arene) would), giving twenty six or 2n (where n = the number of vertices) Polyhedral Skeletal Electrons (PSEs), as opposed to the twenty eight (2n + 2) required for a closo structure.[6a] The structure of **VIII** can therefore be described as hypercloso. It has been shown that the hypothetical docosahedral compounds $B_{13}H_{13}$ and $[B_{13}H_{13}]^{2-}$ should have similar stabilities, as removal of a pair of electrons from the latter should not be significantly destabilising.[6b] Similar predictions were made for $B_{15}H_{15}$ and $B_{17}H_{17}$ and their respective dianions. Thus the stability of non-Wadian **VIII** can be rationalised based on its similarity to $B_{13}H_{13}$.

Upon attempting to repeat the reaction of $Tl[TlC_2B_9H_{11}]$ and $[RuClCp^*]_4$, we isolated a new twelve vertex compound with a pendant THF molecule 7-(THF)-3-(η-C_5Me_5)-3,1,2-*closo*-$RuC_2B_9H_{10}$ (compound **17**, not reported by Kudinov et al) and compound **VIII** (slightly more of **17** (17% yield) than **VIII** (13% yield) is formed).

We wished to see whether substituting the eleven vertex nido species for a twelve vertex one would lead to the synthesis of non-Wadian fourteen vertex compounds. Upon reaction of $[RuClCp^*]_4$ and $Na_2[7,9\text{-}nido\text{-}C_2B_{10}H_{12}]$ in THF, a number of coloured compounds were observed upon TLC.

Most of the bands have been identified, but owing to time constraints the complete characterisation of all the compounds was not possible. The following bands were observed during chromatographic work up: unidentified yellow band; green 3,6-(η-$C_5Me_5)_2$-3,6,?,?-

closo-$Ru_2C_2B_{10}H_{12}$ (**21**)*; yellow band from which 4,5-(η-C_5Me_5)$_2$-4,5,2,11-*closo*-$Ru_2C_2B_9H_{11}$ (**19**) crystallises; partially identified purple band; purple 3,6-(η-C_5Me_5)$_2$-3,6,2,?-*closo*-$Ru_2C_2B_{10}H_{12}$ (**22**)*; orange 4,5-(η-C_5Me_5)$_2$-4,5,1,6-*closo*-$Ru_2C_2B_9H_{11}$ (**18**); pink 4,5-(η-C_5Me_5)$_2$-4,5,2,3-*closo*-$Ru_2C_2B_9H_{11}$ (**VIII**); pink (μ^3-dicarba-*closo*-dodecaborane-B^1,B^2,B^3,H^1,H^2,H^3)-(μ^3-ethylidyne)-tris(η^5-pentamethylcyclopentadienyl)-triruthenium (**23**)*; yellow 8-(*n*-BuO)-4,5-(η-C_5Me_5)$_2$-4,5,1,6-*closo*-$RuC_2B_9H_{10}$ (**20**).

*For these compounds we have not been able to locate one or both of the cage carbon atoms during crystallographic refinement.

Compounds **18**, **19** and **20** are thirteen vertex non-Wadian metallacarboranes with similar structures to compound **VIII**. Compounds **21** and **22** are fourteen vertex non-Wadian metallacarboranes, displaying a previously unseen cage architecture. Compound **23** is an exo-polyhedral bonded tri-metallic icosahedral compound.

Having established that the DEI of {$Ru(Cp^*)^+$} into reduced 1,2-*closo*-$C_2B_{10}H_{12}$ gives fourteen vertex products, we went on to study the reaction of [RuClCp*]$_4$ with a thirteen vertex nido carborane. The tethered species 1,2-μ-$(CH_2)_3$-1,2-*closo*-$C_2B_{11}H_{11}$ was synthesised by the reduction/capitation of 1,2-μ-$(CH_2)_3$-1,2-*closo*-$C_2B_{10}H_{10}$,[7] then the thirteen vertex compound reduced with sodium metal/naphthalene, and reacted with [RuClCp*]$_4$ in THF. We hoped that we would be able to isolate a fifteen vertex non-Wadian bimetallic from this reaction, but only two isomers of a mono-metallated fourteen vertex compound with a cage-coordinated molecule of THF (compounds 5-(THF)-2,3-$(CH_2)_3$-1-(η-C_5Me_5)-1,2,3-*closo*-$RuC_2B_{11}H_{10}$ (**24**) and 11-(THF)-2,3-$(CH_2)_3$-1-(η-C_5Me_5)-1,2,3-*closo*-$RuC_2B_{11}H_{10}$ (**25**)), and two unidentified compounds could be isolated.

All compounds were characterised by ^{11}B and ^1H NMR spectroscopy and mass spectrometry (and selected compounds by CHN microanalysis), and studied by *X*-ray crystallography.

5.2 Synthesis of 7-(THF)-3-(η-C_5Me_5)-3,1,2-*closo*-$RuC_2B_9H_{10}$ (17)

$Tl[TlC_2B_9H_{11}]$ and $[RuClCp^*]_4$ were added together in THF and stirred at room temperature for 72 hrs. Upon chromatography of the resulting grey/brown mixture, yellow **17** is isolated in 17.0% yield. A slightly smaller amount of **VIII** was also recovered.

The MS of **17** contains an envelope centred on *m/z* 438 (M^+) (M_w **17** = 439.71 g/mol).

Crystals of **17** were grown by diffusion of 40-60 petroleum ether and a DCM solution of **17**, then analysed by *X*-ray diffraction. This revealed **17** to be 7-(THF)-3-(η-C_5Me_5)-3,1,2-*closo*-$RuC_2B_9H_{10}$, which has two crystallographically independent molecules in the asymmetric unit (figure 5.2.1).

Compound **17** is presumably zwitterionic, with the positive charge imposed on the three coordinate oxygen atom cancelling the overall negative charge of the [3-(η-C_5Me_5)-3,1,2-*closo*-$RuC_2B_9H_{10}$]$^-$ anion.

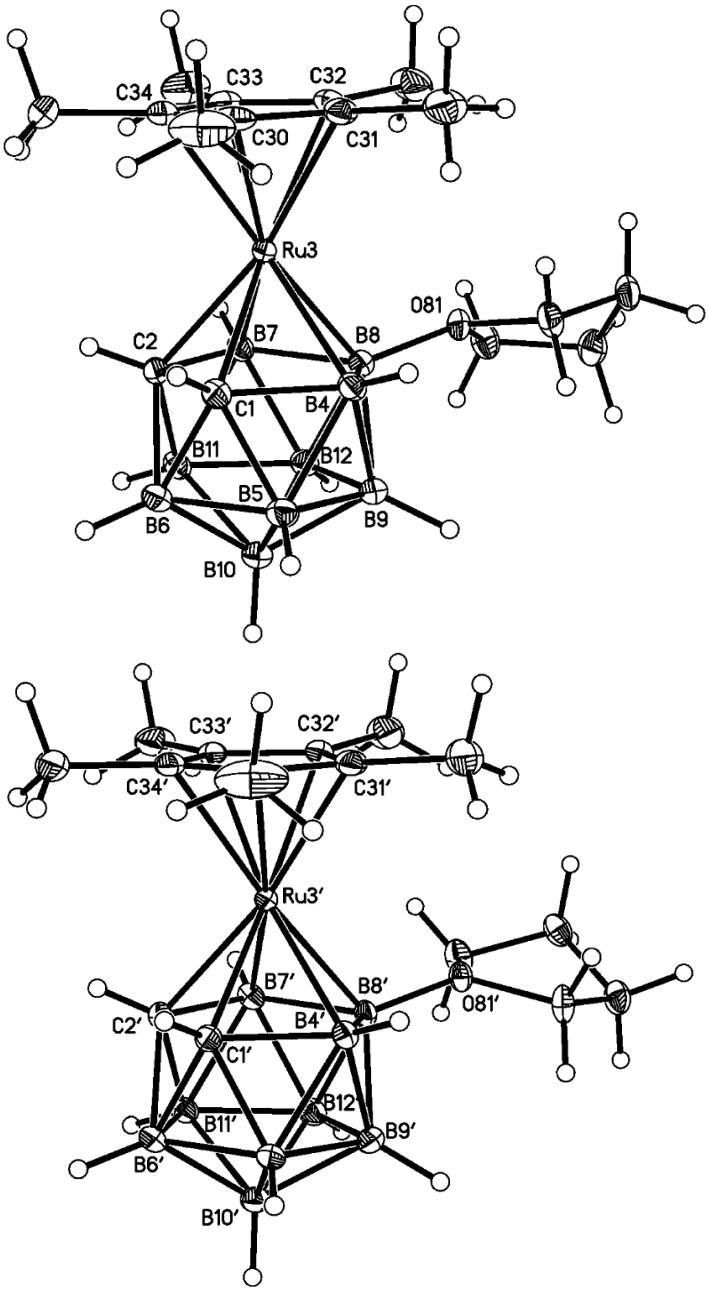

Figure 5.2.1 Molecular structures of 7-(THF)-3-(η-C_5Me_5)-3,1,2-*closo*-$RuC_2B_9H_{10}$ (**17**).

The cages of the two molecules in **17** both show icosahedral structures which resemble that reported for $[N(PPh_3)_2][3\text{-}(\eta\text{-}C_5Me_5)\text{-}3,1,2\text{-}RuC_2B_9H_{11}]$,[4] albeit with a pendant molecule of THF.

Both molecules show the pendant THF attached to B7, which is directly opposite the two cage carbon atoms. In the molecule containing Ru3 (figure 5.2.2 (a)) the Cp* ligand is roughly eclipsed with respect to the cage (each CMe unit is rotated ~ 10^o from perfectly eclipsing a cage vertex). In the molecule containing Ru3' (figure 5.2.2 (b)) the Cp* ligand is

roughly staggered with respect to the cage (each CMe unit is rotated ~ 10° from perfectly eclipsing the centre of a vertex-vertex connectivity).

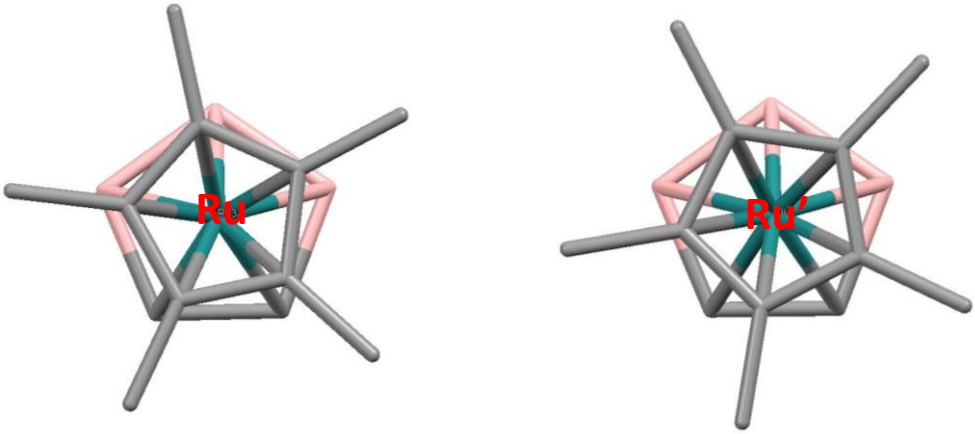

(a) (b)

Figure 5.2.2 Molecular structures (a) and (b) of 7-(THF)-3-(η-C_5Me_5)-3,1,2-*closo*-$RuC_2B_9H_{10}$ (**17**) looking down the M-Cb (Cb = centroid of C1C2B7B8B4) bond (lower section of cages, pendant THF and all hydrogens omitted for clarity).

The ^{1}H NMR spectrum of **17** shows a singlet at 1.80 ppm corresponding to the Cp* group and a broad singlet at 2.50 ppm corresponding to the two cage CHs. This is consistent with cage C_s symmetry and rotation of the Cp* ligand on the NMR timescale. The ^{1}H NMR spectrum also contains multiplets at 4.10-4.20 and 2.05-2.12 ppm corresponding to the hydrogen atoms on the pendant THF.

The ^{11}B{^{1}H} NMR spectrum consists of six peaks in a 1:2:1:2:2:1 ratio between 19.7 and -32.8 ppm. The signal at 19.7 ppm is the only to remain a singlet in the ^{11}B spectrum, meaning that it must correspond to THF bound B7. This signal's relatively downfield position in the ^{11}B NMR spectrum is likely due to B7 being connected to an electronegative (deshielding) oxygen atom.

5.3 Synthesis of 4,5-(η-C_5Me_5)$_2$-4,5,1,6-*closo*-$Ru_2C_2B_9H_{11}$ (18)

Reduction of 1,2-*closo*-$C_2B_{10}H_{12}$ with Na in THF results in [7,9-*nido*-$C_2B_{10}H_{12}]^{2-}$. To this was added [RuClCp*]$_4$ in THF to give a brown solution which was stirred overnight. Upon chromatography orange **18** is isolated in 6.1% yield, along with other compounds which will be described in subsequent sections. This reaction will be described as reaction One in the following sections.

Compound **18** has seven peaks in the ^{11}B NMR spectrum in the ratio 1:2:1:1:2:1:1 between 31.1 and -14.2 ppm, meaning that **18** contains nine boron atoms. There do not appear to be any peaks exceptionally downfield as there are in the ^{11}B NMR spectrum of **VIII**, indicating that there is no degree four boron atom connected to two metals.[8] The structure of **18** is asymmetric, so the integral two peaks must be coincidences.

The MS of **18** contains an envelope centred on *m/z* 604 (M^+) (M_w **1** = 604.94 g/mol), and the elemental analysis is in good agreement with that expected for $C_{22}H_{41}B_9Ru_2$.

The ^{1}H NMR spectrum of **18** has a singlet of integral fifteen at 1.50 ppm and a singlet of integral fifteen at 1.55 ppm, indicating the presence of two symmetry non-equivalent Cp* groups. The ^{1}H NMR spectrum also contains a broad singlet at 2.90 ppm, attributable to a cage CH. The other cage CH signal did not seem to appear in the original spectrum, but running a wider frequency NMR experiment[9] located the other CH at 16.62 ppm, an exceptionally downfield chemical shift for a metallacarborane.

Crystals of **18** were grown by diffusion of 40-60 petroleum ether and a DCM solution of **18** at -30 ^{o}C. *X*-ray analysis of these crystals shows compound **18** to be non-Wadian 4,5-(η-C_5Me_5)$_2$-4,5,1,6-*closo*-$Ru_2C_2B_9H_{11}$ (figure 5.3.1), an isomer of compound **VIII.**

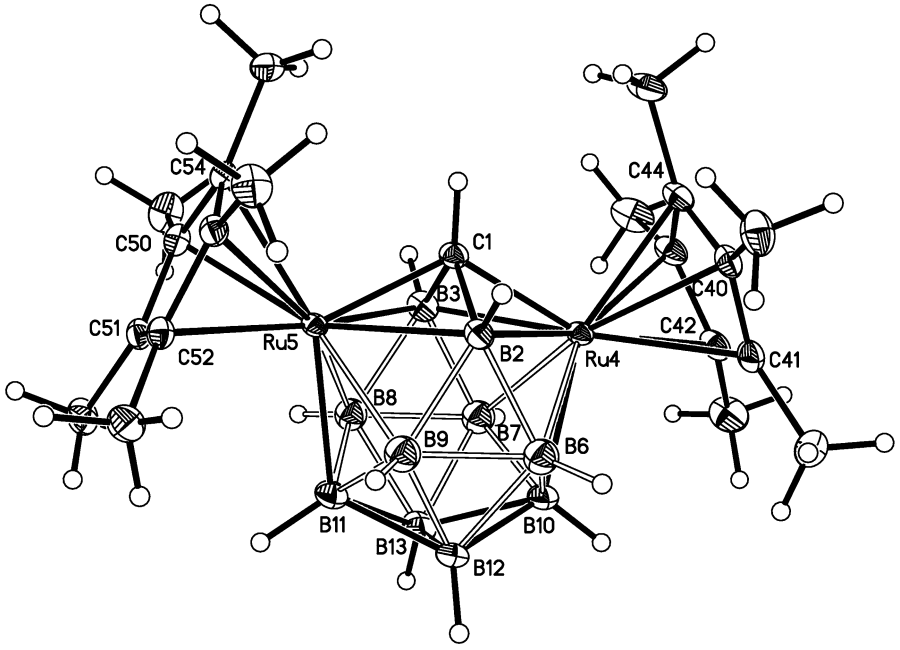

Figure 5.3.1 Molecular structure of 4,5-(η-C_5Me_5)$_2$-4,5,1,6-*closo*-$Ru_2C_2B_9H_{11}$ (**18**). The degree five carbon atom is disordered over vertices 6, 7, 8 and 9.

The structure of **18** is similar to that of **VIII**, but the two compounds differ in the location of the cage carbon atoms. Both clusters are docosahedral with the metal atoms occupying the two degree six vertices and both structures are very similar to 4,5-Cp_2-4,5,2,3-*closo*-$Fe_2C_2B_9H_{11}$ (compound **IX**),[10] which was made by reduction/metallation of 3-Cp-3,1,2-*closo*-$FeC_2B_9H_{11}$. In compound **VIII** the degree four vertex is occupied by a boron atom, but in compound **18** this vertex is occupied by a carbon atom. The assignment of this vertex as carbon was made both because it refined better as carbon than boron, and because of the absence of a high field resonance in the ^{11}B NMR spectrum (something which was also present in **IX**).

The other cage carbon atom is disordered over the symmetry equivalent vertices 6, 7, 8 and 9. The assignment of vertex 6 as carbon was made based on the fact that occupancy of vertices 2/3 or 12/13 would create a mirror plane which would make the Cp* ligands equivalent in the ^{1}H NMR spectrum and occupancy of vertex 10/11 would lead to a 2:2:2:2:1 pattern in the ^{11}B NMR spectrum, leaving only vertex 6.

In **VIII** the two equivalent CH protons are at degree five vertices and both are connected to both metals. The chemical shift of these protons is at -1.27 ppm in the ^{1}H NMR spectrum,

quite upfield for a cage CH proton. In compound **18** one of the CH protons is at a degree four vertex and is connected to both metals, while the other one is on a degree five vertex and is connected to only one of the metals. It cannot be said for certain which signal corresponds to which CH, but it is possible that if when BH is in the degree four position it is very deshielded, then a proton attached to a carbon in the same position would also be very deshielded - i.e. $CH_{deg\ 4}$ = 16.62 ppm, $CH_{deg\ 5}$ = 2.90 ppm.

5.4 Synthesis of 4,5-(η-C_5Me_5)$_2$-4,5,2,11-*closo*-$Ru_2C_2B_9H_{11}$ (19)

Compound **19** is isolated from reaction One in low yield, but its separation during chromatography is somewhat more complicated than that of **18**. Upon initial chromatography, a large purple band is obtained which has signals in the ^{11}B and ^{1}H NMR spectra corresponding to two compounds. Further TLC with a less polar solvent combination leads to a small yellow band slightly above the purple band. The purple band has been partially identified and is described in section 5.9.

The $^{1}H/^{11}B$ NMR spectra of the yellow band reveal the peaks observed in the spectra of the purple band, minus those which correspond to the purple band.

The ^{11}B NMR spectrum of the yellow band contains nine resonances, all of integral one between 116.0 and -19.1 ppm, the downfield boron signal presumably corresponding to a degree four boron at vertex 1 of a 4,5-(η-C_5Me_5)$_2$-4,5,X,Y-*closo*-$Ru_2C_2B_9H_{11}$ (X, Y = carbon position) compound.

The ^{1}H NMR spectrum of the yellow band contains two singlets at 1.60 and 1.48 ppm, both integrating for fifteen protons and likely resulting from two Cp* groups. There is also a broad singlet at 5.20 ppm of integral one, corresponding to a cage CH proton.

The MS of the yellow band contains an envelope centred on *m/z* 604 (M^+) (M_w **19** = 604.94 g/mol) and an envelope centred on *m/z* 357. The MS of the purple compound contains an envelope centred on *m/z* 604 and an envelope centred on *m/z* 644 (which is roughly in agreement with the partially identified structure of the purple compound)

The $^{11}B/^{1}H$ NMR spectra and MS all support compound **19** being the yellow band, which was initially mixed with the purple band, but then separates upon further chromatography.

However, when the yellow band is crystallised (from a 40-60 petroleum ether/THF solution of yellow band), two different types of crystals were grown. The first were red crystals which were analysed by *X*-ray diffraction to give the structure assigned to compound **19**, non-Wadian 4,5-(η-C_5Me_5)$_2$-4,5,2,11-*closo*-$Ru_2C_2B_9H_{11}$, as shown in figure 5.4.1. The

second (green) crystals were found to give the structure of an eleven vertex species, with only one RuCp* unit (figure 5.4.2).

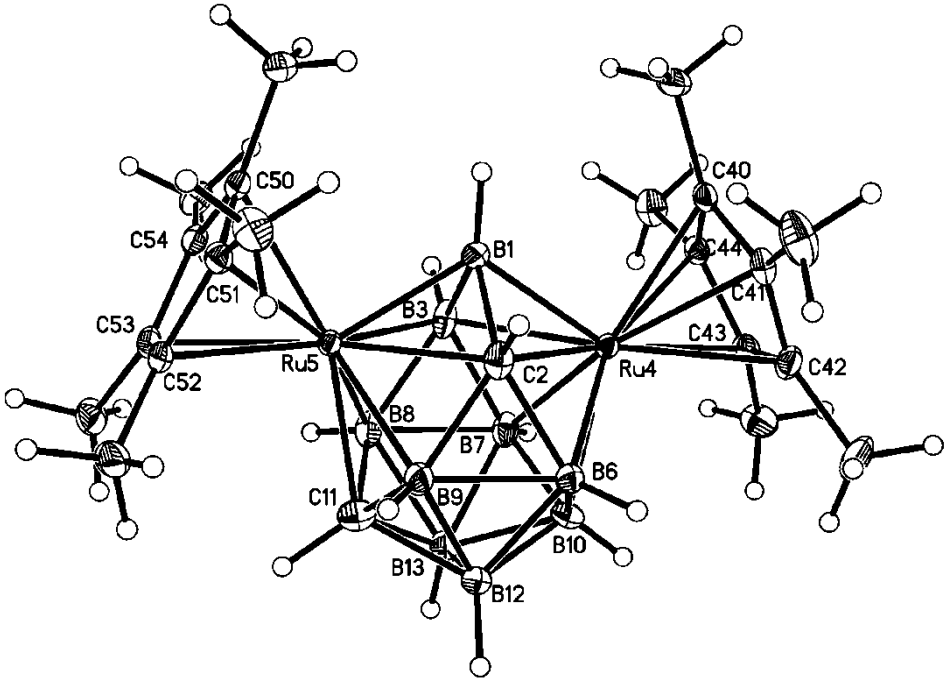

Figure 5.4.1 Molecular structure of 4,5-(η-C_5Me_5)$_2$-4,5,2,11-*closo*-$Ru_2C_2B_9H_{11}$ (**19**).

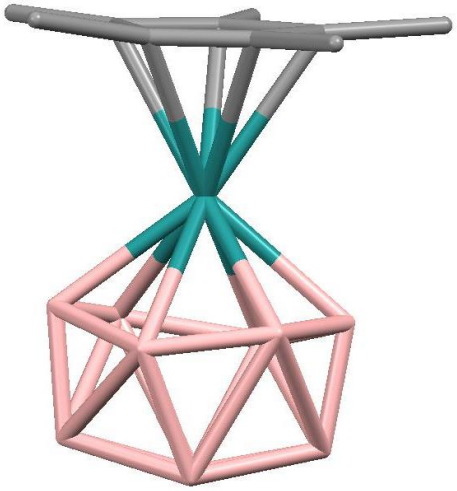

Figure 5.4.2 Molecular structure of compound with formula (Cp*Ru)$C_xB_{10-x}H_{10}$ (x =0, 1 or 2). All non-metal vertices have been refined as boron.

This second structure does not fit well with the NMR data of the yellow band (2 x Cp* in ^{1}H NMR spectrum, nine signals in ^{11}B NMR spectrum), but would have a peak at around *m/z* 357 if the structure is (Cp*Ru)$C_xB_{10-x}H_{10}$ (x = 0, 1 or 2). The structure obtained for this eleven vertex compound is not very good, and the position of any carbon atom(s) could not

be determined. The compound has either no cage carbon atoms and is paramagnetic (2n – 1 PSEs), one cage carbon and is diamagnetic (2n PSEs), or two cage carbon atoms and is paramagnetic (2n + 1 PSEs).

If the NMR data for the yellow band do in fact correspond to this eleven vertex compound, there would have to be one cage carbon (the NMR spectra does not appear to be that of a paramagnetic compound) and impurities in the ^{1}H NMR spectra to account for the two Cp* signals. The eleven vertex compound would account for the single CH resonance found in the ^{1}H NMR spectrum, and potentially the downfield boron signal in the ^{11}B NMR spectrum (there would be a degree four boron adjacent to the metal). However the downfield signal only integrates for one boron atom, and so the CH would have to occupy the other degree four vertex, which would give the molecule C_s symmetry - which is not reflected in the ^{11}B NMR spectrum (nine different signals = asymmetry).

For these reasons the yellow band is assumed to be compound **19** (4,5-(η-C_5Me_5)$_2$-4,5,2,11-*closo*-$Ru_2C_2B_9H_{11}$), and the second CH signal in the ^{1}H NMR spectrum simply lies off the scale of the routine NMR experiment frequency window. Unfortunately time constraints meant that a broader frequency NMR experiment could not be run.

It is supposed that either compound **19** is not as stable as compound **18** in solution and that the presence of the eleven vertex compound is as a decomposition product of **19** (which happens to crystallise alongside **19**), or that the eleven vertex compound is an impurity which is present in such small amounts that it does not appear spectroscopically, but does crystallise out during solvent/vapour diffusion. Both of these explanations would account for the peak at *m/z* 357 in the MS.

The structure of compound **19** has the basic architecture of **18**, but with different cage carbon positions. Compound **19** refined best with the carbon atoms assigned to vertices 2 and 11, which can be rationalised in terms of the spectroscopic data as these two positions give an asymmetric cage, a boron atom at the degree four vertex, and inequivalent Cp* ligands. The 4,5,2,11- isomer has not previously been reported for $M_2C_2B_9$ compounds.

5.5 Synthesis of 8-(*n*-BuO)-4,5-(η-C_5Me_5)$_2$-4,5,1,6-*closo*-$RuC_2B_9H_{10}$ (20)

Compound **20** is isolated from reaction One (after chromatography) as a yellow solid in 1.8% yield at low R_f.

Diffusion of 40-60 petroleum ether and a THF solution of **20** at -30 ^oC gave crystals which were analysed by *X*-ray diffraction, and revealed the structure of **20** to be non-Wadian 8-(*n*-BuO)-4,5-(η-C_5Me_5)$_2$-4,5,1,6-*closo*-$RuC_2B_9H_{10}$ (figure 5.5.1).

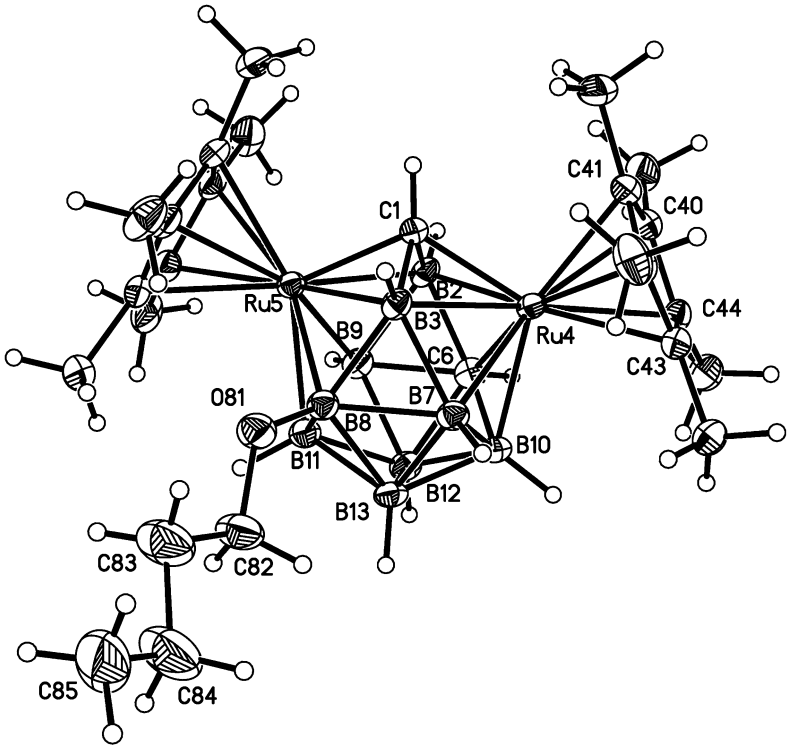

Figure 5.5.1 Molecular structure of 8-(*n*-BuO)-4,5-(η-C_5Me_5)$_2$-4,5,1,6-*closo*-$RuC_2B_9H_{10}$ (**20**).

The structure shows a covalent B-O bond between B8 and an *n*-BuO group, as opposed to compound **17**, which has a dative covalent B-O^+ bond. The *n*-BuO group has almost certainly come from a molecule of THF, but at what point the THF becomes decyclised in not clear. The cage structure of **20** is the same as that observed for **18**, with the carbon atoms located at vertices 1 and 6.

The *n*-BuO group is evident in the ^1H NMR spectrum of compound **20**, with a triplet at 0.75 ppm (3H), and multiplets at 3.30-3.50 (2H) and 1.60-1.70 (4H) ppm corresponding to the butyl protons. There are also two Cp* signals, but only one cage CH signal in the proton

NMR. A wider frequency window NMR would presumably be needed to locate the second CH group (based on the fact that one of the CH groups in **18** resonates at 16.62 ppm).

The ^{11}B NMR spectrum of **20** contains nine resonances between 43.5 and -17.5 ppm, with no coincidental overlaps (as there were in compound **18**). The lack of a very downfield signal indicates that there is a carbon atom occupying the degree four vertex. The relatively downfield signal at 43.5 ppm is not coupled to a proton, and therefore must correspond to B8, the high chemical shift being explained by the attached electronegative oxygen atom.

The MS of **20** contains an envelope centred on *m/z* 676 (M^+) (M_w **20** = 677.76 g/mol) and an envelope centred on *m/z* 603 (compound **20** minus *n*-BuO).

5.6 Synthesis of 3,6-(η-C_5Me_5)$_2$-3,6,?,?-*closo*-$Ru_2C_2B_{10}H_{12}$ (21) and 3,6-(η-C_5Me_5)$_2$-3,6,2,?-*closo*-$Ru_2C_2B_{10}H_{12}$ (22)

Compounds **21** and **22** were recovered from reaction One (upon chromatography) as a green (2.0%) and a purple (1.7%) band respectively.

The MS of **21** shows an envelope centred on *m/z* 618 (M^+) (M_w **21/22** = 616.76 g/mol) and an envelope centred on *m/z* 604 (compound **21** minus BH), while the MS of **22** shows an envelope centred on *m/z* 615 (M^+) and an envelope centred on *m/z* 603 (compound **22** minus BH).

Crystals of compound **21** were grown from diffusion of 40-60 petroleum ether and a THF solution of **21**, while crystals of compound **22** were grown by others in the group[9] from diffusion of 40-60 petroleum ether and a DCM solution of **22**. Analysis by *X*-ray diffraction reveals compounds **21** (figure 5.6.1) and **22** (figure 5.6.2) to be 3,6-(η-C_5Me_5)$_2$-3,6,?,?-*closo*-$Ru_2C_2B_{10}H_{12}$ (**21**) and 3,6-(η-C_5Me_5)$_2$-3,6,2,?-*closo*-$Ru_2C_2B_{10}H_{12}$ (**22**) Both compounds are non-Wadian and have the same basic cage structure, a previously unreported fourteen vertex bimetallic architecture.

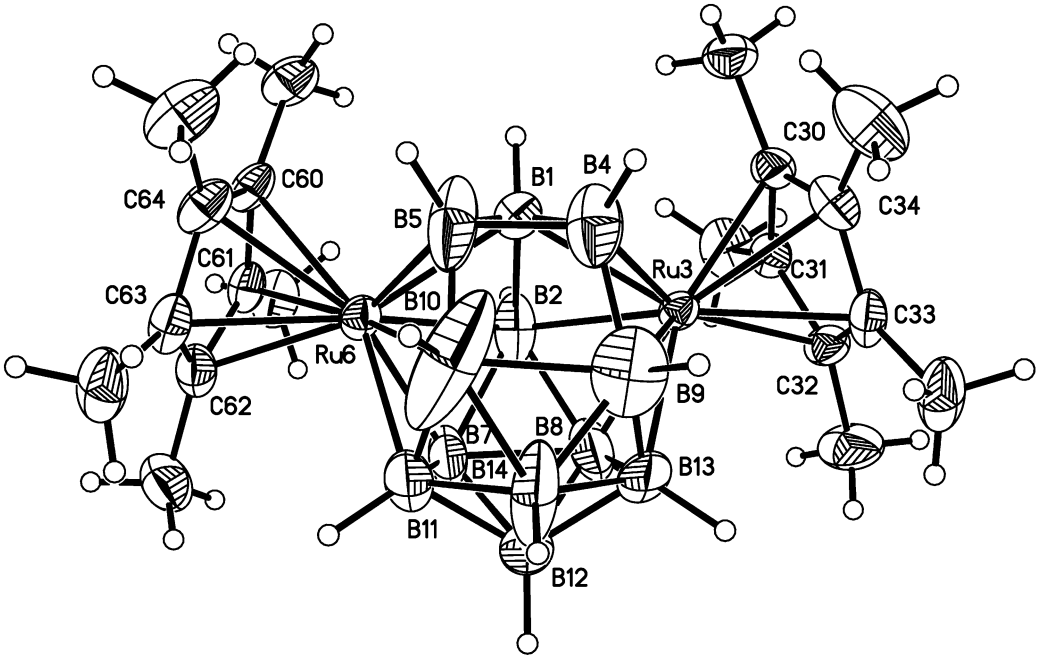

Figure 5.6.1 Molecular structure of 3,6-(η-C_5Me_5)$_2$-3,6,?,?-*closo*-$Ru_2C_2B_{10}H_{12}$ (**21**).

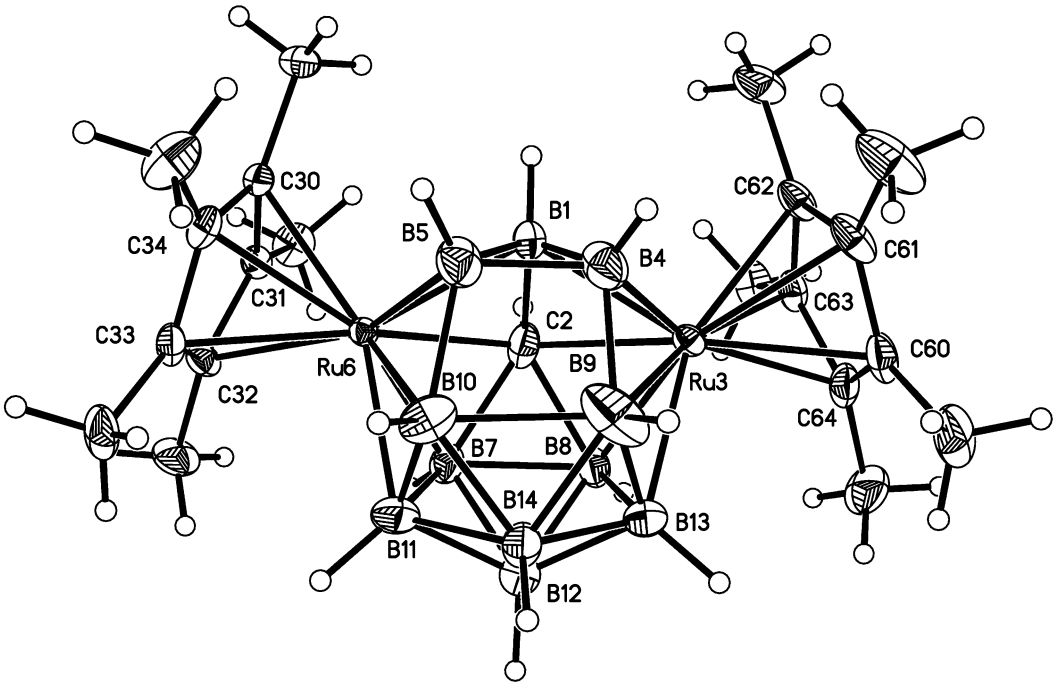

Figure 5.6.2 Molecular structure of 3,6-(η-C_5Me_5)$_2$-3,6,2,?-*closo*-$Ru_2C_2B_{10}H_{12}$ (**22**).

There are ten degree five vertices, two degree six vertices (both occupied by Ru) and two degree four vertices which sit on a quadrilateral face (along with two degree five vertices). The structure is perhaps best described as a henicosahedron, but with a triangular B_3 unit (although some of these vertices may be carbon) capping the top pentagonal face as opposed to a B-B unit (figure 5.6.3).

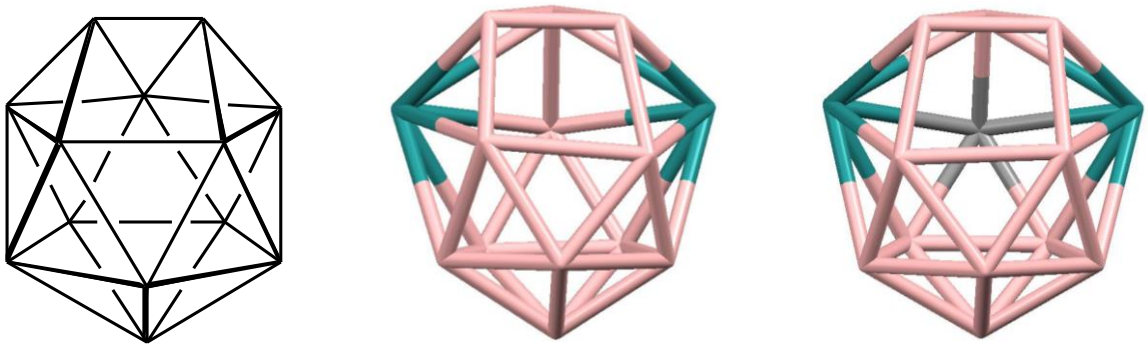

(a) (b) (c)

Figure 5.6.3 (a) Henicosahedral cage structure, (b) and (c), cage structures of compounds **21** and **22**.

Neither cage carbon atom could be located during refinement of **21** (all the non-metal vertices in figure 5.6.1 have been refined as boron), while only one of the cage carbon atoms could be located in **22** (nine of the non-metal vertices in figure 5.6.2 have been refined as boron), and

occupies a degree five vertex. That **21** has two CH units is evident from the ^{1}H NMR spectrum, and **22** must also have two CH units to avoid paramagnetism.

The ^{1}H NMR spectrum of **21** contains two integral fifteen signals (Cp*), one at 1.55 ppm and the other at 1.65 ppm. There are two broad singlets corresponding to cage CHs, one at a moderate chemical shift (3.85 ppm), the other one with quite a high chemical shift (10.40 ppm). Similar resonances are seen in the ^{1}H NMR spectrum of **22** (peaks corresponding to Cp* at 1.68 and 1.72 ppm), but only one, quite high chemical shift, CH peak (8.50 ppm) is present. The other CH peak has not been located at this time (lack of a second CH would render the compound paramagnetic and require an additional boron resonance in the ^{11}B NMR spectrum).

Both compounds have ten peaks in the ^{11}B NMR spectrum (compound **21** = 58.2 to -22.9 ppm, compound **22** = 72.1 to -11.7 ppm), indicating cage asymmetry. In both spectra there are two relatively downfield peaks (compound **21** = 58.2 and 53.8 ppm, compound **22** = 72.1 and 63.3 ppm). These signals may indicate that the two degree four vertices (each bonded to one metal) in each compound are occupied by boron, but location of the two cage carbon atoms during crystallographic refinement would be needed to confirm this.

The positions of the two cage carbon atoms in **21** and the second cage carbon atom in **22** is not easily determined from the NMR data. The quadrilateral face in **21** and **22** is an irregular quadrilateral (all four lengths and angles different), but cage fluxionality may cause it to be 'seen' as a more symmetric quadrilateral on the NMR time-scale, giving the molecule C_s symmetry (assigning all atoms as boron). If this is the case, then all that can be said about the positions of the cage carbon atoms in **21** is that they must occupy vertices that break this C_s symmetry, as the ^{11}B NMR spectrum of **21** shows clearly that the molecule is asymmetric and there are two peaks corresponding to (inequivalent) Cp* groups in the ^{1}H spectrum. For **22**, the cage carbon which has been located would sit on the mirror plane in C_s symmetry, meaning that the second cage carbon must occupy a vertex which does not sit on the mirror plane (i.e. vertices 1, 12 and 14 are precluded), in order for the asymmetry in the NMR spectra of **22** to be rationalised.

The large ADPs on some of the vertices in compound **21** (see figure 5.6.1, particularly vertices 9, 10 and 14) led to the suspicion of a disordered thirteen vertex compound, where a

number of vertices were disordered over more than one position. However this is not in agreement with the ^{11}B NMR spectrum for compound **21** (ten peaks) or the MS (although there is a peak that corresponds to a thirteen compound as noted above). In terms of the structure itself, it seems unlikely that the structures of compounds **21** and **22** (the latter of which has relatively small ADPs) would refine to give such a similar architecture if the cage in the former was merely the disordered cage of a thirteen vertex compound.

Further evidence is in the form of the Ru-Ru distance which should not be affected by the disorder, if it were present. The Ru-Ru distances for the thirteen vertex compounds **VIII**, **18** and **19** are 3.531 Å, 3.567 Å and 3.535 Å, respectively, while the Ru-Ru distances for compounds **21** and **22** are 3.784 Å and 3.795 Å, respectively. The larger Ru-Ru distances of **21** and **22** reflects the extra M-M separation necessitated by the extra boron atom in the cage (compared to the thirteen vertex compounds).

It therefore seems that although the quality of structure **21** is not as good as that of **22**, it is nevertheless a fourteen vertex species and that better quality crystals would be needed to give a structure with smaller ADPs.

5.7 Synthesis of (μ^3-dicarba-*closo*-dodecaborane-B^1,B^2,B^3,H^1,H^2,H^3)-(μ^3-ethylidyne)-tris(η^5-pentamethylcyclopentadienyl)-triruthenium (23)

Compound **23** is isolated from reaction One after chromatography as a pink band at low R_f (1.6% yield based on title structure).

The structure of **23** - shown in figure 5.7.1 - was obtained by *X*-ray analysis of crystals grown from diffusion of diethyl ether and a DCM solution of **23**.

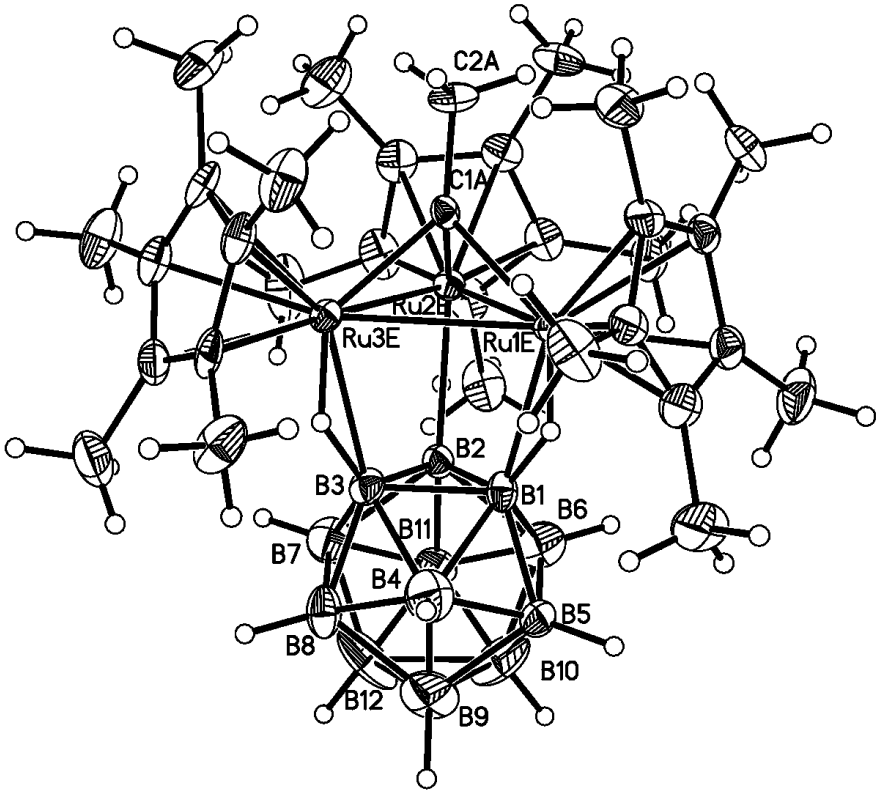

Figure 5.7.1 Molecular structure of (μ^3-dicarba-*closo*-dodecaborane-B^1,B^2,B^3,H^1,H^2,H^3)-(μ^3-ethylidyne)-tris(η^5-pentamethylcyclopentadienyl)-triruthenium (**23**).

The compound is not a metallacarborane, as the ruthenium atoms do not occupy polyhedral sites, but rather lie exo- to the cage, obtaining two electrons per metal from agostic B-H→Ru interactions. Exo-metal bound heteroboranes with agostic B-H→M interactions are well known in the literature, with compounds containing a wide variety of metals reported.[11a,b]

The three RuCp* units have captured a two atom fragment in the middle of the triangle which they form. Assignment of these two atoms has not been made definitively, and they have both been assigned as carbon on the basis of precedent and the eighteen electron rule (see section 5.10) until more evidence as to their identity becomes available. The cage is icosahedral, and

is presumably $C_2B_{10}H_{12}$, although the cage CHs could not be located during refinement, and so the cage in figure 5.7.1 has been refined as all boron.

In the ^{1}H NMR spectrum there are two Cp* peaks, one integrating for 2 x Cp* (30H, 1.80 ppm) and one one integrating for 1 x Cp* (15H, 1.75 ppm). The fact that there are two different Cp* environments indicates the presence of at least one cage CH, as if the cage was all boron the molecule would have C_{3v} symmetry and the Cp* ligands would be symmetry equivalent. There were no peaks corresponding to cage CHs in the proton NMR spectrum, the signal(s) presumably either lying out with the frequency range of the NMR experiment, or being broadened into the baseline for some reason.

The ^{11}B NMR spectrum of this compound suffers from poor signal to noise ratio, but from what can be made out, there are six signals apparently integrating for eleven boron atoms in the ratio 1:3:3:2:1:1, the first signal being at 87.0 ppm, and the other five being between -8.7 ppm and -46.7 ppm. An integral three signal at -12.0 ppm appears to be either uncoupled to protons, or at least coupled less strongly than the remainder of the peaks. This signal is assumed to correspond to the vertices involved in the B-H→Ru agostic interactions. The agostic interactions presumably reduce the B-H coupling, explaining why this peak is observed as a singlet (or very weakly coupled doublet) in the ^{1}H coupled boron NMR spectrum. This relatively weak coupling for boron atoms involved in B-H→M agostic interactions has been observed previously in heteroboranes with exo-polyhedral bound metal fragments.[11a,b]

The signal at 87.0 ppm in the ^{11}B NMR spectrum does not appear to be part of the cage (based on its high chemical shift), and was initially suspected to be bonded to the Ru_3 triangle as BMe. However, if the fragment was BMe, with the boron atom coordinated to the metals, only two electrons would be available for bonding to the metal atoms, which would give a paramagnetic compound as one of the ruthenium atoms would be an electron short of an eighteen electron count. Each metal centre without the electrons from the two atom fragment would have 17 electrons:

Ru	$8e^-$
2 x Ru-Ru bond	$2e^-$
Cp*	$5e^-$
B-H bond	$2e^-$
	$17e^-$

Most small atom fragments capping a triangle of metals found during a search of the CSD[12] have a carbon bound to the metals, as it can provide the necessary three electrons and still have one remaining to bond to the next atom of the fragment. It would therefore seem that the downfield peak in the ^{11}B NMR spectrum is an impurity (it would appear to be too downfield to correspond to a cage boron) and that the fragment is in fact CMe. There is a singlet in the ^{1}H NMR spectrum at 3.30 ppm which appears to integrate for three hydrogens, supporting assignment of the small fragment as CMe (although during crystallographic refinement the methyl group was set as such with an HFIX command - the three hydrogen atoms were not located in the difference Fourier map or freely refined).

Alternative explanations are that the fragment is in fact BOH_2 and the downfield signal does correspond to a boron that is part of the compound, or that the fragment is CBH_2 and the boron signal is very downfield despite not being directly bonded to the Ru_3 triangle. For these explanations to be correct the singlet at 3.30 ppm in the ^{1}H NMR spectrum would have to be either an impurity, or overlapping with a small amount of impurity, as BOH_2 or CBH_2 would both give a signal integrating for only two protons. The poor quality of the ^{11}B NMR spectrum and broadness of the downfield resonance makes it difficult to tell whether it is coupled to a proton(s) in the ^{1}H coupled boron NMR spectrum.

The MS of **23** shows an envelope centred on *m/z* 876 (M^+) and an envelope centred on *m/z* 732 (compound **23** minus $C_2B_{10}H_{12}$). The envelope at *m/z* 876 fits best with assignment of the small fragment as CBH_2 (M_w = 877.9 g/mol), although it also fits moderately well with CMe (M_w = 880.1 g/mol), or BOH_2 (M_w = 881.9 g/mol).

The origin of the small fragment is not clear. The isolation of compounds which have lost BH vertices would account for the presence of boron, trace amounts of water are likely regardless of the dryness of the equipment/reagents/solvents, and carbon atoms could be extruded from other cages, solvent molecules or Cp*. Better quality NMR data would help to assign the small fragment unambiguously, and a wider frequency ^{1}H NMR experiment may help to find the cage CH resonances.

5.8 Synthesis of 5-(THF)-2,3-$(CH_2)_3$-1-(η-C_5Me_5)-1,2,3-*closo*-$RuC_2B_{11}H_{10}$ (24) and 11-(THF)-2,3-$(CH_2)_3$-1-(η-C_5Me_5)-1,2,3-*closo*-$RuC_2B_{11}H_{10}$ (25)

Reduction of 1,2-μ-$(CH_2)_3$-1,2-*closo*-$C_2B_{11}H_{11}$ with Na in THF results in [μ-$(CH_2)_3$-*nido*-$C_2B_{11}H_{11}]^{2-}$. To this was added [RuClCp*]$_4$ in THF to give a brown/orange solution which was stirred overnight (reaction Two). Upon chromatography orange **24** and yellow **25** are isolated in trace amounts, along with a pink and a yellow band which remain at this point unidentified (see section 5.9).

Crystals of both compounds **24** and **25** were grown by diffusion of 40-60 petroleum ether and a THF solution of the metallacarborane at -30 ^oC. Analysis by *X*-ray diffraction revealed the two compounds to be 5-(THF)-2,3-$(CH_2)_3$-1-(η-C_5Me_5)-1,2,3-*closo*-$RuC_2B_{11}H_{10}$ (**24**) and 11-(THF)-2,3-$(CH_2)_3$-1-(η-C_5Me_5)-1,2,3-*closo*-$RuC_2B_{11}H_{10}$ (**25**) as shown in figures 5.8.1 and 5.8.2 respectively.

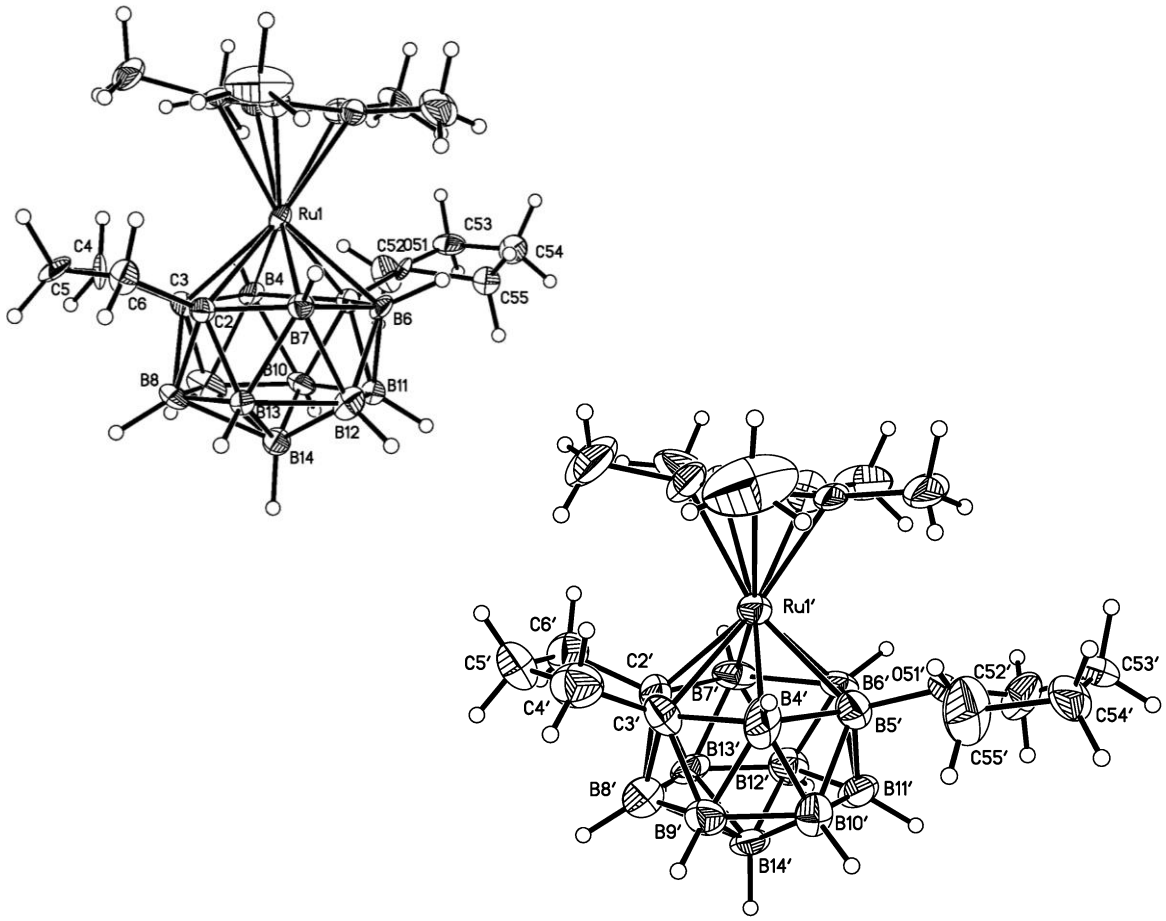

Figure 5.8.1 Molecular structures of 5-(THF)-2,3-$(CH_2)_3$-1-(η-C_5Me_5)-1,2,3-*closo*-$RuC_2B_{11}H_{10}$ (**24**).

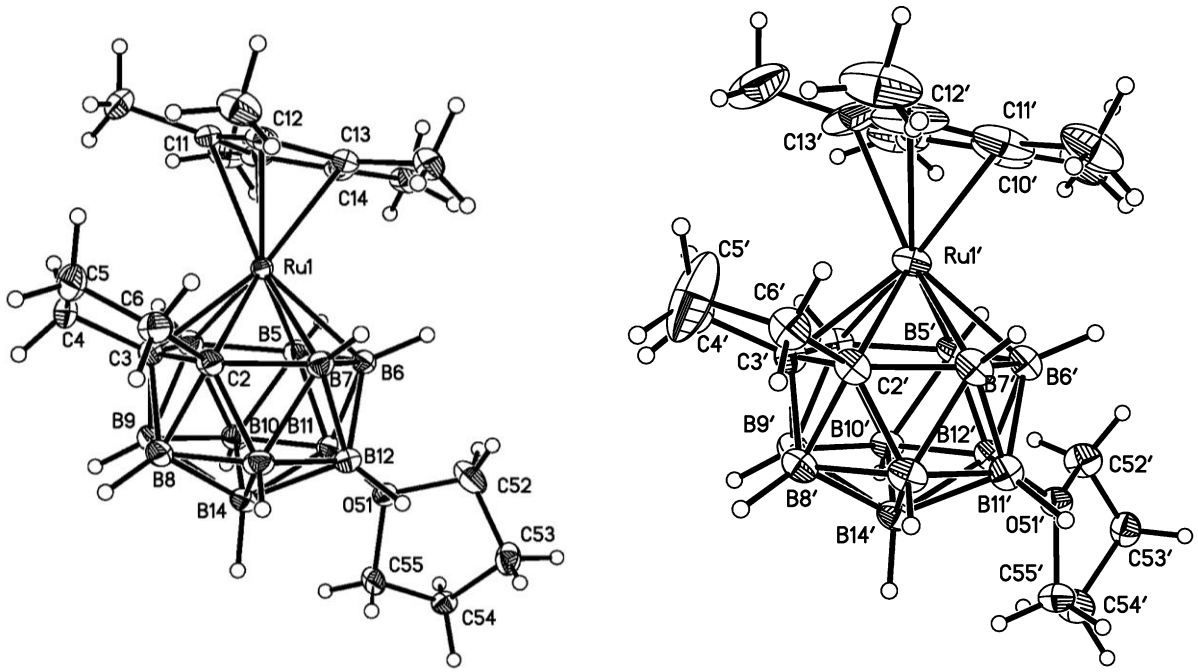

Figure 5.8.2 Molecular structures of 11-(THF)-2,3-$(CH_2)_3$-1-(η-C_5Me_5)-1,2,3-*closo*-$RuC_2B_{11}H_{10}$ (**25**).

Both compounds crystallise with two independent molecules in the asymmetric unit. Compound **24** was solved as a two component twin, whilst compound **25** had a Cp* ligand disordered over two positions in one molecule, and the alkyl ring of the pendant THF disordered over two positions in the other. Only one component of the disorder is shown for each molecule in figure 5.8.2.

Compounds **24** and **25** are both fourteen vertex bicapped hexagonal antiprismatic compounds with a single RuCp* unit incorporated into the cage. Both compounds are Wadian, and they each have a pedant THF molecule containing a positively charged oxygen atom, which balances with the overall negative charge of the molecule to give a zwitterionic species which is mobile during chromatography on silica. Compounds **24** and **25** differ in that the former has the pendant THF on the upper hexagonal belt, while the latter has the pendant THF on the lower hexagonal belt and has approximate C_s symmetry.

The ^{11}B NMR spectrum of **24** contains seven peaks in the ratio 1:2:1:1:2:1:3 between 19.2 and -26.2 ppm, while **25** has a 1:2:2:1:2:3 pattern between 0.2 and -29.1 ppm. In the ^{11}B NMR spectra of both compounds the furthest downfield signal is not coupled to a proton and must therefore correspond to the THF bound boron atom. The structure of **24** is asymmetric, with the integral two/three resonances being coincidences, while the C_s symmetry of **25** is

reflected in the integration of the boron peaks, with only the integral three signal being a 2 + 1 coincidence.

The ^{1}H NMR spectra of both compounds contain a single Cp* resonance (both compounds at 1.50 ppm) and peaks relevant to the C_3 tether (2.05-2.23 ppm (3H), and 2.60-2.80 ppm (3H)) and the pendant THF (1.95-2.12 ppm (4H) and 4.20-4.35 ppm (4H)).

The MS of both compounds show an envelope centred on *m/z* 504 (M^+) (M_w **23**/**24** = 503.40 g/mol).

An attempt to repeat the reaction of [μ-$(CH_2)_3$-*nido*-$C_2B_{11}H_{11}]^{2-}$ with [RuClCp*]$_4$ in a non-coordinating solvent (the reduced carborane solution had the THF removed *in vacuo*, then a DCM solution of [RuClCp*]$_4$ was added) only resulted in smaller amounts of the fourteen vertex THF bound compounds being formed. Presumably either the solid state reduced thirteen vertex species is associated with $Na_2 \cdot (THF)_x$, or there are trace amounts of THF left over after solvent removal which explains how THF is still able to coordinate to the cage in the absence of the bulk solvent.

5.9 Partially identified compounds

Two compounds from reaction One remain unidentified (not including the eleven vertex compound noted in section 5.4). One of these compounds is the purple band observed at R_f 0.56. A crystal structure of this compound has been determined but the quality of the data is poor. The structure (figure 5.9.1) appears to show an open cage, with two RuCp* units involved in B-H→Ru agostic interactions. The cage CHs have been assigned based on BHD arguments.[3,13]

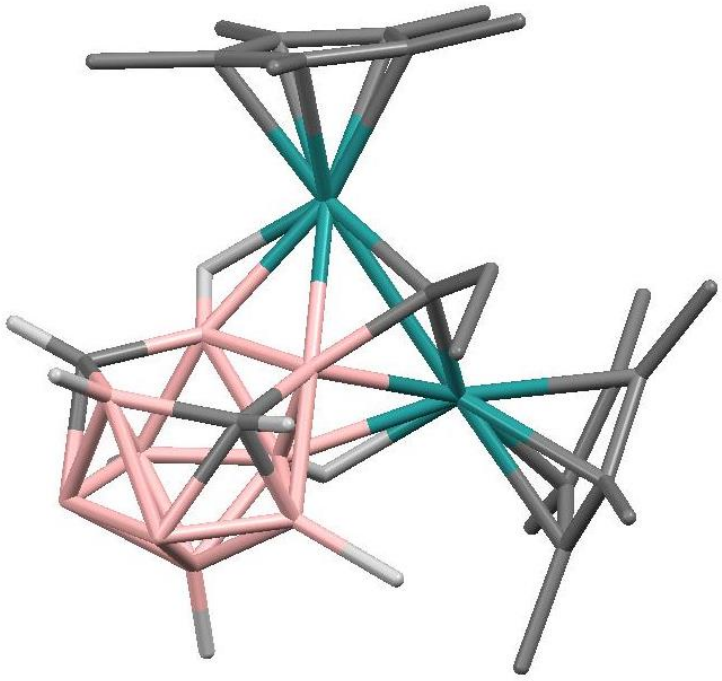

Figure 5.9.1 Approximate molecular structure of partially identified compound crystallised from purple band.

The ruthenium atoms appear to be bonded to each other and to a small three atom fragment which is also bonded to a cage boron atom. There is also a four atom sequence in the asymmetric unit (omitted from figure 5.9.1 for clarity) which is likely solvent of some sort. The molecule seems to be zwitterionic, with a positive charge on each ruthenium atom offset by the two negative charge of the nido cage.

Impurities in the NMR spectra make confident interpretation difficult. The ^{1}H NMR spectrum seems to show two broad singlets which are presumably cage CHs, and two Cp* resonances. The ^{11}B NMR spectrum appears to show nine peaks of integral one, two of which appear to be either weakly coupled or uncoupled to protons. The cage boron atom bonded to the three atom fragment will not be coupled, accounting for one of the uncoupled resonances.

There would be expected to be two other signals in the ^{11}B NMR spectrum with weak B-H coupling corresponding to the two boron atoms involved in B-H→Ru agostic interactions. The reason why there is only one other weakly proton coupled boron signal in the ^{11}B NMR spectrum is not known at this time, nor is the identity of the three atom fragment. However, as for compound **23**, the atom bonded directly to the ruthenium atoms is likely to be carbon in order for it to provide enough electrons for bonding to both of the metals, the cage boron atom and the next atom in the three atom fragment.

The MS contains an envelope centred on *m/z* 644, and one centred on *m/z* 604 (attributable to just the cage and the two RuCp* units). This indicates that the three atom fragment could be CEt, as this would account for the ~ 40 Da difference between the two MS peaks.

The other compound which remains unidentified is a yellow band which was observed at high R_f (0.75) upon chromatography. This compound contained ~ ten peaks between about 30 and -30 ppm in the ^{11}B{^{1}H} NMR spectrum, but also contained peaks corresponding to 1,2-*closo*-$C_2B_{10}H_{12}$. Attempted purification of this compound by further chromatography did not separate it from the 1,2-*closo*-$C_2B_{10}H_{12}$, and crystallisation was not attempted.

The reaction of [RuClCp*]$_4$ with reduced 1,2-μ-$(CH_2)_3$-1,2-*closo*-$C_2B_{11}H_{11}$ was performed on quite a small scale (90 mg of carborane), and there were two mobile band in the TLC which could not be properly isolated due to their small amounts. The first of these bands was yellow (R_f 0.65), and the ^{11}B NMR spectrum of this band shows peaks between -0.5 and -29.1 ppm, and a small peak at 52.0 ppm. However the signal to noise ratio is poor and it is not clear which peaks correspond to impurities. The mass spectrum (figure 5.9.2) is more interesting however, as there appears to be a peak at *m/z* 667 which corresponds to the thirteen vertex cage plus two Ru(Cp*) units.

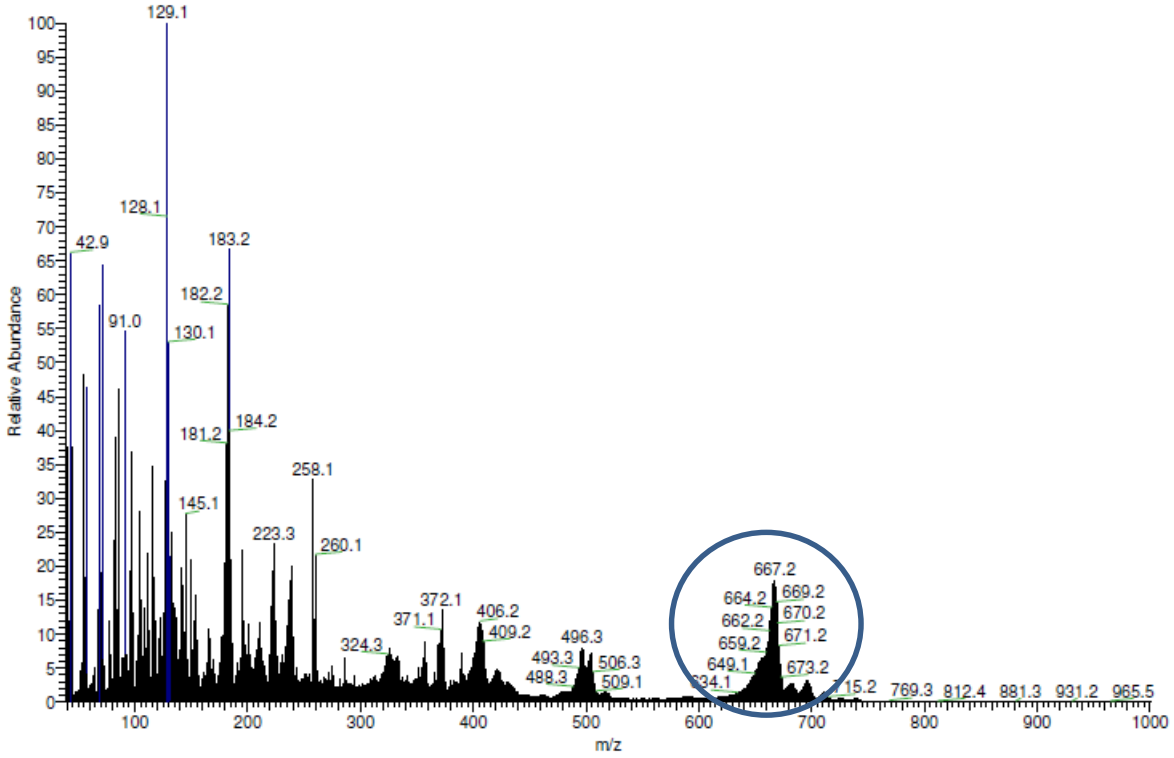

Figure 5.9.2 MS of unidentified yellow band from reaction of $[RuClCp^*]_4$ with reduced 1,2-μ-$(CH_2)_3$-1,2-*closo*-$C_2B_{11}H_{11}$. Peak at *m/z* 667 is circled.

The MS of compound **24** - which sits immediately below the yellow band on the TLC plate - also shows a peak at *m/z* 667 as a minor contaminant. This peak could correspond to a species with exo-bound metal fragments, or could be from a fifteen vertex compound. Unfortunately owing to time constraints this reaction could not be repeated to try and characterise this yellow band responsible for the mass spectral peak at *m/z* 667.

The second unidentified band was pink and the ^{11}B NMR spectrum of this band shows peaks between 21.3 and -25.9 ppm, again with poor signal to noise ratio. The signal at 23.1 ppm does not appear to be coupled to a proton, and there is a peak at *m/z* 503 in the MS. This band is likely another isomer of compound **24**/**25**, but a crystallographic study would be needed to determine which boron atom the THF is attached to.

5.10 Discussion and suggested future work

Thirteen vertex bimetallacarboranes

Compound **18** is presumably made from DEI of {$RuCp^{*+}$} into [4-Cp*-4,1,6-*closo*-$RuC_2B_{10}H_{12}]^-$, followed by loss of a {BH} vertex (figure 5.10.1). For compound **VIII** the DEI appears to be adjacent to the two cage carbon atoms of [3-Cp*-3,1,2-*closo*-$RuC_2B_9H_{11}]^-$, which end up separated by one boron atom in the final product. The DEI into [4-Cp*-4,1,6-*closo*-$RuC_2B_{10}H_{12}]^-$ to make compound **18** appears to happen adjacent to the degree four carbon atom, and it is not easily determined which BH vertex is subsequently lost.

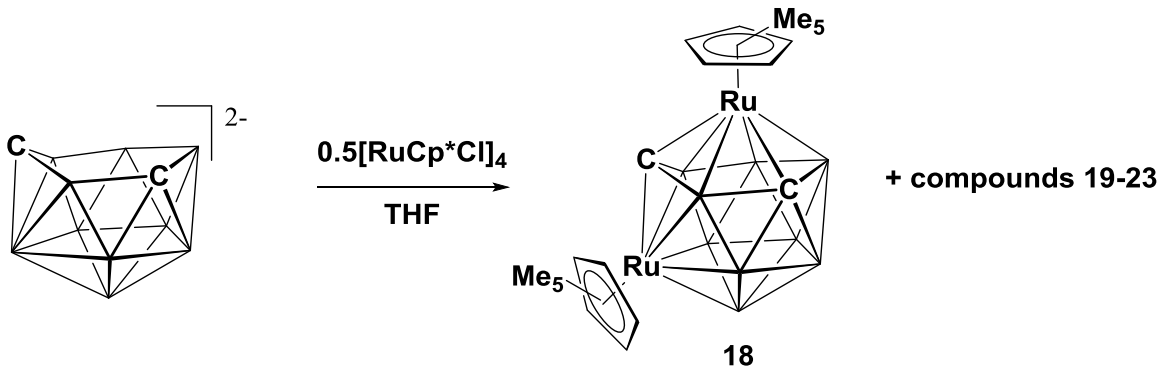

Figure 5.10.1 Reaction of $[7,9\text{-}nido\text{-}C_2B_{10}H_{12}]^{2-}$ with $[RuClCp^*]_4$ to ultimately give, amongst other things, compound **18**.

A small amount of compound **VIII** was recovered from reaction One, meaning that, in all, three isomers of the type 4,5-Cp^*_2-4,5,X,Y-*closo*-$Ru_2C_2B_9H_{11}$ (X, Y = carbon positions) were recovered from the reaction. Compound **18** is presumed to be the most thermodynamically stable product as it has a carbon atom at the degree four vertex. The Wadian (2n + 2 PSEs) compounds 4,5-L_2-4,5,2,3-*closo*-$M_2C_2B_9H_{11}$ (M = Co L = Cp,[14,15] M = Ru L = *p*-cymene[14]) were made by reduction/metallation of 3-L-3,1,2-*closo*-$MC_2B_9H_{11}$ and isomerise to the 4,5,1,6- isomers upon heating (the Co one in refluxing THF, the Ru one in tetra(ethyleneglycol)dimethylether at 150°C). The 4,5,1,6- $(CoCp)_2$ compound isomerises again to the 4,5,1,12- isomer in refluxing cyclooctane.[16]

The 4,5,1,6- isomers were also isolated as minor products from the reduction/metallation of the 3-L-3,1,2-*closo*-$MC_2B_9H_{11}$ compounds, and it therefore seems that isomerism of the carbon atoms in the open face of reduced 3-L-3,1,2-*closo*-$MC_2B_9H_{11}$ occurs pre-metallation to give both the 4,5,2,3- and 4,5,1,6- isomers upon addition of the metal.[14]

Alternatively, the 4,5,1,6- and 4,5,1,12- CpCo isomers can be made from subrogation of a BH vertex from 4-Cp-4,1,8-*closo*-$CoC_2B_{10}H_{12}$ and 4-Cp-4,1,12-*closo*-$CoC_2B_{10}H_{12}$ respectively, followed by addition of a source of CpCo.[16] The general structures of these Wadian compounds are similar to their non-Wadian counterparts. The syntheses of the various 4,5-Cp_2-4,5,X,Y-*closo*-$Co_2C_2B_9H_{11}$ (X, Y = carbon positions) isomers is summarised in figure 5.10.2. The non-Wadian compounds **VIII**, 4-Cp*-5-Cp-4,5,2,3-*closo*-$Ru_2C_2B_9H_{11}$ and **IX** were found not to isomerise to the 4,5,1,6- isomers upon heating,[4] while the paramagnetic compound 4,5-Cp_2-4,5,1,6-*closo*-$FeCoC_2B_9H_{11}$ (made from $\{FeCp^+\}$ + subrogated 4-Cp-4,1,8-*closo*-$CoC_2B_{10}H_{12}$) decomposes upon heating in refluxing cyclooctane.[16]

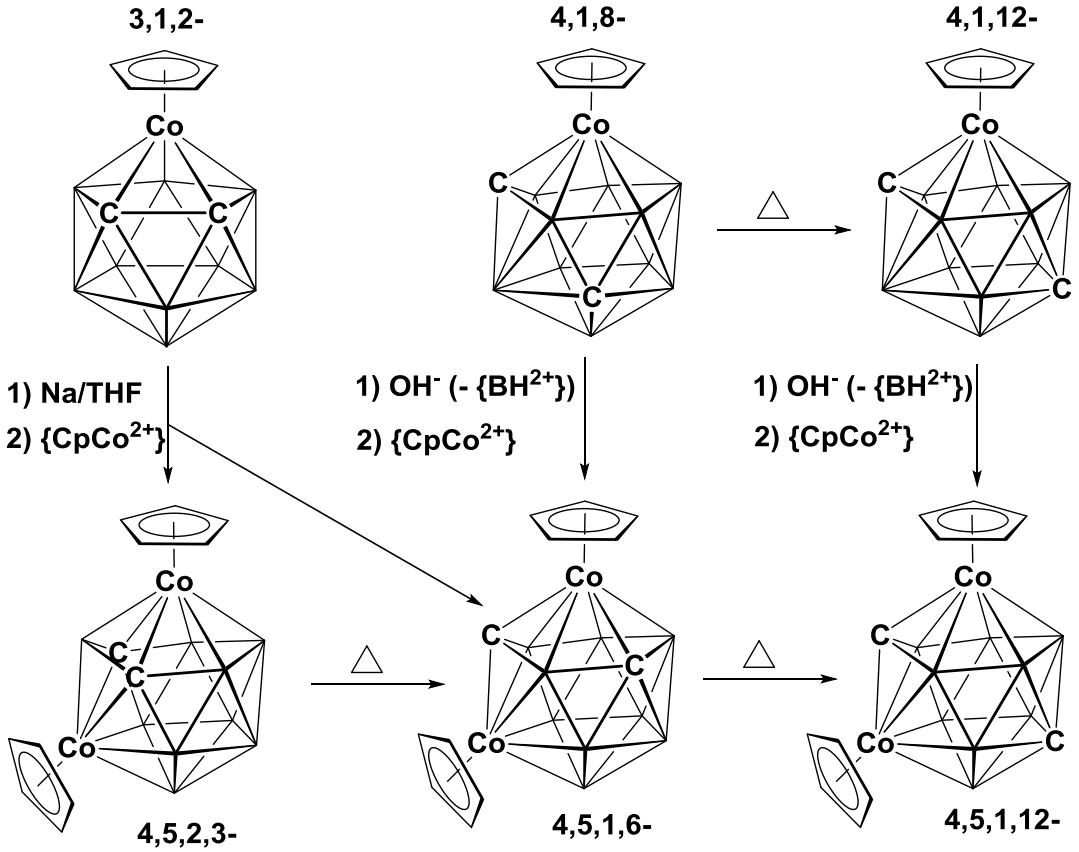

Figure 5.10.2 Routes to different Wadian thirteen vertex bimetallacarboranes of the type 4,5-Cp_2-4,5,X,Y-*closo*-$Co_2C_2B_9H_{11}$ (X, Y = cage carbon positions).

It would appear that during reaction One compounds **18**, **19** and **VIII** are formed from either DEI at different points on the cage, subsequent loss of a different BH vertex, or a combination of both. Compound **VIII** is then 'stuck' as the kinetic 4,5,2,3- isomer which cannot isomerise to the thermodynamically more stable 4,5,1,6- isomer. A similar argument could be made for compound **19** (4,5,2,11- isomer), but attempts at isomerising this

compound to the 4,5,1,6- isomer would be needed to confirm this. It seems possible that if it could isomerise, then the 4,5,2,11- isomer would isomerise to the (presumably) thermodynamically most stable 4,5,1,12- isomer. It is not known whether the 4,5,1,6- isomer would convert to the 4,5,1,12- isomer upon heating, although it seems unlikely based on the fact that the 4,5,2,3- to 4,5,1,6- isomerisation does not appear to take place for these non-Wadian compounds.

The only other known thirteen vertex bimetallacarboranes are the compound [6-SMe_2-4,5-Cp^*_2-4,5,2,3-*closo*-$Ru_2C_2B_9H_{10}]^+$ (which is **VIII**, but with a pendant molecule of SMe_2)[17] and the subcloso (2n + 1 PSEs) tricarbon compounds 4,5-Cp_2-4,5,1,6,7-$Fe_2C_3B_8H_{11}$, 4,5-Cp_2-4,5,1,7,12-$Fe_2C_3B_8H_{11}$ and 7-^{t}BuNH-4,5-Cp_2-4,5,1,7,12-$Fe_2C_3B_8H_{10}$.[18] These paramagnetic compounds, which are formed from the reaction of reduced 2-Cp-9-^{t}BuNH-*closo*-2,1,7,9-$FeC_3B_8H_{10}$ with $CpFe(CO)_2I$ or $[CpFe(CO)_2]_2$, adopt very similar structures to those found in the dicarbon compounds. The compound 4-(η-C_4Me_4)-5-Cp-4,5,2,3-$CoRuC_2B_9H_{11}$ has reportedly[19] been made from insertion of {(η-C_4Me_4)Co}$^+$ into Tl[3-Cp*-3,1,2-*closo*-$RuC_2B_9H_{11}$], but details of this compound have not been published.

Reactions of {$RuCp^{*+}$} and other reduced twelve vertex compounds could potentially lead to more non-Wadian bimetallic compounds. For example reduced 1,12-*closo*-$C_2B_{10}H_{12}$ would have the cage carbon atoms at vertices 7 and 10 in the nido species (two carbons separated by two boron vertices as opposed to one boron vertex for reduced 1,2-*closo*-$C_2B_{10}H_{12}$), while reduced 1,2-μ-$(CH_2)_3$-1,2-*closo*-$C_2B_{10}H_{10}$ would have adjacent carbon atoms in the nido species. This could lead to new isomers (of thirteen and fourteen vertex compounds) being formed upon metallation/DEI. Metallation/DEI using reduced 1,2-Me_2-1,2-*closo*-$C_2B_{10}H_{10}$ would unambiguously locate the cage carbon atoms in the thirteen and fourteen vertex products, but the reaction may proceed differently or in poorer yields (which are already low) to the reaction using reduced 1,2-*closo*-$C_2B_{10}H_{12}$ due to the steric repulsion between the methyl groups and the Cp* ligands.

Comparison of the NMR data between the Wadian CpCo/Ru(*p*-cymene) and non-Wadian **VIII**, **IX**, 4-Cp*-5-Cp-4,5,2,3-*closo*-$Ru_2C_2B_9H_{11}$, **18** and **19** is interesting. The Wadian 4,5,2,3- compounds do not have the very downfield boron resonance in their ^{11}B NMR spectra which would be expected due to their containing a degree four boron at vertex 1. Eight, nine and ten vertex compounds which have a degree four boron vertex connected to

two polyhedral metal atoms tend to have a very downfield resonance (~75-120 ppm) in the ^{11}B NMR spectrum,[8] although there are examples which do not.[20]

The lack of a downfield ^{11}B NMR signal in the Wadian compounds could be the result of a fluxional DSD type mechanism - as observed in 4,1,6- mono-metallacarboranes[1] - which would 'average out' the degree four boron's ^{11}B NMR signal with a degree five vertex position, leading to the absence of such a downfield signal. If this were the case then the non-Wadian compounds would presumably not be undergoing this fluxional process.

If the CH resonance at 16.62 ppm in the ^{1}H NMR spectrum of **18** (see section 5.3) does correspond to the degree four cage CH proton, then a fluxional DSD type mechanism also would be expected to 'average out' the $CH_{deg\ 4}$ signal with a degree five vertex position.

The CH chemical shifts in the ^{1}H NMR spectra of the Wadian compounds are in the range 2.60-3.70 ppm. This is in contrast to the non-Wadian 4,5,2,3- compounds **VIII**, 4-Cp*-5-Cp-4,5,2,3-*closo*-$Ru_2C_2B_9H_{11}$ and **IX**, which have fairly upfield CH resonances (-1.27, -0.67 and -0.81 ppm respectively), and the 4,5,1,6- compound **18** which has one 'normal' CH resonance (2.90 ppm), and one very downfield resonance (16.62 ppm). Based on the respective CH resonance chemical shifts in compounds **VIII**, 4-Cp*-5-Cp-4,5,2,3-*closo*-$Ru_2C_2B_9H_{11}$, **IX** and **18**, the unfound CH resonance in compound **19** would be expected to be at a fairly upfield resonance, while the unfound CH resonance in compound **20** would be expected to be at a very downfield resonance. It is not clear why the degree five cage carbon atoms at vertices 2 and 3 in compounds **VIII,** 4-Cp*-5-Cp-4,5,2,3-*closo*-$Ru_2C_2B_9H_{11}$ and **IX** have such upfield resonances compared to the Wadian 4,5,2,3- compounds, but as for the downfield degree four boron resonance, a fluxional DSD mechanism could potentially average out the carbon atoms which correspond to the upfield CH resonances on the NMR timescale.

Alternatively, there may not be a DSD mechanism operating, and the deshielding effect for the degree four vertex between two metals may be observed only in subicosahedral and non-Wadian thirteen vertex bimetallics, but not the Wadian thirteen vertex bimetallics. However it is not clear how the electronic change in going from the Wadian compounds to the non-Wadian compounds would cause NMR shielding at vertices 2 and 3, and deshielding at vertex 1.

Low temperature NMR experiments could be used to try to freeze out any fluxional DSD mechanisms if they exist. Reduction of the non-Wadian compounds (if they are indeed reducible) would potentially lead to dianionic Wadian compounds which are isoelectronic with the Wadian Ru(*p*-cymene)/CpCo compounds. Any changes in the NMR spectra in going from the non-Wadian to the reduced species could be useful in understanding the differences in the NMR spectra of Wadian/non-Wadian bimetallic compounds.

If *X*-ray structures of the reduced species could be studied, then comparing cage bond lengths with the cage bond lengths of the structures of the non-Wadian species could also give experimental information on the nature of the LUMO of the non-Wadian compounds (i.e. the HOMO of the reduced, Wadian compounds).

Fourteen vertex bimetallacarboranes

Compounds **21** and **22** appear to be reasonably stable in solution for moderate amounts of time, which is perhaps surprising given that the thirteen vertex compounds are presumably formed from an initial fourteen vertex bimetallic which subsequently loses a boron vertex. The alternative would be that the intermediate [4-Cp*-4,1,6-*closo*-$RuC_2B_{10}H_{12}]^-$ loses a BH vertex, which is then replaced by a RuCp* unit. However this seems unlikely in the absence of a base.

Experiments where compounds **21** and **22** were left in solution for prolonged periods, or heated, would be needed to give a better idea of how stable these compounds are. The compound's non-Wadian architectures (i.e. not bicapped hexagonal antiprismatic) indicates that they are either kinetic products, meaning that they have been formed by DEI, but that rearrangement to the bicapped hexagonal antiprism is for some reason not feasible, or thermodynamic products whereby the adopted structure is one which is stable with only 2n PSEs.

A series of fourteen vertex $Cp_2Fe_2(CH_3)_4C_4B_8H_8$ isomers was prepared by Grimes et al.[21] Three of these isomers have non-Wadian shapes - one of which has an open quadrilateral face, and the other two an open pentagonal face (similar to the structure of reduced 2,3-$(CH_2)_3$-2,3-*closo*-$C_2B_{12}H_{12}$)[22] - which ultimately convert to Wadian bicapped hexagonal antiprisms without open faces upon heating. The non-Wadian compounds were described by Grimes et al as kinetic isomers, although unlike in compounds **21** and **22** these tetracarbon compounds are non-Wadian only because they have open faces, giving nido like structures which would be expected to be closo (they have 2n + 2 PSEs).

The architecture of the kinetic tetracarbon isomers which have pentagonal open faces (isomers I and II) are similar to those of compounds **21** and **22** (figure 5.10.3), differing only in that the former have pentagonal open faces, while the latter have quadrilateral faces (i.e. breaking the v9-v10 connectivity in **21**/**22** generates a very similar cage architecture to the pentagonal face tetracarbon compounds). The tetracarbon isomer which has a quadrilateral open face (isomer III) incorporates a metal vertex in the open face and so has an architecture which is less like that of compounds **21**/**22**.

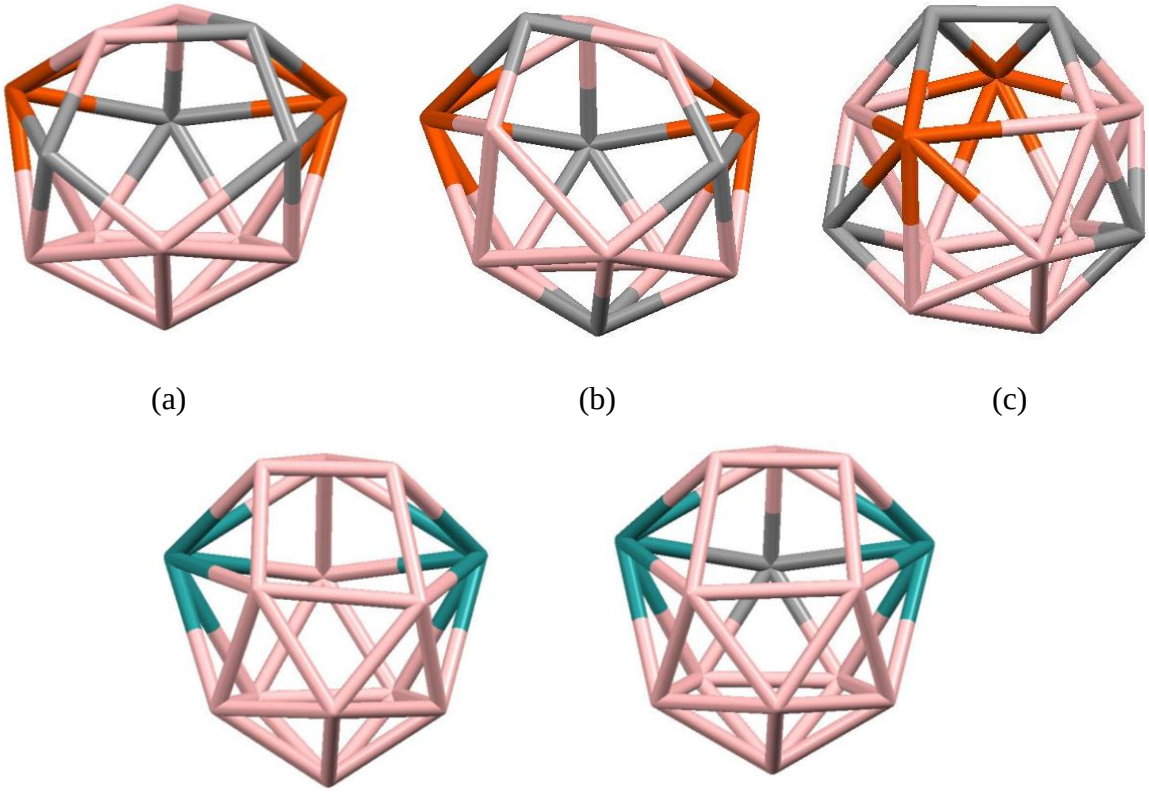

Figure 5.10.3 Cage structures of $Cp_2Fe_2(CH_3)_4C_4B_8H_8$ (a) isomer I, (b) isomer II, (c) isomer III, (d) **21** and (e) **22**.

Heating compounds **21** and **22** could potentially result in either loss of a boron vertex to give thirteen vertex bimetallic compounds or rearrangement of the cage to give a different architecture.

Based on the lack of cage carbon migration observed in compounds **VIII** and **IX** upon heating, it seems unlikely that compound **21** isomerised from **22** or vice versa (**21** does not change to **22** in solution or vice versa), but rather that they are formed by DEI at different positions on the cage. The lack of cage carbon migration observed in compounds **VIII** and **IX** also suggests that compounds **21** and **22** will not be expected to display cage carbon migration upon heating, but experimental evidence would be needed to confirm this as such migration across the surface of these fourteen vertex non-Wadian species may be more energetically favourable than for the thirteen vertex compounds.

Reduction of compounds **21** or **22** would lead to them having 2n + 2 PSEs, and could potentially effect a cage rearrangement to a Wadian bicapped hexagonal antiprism, which

could then hopefully be isolated as the dianion. Such a reduction may also be possible for compounds **18** and **19**, but would not be predicted to be accompanied by significant structural rearrangement.

The susceptibility of compounds **21** and **22** towards direct nucleophilic insertion (the quadrilateral face being a possible insertion site) could also be investigated. However nucleophilic metal insertions may only be applicable to subicosahderal compounds, as the direct insertion of nucleophilic metal fragments into supraicosahedral compounds (such as the open faced fourteen vertex bimetallic tetracarbon compounds) has not been reported. Also, reaction of a nucleophilic metal fragment with a compound which has 2n PSEs like **21** or **22** may result in oxidation of the metal fragment, and reduction of the metallacarborane, rather than insertion of the metal into the polyhedral framework.

Structures of non-Wadian compounds

The compounds **VII**, **IX**, 4,5-Cp_2-4,5,2,3-*closo*-$Co_2C_2B_9H_{11}$, 4,5-(*p*-cymene)$_2$-4,5,2,3-*closo*-$Ru_2C_2B_9H_{11}$ and the theoretical compounds $B_{13}H_{13}$ and $[B_{13}H_{13}]^{2-}$ belong to the non-degenerate C_{2v} point group. The HOMO of $[B_{13}H_{13}]^{2-}$ (figure 5.10.4) has been calculated[14a] to be bonding along certain edges (particularly between the degree four vertex and the two adjacent degree five vertices) but is evidently high enough in energy that its occupation is not essential to the stability of the molecule[6b,14b] as stable bimetallacarborane compounds are observed with this orbital both empty and occupied.

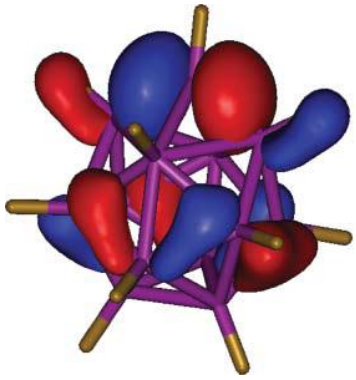

Figure 5.10.4 Calculated HOMO of $[B_{13}H_{13}]^{2-}$

The Wadian 4,5,1,6- compounds, whilst not of C_{2v} symmetry, must have a HOMO of similarly high energy in order for the non-Wadian 4,5,1,6- compounds to be observed.

If the fourteen vertex non-Wadian compounds are thermodynamic products, then the adopted structure is evidently one which has a LUMO whose occupation is not essential to the stability of the molecule. This is not a bicapped hexagonal antiprism, which would not be predicted to be stable with only 2n PSEs based on the calculated orbitals of $[B_{14}H_{14}]^{2-}$.[6b]

Compounds **VIII**, **18**, **21** and **22** all crystallise in the same space group ($P2_1/n$), and all have similar unit cell dimensions (table 5.10.1) despite being confirmed as different compounds spectroscopically. This phenomenon has been observed before[23] in 2-H-2,2-(Et$_3$P)$_2$-2,1,6-$CoC_2B_7H_9$, 2-H-2,2-(Et$_3$P)$_2$-2,1,6-$RhC_2B_7H_9$ and 1,1-(Et$_3$P)$_2$-1,2,4-$CoC_2B_8H_{10}$, which differ in either the size of the cage or as rotational conformers. It is not known why these compounds crystallise in identical space groups with such close unit cell dimensions. Compound **19** crystallises in the same space group, but has different unit cell dimensions to the other four compounds.

Table 5.10.1 Unit cell parameters of compounds **VIII**, **18**, **19**, **20** and **21**.

Compound	Unit cell parameters (Å, ^{o})
VIII	a = 8.3431(13), b = 15.782(3), c = 20.446(3) α = 90, β = 101.483(3), γ = 90
18	a = 8.3601(17), b = 15.643(3), c = 20.547(4) α = 90.00, β = 101.31(3), γ = 90.00
21	a = 8.4816(6), b = 15.5241(11), c = 20.8045(15) α = 90.00, β = 101.3680(10), γ = 90.00
22	a = 8.3871(5), b = 15.5825(9), c = 20.8076(13) α = 90.00, β = 101.538(3), γ = 90.00
19	a = 8.2910(6), b = 26.1610(17), c = 12.0948(8) α = 90.00, β = 99.394(4), γ = 90.00

*Compound **23***

Discussion of compound **23** is somewhat limited by the ambiguous nature of the small fragment connected to the three metal centres, but the general structure of a triangle of metal centres participating in B-H→Ru agostic interactions is clear, and can be compared to other known compounds which display similar structural motifs.

For example a search of the CSD[12] returned ten hits which have a similar triangular Ru_3 fragment with C_{3v} symmetry (for example (μ_3-methylidyne)-tris(μ_2-carbonyl)-tris(η^5-pentamethyl-cyclopentadienyl)-tri-ruthenium[24] (figure 5.10.5)). Instead of getting two electrons from B-H→Ru agostic interactions, these compounds have bridging carbonyls to give eighteen electron count metals. In all these compounds the atom of the small fragment which is connected to the metals is carbon, making it more likely that the equivalent atom in compound **23** is the same.

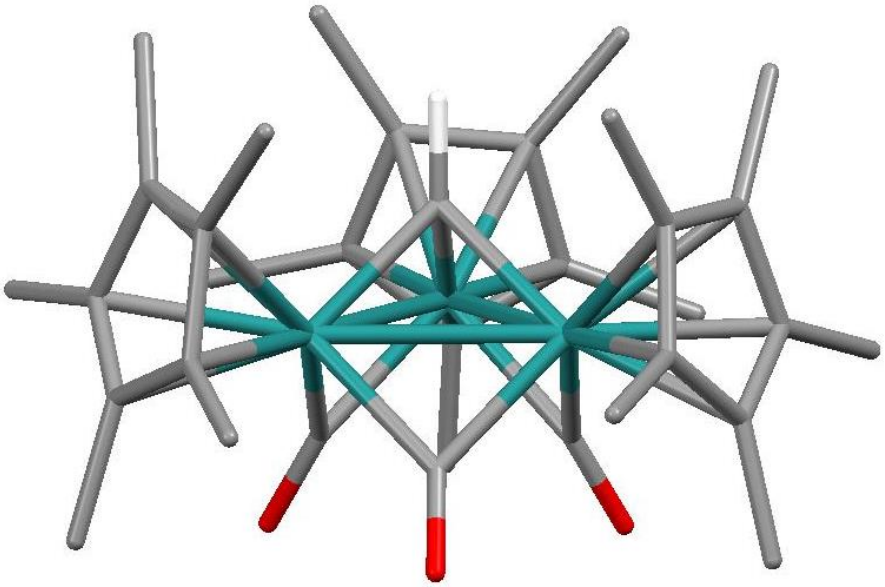

Figure 5.10.5 Molecular **s**tructure of (μ_3-methylidyne)-tris(μ_2-carbonyl)-tris(η^5-pentamethyl-cyclopentadienyl)-tri-ruthenium.

With respect to the $C_2B_{10}H_{12}$ cage in compound **23**, there are many examples of compounds with metal atoms bound via the electrons in the B-H bond, particularly metallacarborane compounds[11a] where there is also a polyhedral metal atom - although numerous examples also exist with only carbon/boron cage vertices.[11b] However compound **23** is believed to be the first example of a Ru_3 triangle involved in B-H→Ru agostic interactions with one of the triangular faces of an icosahedral carborane cage (figure 5.10.6).

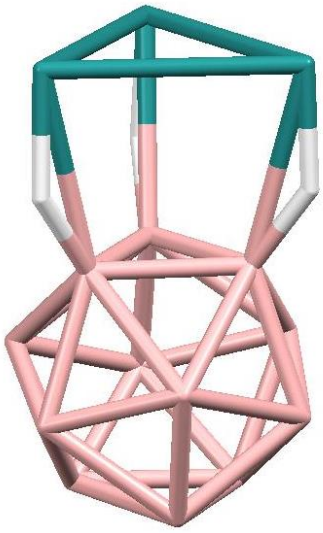

Figure 5.10.6 Structure of compound **23** (all, vertices refined as boron and Cp* ligands, small fragment and non-bridging hydrogen atoms removed for clarity).

THF bound mono-metallacarboranes

For the reactions using $Tl[TlC_2B_9H_{11}]$ or reduced 1,2-μ-$(CH_2)_3$-1,2-*closo*-$C_2B_{11}H_{11}$ as the carborane sources, the initial metallation has been successful, but coordination of THF appears to be more favourable than DEI of a second {$RuCp^{*+}$} unit. The THF blocks the DEI, as the cage is now zwitterionic and has no overall negative charge.

Compound **20** has a σ-bonded *n*-BuO group attached to the cage, the *n*-BuO likely coming from a molecule of THF. It is not clear exactly how this occurs, or whether it happens after the first metallation or the DEI, but it results in a compound which unlike **17**, **24** and **25**, is not zwitterionic.

Previous work[25a,b,c] on icosahedral and thirteen vertex carboranes has shown the attack of donor molecules, including THF, on the cage in the presence of hydride abstracting reagents such as $[CPh_3][BF_4]$. It is possible that {$RuCp^{*+}$} is acting as a hydride abstraction reagent, giving a positive charge on the mono-metallated cage which is then attacked by a molecule of THF (figure 5.10.7).

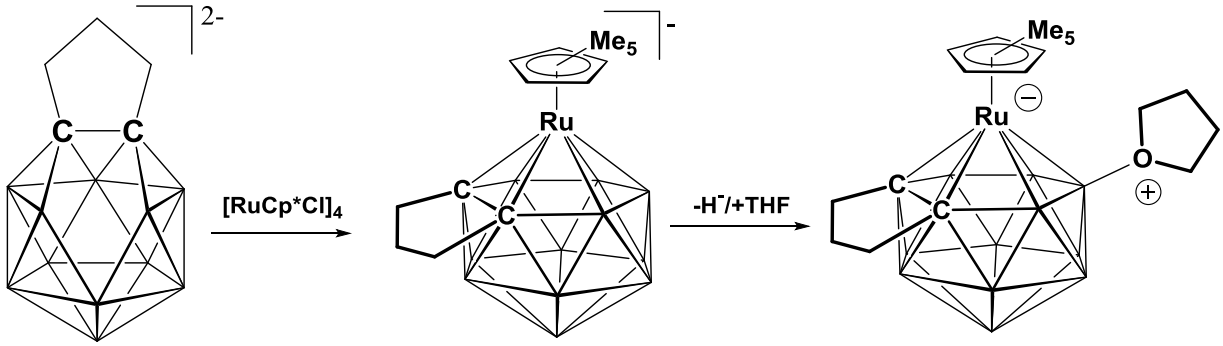

Figure 5.10.7 Possible sequence of metallation and hydride abstraction/THF coordination in compound **24** (a similar sequence could be drawn for compound **25**).

It is also possible that the hydride abstraction/THF coordination is occurring pre-metallation, followed by metallation of a singularly negatively charged nido zwitterionic species, or even that the hydride is somehow being abstracted by sodium metal and replaced with THF during the reduction step (although this would not account for the formation of **17**). The latter process would give a pseudo-zwitterionic species with a nido structure, but a single positive charge, which would only give a neutral (and hence chromatographically mobile) species

upon reaction with an M^+ source, but not with the more conventional reaction with an M^{2+} source.

Why the hydride abstraction/THF attack only occurs when using $Tl[TlC_2B_9H_{11}]$ or reduced 1,2-μ-$(CH_2)_3$-1,2-*closo*-$C_2B_{11}H_{11}$ as the carborane sources, and not when using reduced 1,2-*closo*-$C_2B_{10}H_{12}$ (i.e. why X-THF-4-Cp*-4,1,6-*closo*-$RuC_2B_{10}H_{11}$ is not isolated from reaction One) is not known.

Nor is it not clear why Kudinov et al report formation of exclusively **VIII** from the reaction of $Tl[TlC_2B_9H_{11}]$ and $\{RuCp^{*+}\}$. One explanation is that Kudinov et al isolated **VIII** by recrystallising it from the crude reaction mixture, and not by chromatography, so **17** could have been missed. Another explanation is that an experimental oversight/impurity of reagents could have led to hydride abstraction/THF attack and the formation of **17** as opposed to **VIII** in our hands. Determining why **17** is being formed in the reaction of $Tl[TlC_2B_9H_{11}]$ and $\{RuCp^{*+}\}$, and optimizing the reaction to give exclusively **VIII** and no **17** (i.e. stopping the hydride abstraction from happening) may provide insights that could be used to get reaction Two to proceed with less/no hydride abstraction.

If $\{RuCp^{*+}\}$ is acting as a hydride abstracting reagent then it may be possible to take measures which limit the amount of hydride abstraction/THF coordination occurring, and increase the amount of metallation/DEI.

A similar sort of reaction to the one which yielded compounds **24** and **25**, but using a different thirteen vertex carborane source may give a mono-metallated fourteen vertex anion which is less prone to hydride abstraction, and more likely to undergo DEI. This could involve using a species with a different tether,[7] or 1,6-Me_2-1,6-*closo*-$C_2B_{11}H_{11}$[26] as the carborane sources. Performing the reactions at low temperature (DEI into Tl[3-Cp*-3,1,2-*closo*-$RuC_2B_9H_{11}$] could be carried out at -78°C)[4] may prevent the hydride abstraction to some degree.

$[NR_4]X$ (R = Et, Bu^n, X = I, F, Cl) salts have been shown[25a,27] to react with icosahedral THF bound zwitterionic metallacarboranes at room temperature to give compounds of the type $[MC_2B_9H_{10}$-8-$O(CH_2)_3CH_2X]^-$, where cleavage of an O-C bond gives an anionic metallacarborane. Such tertiary amine halide salts would be predicted to be unreactive

towards a reduced carborane or $[RuClCp^*]_4$, and so could conceivably be added alongside the $[RuClCp^*]_4$ to react with the hydride abstracted/THF bound zwitterionic metallacarborane and give an anionic species, allowing a DEI. The $-O(CH_2)_3CH_2X$ group would hopefully not be sterically repulsive towards a DEI as it would be located on the other side of the molecule to the (predicted) insertion site adjacent to the cage carbon atoms.

Subrogation of fourteen vertex 2,3-$(CH_2)_3$-2,3-*closo*-$C_2B_{12}H_{12}$ gives a thirteen vertex dianion which appears to be less susceptible to reoxidation than reduced 1,2-μ-$(CH_2)_3$-1,2-*closo*-$C_2B_{11}H_{11}$,[28] presumably as the resulting nido carborane has a hexagonal open face, as opposed to reduced 1,2-μ-$(CH_2)_3$-1,2-*closo*-$C_2B_{11}H_{11}$ which has a pentagonal open face which rearranges to a hexagonal metal bound face upon metallation with $\{Ru(p\text{-cymene})^{2+}\}$[29] (the pentagonal metal bound face product can also be made by metallating with $\{Ni(dppe)^{2+}\}$[7]). Using this subrogated carborane as the nido carborane source could lead to a greater amount of metallation, which in turn could lead to a greater amount of DEI product, although the ratio of hydride abstraction product to DEI product would likely be the same as metallation of reduced 1,2-μ-$(CH_2)_3$-1,2-*closo*-$C_2B_{11}H_{11}$.

Alternatively, instead of using a reduced carborane as the nido cage source, the metallation/DEI could be attempted using a reduced/subrogated metallacarborane (for example [1-(arene)-1,2,10-*nido*-$RuC_2B_{10}H_{12}]^{2-}$, made by reducing 4-(arene)-4,1,12-*closo*-$RuC_2B_{10}H_{12}$)[30] (figure 5.10.8).

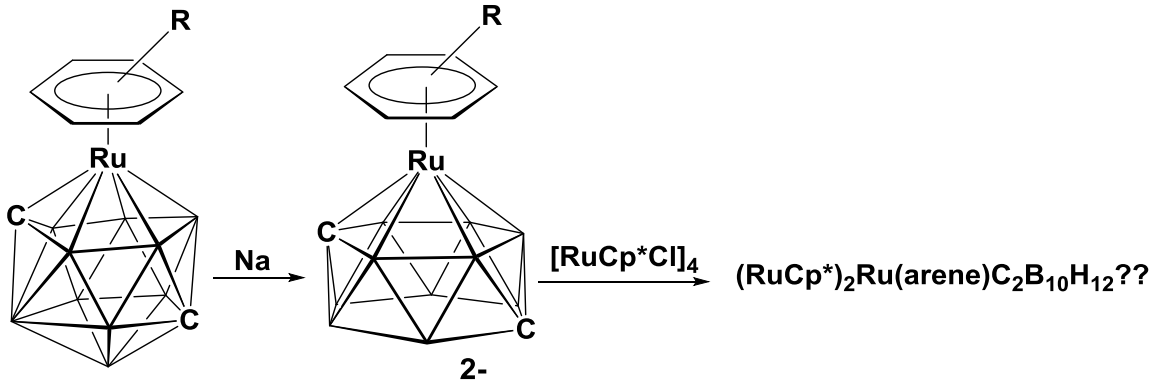

Figure 5.10.8 Reduction of 4-(arene)-4,1,12-*closo*-$RuC_2B_{10}H_{12}$ followed by addition of $[RuClCp^*]_4$ could lead to metallation/DEI (exact structure of resulting compound not easy determined).

The reaction could also be attempted using $[(\eta\text{-}C_5R_5)Ru(MeCN)_3]^+$ (R = H, Me) or $[(\eta\text{-}C_4Me_4)Co]^+$ which have been shown to undergo DEI into Tl[3-Cp*-3,1,2-*closo*-$RuC_2B_9H_{11}$],[19] although the initial metallation step using these metal fragments has not been reported. $[(\eta\text{-}C_4Me_4)Co]^+/[(\eta\text{-}C_5R_5)Ru(MeCN)_3]^+$ may not be as strong hydride abstracting reagents as $[RuClCp^*]_4$ (if indeed $[RuClCp^*]_4$ is responsible for abstracting the hydride in the reaction to make **17** and reaction Two), although they could potentially be equally strong or even stronger ones.

Metallation/DEI could be attempted using reduced 2,3-$(CH_2)_3$-2,3-*closo*-$C_2B_{12}H_{12}$[22] as the nido carborane source. This could give a sixteen vertex non-Wadian bimetallacarborane, if the DEI occurs, or a fifteen vertex zwitterionic mono-metallic species with a pendant THF if the hydride abstraction occurs (figure 5.10.9).

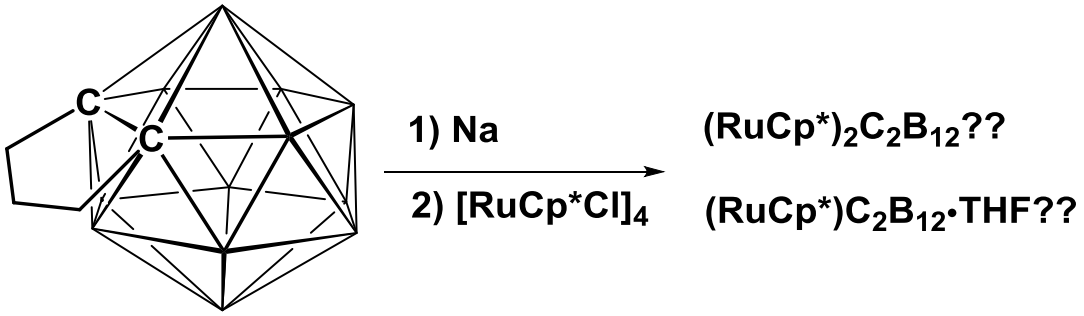

Figure 5.10.9 Reduction of 2,3-$(CH_2)_3$-2,3-*closo*-$C_2B_{12}H_{12}$ followed by addition of $[RuClCp^*]_4$ could lead to a sixteen vertex bimetallacarborane, or fifteen vertex THF bound mono-metallacarboranes.

Other anionic closo metallaheteroboranes (for example [2-Cp-2,1-$CoCB_{10}H_{11}]^-$, [1-Me-2-Cp*-2,1-$CoSiB_{10}H_{10}]^-$, [4-Cp-4,1,6-*closo*-$FeC_2B_{10}H_{11}]^-$ or [4,4′-Co-(1,6-*closo*-$C_2B_{10}H_{12})_2]^-$)[31a,b,c,] could potentially undergo DEI to give thirteen vertex mixed metal non-Wadian bimetallic compounds. Such reactions are unlikely to occur with closo dianionic metallaheteroboranes though, as the resulting trimetallic (metallacarborane^{2-} + 2{$RuCp^{*+}$}) would have 2n - 2 PSEs and so would not be predicted to be stable.

The DEI of {$RuCp^{*+}$} into [1-*closo*-$CB_{11}H_{12}]^-$ does not proceed in THF at room temperature or at reflux, with no mobile bands being observed in the TLC, indicating that a metal vertex must be present for this type of reaction to occur. Reactions with metallacarboranes bearing exo-polyhedral substituents other that Cp/Cp*/arene are also unlikely to be successful, as the {$RuCp^{*+}$} units could undergo insertion into M-L bonds as opposed to DEI into the cage.

5.11 Summary

The reaction of $[RuCp^*Cl]_4$ and reduced 1,2-*closo*-$C_2B_{10}H_{12}$ leads to a range of different compounds. If metallation occurs, then the resulting thirteen vertex compound can undergo DEI to give non-Wadian fourteen vertex species (compounds **21** and **22**) or undergo DEI accompanied by loss of a BH vertex to give a non-Wadian thirteen vertex compound (compounds **18**, **19** and **20**). In the case of compound **20** this process is accompanied by coordination of either a decyclised molecule of THF, or a cyclic molecule of THF which is subsequently decyclised. From the same reaction species with closo (compound **23**) or nido (partially identified purple compound) cages bound to RuCp* fragments via B-H→Ru agostic interactions are also isolated.

The non-Wadian fourteen vertex compounds and have a novel cage architecture, which is either the thermodynamically favoured cage structure for a 2n PSE fourteen vertex heteroborane, or a kinetic structure formed by the DEI mechanism. The non-Wadian thirteen vertex compounds have similar structures to their Wadian analogues, but have different spectroscopic characteristics, most notably for the atoms occupying vertices 1, 2, and 3.

An attempted repeat of the previously reported reaction between $[RuCp^*Cl]_4$ and $Tl[TlC_2B_9H_{11}]$ gave a mixture of compound **VIII** and compound **17**. Compound **17** was not reported in the original synthesis, and the reasons for its formation during our attempted recreation of the original synthesis are not clear at this point.

Reaction of $[RuCp^*Cl]_4$ and reduced 1,2-μ-$(CH_2)_3$-1,2-*closo*-$C_2B_{11}H_{11}$ gives small amounts of two isomers of a fourteen vertex THF bound zwitterionic species (compounds **24** and **25**). There is some evidence that a third isomer is also formed during this reaction, and that possibly a fifteen vertex non-Wadian bimetallic compound is also formed, although further work is needed to confirm this.

It seems possible that other reducible carboranes could undergo metallation followed by DEI when reacted with $[RuCp^*Cl]_4$, but hydride abstraction/THF coordination of the mono- metallated anionic intermediate might be a limiting factor in the applicability of this method. Further work is needed to both fully characterise and understand the chemistry of the

compounds outlined in this chapter and test the DEI reaction on other nido carborane/anionic metallacarborane sources.

5.12 References

5.1 For example: G.B. Dunks, M.M. McKown and M.F. Hawthorne, *J. Am. Chem. Soc.*, 1971, **93**, 2541; D.F. Dustin, G.B. Dunks and M.F. Hawthorne, *J. Am. Chem. Soc.*, 1973, **95**, 1109; D. Ellis, M.E. Lopez, R. McIntosh, G.M. Rosair, A.J. Welch and R. Quenardelle, *Chem, Commun.*, 2005, 1348; A. McAnaw, M.E. Lopez, G. Scott, D. Ellis, D. McKay, G.M. Rosair and A.J. Welch, *Dalton Trans.*, 2012, **41**, 10957.

5.2 G.K. Barker, M.P. Garcia, M. Green, F.G.A. Stone and A.J. Welch, *J. Chem. Soc., Chem. Commun.*, 1983, 137.

5.3 A. McAnaw, M.E. Lopez, D. Ellis, G.M. Rosair and A.J. Welch, *Dalton Trans.*, 2014, **43**, 5095.

5.4 A.R. Kudinov, D.S. Perekalin, S.S. Rynin, K.A. Lyssenko, G.V. Grintselev-Knyazev and P.V. Petrovskii, *Angew. Chem., Int. Ed.*, 2002, **41**, 4112.

5.5 For example: M.P. Garcia, M. Green, F.G.A. Stone, R.G. Somerville, A.J. Welch, C.E. Briant, D.N. Cox and D.M.P. Mingos, *J. Chem. Soc., Dalton Trans.*, 1985, 2343; T.D. McGrath, A. Franken, J.A. Kautz, and F.G.A. Stone, *Inorg. Chem.*, 2005, **44**, 8135; M. Green, J.L. Spencer, F.G.A. Stone and A.J. Welch, *J. Chem. Soc., Dalton Trans.*, 1975, 179; M. Green, J.A.K. Howard, J.L. Spencer and F.G.A. Stone, *J. Chem. Soc., Dalton Trans.*, 1975, 2275.

5.6 (a) K. Wade, *J. Chem. Soc. D*, 1971, 792.
(b) P.W. Fowler, *Polyhedron*, 1985, **4**, 2051.

5.7 L. Deng, H.-S. Chan, and Z. Xie, *J. Am. Chem. Soc.*, 2006, **128**, 5219.

5.8 For example: V.R. Miller and R.N. Grimes, *J. Am. Chem. Soc.*, 1973, **95**, 2830; K.P. Callahan, W.J. Evans, F.Y. Lo, C.E. Strouse and M.F. Hawthorne, *J. Am. Chem. Soc.*, 1975, **97**, 296; C.G. Salentine, C.E. Strouse and M. F. Hawthorne, *Inorg. Chem.*, 1976, **15**, 1832; A. Franken, B.E. Hodson, T.D. McGrath and F.G.A. Stone, *Dalton Trans.*, 2007, 2254; S. Ghosh, M. Shang, Y. Li, and T. P. Fehlner, *Angew. Chem. Int. Ed.*, 2001, **40**, 1125.

5.9 W.Y. Man, unpublished results, Heriot-Watt University, 2014.

5.10 C.G. Salentine and M.F. Hawthorne, *Inorg. Chem.*, 1978, **17**, 1948.

5.11 (a) For example: N. Carr, M.C. Gimeno, J.E. Goldberg, M.U. Pilotti, F.G.A. Stone and I. Topaloğlu, *J. Chem. Soc., Dalton Trans.*, 1990, 2253; M. Elrington, N.N. Greenwood, J.D. Kennedy and M. Thornton-Pett, *J. Chem. Soc., Chem. Commun.*, 1984, 1398; M.J. Carr, T.D. McGrath and F.G.A. Stone, *Inorg. Chem.*, 2008, **47**, 713;

F.-E. Baumann, J.A.K. Howard, O. Johnson and F.G.A. Stone, *J. Chem. Soc., Dalton Trans.*, 1987, 2917; B.E. Hodson, T.D. McGrath and F.G. A. Stone, *Organometallics*, 2005, **24**, 3386.

(b) For example: K. Shelly, C.A. Reed, Y.J. Lee and W.R. Scheidt, *J. Am. Chem. Soc.*, 1986, **108**, 3117; E. Molinos, G. Kociok-Kohn and A.S. Weller, *Chem, Commun.*, 2005, 3609; K. Shelly, D.C. Finster, Y.J. Lee, W.R. Scheidt and C.A. Reed, *J. Am. Chem. Soc.*, 1985, **107**, 5955.

5.12 F.H. Allen, *Acta Crystallogr., Sect. B: Struct. Sci.*, 2002, **B58**, 380. For this study we used CSD Version 5.33 (November 2011).

5.13 A. Burke, R. McIntosh, D. Ellis, G.M. Rosair and A.J. Welch, *Collect. Czech. Chem. Commun.*, 2002, **67**, 991.

5.14 (a) M.E. Lopez, M.J. Edie, D. Ellis, A. Horneber, S.A. Macgregor, G.M. Rosair and A.J. Welch, *Chem, Commun.*, 2007, 2243.

(b) M.E. O'Neill and K. Wade, *Polyhedron*, 1984, **3**, 199.

5.15 W.J. Evans and M.F. Hawthorne, *Inorg. Chem.*, 1974, **13**, 869.

5.16 D.F. Dustin and M.F. Hawthorne, *J. Am. Chem. Soc.*, 1974, **96**, 3462.

5.17 A.R. Kudinov, M.I. Rybinskaya, D.S. Perekalin, V.I. Meshcheryakov, Y.A. Zhuravlev, P.V. Petrovskii, A.A. Korlyukov, D.G. Golovanov and K.A. Lyssenko, *Izv. Akad. Nauk SSSR, Ser. Khim. (Russ.)(Russ. Chem. Bull.)*, 2004, 1879.

5.18 B. Grüner, B. Štíbr, R. Kivekäs, R. Sillanpää, P. Stopka, F. Teixidor and C. Viňas, *Chem. Eur. J.*, 2003, **9**, 6115.

5.19 A.R. Kudinov, E.V. Mutseneck and D.A. Loginov, *Coord. Chem. Rev.*, 2004, **248**, 571.

5.20 A. Franken, T.D. McGrath and F.G.A. Stone, *J. Am. Chem. Soc.*, 2006, **128**, 16169.

5.21 W.M. Maxwell, R.F. Bryan and R.N. Grimes, *J. Am. Chem. Soc.*, 1977, **99**, 4008; W.M. Maxwell, R. Weiss, E. Sinn and R.N. Grimes, *J. Am. Chem. Soc.*, 1977, **99**, 4016.

5.22 L. Deng, J. Zhang, H.-S. Chan, and Z. Xie, *Angew. Chem., Int. Ed.*, 2006, **45**, 4309.

5.23 G.K. Barker, M.P. Garcia, M. Green, G.N. Pain, F.G.A. Stone, S.K.R. Jones, and A.J. Welch, *J. Chem. Soc., Chem. Commun.*, 1981, 652; G.K. Barker, M.P. Garcia, M. Green, F.G.A. Stone, J.-M. Bassett, and A.J. Welch, *J. Chem. Soc., Chem. Commun.*, 1981, 653.

5.24 R. Tenjimbayashi, E. Murotani, T. Takemori, T. Takao and H. Suzuki, *J. Organomet. Chem.*, 2007, **692**, 442.

5.25 (a) D.F. Mullica, E.L. Sappenfield, F.G.A. Stone and S.F. Woollam, *Organometallics*, 1994, **13**, 157.

(b) D.D. Ellis, A. Franken, P.A. Jelliss, F.G.A. Stone and P.-Y. Yu, *Organometallics*, 2000, **19**, 1993.

(c) B.E. Hodson, T.D. McGrath and F.G.A. Stone, *Organometallics*, 2005, **24**, 1638.

5.26 J. Zhang, L. Deng, H.-S. Chan and Z. Xie, *J. Am. Chem. Soc.*, 2007, **129**, 18.

5.27 M. Gomez-Saso, D.F. Mullica, E. Sappenfield and F.G.A. Stone, *Polyhedron*, 1996, **15**, 793.

5.28 F. Zheng and Z. Xie, *Dalton Trans.*, 2014, **43**, 4986.

5.29 R.D. McIntosh, D. Ellis, G.M. Rosair and A.J. Welch, *Angew. Chem. Int. Ed*., 2006, **45**, 4313.

5.30 D. Ellis, M.E. Lopez, R. McIntosh, G.M. Rosair and A.J. Welch, *Chem. Commun*., 2005, 1917.

5.31 (a) R.R. Rietz, D.F. Dustin and M.F. Hawthorne, *Inorg. Chem.*, 1974, **13**, 1580.

(b) L. Wesemann, Y. Ramjoie, M. Trinkaus and T.P. Spaniol, *Eur. J. Inorg. Chem.*, 1998, 1263.

(c) D.F. Dustin, G.B. Dunks and M.F. Hawthorne, *J. Am. Chem. Soc.*, 1973, **95**, 1109.

Thesis summary

The indenyl orientations of the supraicosahedral compounds described in chapter two show that the bridging carbon atoms lie trans to cage boron atoms and not cage carbon atoms. This can be rationalised by the fact that cage boron atoms are expected to have a stronger trans influence than cage carbon atoms. Methylation on the cage results in either rotation of the indenyl ligand away from the orientation observed in the non-methylated analogues or inclination of the indenyl ligand away from the methyl groups.

Similarly, the naphthalene bridging carbon atoms of the supraicosahedral naphthalene ruthenacarboranes lie trans to cage boron atoms and not cage carbon atoms. The observed orientations in both the indenyl and naphthalene compounds agree only moderately well with DFT calculated energy minima for rotation of a naphthalene ligand about 360^{o} in $(C_{10}H_8)FeC_2B_{10}H_{12}$ compounds.

The results of the database search from chapter four suggest that (a) exo-polyhedral ligands which lie trans to the carbon (or heteroatom) part of the cage will have a shorter M-L bond than identical ligands which lie trans to the boron part of the cage and (b) if the exo-polyhedral ligand set comprises ligands of different trans influence, the ligand(s) with the stronger trans influence will be orientated trans to the carbon (or heteroatom) part of the cage at the expense of the ligand(s) with the weaker trans influence.

The results of chapters two, three and four indicate that in metallacarboranes the trans influence is an important factor in determining the exo-polyhedral ligand orientation, with strong cage-to-metal bonding being compensated by weak exo-polyhedral-to-metal bonding and weak cage-to-metal bonding being compensated by strong exo-polyhedral-to-metal bonding.

Chapter five has shown that direct electrophilic insertion is possible for anionic thirteen vertex metallacarboranes, giving either fourteen vertex non-Wadian bimetallacarboranes or undergoing subsequent loss of BH to give fourteen vertex non-Wadian bimetallacarboranes. For anionic fourteen vertex metallacarboranes, hydride abstraction and coordination of solvent to the cage appears to be favourable to direct electrophilic insertion.

Chapter 6
Experimental

6.1 General experimental

Syntheses

All experiments were carried out under a dry, oxygen free, nitrogen atmosphere, using Schlenk line techniques, with some subsequent manipulation being carried out in the open laboratory. Most of the compounds reported are air stable. All solvents were freshly distilled from the appropriate drying agents under nitrogen immediately before use (DCM and MeCN, CaH_2; THF and diethyl ether, sodium wire/benzophenone; toluene and petroleum ether (b.p. 40-60^oC), sodium wire), or were stored over 4 Å molecular sieves and were degassed (3 x freeze-pump-thaw cycles) before use. Preparative thin layer chromatography (TLC) employed 20 x 20 cm Kiesegel 60 F_{254} glass plates.

Analyses

NMR spectroscopy was carried out on Bruker AC200, AVIII300, DPX400 and AVIII400 spectrometers at ambient temperature from $CDCl_3$ solutions. Chemical shifts were recorded relative to tetramethylsilane (^1H - 200, 300 or 400 MHz), boron trifluoride etherate (^{11}B - 64, 96 or 128 MHz) or phosphoric acid (^{31}P - 81, 121.5 or 162 MHz). EI mass spectra were recorded using a Kratos Concept mass spectrometer at Heriot-Watt University or a Finnigan (Thermo) LCQ Classic ion trap mass spectrometer at the University of Edinburgh. Elemental analyses were carried out using an Exeter CE-440 elemental analyser at Heriot-Watt University.

Hazards

Standard principles of safe handling and good general laboratory practice were followed, including the wearing of protective clothing and safety glasses. Extra care and attention was exercised when handling flammable solvents, alkali metals and toxic chemicals.

Standard preparations

The compounds[$RuCl_2(COD)]_x$,[1] [$HNEt_3$][7,8-*nido*-$C_2B_9H_{12}$],[2] Tl[$TlC_2B_9H_{11}$],[3] 1,2-μ-$(CH_2)_3$-1,2-*closo*-$C_2B_{10}H_{10}$,[4] 1,2-μ-$(CH_2)_3$-1,2-*closo*-$C_2B_{11}H_{11}$,[5] [$RuCl_2Cp^*]_n$[6] and [$RuClCp^*]_4$[7] were prepared by literature methods or slight variants thereof. The compound 1,2-Me_2-1,2-*closo*-$C_2B_{10}H_{10}$ was prepared by treatment of Li_2[1,2-*closo*-$C_2B_{10}H_{10}$] with MeI in Et_2O.[8] All other reagents and solvents were supplied commercially and were used as received.

Computational calculations

Calculations performed by D. McKay at Heriot-Watt University. All geometries was optimised without constraints using Gaussian 03, Revision D.01[9] employing the BP86 functional.[10] 6-31G** basis sets were used for B, C and H atoms[11] whilst for Fe and Co the Stuttgart relativistic ECP[12] and the associated basis sets were employed. Local minima were confirmed as such through analytical frequency calculations. Geometry measurements were made using Mercury[13] and orbital representations generated *via* Molekel.[14]

Crystallographic data collection

For most compounds intensity data were collected from single crystals on a Bruker X8 APEX2 diffractometer using Mo-K_α *X*-radiation, with crystals mounted in inert oil on a cryoloop and cooled to 100 K by an Oxford Cryosystems Cryostream. Single crystals of compounds **21** and **23** were studied by the National Crystallography Service on a Rigaku FR-E+ diffractometer using Mo-K_α *X*-radiation, with crystals mounted in inert oil on a cryoloop and cooled to 100 K by an Oxford Cryosystems Cobra. Indexing, data collection and absorption correction were performed using the APEXII suite of programs[15] or CrystalClear-SM Expert 3.1 b27 (Rigaku, 2012).[16] Structures were solved by direct methods and refined by full-matrix least-squares using either SHELXL-97[17] or OLEX2.[18]

Details of compounds which co-crystallised with molecules of solvent are listed in table 6.1.1

Table 6.1.1 Details of co-crystallised solvents in applicable compounds.

Compound	Number (per asymmetric unit)/type of co-crystallised solvent
7	1xDCM
11	1x(partially disordered)THF
16	1xDCM
V	1xDCM
VI	1xDCM, 0.5x(partially disordered)DCM
VII	1x(partially disordered)DCM
24	0.75x(disordered) DCM

The structure of **5** is partially disordered across a crystallographic mirror plane (see chapter two for details) and stable refinement required the application of restraints [B2–B3, 1.9(2) Å; C1–B2, 1.53(2) Å; C1–B3A, 1.53(2) Å].

In the THF of solvation of **11** all C-C distances were restrained to 1.50(2) Å, atoms C4T and C4S had occupancies of 0.505(18) and 0.495(18), respectively, and all H atoms were set in calculated positions with C-H = 0.99 Å.

The structure of compound **13** was solved as a three component twin. Four atoms in **13** were found to have unstable or irregular anisotropic displacement parameters when freely refined, so for these atoms (C1, B6, B12 and C42) restraints were applied.

Four molecules of compound **14** crystallise in space group Pnma, requiring crystallographically-imposed mirror symmetry, which bisects the cage and lies perpendicular to the C-C junction of the naphthalene ligand (see chapter three for details).

The hydride ligand in **V** was located from a difference Fourier map and freely refined, including an isotropic temperature factor.

For compound **VI** (which was solved as a three component twin) the complete DCM molecule per asymmetric unit is ordered, but the half-occupancy one is partially disordered,

with Cl atoms Cl3A and Cl3B each assigned occupancies of 0.5 (0.25Cl each). For these disordered Cl atoms the C–Cl distance was restrained to 1.70(2) Å.

For the partially disordered molecule of DCM which co-crystallises with **VII**, all C-Cl distances were restrained to 1.70(2) Å, atoms C13A and Cl4A both had assigned occupancies of 0.5 and all H atoms were set in calculated positions with C-H = 0.99 Å. A solvent mask was also used during the refinement of **VII** as what was presumed to be a highly disordered molecule of $CDCl_3$ could not be satisfactorily modelled.

For compound **19** one of the cage carbon atoms is disordered over vertices 6, 7, 8 and 9, with each vertex assigned an occupancy of 0.25 (C) and 0.75 (B).

For the disordered 0.75 molecules of DCM which co-crystallise with **24** (0.75 DCM per asymmetric unit, 3 DCM per unit cell) all C-Cl distances were restrained to 1.70(2) Å, the following occupancies were assigned to the following atoms: C1S 0.125; Cl1T 0.5; Cl2S 0.375; C2S 0.625; Cl1S 0.25; Cl2T 0.375 and all H atoms were set in calculated positions with C-H = 0.99 Å. The structure of **24** was solved as a two component twin. Eleven atoms in **24** were found to have unstable or irregular anisotropic displacement parameters when freely refined, so for these atoms (C55, C10', C2, C13, B11, B13, B5, C11', C12, B7, C15) restraints were applied.

For compound **25**, the C_5Me_5 group of one of the two molecules in the asymmetric unit is disordered over two positions. All C-C (ring) distances were restrained to be the same and all C-CMe distances were restrained to be the same. Atoms C10'-19' had occupancies of 0.591 (4), while atoms 10A-19A had occupancies of 0.409 (4), and all H atoms were set in calculated positions with C-H = 0.98 Å. The other molecule in the asymmetric unit has a cage bound THF molecule which is disordered over two positions. All C-O distances were restrained to be the same and all C-C distances were restrained to be the same. Atoms C52-C55 had occupancies of 0.591 (4), while atoms C56-C59 had occupancies of 0.409 (4), and all H atoms were set in calculated positions with C-H = 0.99 Å

For compounds **5** (except H5), **11** (except H1 and H5), **12** (except H1, H5 and H8), **13** (except H5), **14** (except H5 and H7 (although B7-H7 distance was restrained to 1.12(2) Å)),

15 (except H5), **16** (except H5), **V**, **VI**, **VII**, **17**, **21**, **23**, **24** and **25** (except H14 and H14') the cage hydrogens were set in idealised (riding) positions with C-H = B-H = 1.12 Å (except in selected compounds where idealised (riding) positions were as follows: **5** C-H = B-H = 1.10 Å; **V** C-H 1.00 Å, B-H = 1.12 Å; **VII** C-H = B-H = 1.00 Å). For all other compounds cage-bound H atoms were located in difference Fourier maps and freely refined. Non-cage H atoms were set in idealised positions in all compounds (CH_2, C–H 0.99 Å; CH_3, C–H 0.98 Å; CH [metal bound ring], C-H 1.0 Å; CH [non-metal bound ring], C–H 0.95 Å). Some cage H atom thermal parameters were set to 1.2xU_{eq} of the attached B or C atom, while others were successfully refined with individual thermal parameters.

In most cases cage C atoms were identified by a combination of low isotropic thermal parameters following refinement as B atoms, a short C1-C2 connectivity (in the case of twelve vertex icosahedral compounds), vertex-to-centroid distances (VCD)[19] and boron-to-hydrogen-distances (BHD).[20]

For compound **22** one of the cage carbon atoms could not be found and so eleven of the twelve (non-metal) cage vertices were refined as boron. For compound **21** neither of the two cage carbon atoms could be found and so all twelve of the (non-metal) cage vertices were refined as boron. For compound **23** neither of the two cage carbon atoms could be found and so all twelve of the (non-metal) cage vertices were refined as boron. For compound **23** the atoms labelled C1A and C2A could not be definitively assigned as such, but refinement as these atoms best fits the isotropic thermal parameters and available spectroscopic data.

Compounds **18**, **21**, **22** and 4,5-Cp*$_2$-4,5,2,3-*closo*-$Ru_2C_2B_9H_{11}$[21] are isostructural (see chapter five for details).

6.2.1 Synthesis of 4-(η-C_9H_7)-4,1,6-*closo*-$CoC_2B_{10}H_{12}$ (1)

1,2-*closo*-$C_2B_{10}H_{12}$ (0.700 g, 4.85 mmol) was dissolved in degassed THF (30 mL). Na metal (0.34 g, 14.79 mmol) was added and the solution stirred overnight. In a separate Schlenk tube a solution of Li[C_9H_7] was prepared by adding indene (1.69 mL, 14.55 mmol) and *n*-BuLi (6.40 mL, 16.00 mmol) to degassed THF (10 mL) in an ice bath, stirring the solution at room temperature for 1 h, then at reflux for 15 min, giving a dark red solution. Excess Na was removed from the reduced carborane solution which was then added to the Li[C_9H_7] solution via gas-tight syringe. The resulting red solution was cooled in an ice bath, and $CoCl_2$ (2.330 g, 17.95 mmol) was added, affording a brown solution which was stirred at room temperature overnight then aerially oxidised (0.5 h). The solution was filtered through a short silica column eluting with DCM to afford a brown solution, removal of solvent from which yielded a brown solid. This was further purified by column chromatography (1:4 DCM:40-60 petroleum ether), followed by preparative TLC on silica (3:2 DCM:40-60 petroleum ether, R_f 0.62) yielding, as major product, **1** as a brown solid on removal of solvent.

Compound 1	**4-(η-C_9H_7)-4,1,6-*closo*-$CoC_2B_{10}H_{12}$**
	Yield = 0.730 g, 47.3%.
CHN	Calculated for $C_{11}H_{19}B_{10}Co$: C 41.5, H 6.02. Found: C 41.6, H 6.18%.
NMR ($CDCl_3$)	$^{11}B\{^1H\}$ NMR: δ 14.5 (1B), 2.0 (2B), -0.5 (1B), -3.8 (3B), -11.9 (2B), -16.9 (1B) ppm.
	^1H NMR: δ 7.70 (m, 2H, C_6H_4), 7.60 (m, 2H, C_6H_4), 5.90 (d, 2H, C_5H_3), 5.60 (t, 1H, C_5H_3), 3.70 (br s, 2H, $C_{cage}H$) ppm.
MS (low res. EI)	M_w = 318.19 g mol^{-1}.
	Envelope centred on *m/z* 317 (M^+).

Red block crystals grown by solvent diffusion of diethyl ether and a THF solution of **1** at -30 ^oC.

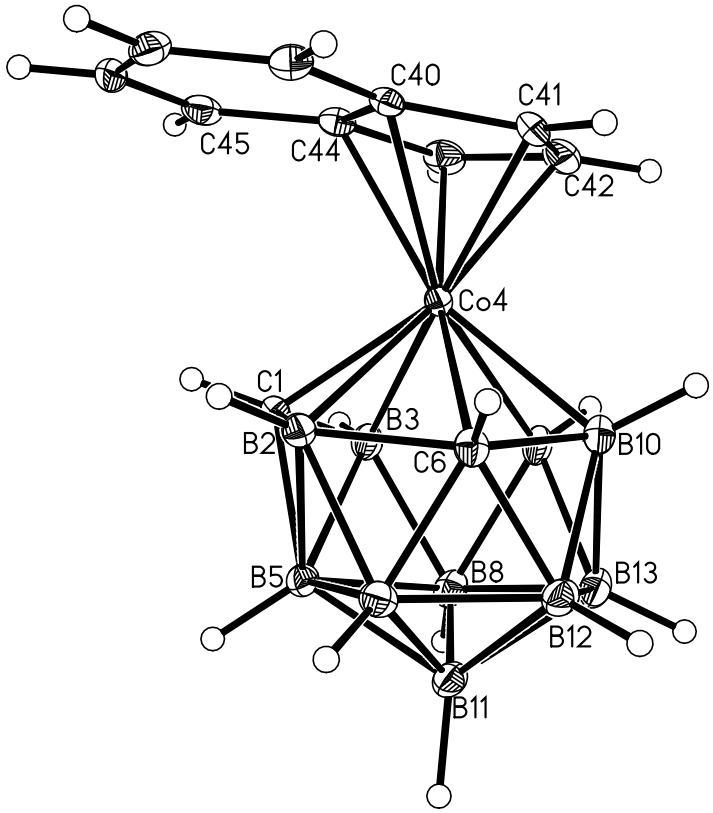

6.2.2 Synthesis of 1,6-Me_2-4-(η-C_9H_7)-4,1,6-*closo*-$CoC_2B_{10}H_{10}$ (2)

1,2-Me_2-1,2-*closo*-$C_2B_{10}H_{10}$ (0.500 g, 2.90 mmol) was dissolved in degassed THF (30 mL). Na metal (0.24 g, 10.4 mmol) was added and the solution stirred overnight. Excess Na was removed from the reduced carborane solution which was then added via gas-tight syringe to a THF solution of Li[C_9H_7] (8.70 mmol). The resulting red solution was cooled in an ice bath, and $CoCl_2$ (1.393 g, 10.73 mmol) was added, affording a brown solution which was stirred at room temperature overnight then aerially oxidised (0.5 h). The solution was filtered through a short silica column eluting with DCM to afford a brown solution, removal of solvent from which yielded a brown solid. This was further purified by column chromatography (1:4 DCM:40-60 petroleum ether), followed by preparative TLC on silica (3:2 DCM:40-60 petroleum ether, R_f 0.62) yielding, as major product, **2** as a brown solid on removal of solvent.

Compound 2	**1,6-Me$_2$-4-(η-C$_9$H$_7$)-4,1,6-*closo*-CoC$_2$B$_{10}$H$_{10}$**
	Yield = 0.340 g, 33.8%.
CHN	Calculated for $C_{13}H_{23}B_{10}Co$: C 45.1, H 6.69. Found: C 44.9, H 6.77%.
NMR ($CDCl_3$)	$^{11}B\{^1H\}$ NMR: δ 15.1 (1B), 4.9 (2B), 0.3 (1B), -0.5 (1B), -4.8 (2B), -7.3 (2B), -12.1 (1B) ppm.
	^1H NMR: δ 7.80 (m, 2H, C_6H_4), 7.60 (m, 2H, C_6H_4), 5.80 (d, 2H, C_5H_3), 5.75 (t, 1H, C_5H_3), 2.15 (s, 6H, CH_3) ppm.
MS (low res. EI)	M_w = 346.24 g mol^{-1}.
	Envelope centred on *m/z* 346 (M^+).

Red block crystals grown by solvent diffusion of 40-60 petroleum ether and a DCM solution of **2** at -30 °C.

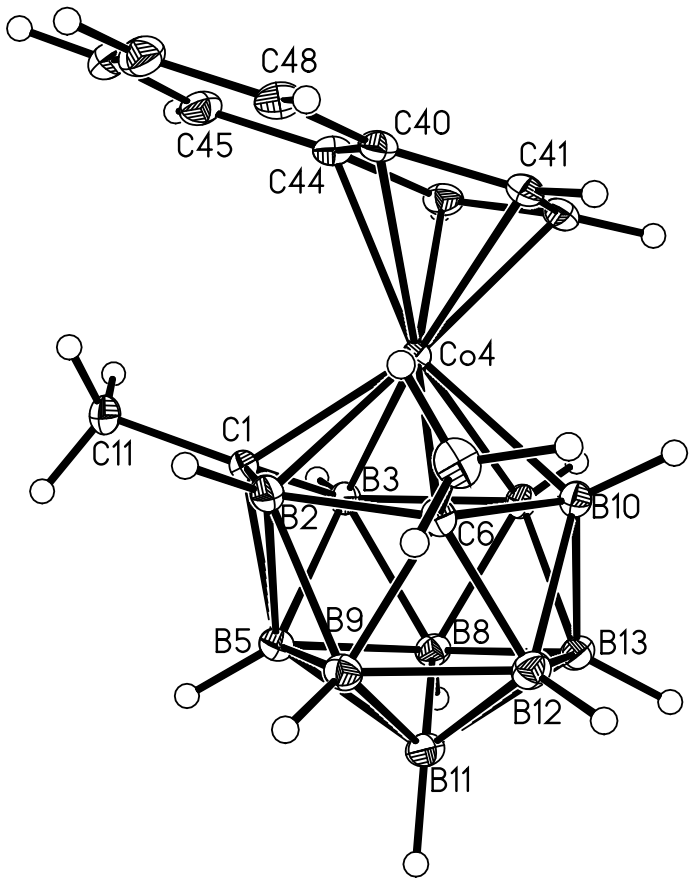

6.2.3 Synthesis of 4-(η-C_9H_7)-4,1,8-*closo*-$CoC_2B_{10}H_{12}$ (3)

Compound **1** (0.208 g, 0.65 mmol) was stirred at reflux overnight in THF (25 mL). Removal of solvent from the resulting brown solution yielded a bronze solid. Preparative TLC on silica (3:2 DCM:40–60 petroleum ether) separated **3** as a bronze product at R_f 0.77 from minor amounts of the corresponding 4,1,12- isomer (R_f 0.84) and unchanged 4,1,6- isomer (R_f 0.60).

Compound 3 **4-(η-C_9H_7)-4,1,8-*closo*-$CoC_2B_{10}H_{12}$**

Yield = 0.153 g, 73.6%.

NMR ($CDCl_3$) $^{11}B\{^1H\}$ NMR: δ 22.6 (1B), 9.3 (1B), 7.4 (1B), 6.3 (1B), -0.9 (1B), -5.8 (1B), -7.2 (1B), -8.7 (1B), -9.7 (1B), -12.5 (1B) ppm.

^1H NMR: δ 7.60 (m, 2H, C_6H_4), 7.50 (m, 2H, C_6H_4), 5.86 (m, 1H, C_5H_3), 5.80 (m, 1H, C_5H_3), 5.10 (app. t, 1H, C_5H_3), 3.75 (br s, 1H, $C_{cage}H$), 2.50 (br s, 1H, $C_{cage}H$) ppm.

MS (low res. EI) M_w = 318.19 g mol^{-1}.

Envelope centred on *m/z* 317 (M^+).

6.2.4 Synthesis of 1,8-Me_2-4-(η-C_9H_7)-4,1,8-*closo*-$CoC_2B_{10}H_{10}$ (4)

Compound **2** (0.200 g, 0.58 mmol) was heated to reflux in THF (25 mL) to afford, following TLC on silica (3:2 DCM:40-60 petroleum ether, R_f 0.75), **4** as an orange solid together with a smaller amount (57 mg, 28.5%) of the corresponding Me_2-4,1,12- isomer (R_f 0.87).

Compound 4	**1,8-Me$_2$-4-(η-C$_9$H$_7$)-4,1,8-*closo*-CoC$_2$B$_{10}$H$_{10}$**
	Yield = 0.133 g, 66.5%.
CHN	Calculated for $C_{13}H_{23}B_{10}Co$: C 45.1, H 6.69. Found: C 44.9, H 6.71%.
NMR ($CDCl_3$)	$^{11}B\{^1H\}$ NMR: δ 21.2 (1B), 13.2 (1B), 10.8 (1B), 5.2 (1B), 3.3 (1B), -2.1 (1B), -2.6 (1B), -3.0 (1B), -5.7 (1B), -13.2 (1B) ppm.
	^1H NMR: δ 7.60 (m, 2H, C_6H_4), 7.50 (m, 2H, C_6H_4), 5.65 (m, 1H, C_5H_3), 5.60 (m, 1H, C_5H_3), 5.25 (app. t, 1H, C_5H_3), 2.60 (s, 3H, CH_3), 1.75 (s, 3H, CH_3) ppm.
MS (low res. EI)	M_w = 346.24 g mol^{-1}.
	Envelope centred on *m/z* 346 (M^+).

Red plate crystals grown by solvent diffusion of 40-60 petroleum ether and a DCM solution of **4** at -30 °C. There are two crystallographically independent molecules in the asymmetric unit.

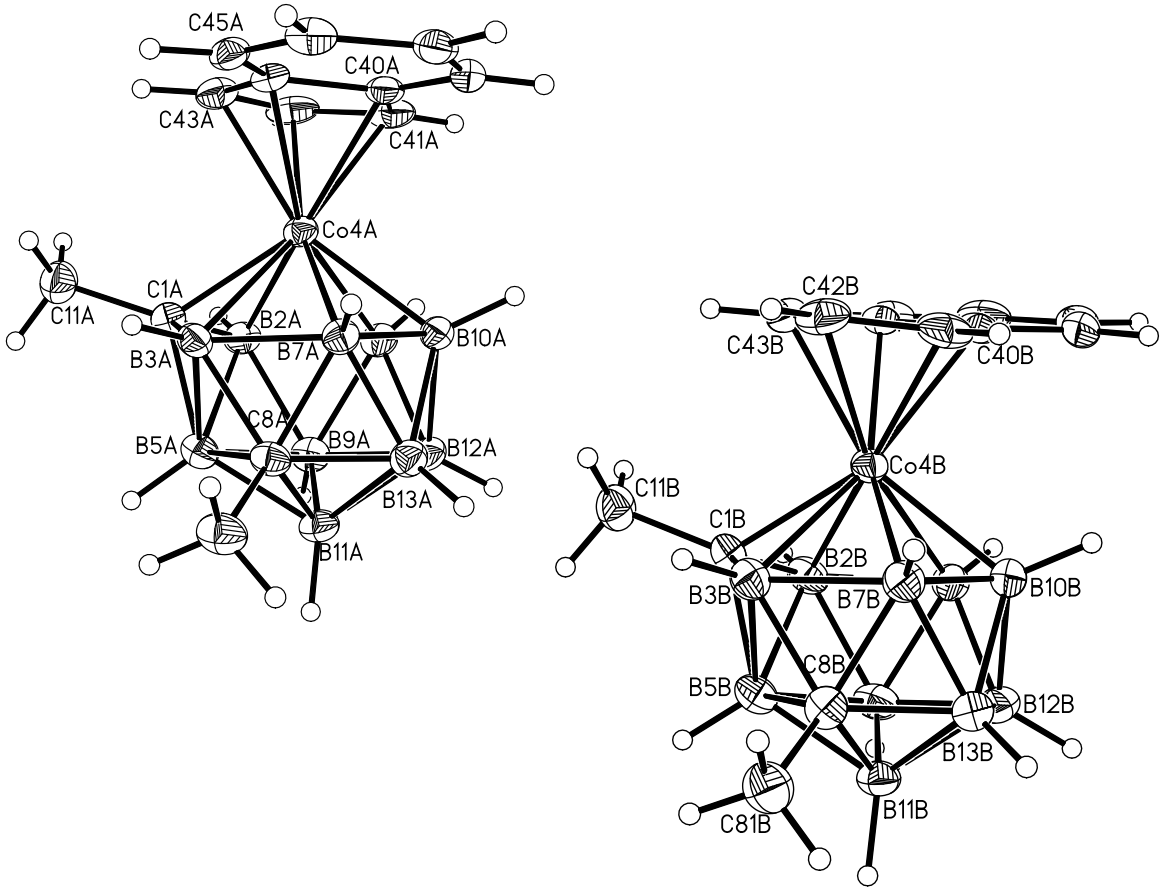

6.2.5 Synthesis of 4-(η-C_9H_7)-4,1,12-*closo*-$CoC_2B_{10}H_{12}$ (5)

Compound **7** (0.850 g, 2.67 mmol) was stirred at reflux overnight in THF (25 mL). The resulting brown solution was cooled to room temperature, and solvent removed leaving a brown solid. Preparative TLC on silica (3:2 DCM:40-60 petroleum ether) yielded **5** as a brown band at R_f 0.84.

Compound 5 **4-(η-C_9H_7)-4,1,12-*closo*-$CoC_2B_{10}H_{12}$**

Yield = 0.775 g, 91.2%.

CHN Calculated for $C_{11}H_{19}B_{10}Co$: C 41.5, H 6.02. Found: C 41.4, H 6.02%.

NMR ($CDCl_3$) $^{11}B\{^1H\}$ NMR: δ 8.8 (1B), 6.7 (1B), 4.0 (1B), 3.2 (1B), -2.8 (1B), -10.0 (2B), -14.3 (1B), -15.9 (1B), -17.3 (1B) ppm.

^1H NMR: δ 7.55 (m, 2H, C_6H_4), 7.45 (m, 2H, C_6H_4), 5.86 (m, 1H, C_5H_3), 5.76 (m, 1H, C_5H_3), 5.15 (app. t, 1H, C_5H_3), 3.70 (br s, 1H, $C_{cage}H$), 3.15 (br s, 1H, $C_{cage}H$) ppm.

MS (low res. EI) M_w = 318.19 g mol^{-1}.

Envelope centred on *m/z* 317 (M^+).

Red plate crystals grown by solvent diffusion of diethyl ether and a DCM solution of **5** at -30 ^oC.

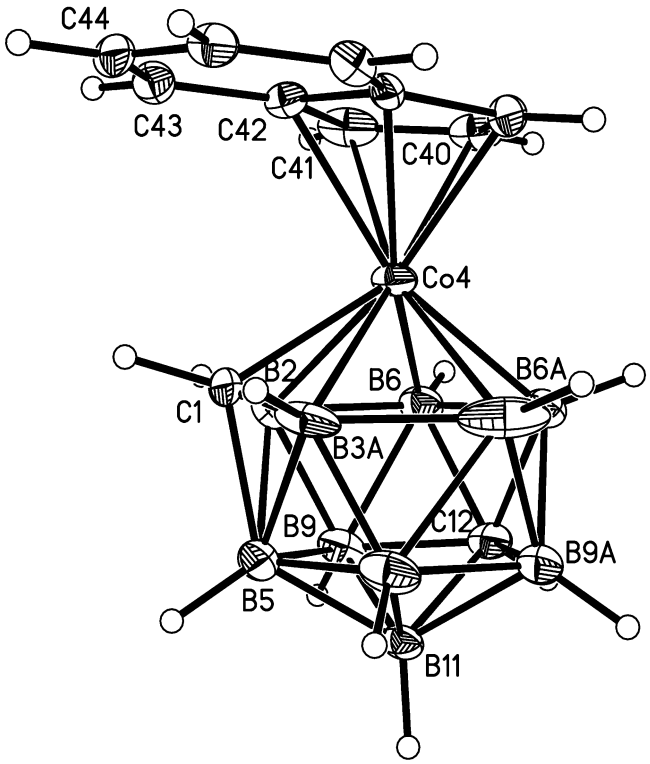

6.2.6 Synthesis of 1,12-Me_2-4-(η-C_9H_7)-4,1,12-*closo*-$CoC_2B_{10}H_{10}$ (6)

Compound **4** (0.075 g, 0.22 mmol) was stirred at reflux overnight in toluene (25 mL). Preparative TLC on silica (1:1 DCM:40-60 petroleum ether) yielded **6** as a dark brown band at R_f 0.86 (also recovered from the TLC plates was unchanged Me_2-4,1,8- isomer, R_f 0.74, 0.013 g, 17.3%).

Compound 6	**1,12-Me$_2$-4-(η-C$_9$H$_7$)-4,1,12-*closo*-CoC$_2$B$_{10}$H$_{10}$**
	Yield = 0.056 g, 74.7%.
CHN	Calculated for $C_{13}H_{23}B_{10}Co$: C 45.1, H 6.69. Found: C 44.9, H 6.76%.
NMR (CDCl$_3$)	$^{11}B\{^1H\}$ NMR: δ 10.2 (1B), 9.0 (1B), 8.2 (1B), 4.2 (1B), 1.9 (1B), -5.2 (1B), -5.8 (1B), -8.0 (1B), -14.4 (2B) ppm.
	^1H NMR: δ 7.55 (m, 4H, C_6H_4), 5.64 (m, 1H, C_5H_3), 5.55 (m, 1H, C_5H_3), 5.31 (app. t, 1H, C_5H_3), 2.38 (s, 3H, CH_3), 1.72 (s, 3H, CH_3) ppm.
MS (low res. EI)	M_w = 346.24 g mol^{-1}.
	Envelope centred on *m/z* 346 (M^+).

Red block crystals grown by solvent diffusion of diethyl ether and a DCM solution of **6** at -30 ^oC.

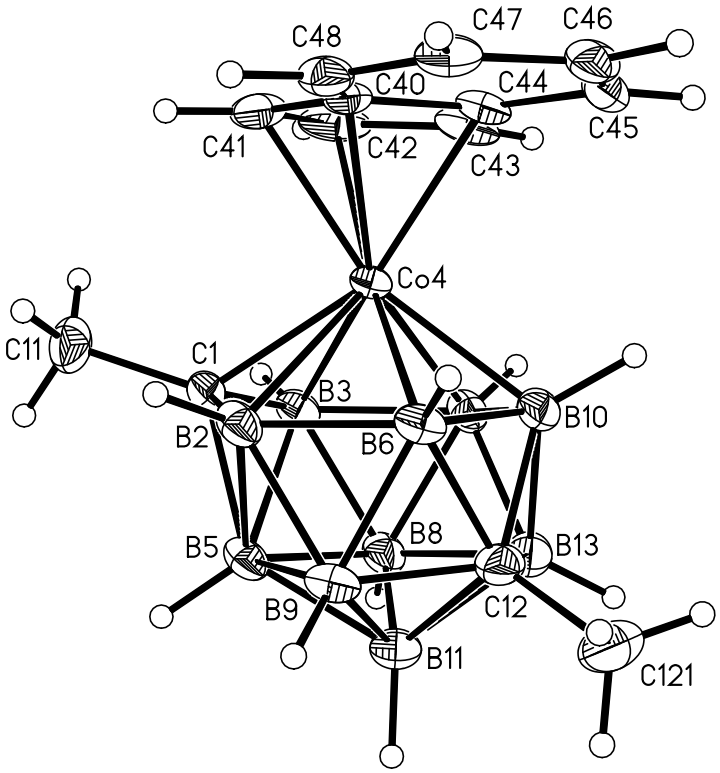

6.2.7 Synthesis of 4-(η-C_9H_7)-4,1,10-*closo*-$CoC_2B_{10}H_{12}$ (7)

Ammonia (30 mL) was condensed onto 1,12-*closo*-$C_2B_{10}H_{12}$ (1.000 g, 6.94 mmol) at -78 ^oC. Na metal (1.116 g, 48.70 mmol) was added and the resulting dark blue solution left stirring at -78 ^oC for 3 h. After warming to room temperature and evaporation of ammonia the resulting Na_2[7,10-*nido*-$C_2B_{10}H_{12}$] was dissolved in degassed THF (40 mL) giving a purple solution. This was then added via gas-tight syringe to a freshly prepared THF solution of Li[C_9H_7] (20.82 mmol). Following addition of $CoCl_2$ (3.330 g, 25.68 mmol) and stirring at room temperature overnight, aerial oxidation (0.5 h) afforded the final product. Purification as for compound **1** concluding with preparative TLC on silica (3:2 DCM:40-60 petroleum ether, R_f 0.60) yielded brown **7** as the major product. A small amount of the corresponding 4,1,12-isomer was also visible (R_f 0.84).

Compound 7 **4-(η-C_9H_7)-4,1,10-*closo*-$CoC_2B_{10}H_{12}$**

Yield = 1.050 g, 47.5%

CHN Calculated for $C_{11}H_{19}B_{10}Co$: C 41.5, H 6.02. Found: C 41.6, H 6.14%.

NMR (CD_2Cl_2) $^{11}B\{^1H\}$ NMR: δ 4.9 (2B), 3.9 (2B), -7.3 (1B), -9.8 (3B), -12.8 (2B) ppm.

^1H NMR: δ 7.70 (m, 2H, C_6H_4), 7.55 (m, 2H, C_6H_4), 5.80 (d, 2H, C_5H_3), 5.65 (t, 1H, C_5H_3), 5.05 (br s, 1H, $C_{cage}H$), 1.90 (br s, 1H, $C_{cage}H$) ppm.

MS (low res. EI) M_w = 318.19 g mol^{-1}.

Envelope centred on *m/z* 317 (M^+).

Red needle crystals grown by solvent diffusion of 40-60 petroleum ether and a DCM solution of **7** at -30 °C. Compound **7** co-crystallises with one molecule of DCM of solvation per asymmetric unit which is omitted from the structure below for clarity.

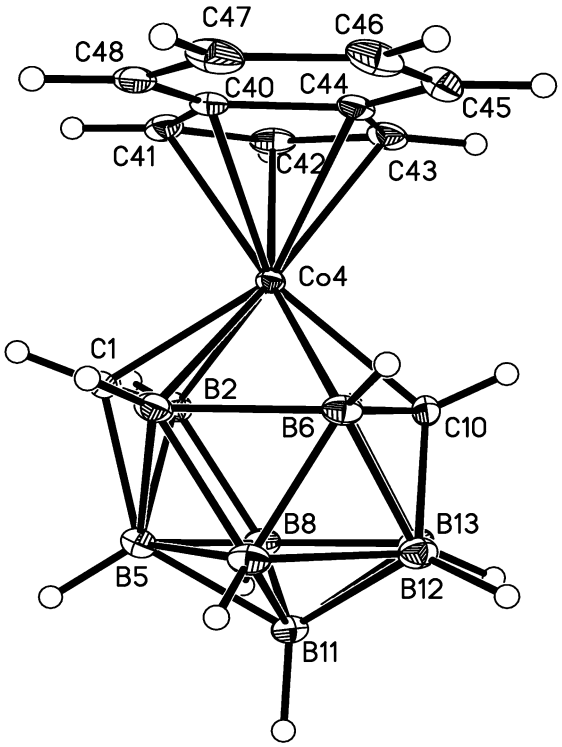

6.2.8 Synthesis of 1,14-(η-C_9H_7)$_2$-1,14,2,10-*closo*-$Co_2C_2B_{10}H_{12}$ (8)

Compound **5** (0.75 g, 2.36 mmol) in THF (30 mL) was treated with sodium (0.38 g, 16.5 mmol) and naphthalene (0.015 g) then transferred via gas-tight syringe to a solution of freshly prepared Li[C_9H_7] (7.08 mmol) in THF (10 mL) to which was added $CoCl_2$ (1.13 g, 8.73 mmol). Following reaction, oxidation and filtration through silica the brown filtrate was concentrated and purified by TLC (3:2 DCM:40-60 petroleum ether). A complex mixture of mobile bands were observed including that at R_f 0.84 (unchanged 4,1,12-isomer) and the dark blue target compound **8** at R_f 0.49.

Compound 8 **1,14-(η-C_9H_7)$_2$-1,14,2,10-*closo*-$Co_2C_2B_{10}H_{12}$**

Yield = 0.020 g, 2%.

NMR ($CDCl_3$) $^{11}B\{^1H\}$ NMR: δ -6.2 (2B), -11.7 (2B), -13.2 (2B), -14.7 (2B), -18.7 (2B) ppm.

^1H NMR: δ 7.32 (m, 4H, C_6H_4), 7.10 (m, 4H, C_6H_4), 5.25 (m, 4H, C_5H_3), 4.63 (app. t, 2H, C_5H_3), 0.94 (br. s, 2H, $C_{cage}H$) ppm.

MS (low res. EI) M_w = 492.27 g mol^{-1}.

Envelope centred on *m/z* 493 (M^+).

Red lozenge crystals grown by vapour diffusion of 40-60 petroleum ether and a DCM solution of **8** at -30 °C.

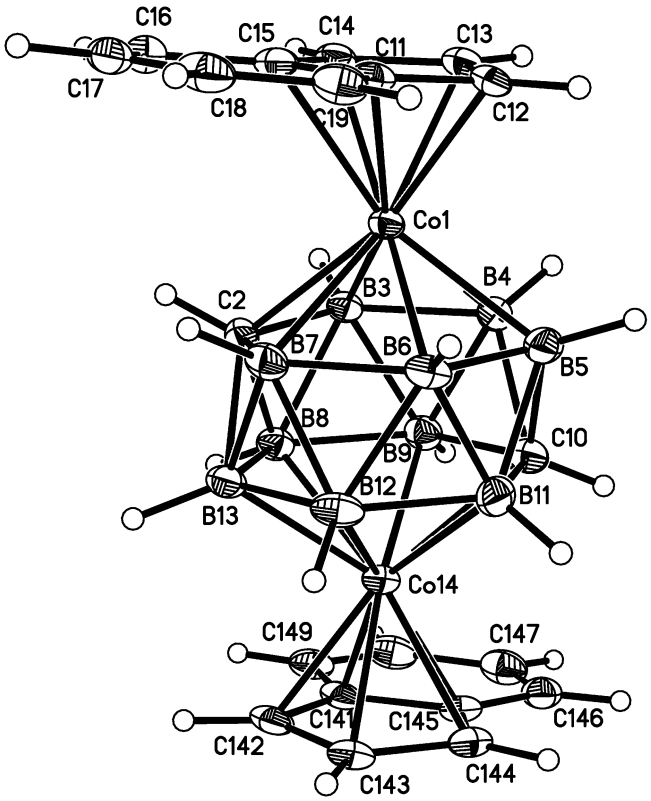

6.3.1 Synthesis of 3-(η-$C_{10}H_8$)-3,1,2-*closo*-$RuC_2B_9H_{11}$ (9)

[$HNEt_3$][7,8-*nido*-$C_2B_9H_{12}$] (0.400 g, 1.71 mmol) was suspended in degassed ether (35 mL). n-BuLi (1.40 mL, 3.50 mmol) was added, giving a pale yellow suspension which was stirred under N_2 for 1 h, then heated at reflux for 90 min. The resulting solution was filtered, and the ether removed *in vacuo* to give a yellow oily solid which was subsequently dissolved in degassed THF (35 mL). $[RuCl_2(COD)]_x$ (0.560 g, 2.00 mmol) and a large excess of naphthalene were added to the THF solution. The resulting brown mixture was heated at reflux for 90 min, then allowed to cool to room temperature. The brown mixture was filtered through a short silica column eluting with DCM to afford a brown solution, removal of solvent from which yielded a brown solid. This was further purified by column chromatography (1:2 DCM:40-60 petroleum ether) giving a yellow band, followed by preparative TLC (2:1 DCM:40-60 petroleum ether, R_f 0.82) yielding, as major product, **9** as a yellow solid on removal of solvent (0.065 g, 10.6%).

Compound 9 **3-(η-$C_{10}H_8$)-3,1,2-*closo*-$RuC_2B_9H_{11}$**

Yield = 0.065 g, 10.6%.

CHN Calculated for $C_{12}H_{19}B_9Ru$: C 39.9, H 5.30. Found: C 39.9, H 5.53%.

NMR ($CDCl_3$) $^{11}B\{^1H\}$ NMR: δ 2.0 (1B), 0.8 (1B), -7.3 (2B), -8.6 (2B), -19.5 (2B), -24.5 (1B) ppm.

^1H NMR: δ 7.55 (app. s, 4H, C_6H_4), 6.75 (dd, 2H, C_6H_4), 6.35 (dd, 2H, C_6H_4), 2.95 (br. s, 2H, $C_{cage}H$) ppm.

MS (low res. EI) M_w = 361.57 g mol^{-1}.

Envelope centred on *m/z* 361 (M^+).

Yellow block crystals grown by solvent diffusion of 40-60 petroleum ether and a DCM solution of **9** at -30 ºC.

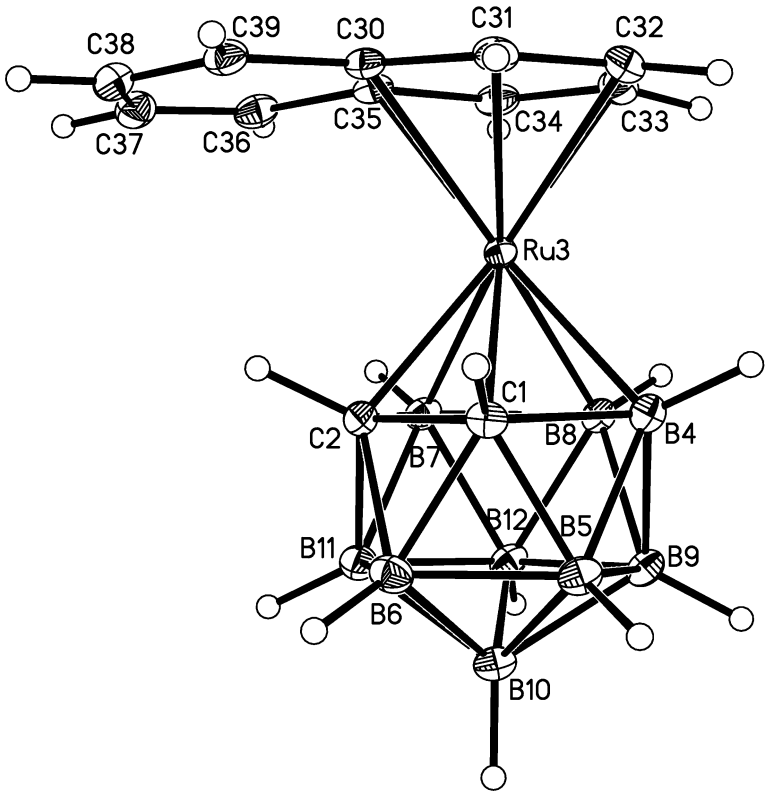

6.3.2 Synthesis of 3-(η-EtPh)-3,1,2-*closo*-$RuC_2B_9H_{11}$ (10)

To a three-necked round bottom flask was added $Tl[TlC_2B_9H_{11}]$ (0.405 g, 0.748 mmol), $[RuCl_2(COD)]_x$ (0.210 g, 0.749 mmol) and naphthalene (0.289 g, 2.26 mmol). To this was added DCM (35 mL) and the mixture was stirred at room temperature overnight. The brown mixture was then stirred at the reflux temperature for 2 h, cooled to room temperature, then the DCM removed on the line - giving a brown mixture. THF (50 mL) was added and the brown mixture stirred at the reflux temperature for 6 h, cooled to room temperature, then filtered. The brown mixture was filtered through a short silica column eluting with pure DCM to afford a brown solution. This was further purified by preparative TLC on silica (1:1 DCM:40-60 petroleum ether, R_f 0.62) to yield yellow **10** as the major product. Small amounts of **9** were also recovered.

Compound 10 **3-(η-EtPh)-3,1,2-*closo*-$RuC_2B_9H_{11}$**

Yield = 0.024 g, 9.51%.

CHN Calculated for $C_{10}H_{21}B_9Ru$: C 35.4 H 6.23. Found: C 36.6 H 5.87%.

NMR ($CDCl_3$) $^{11}B\{^1H\}$ NMR: δ 1.9 (1B), 1.0 (1B), -7.9 (2B), -8.8 (2B), -19.2 (2B), -24.0 (1B) ppm.

^1H NMR: δ 5.95 (m, 5H, C_6H_5), 3.85 (br s, 2H, $C_{cage}H$), 2.60 (q, 2H, CH_2), 1.25 (t, 3H, CH_3) ppm.

MS (low res. EI) M_w = 339.57 g mol^{-1}.

Envelope centred on *m/z* 339 (M^+).

Yellow plate crystals grown by solvent diffusion of 40-60 petroleum ether and a DCM solution of **10**/**9** at -30 °C, with **10** crystallising preferentially.

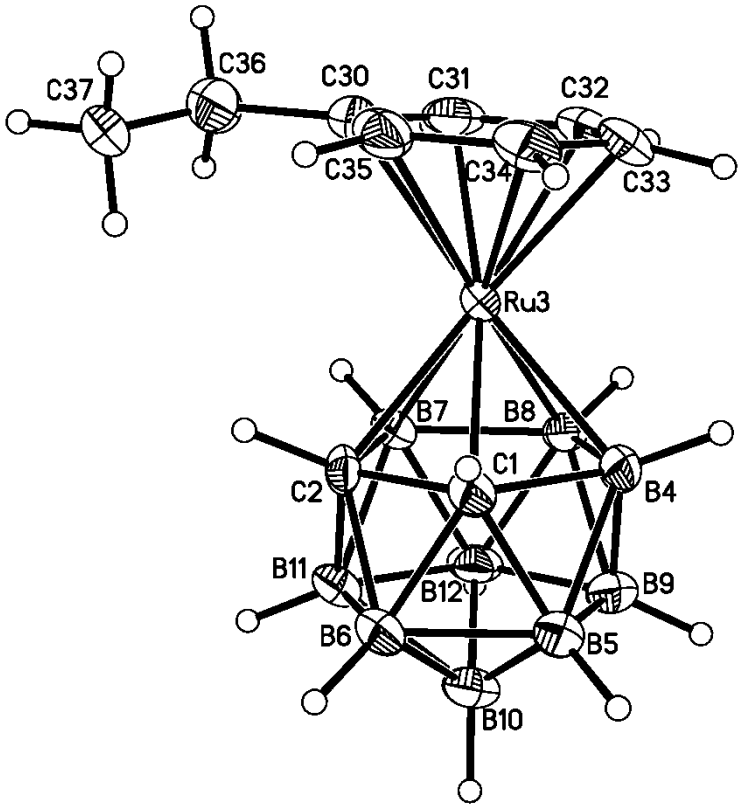

6.3.3 Synthesis of 4-(η-$C_{10}H_8$)-4,1,6-*closo*-$RuC_2B_{10}H_{12}$ (11)

1,2-*closo*-$C_2B_{10}H_{12}$ (0.400 g, 2.77 mmol) was dissolved in degassed THF (35 mL). Na metal (0.300 g, 13.04 mmol) and naphthalene (ca. 15 mg) were added and the solution stirred overnight. The resulting dark green solution was transferred via a gas-tight syringe into a second Schlenk tube containing $[RuCl_2(COD)]_x$ (0.650 g, 2.32 mmol) and a large excess of naphthalene. The resulting brown mixture was heated at reflux for 90 min then allowed to cool to room temperature. The brown mixture was filtered through a short silica column eluting with DCM to afford a brown solution, removal of solvent from which yielded a brown solid. This was further purified by column chromatography (1:2 DCM:40-60 petroleum ether), giving a yellow band, followed by preparative TLC (4:3 DCM:40-60 petroleum ether, R_f 0.55) yielding, as major product, **11** as a yellow solid on removal of solvent.

Compound 11 **4-(η-$C_{10}H_8$)-4,1,6-*closo*-$RuC_2B_{10}H_{12}$**

Yield = 0.093 g, 9.0%.

CHN Calculated for $C_{12}H_{20}B_{10}Ru$: C 38.6, H 5.40. Found: C 38.0, H 5.67%.

NMR ($CDCl_3$) $^{11}B\{^1H\}$ NMR: δ 9.1 (1B), -1.1 (1B), -3.8 (2B), -8.3 (1B), -9.5 (2B), -13.3 (2B), -23.4 (1B) ppm.

^1H NMR: δ 7.80 (dd, 2H, C_6H_4), 7.60 (dd, 2H, C_6H_4), 6.35 (dd, 2H, C_6H_4), 6.20 (dd, 2H, C_6H_4), 3.55 (br. s, 2H, $C_{cage}H$) ppm.

MS (low res. EI) M_w = 373.38 g mol^{-1}.

Envelope centred on *m/z* 374 (M^+).

Yellow plate crystals grown by solvent diffusion of 40-60 petroleum ether and a THF solution of **11** at -30 °C. Compound **11** co-crystallises with one molecule of partially disordered THF of solvation per asymmetric unit which is omitted from the structure below for clarity.

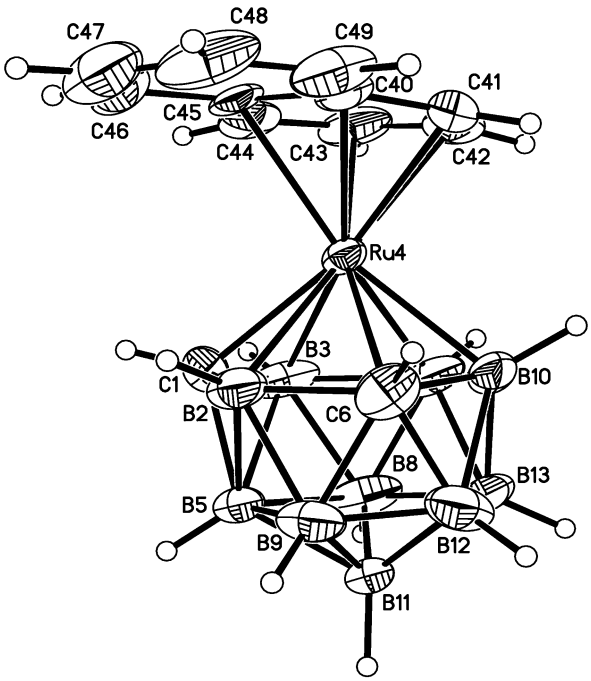

6.3.4 Synthesis of 4-(η-$C_{10}H_8$)-4,1,8-*closo*-$RuC_2B_{10}H_{12}$ (12)

Compound **11** (0.060 g, 0.16 mmol) was stirred at reflux overnight in toluene (25 mL). Removal of solvent from the resulting yellow solution yielded a yellow solid. Preparative TLC (1:1 DCM:40-60 petroleum ether) separated **12** as a yellow product at R_f 0.58 from unchanged **11** (R_f 0.38).

Compound 12 **4-(η-$C_{10}H_8$)-4,1,8-*closo*-$RuC_2B_{10}H_{12}$**

Yield = 0.02 g, 33.3%.

CHN Calculated for $C_{12}H_{20}B_{10}Ru$: C 38.6, H 5.40. Found: C 38.4, H 5.55%.

NMR ($CDCl_3$) $^{11}B\{^1H\}$ NMR: δ 15.7 (1B), 3.4 (1B), 1.8 (1B), -2.0 (1B), -6.3 (1B), -7.7 (1B), -10.0 (1B), -10.2 (1B), -13.4 (1B), -19.4 (1B) ppm.

^1H NMR: δ 7.72-7.70 (m, 2H, C_6H_4), 7.65-7.55 (m, 2H, C_6H_4), 6.57 (d, 1H, C_6H_4), 6.56 (d, 1H, C_6H_4), 6.15 (app. t, 1H, C_6H_4), 6.08 (app. t, 1H, C_6H_4), 3.18 (br. s, 1H, $C_{cage}H$), 2.10 (br. s, 1H, $C_{cage}H$) ppm.

MS (low res. EI) M_w = 373.38 g mol^{-1}.

Envelope centred on *m/z* 374 (M^+).

Yellow needle crystals grown by solvent diffusion of 40-60 petroleum ether and a DCM solution of **12** at -30 ºC.

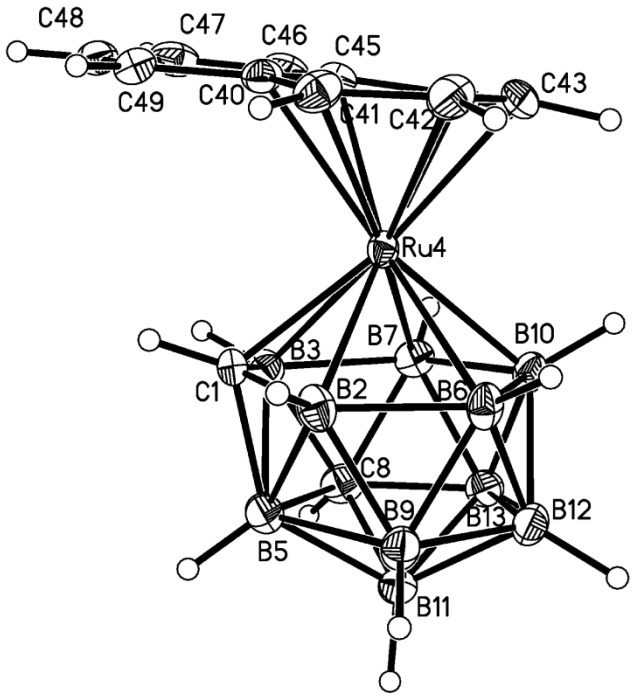

6.3.5 Synthesis of 4-(η-$C_{10}H_8$)-4,1,10-*closo*-$RuC_2B_{10}H_{12}$ (13)

Ammonia (50 mL) was condensed onto 1,12-*closo*-$C_2B_{10}H_{12}$ (0.400 g, 2.78 mmol) at -78 ^oC. Na metal (0.450 g, 19.56 mmol) was added and the resulting dark blue solution left stirring at -78 ^oC for 3 h. After warming to room temperature and evaporation of ammonia the resulting Na_2[7,10-*nido*-$C_2B_{10}H_{12}$] was dissolved in degassed THF (45 mL) giving a purple solution. Excess Na was removed from the reduced carborane solution to give a colourless solution which was then transferred via gas-tight syringe into a Schlenk tube containing $[RuCl_2(COD)]_x$ (0.780 g, 2.78 mmol) and a large excess of naphthalene. The resulting brown mixture was heated at reflux for 90 min then allowed to cool to room temperature. The brown mixture was filtered through a short silica column eluting with DCM to afford a brown solution, removal of solvent from which yielded a brown solid. This was further purified by column chromatography (1:2 DCM:40-60 petroleum ether), giving a yellow band, followed by preparative TLC (2:1 DCM:40-60 petroleum ether), yielding **13** (R_f 0.38) as a yellow solid on removal of solvent.

Compound 13 **4-(η-$C_{10}H_8$)-4,1,10-*closo*-$RuC_2B_{10}H_{12}$**

Yield = 0.03 g, 3%.

CHN Calculated for $C_{12}H_{20}B_{10}Ru$: C 38.6, H 5.40. Found: C 39.5, H 4.87%.

NMR ($CDCl_3$) $^{11}B\{^1H\}$ NMR: δ -0.1 (2B), -4.1 (2B), -9.1 (2B), -14.7 (2B), -16.4 (2B) ppm.

^1H NMR: δ 7.65 (dd, 2H, C_6H_4), 7.45 (dd, 2H, C_6H_4), 6.40 (dd, 2H, C_6H_4), 6.10 (dd, 2H, C_6H_4), 4.05 (br. s, 1H, $C_{cage}H$), 1.30 (br. s, 1H, $C_{cage}H$) ppm.

MS (low res. EI) M_w = 373.38 g mol^{-1}.

Envelope centred on *m/z* 374 (M^+).

Yellow plate crystals grown by solvent diffusion of 40-60 petroleum ether and a DCM solution of **13** at -30 °C.

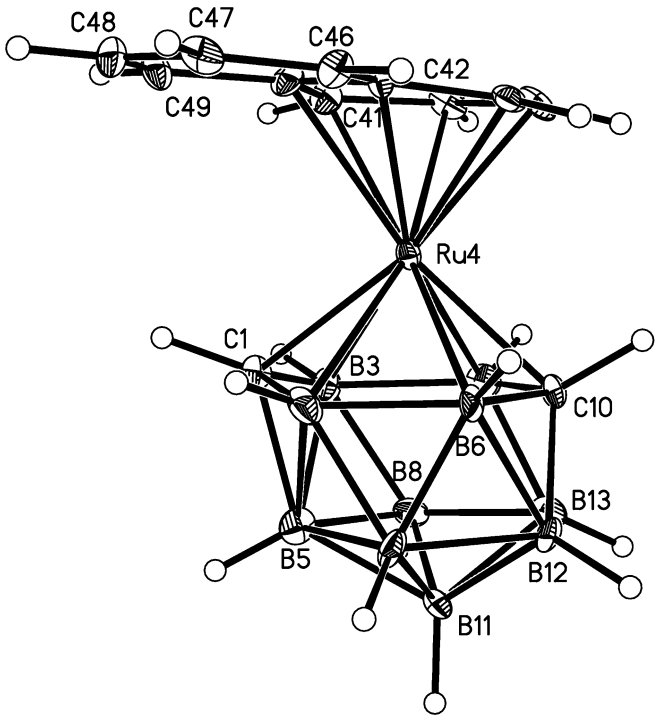

6.3.6 Synthesis of 4-(η-$C_{10}H_8$)-4,1,12-*closo*-$RuC_2B_{10}H_{12}$ (14)

Compound **13** (0.025 g, 0.67 mmol) was stirred at reflux overnight in toluene (25 mL). Removal of solvent from the resulting yellow solution yielded a yellow solid. Preparative TLC (1:1 DCM:40-60 petroleum ether) yielded **14** as a yellow product at R_f 0.53.

Compound 14 **4-(η-$C_{10}H_8$)-4,1,12-*closo*-$RuC_2B_{10}H_{12}$**

Yield = 0.02 g, 80%.

CHN Calculated for $C_{12}H_{20}B_{10}Ru$: C 38.6, H 5.40. Found: C 37.6, H 4.86%.

NMR ($CDCl_3$) $^{11}B\{^1H\}$ NMR: δ 3.4 (1B), 0.0 (2B), -3.2 (1B), -9.3 (1B), -10.2 (1B), -14.1 (2B), -22.7 (2B) ppm.

^1H NMR: δ 7.70-7.60 (m, 2H, C_6H_4), 7.60-7.50 (m, 2H, C_6H_4), 6.48 (d, 1H, C_6H_4), 6.50 (d, 1H, C_6H_4), 6.10 (app. t, 1H, C_6H_4), 5.95 (app. t, 1H, C_6H_4), 3.20 (br. s, 1H, $C_{cage}H$), 3.00 (br. s, 1H, $C_{cage}H$) ppm.

MS (low res. EI) M_w = 373.38 g mol^{-1}.

Envelope centred on *m/z* 374 (M^+).

Yellow needle crystals grown by solvent diffusion of 40-60 petroleum ether and a DCM solution of **14** at -30 °C.

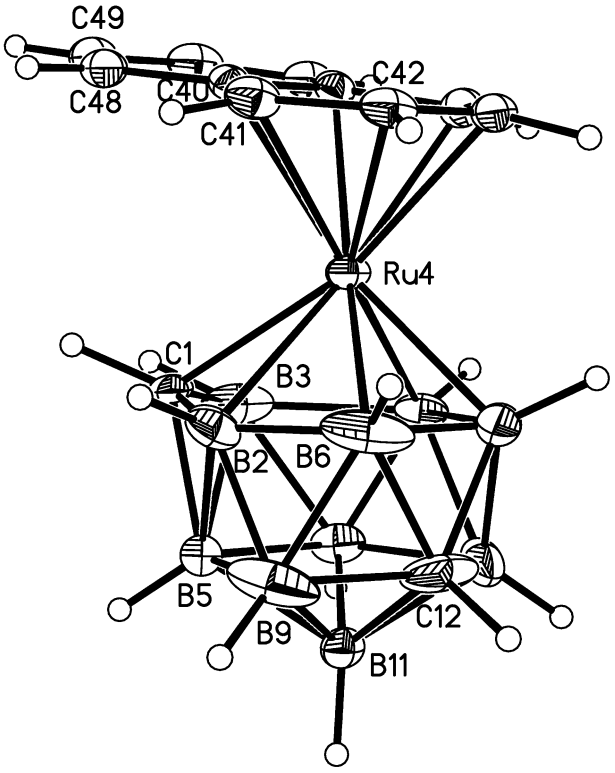

6.3.7 Synthesis of 4-(η-C_8H_{10})-4,1,6-*closo*-$RuC_2B_{10}H_{12}$ (15)

1,2-*closo*-$C_2B_{10}H_{12}$ (0.300 g, 2.083 mmol) was dissolved in degassed THF (25 mL). Na metal (0.200 g, 8.696 mmol) and naphthalene (ca. 15 mg) were added and the solution stirred overnight. The resulting dark green solution was transferred via a gas-tight syringe into a second Schlenk tube containing $[RuCl_2(COD)]_x$ (0.292 g, 1.042 mmol). The resulting brown mixture was stirred overnight at room temperature. THF was removed *in vacuo,* then ethanol (30 ml) added, followed by an ethanol solution (10 mL) of [BTMA]Cl (0.400 g, 2.154 mmol) to give a brown precipitate. The precipitate and the ethanol solution were recombined and the ethanol removed by rotary evaporation, leaving a brown solid. THF (50 mL) was added to the brown solid and the mixture was filtered through a short silica column eluting with DCM to afford a brown solution, removal of solvent from which yielded a brown solid. This was further purified by preparative TLC (1:1 DCM:40-60 petroleum ether) yielding, as major product, **15** (R_f 0.75) as a yellow solid on removal of solvent.

Compound 15 **4-(η-C_8H_{10})-4,1,6-*closo*-$RuC_2B_{10}H_{12}$**

Yield = 0.015 g, 4.10%.

CHN Calculated for $C_{10}H_{22}B_{10}Ru$: C 34.2, H 6.31. Found: C 34.3, H 6.53%.

NMR ($CDCl_3$) $^{11}B\{^1H\}$ NMR: δ 9.4 (1B), 0.7 (1B), -2.9 (2B), -7.6 (2B), -9.3 (1B), -13.2 (2B), -21.7 (1B) ppm.

^1H NMR: δ 6.25 (m, 2H, C_8H_{12} (C*H*)), 5.70 (m, 2H, C_8H_{12} (C*H*)), 5.60 (m, 2H, C_8H_{12} (C*H*)), 4.20 (br s, 2H, $C_{cage}H$), 2.25 (br m, 2H, C_8H_{12} (CH_2)), 1.33 (app. br s, 2H, C_8H_{12} (CH_2)) ppm.

MS (low res. EI) M_w = 351.37 g mol^{-1}.

Envelope centred on *m/z* 346.

Yellow needle crystals grown by solvent diffusion of 40-60 petroleum ether and a THF solution of **15** at -30 ºC.

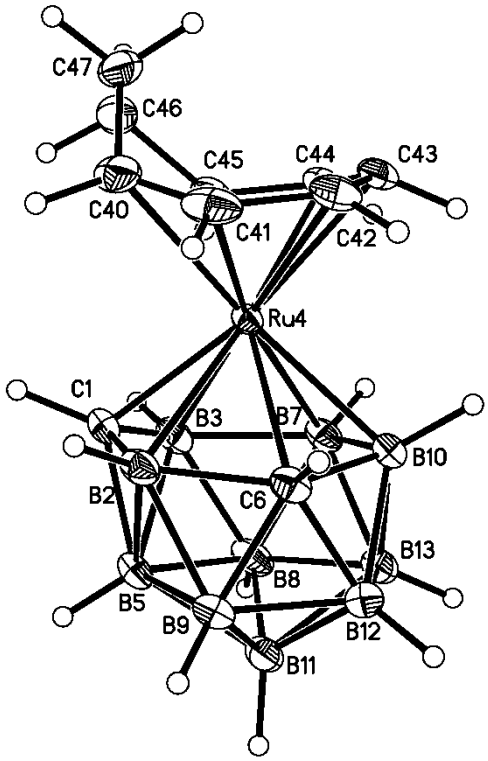

6.3.8 Synthesis of 4-(η-$C_{10}H_{12}$)-4,1,6-*closo*-$FeC_2B_{10}H_{12}$ (16)

1,2-*closo*-$C_2B_{10}H_{12}$ (0.400 g, 2.77 mmol) was dissolved in degassed THF (35 mL). Na metal (0.250 g, 10.87 mmol) and naphthalene (ca. 15 mg) were added and the solution stirred overnight. The resulting dark green solution was transferred via a gas-tight syringe into a second Schlenk tube, then $Li_2[C_{10}H_8]$ in THF (formed by adding Li metal (0.500 g, 71.43 mmol) and naphthalene (1.00 g, 7.8 mmol) in THF (50 mL) and stirring for 1 h to give a purple solution) added at -196 ^oC. $FeCl_2$ (0.650 g, 5.12 mmol) added to frozen solutions, then mixture warmed to 0 ^oC and stirred at this temperature for 1 h, then warmed to RT and stirred overnight at this temperature. The brown mixture was filtered through a short silica column eluting with DCM to afford a brown solution, removal of solvent from which yielded a brown solid. This was further purified by preparative TLC (3:2 DCM:40-60 petroleum ether, R_f 0.41) yielding, as major product, **16** as a pink solid on removal of solvent.

Compound 16 **4-(η-$C_{10}H_{12}$)-4,1,6-*closo*-$FeC_2B_{10}H_{12}$**

Yield = 0.020 g, 2.17%.

NMR ($CDCl_3$) $^{11}B\{^1H\}$ NMR: δ 11.2 (2B), -2.2 (2B), -6.2 (2B), -9.2 (1B), -13.3 (2B), -20.5 (1B) ppm.

^1H NMR: δ 5.90 (m, 2H, C_6H_4), 5.70 (m, 2H, C_6H_4), 2.95 (m, 2H, C_4H_8), 2.50 (m, 2H, C_4H_8), 2.25 (br s, 2H, $C_{cage}H$), 2.10 (m, 2H, C_4H_8), 1.75 (m, 2H C_4H_8) ppm.

MS (low res. EI) M_w = 332.16 g mol^{-1}.

Envelope centred on *m/z* 332 (M^+).

Purple needle crystals grown by solvent diffusion of 40-60 petroleum ether and a DCM solution of **16** at -30 °C. Compound **16** co-crystallises with one molecule of DCM of solvation per asymmetric unit which is omitted from the structure below for clarity.

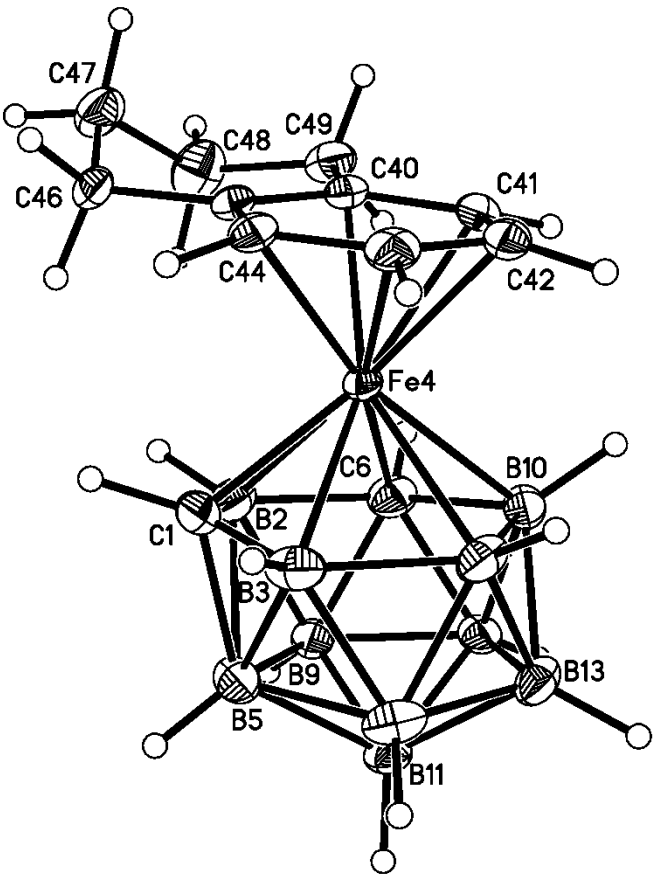

6.4.1 Resynthesis and recrystallisation of compounds 3,3-$(PPh_3)_2$-3-H-3,1,2-*closo*-$RhC_2B_9H_{11}$ (V), 3-(κ^2-NO_3)-3-(PPh_3)-3,1,2-*closo*-$RhC_2B_9H_{11}$ (VI) and 3,3-$(PPh_3)_2$-3-(κ^1- NO_3)-3,1,2-*closo*-$RhC_2B_9H_{11}$ (VII)

Compounds **V**, **VI** and **VII** were synthesised according to the literature methods[22,23] and then recrystallised.

Compound V - 3,3-(PPh$_3$)$_2$-3-H-3,1,2-*closo*-RhC$_2$B$_9$H$_{11}$

Orange block crystals grown by solvent diffusion of 40-60 petroleum ether and a DCM solution of **V** at -30 ^{o}C. Compound **V** co-crystallises with one molecule of DCM of solvation per asymmetric unit which is omitted from the structure below for clarity.

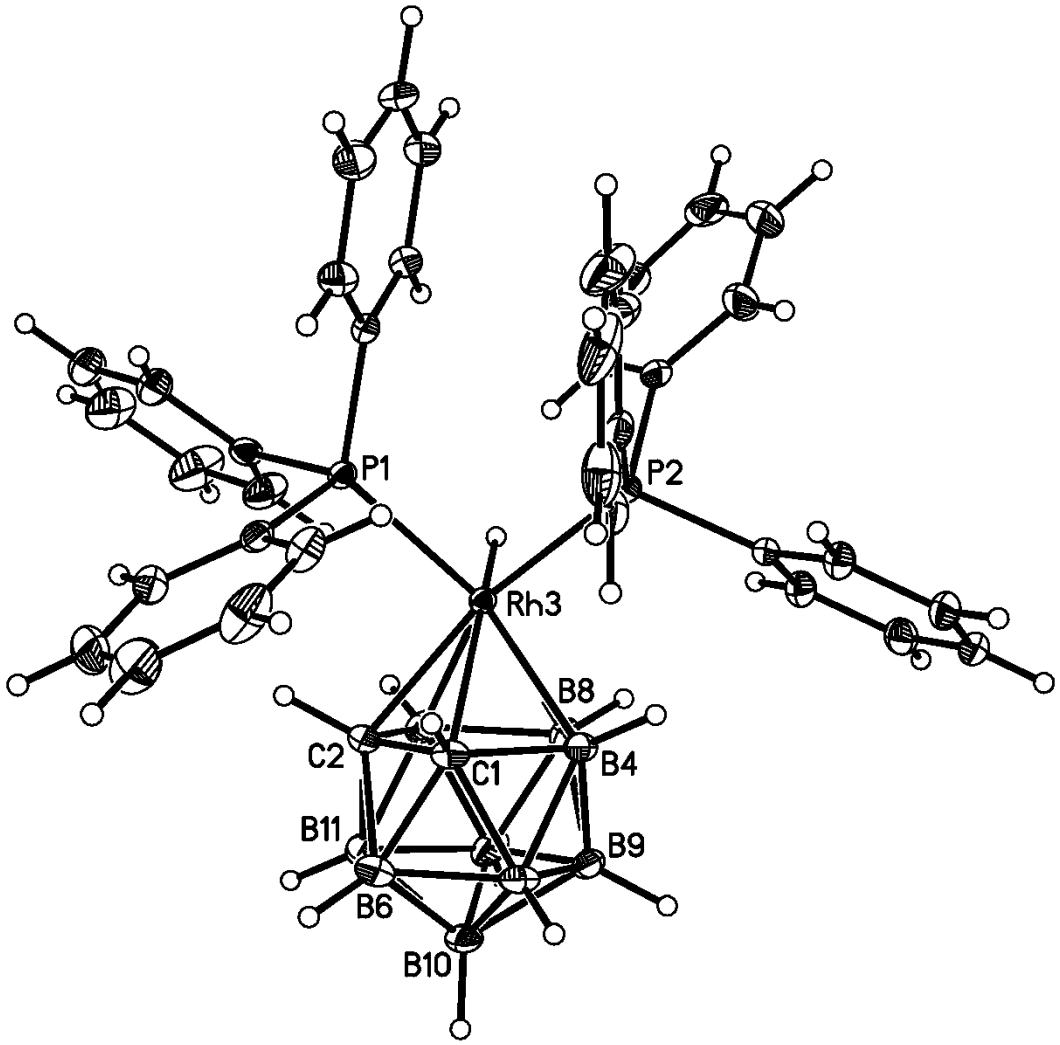

Compound VI - 3-(κ^2-NO_3)-3-(PPh_3)-3,1,2-*closo*-$RhC_2B_9H_{11}$

Red plate crystals grown by solvent diffusion of 40-60 petroleum ether and a DCM solution of **VI** at -30 ^oC. Compound **VI** co-crystallises with one molecule of DCM and half a molecule of partially disordered DCM of solvation per asymmetric unit which are omitted from the structure below for clarity. There are two crystallographically independent molecules in the asymmetric unit.

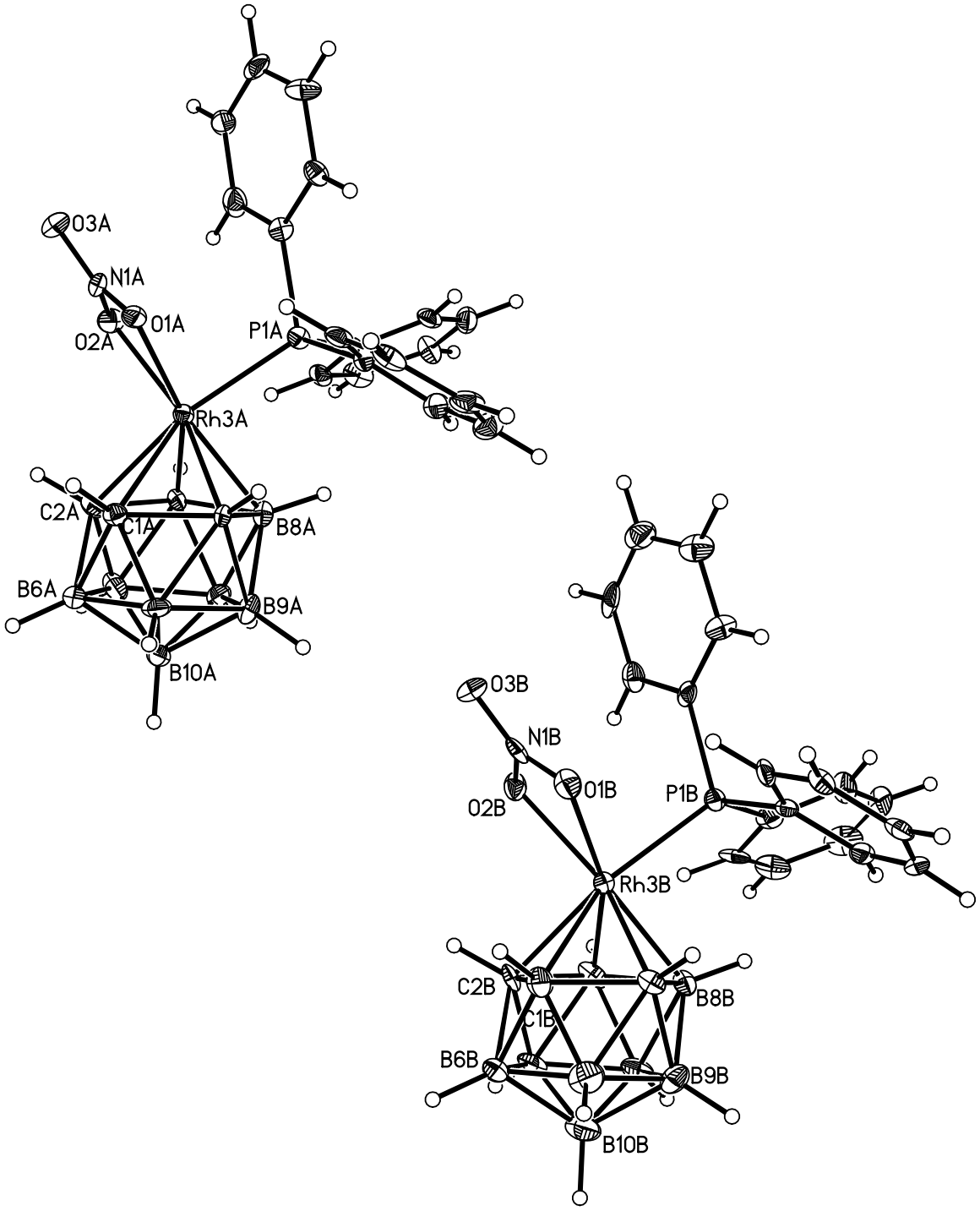

Compound VII - 3,3-$(PPh_3)_2$-3-(κ^1-NO_3)-*closo*-3,1,2-$RhC_2B_9H_{11}$

Orange plate crystals grown by solvent diffusion of 40-60 petroleum ether and a DCM solution of **VII** at -30 ^oC. Compound **VII** co-crystallises with one molecule of partially disordered DCM of solvation per asymmetric unit which is omitted from the structure below for clarity.

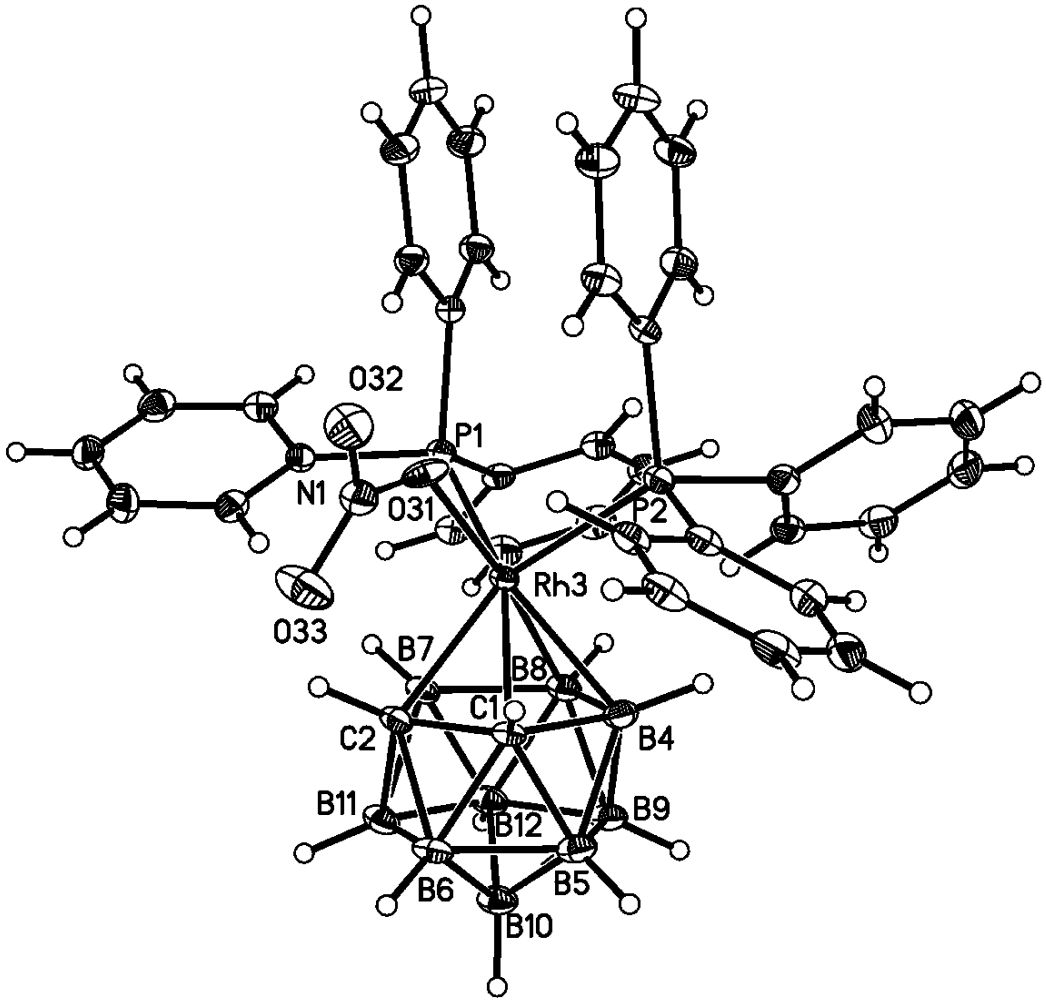

6.5.1 Synthesis of 7-(THF)-3-(η-C_5Me_5)-3,1,2-*closo*-$RuC_2B_9H_{10}$ (17)

$Tl[TlC_2B_9H_{11}]$ (0.162 g, 0.299 mmol) and $[RuClCp^*]_4$ (0.164 g, 0.151 mmol) were placed in a Schlenk tube and the mixture evacuated for 1 h then covered with a blanket of N_2. THF (15 ml) was added via a gas-tight syringe and the resulting brown mixture stirred at room temperature for 72 h. The resulting grey/brown mixture was filtered through a short Al_2O_3 column to afford a yellow solution, removal of solvent from which yielded a brown solid. This was further purified by preparative TLC (3:2 DCM:40-60 petroleum ether) which, on removal of solvent, yielded yellow **17** as the major product (R_f 0.40), and red 4,5-$(C_5Me_5)_2$-4,5,2,3-*closo*-$Ru_2C_2B_9H_{11}$ as the minor product (R_f 0.67).

Compound 17 **7-(THF)-3-(η-C_5Me_5)-3,1,2-*closo*-$RuC_2B_9H_{10}$**

Yield = 0.02 g, 17.0%.

NMR ($CDCl_3$) $^{11}B\{^1H\}$ NMR: δ 19.7 (1B, B-THF), -12.6 (2B), -13.8 (1B), -16.9 (2B), -26.0 (2B), -32.8 (1B) ppm.

^1H NMR: δ 4.10-4.20 (m, 4H, OC_4H_8), 2.50 (br s, 2H, $C_{cage}H$), 2.05-2.12 (m, 4H, OC_4H_8), 1.80 (s, 15H, C_5Me_5) ppm.

MS (low res. EI) M_w = 439.71 g mol^{-1}.

Envelope centred on *m/z* 438 (M^+).

Yellow block crystals grown by solvent diffusion of 40-60 petroleum ether and a DCM solution of **17** at -30 ^oC. There are two crystallographically independent molecules in the asymmetric unit.

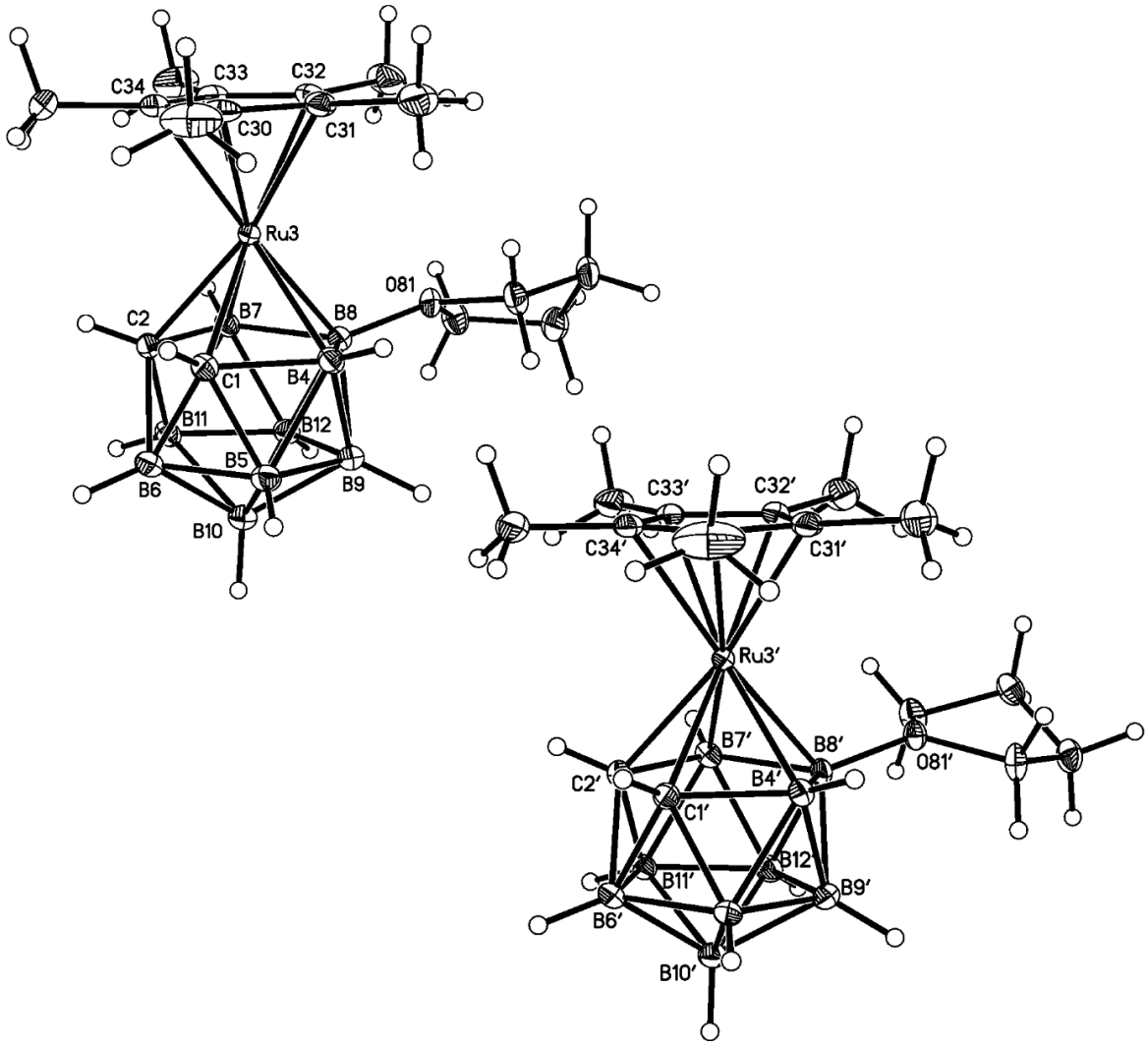

6.5.2 Synthesis of thirteen and fourteen vertex bimetallacarboranes (18-22) and an exo-polyhedral metal bound carborane (23)

Reaction One

1,2-*closo*-$C_2B_{10}H_{12}$ (0.200 g, 1.39 mmol) was dissolved in degassed THF (20 mL). Na metal (0.19 g, 8.26 mmol) was added and the solution stirred overnight. The resulting colourless solution was transferred via a gas-tight syringe into a second Schlenk tube containing a frozen mixture of $[RuClCp^*]_4$ (0.756 g, 0.695 mmol) in THF (20 mL) at -196 ^oC. The solution of reduced carborane was allowed to freeze, then the mixture was warmed to room temperature and stirred for 48 h. The resulting brown mixture was filtered through a short silica column eluting with DCM to afford a brown solution, removal of solvent from which yielded a brown solid. This was further purified by column chromatography (1:2 DCM:40-60 petroleum ether), followed by preparative TLC on silica (2:3 DCM:40-60 petroleum ether), yielding nine mobile bands. These bands were, in order of elution: unidentified yellow band (R_f 0.75); green **21** (R_f 0.69), yellow band (from which **19** crystallises) (R_f 0.60, trace amounts); unidentified purple band (R_f 0.56); purple **22** (R_f 0.40); orange **18** (R_f 0.35); pink 4,5-Cp^*_2-4,5,2,3-*closo*-$Ru_2C_2B_9H_{11}$ (R_f 0.29, trace amounts); pink **23** (R_f 0.24); yellow **20** (R_f 0.22).

Compound 18 **4,5-(η-C_5Me_5)$_2$-4,5,1,6-*closo*-$Ru_2C_2B_9H_{11}$**

Yield = 0.051 g, 6.1%.

CHN Calculated for $C_{22}H_{41}B_9Ru_2$: C 43.7, H 6.83. Found: C 42.9, H 6.80%.

NMR ($CDCl_3$) $^{11}B\{^1H\}$ NMR: δ 31.1 (1B), 28.2 (2B), 23.0 (1B), 16.8 (1B), 0.6 (2B), -8.0 (1B), -14.2 (1B) ppm.

^1H NMR: δ 16.62 (br s, 1H, $C_{cage}H$), 2.90 (br s, 1H, $C_{cage}H$), 1.55 (s, 15H, C_5Me_5), 1.50 (s, 15H, C_5Me_5) ppm.

MS (low res. EI) M_w = 604.94 g mol^{-1}.

Envelope centred on *m/z* 604 (M^+).

Brown needle crystals grown by solvent diffusion of 40-60 petroleum ether and a DCM solution of **18** at -30 °C.

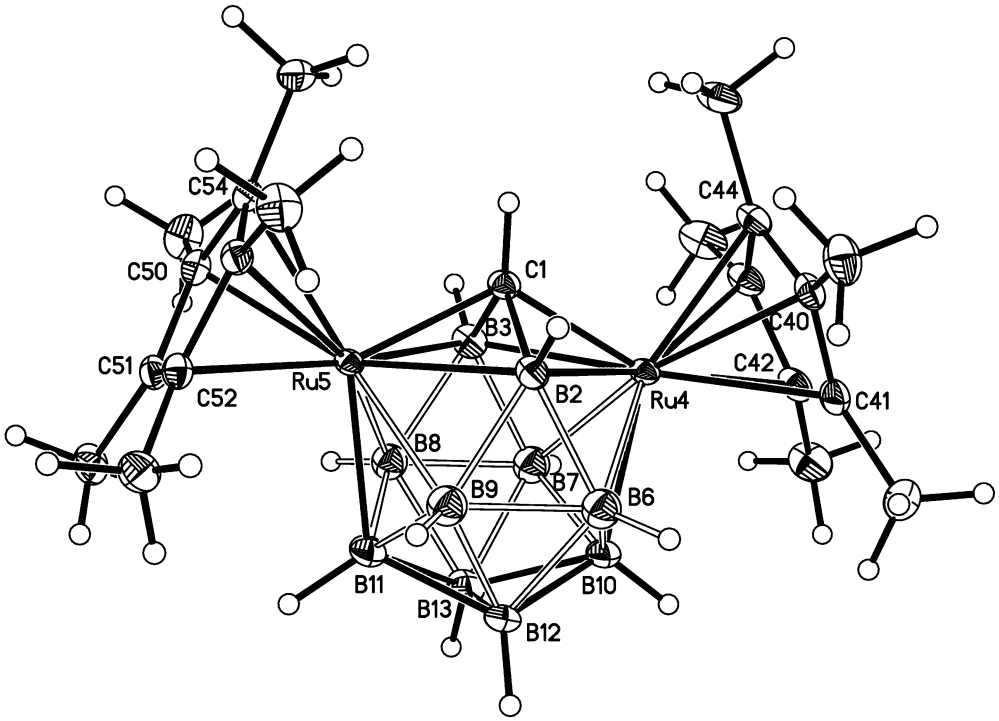

Compound 19 **4,5-(η-C_5Me_5)$_2$-4,5,2,11-*closo*-$Ru_2C_2B_9H_{11}$**

NMR ($CDCl_3$) $^{11}B\{^1H\}$ NMR: δ 116.0 (1B), 35.1 (1B), 14.2 (1B), 11.8 (1B), 10.5 (1B), 7.4 (1B), 6.4 (1B), -9.0 (1B), -19.1 (1B) ppm.

^1H NMR: δ 5.20 (br s, 1H, $C_{cage}H$), 1.60 (s, 15H, C_5Me_5), 1.48 (s, 15H, C_5Me_5) ppm (second $C_{cage}H$ signal not found).

MS (low res. EI) M_w = 604.94 g mol^{-1}.

Envelope centred on *m/z* 604 (M^+).

Red needle crystals grown by solvent diffusion of 40-60 petroleum ether and a THF solution of **19** at -30 ºC.

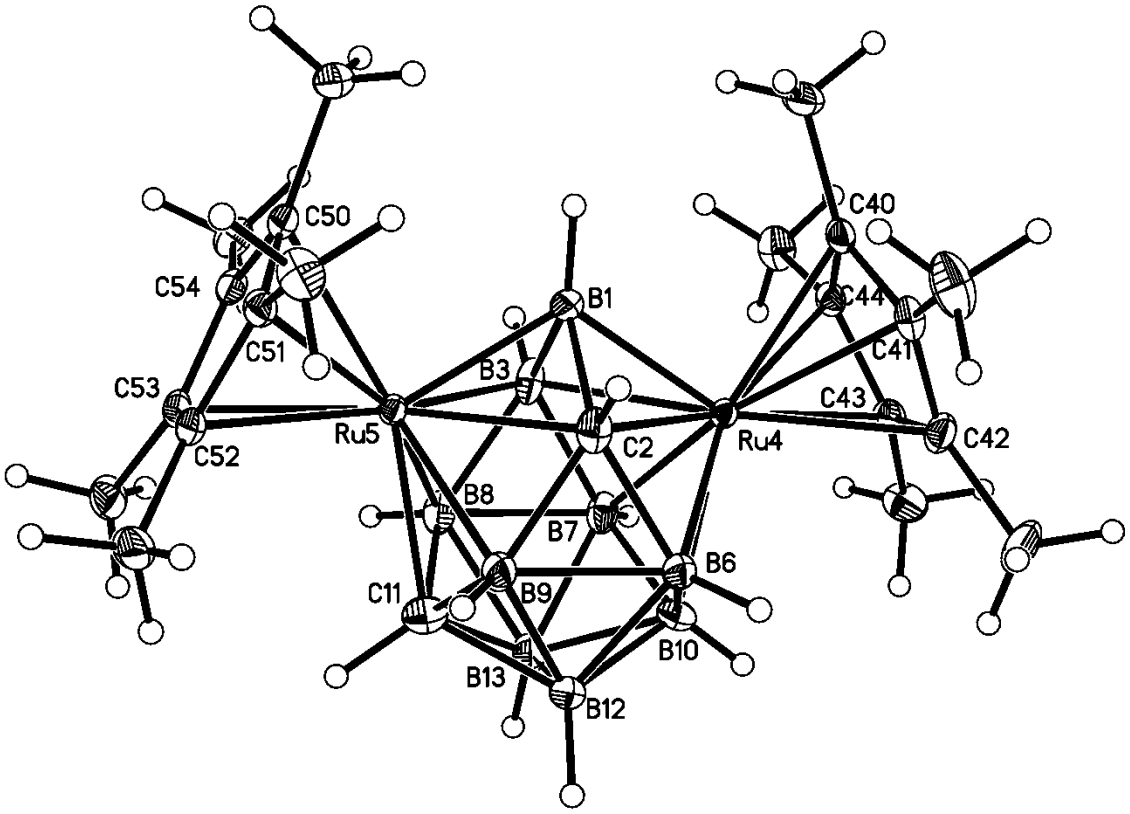

Compound 20 **8-(*n*-BuO)-4,5-(η-C_5Me_5)$_2$-4,5,1,6-*closo*-$Ru_2C_2B_9H_{10}$**

Yield = 0.017 g, 1.8%.

CHN Calculated for $C_{26}H_{48}B_9Ru_2O$: C 46.2, H 7.16. Found: C 46.7, H 7.39%.

NMR ($CDCl_3$) $^{11}B\{^1H\}$ NMR: δ 43.5 (1B, B-*n*-BuO), 29.7 (1B), 22.1 (1B), 19.4 (1B), 15.6 (2B), 1.2 (1B), -10.2 (1B), -17.5 (1B) ppm.

^1H NMR: δ 3.30-3.50 (m, 2H, OC_4H_9 (OCH_2)), 2.70 (br s, 1H, $C_{cage}H$), 1.60-1.70 (m, 4H, OC_4H_9 (2 x CH_2)), 1.55 (s, 15H, C_5Me_5), 1.50 (s, 15H, C_5Me_5), 0.75 (t, 3H, OC_4H_9) ppm (second $C_{cage}H$ signal not found).

MS (low res. EI) M_w = 677.04 g mol^{-1}.

Envelope centred on *m/z* 676 (M^+).

Brown plate crystals grown by vapour diffusion of 40-60 petroleum ether and a THF solution of **20** at -30 °C.

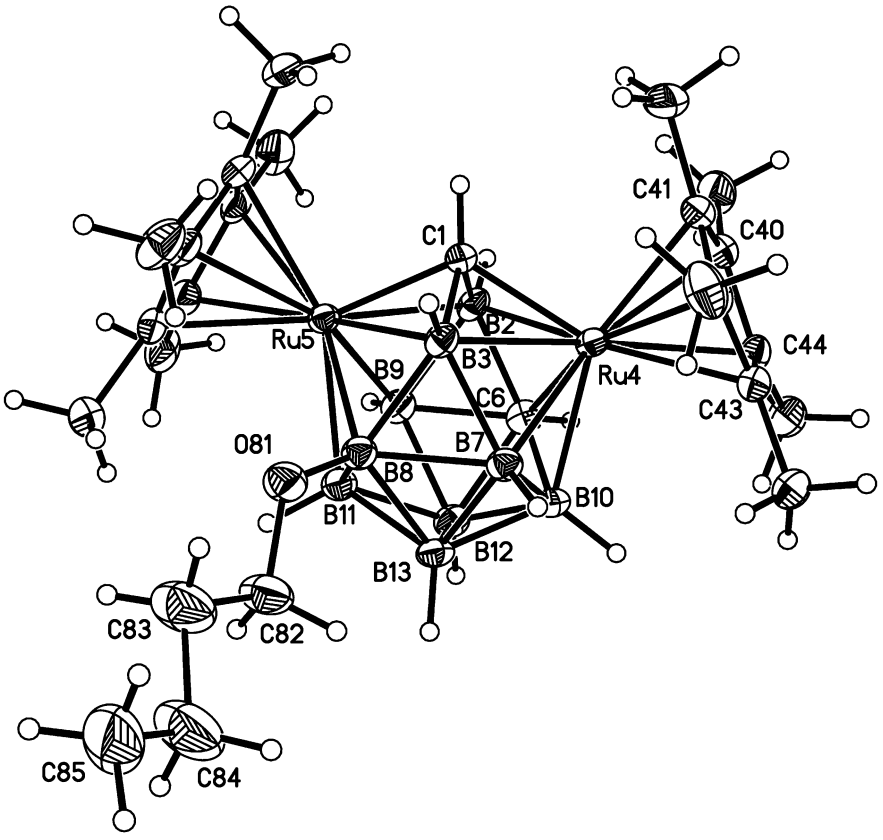

Compound 21 **3,6-(η-C_5Me_5)$_2$-3,6,?,?-*closo*-$Ru_2C_2B_{10}H_{12}$***

Yield = 0.018 g, 2.0%.

NMR ($CDCl_3$) $^{11}B\{^1H\}$ NMR: δ 58.2 (1B), 53.8 (1B), 36.1 (1B), 29.5 (1B), 28.3 (1B), 19.0 (1B), 12.0 (1B) 3.4 (1B), -7.8 (1B), -22.9 (1B) ppm.

^1H NMR: δ 10.40 (br s, 1H, $C_{cage}H$), 3.85 (br s, 1H, $C_{cage}H$), 1.65 (s, 15H, C_5Me_5), 1.55 (s, 15H, C_5Me_5) ppm.

MS (low res. EI) M_w = 616.76 g mol^{-1}.

Envelope centred on *m/z* 618 (M^+).

*Neither of the cage carbon atoms could be located during crystallographic refinement.

Green plate crystals grown by vapour diffusion of 40-60 petroleum ether and a THF solution of **21** at -30 ºC.

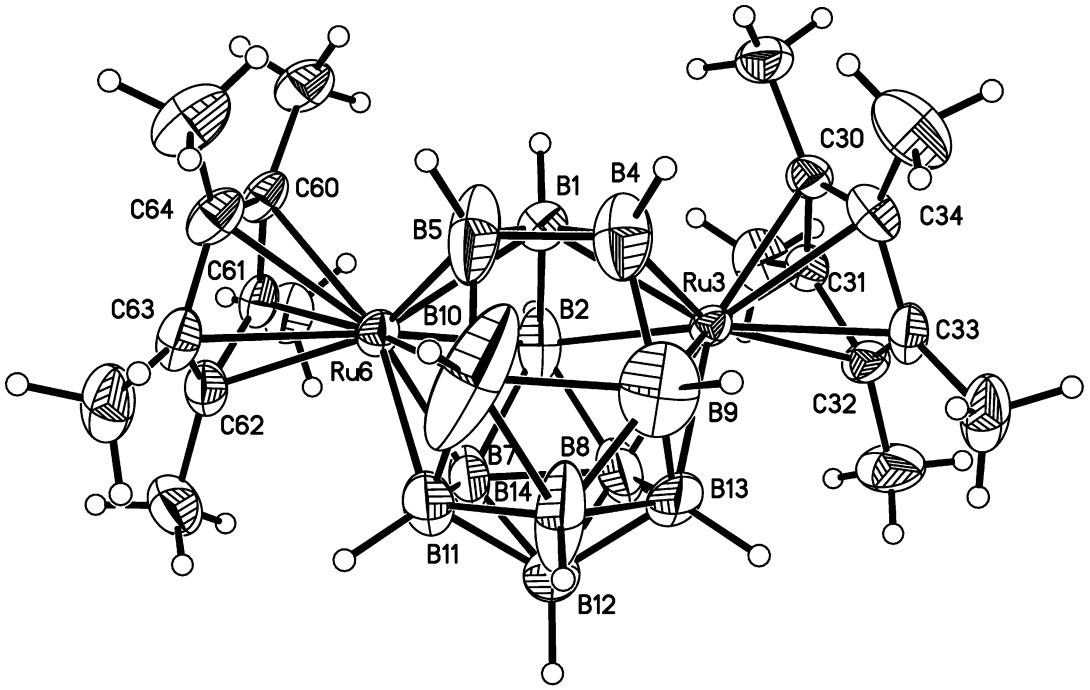

Compound 22 **3,6-(η-C_5Me_5)$_2$-3,6,2,?-*closo*-$Ru_2C_2B_{10}H_{12}$***

Yield = 0.015 g, 1.7%.

NMR ($CDCl_3$) $^{11}B\{^1H\}$ NMR: δ 72.1 (1B), 63.3 (1B), 45.1 (1B), 37.5 (1B), 22.5 (1B), 18.6 (1B), 11.3 (1B) 7.3 (1B), 0.7 (1B), -11.7 (1B) ppm.

^1H NMR: δ 8.50 (br s, 1H, $C_{cage}H$), 1.72 (s, 15H, C_5Me_5), 1.68 (s, 15H, C_5Me_5) ppm (second $C_{cage}H$ signal not found).

MS (low res. EI) M_w = 616.76 g mol^{-1}. g mol^{-1}.

Envelope centred on *m/z* 615 (M^+).

*One of the cage carbon atoms could not be located during crystallographic refinement.

Red needle crystals grown by solvent diffusion of 40-60 petroleum ether and a DCM solution of **22** at -30 ºC.

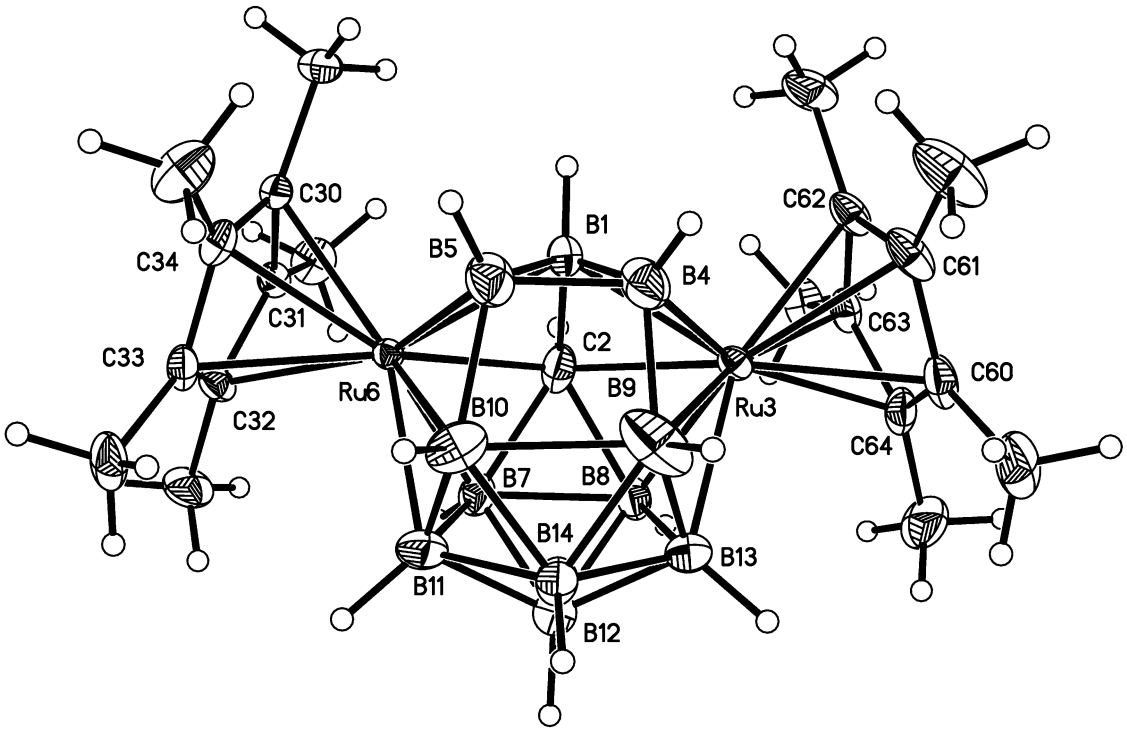

Compound 23	**(μ^3-dicarba-*closo*-dodecaborane-B^1,B^2,B^3,H^1,H^2,H^3)-(μ^3-ethylidyne*)-tris(η^5-pentamethylcyclopentadienyl)-triruthenium**
	Yield = 0.020 g, 1.6% (based on assigned structure).
NMR ($CDCl_3$)	$^{11}B\{^1H\}$ NMR: δ 87.0 (1B)*, -8.7 (3B), -12.0 (3B), -24.2 (2B), -34.4 (1B), -46.7 (1B) ppm.
	^1H NMR: δ 3.30 (s, 3H, CH_3)*, 1.75 (s, 15H, C_5Me_5), 1.80 (s, 30H, C_5Me_5) ppm ($C_{cage}H$ signals not found).
MS (low res. EI)	M_w = 880.11 g mol^{-1}.
	Envelope centred on *m/z* 876 (M^+).

*see chapter five for explanation of assignment.

Red plate crystals grown by vapour diffusion of diethyl ether and a DCM solution of **23** at -30 °C.

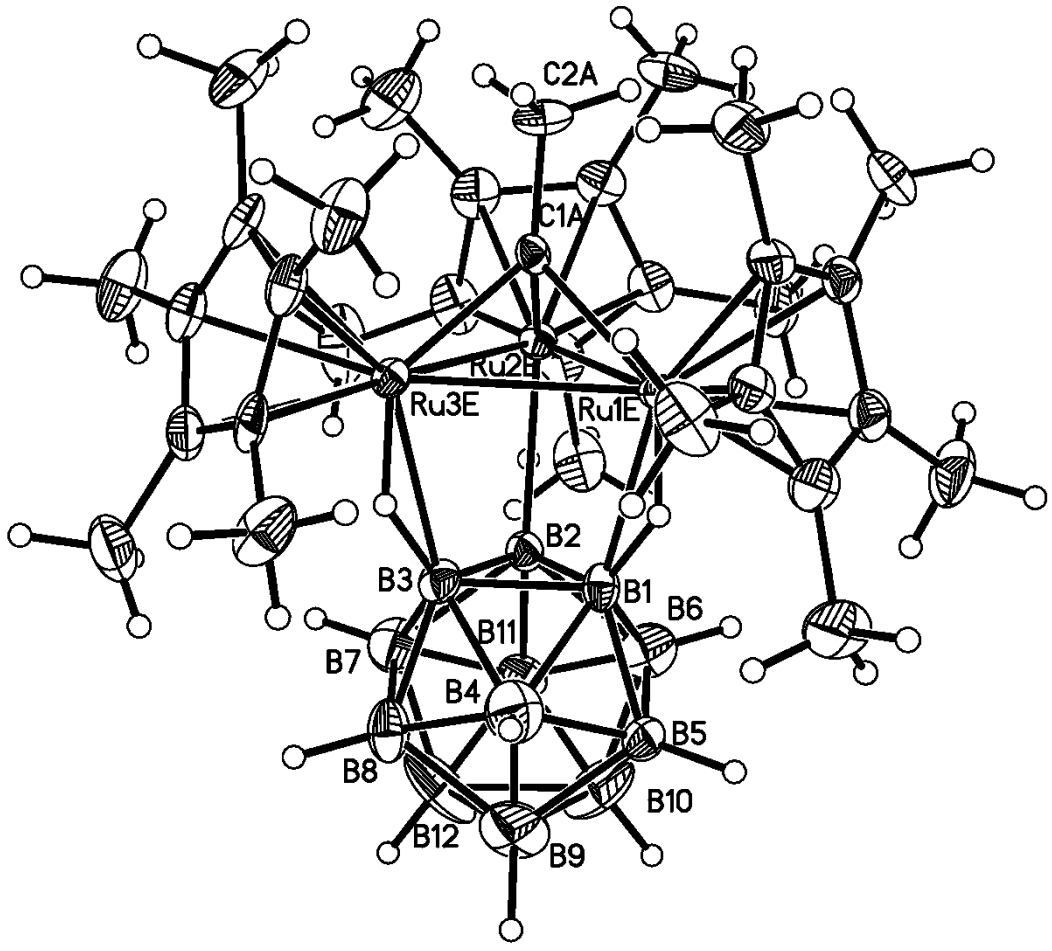

6.5.3 Synthesis of X-(THF)-2,3-$(CH_2)_3$-1-(η-C_5Me_5)-1,2,3-*closo*-$RuC_2B_{11}H_{10}$ (X = 5 and 11) (24 and 25)

Reaction Two

1,2-μ-$(CH_2)_3$-1,2-*closo*-$C_2B_{11}H_{11}$ (0.090 g, 0.459 mmol) was dissolved in degassed THF (25 ml). Na metal (0.080 g, 3.48 mmol) and naphthalene (ca. 15 mg) were added and the solution stirred for 48 h. The resulting dark green solution was transferred via a gas-tight syringe into a second Schlenk tube containing a frozen mixture of $[RuClCp^*]_4$ (0.280 g, 2.58 mmol) in THF (20 mL) at -196 ^oC. The solution of reduced carborane was allowed to freeze, then the mixture was warmed to room temperature and stirred overnight. The resulting brown/orange mixture was purified by preparative TLC (1:1 DCM:40-60 petroleum ether), yielding mobile bands orange **24** (R_f 0.62), yellow **25** (R_f 0.80) and two unidentified bands (pink (R_f 0.55) and yellow (R_f 0.65)) in trace amounts.

Compound 24 **5-(THF)-2,3-$(CH_2)_3$-1-(η-C_5Me_5)-1,2,3-*closo*-$RuC_2B_{11}H_{10}$**

NMR ($CDCl_3$) $^{11}B\{^1H\}$ NMR: δ 19.2 (1B, B-THF), -9.7 (2B), -13.7 (1B), -19.5 (1B), -22.9 (2B), -24.7 (1B), -26.2 (3B) ppm.
^1H NMR: δ 4.25-4.35 (m, 4H, OC_4H_8), 2.60-2.80 (m, 3H, $(CH_2)_3$), 2.13-2.23 (m, 3H, $(CH_2)_3$), 2.05-2.12 (m, 4H, OC_4H_8), 1.50 (s, 15H, C_5Me_5) ppm.

MS (low res. EI) M_w = 503.40 g mol^{-1}.
Envelope centred on *m/z* 504 (M^+).

Yellow needle crystals grown by vapour diffusion of 40-60 petroleum ether and a THF solution of **24** at -30 °C. Compound **24** co-crystallises with three quarters of a molecule of partially disordered DCM of solvation per asymmetric unit which is omitted from the structure below for clarity. There are two crystallographically independent molecules in the asymmetric unit.

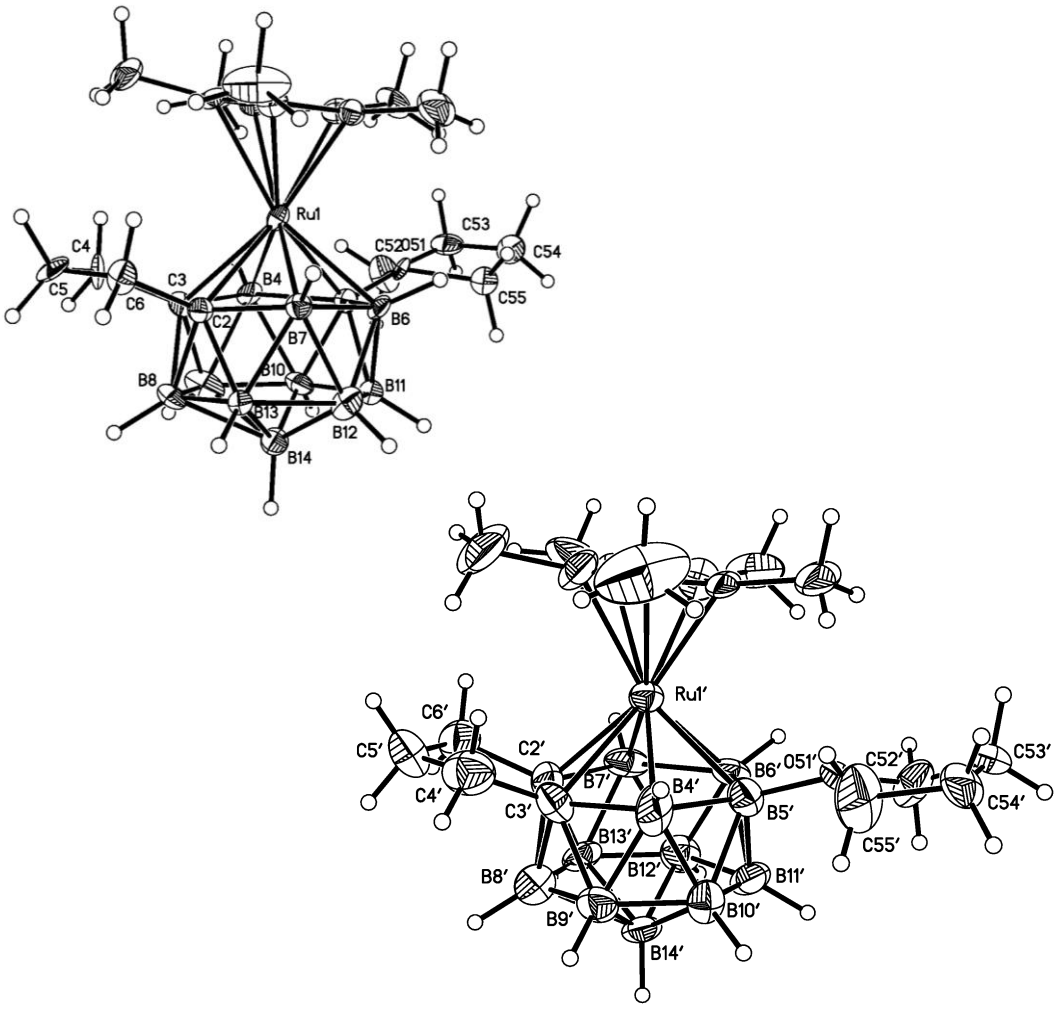

Compound 25 **11-(THF)-2,3-$(CH_2)_3$-1-(η-C_5Me_5)-1,2,3-*closo*-$RuC_2B_{11}H_{10}$**

NMR ($CDCl_3$) $^{11}B\{^1H\}$ NMR: δ 0.2 (1B, B-THF), -8.9 (2B), -18.7 (2B), -24.3 (1B), -26.1 (2B), -29.1 (3B) ppm.

^1H NMR: δ 4.20-4.30 (m, 4H, OC_4H_8), 2.60-2.70 (m, 3H, $(CH_2)_3$), 2.05-2.13 (m, 3H, $(CH_2)_3$), 1.95-2.03 (m, 4H, OC_4H_8), 1.50 (s, 15H, C_5Me_5) ppm.

MS (low res. EI) M_w = 503.40 g mol^{-1}.

Envelope centred on *m/z* 504 (M^+).

Yellow block crystals grown by vapour diffusion of 40-60 petroleum ether and a THF solution of **25** at -30 °C. There are two crystallographically independent molecules in the asymmetric unit, one of which has a disordered Cp^* (molecule containing Ru1'), and the other a disordered pendant THF (molecule containing Ru1). Only one component of the disorder is shown in the below diagrams for clarity.

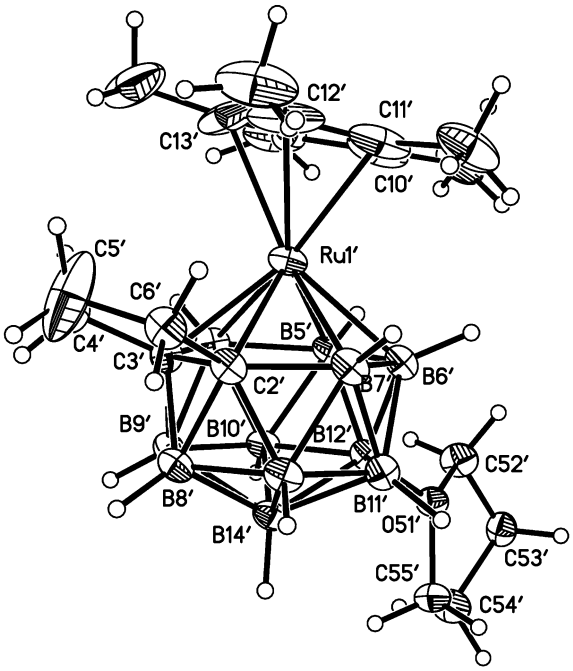

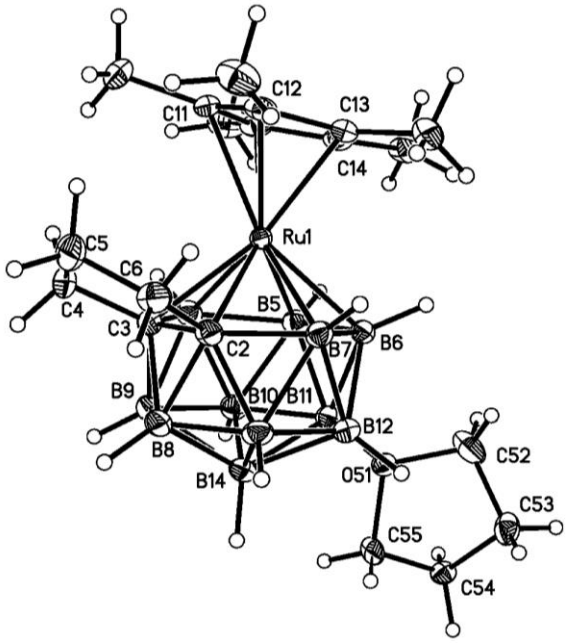

6.6 References

6.1 M.A. Bennett and G. Wilkinson, *Chem. Ind. (London)*,1959, 1516.

6.2 M.F. Hawthorne, D.C. Young, P.M. Garrett, D.A. Owen, S.G. Schwerin, F.N. Tebbe and P.A. Wegner, *J. Am. Chem. Soc.*,1968, **90**, 862.

6.3 M.P. Garcia, M. Green, F.G.A. Stone, R.G. Somerville, A.J. Welch, C.E. Briant, D.N. Cox and D.M.P. Mingos, *J. Chem. Soc., Dalton Trans.*, 1985, 2343.

6.4 T.E. Paxon, M.K. Kaloustian, G.M. Tom, R.J. Wiersema and M.F. Hawthorne, *J. Am. Chem. Soc.*, 1972, **94**, 4882.

6.5 L. Deng, H-S. Chan, and Z. Xie, *J. Am. Chem. Soc.*, 2006, **128**, 5219.

6.6 N. Oshima, H. Suzuki and Y. Moro-oka, *Chem. Lett.*, 1984, **13**, 1161.

6.7 P.J. Fagan, M.D. Ward and J.C. Calabrese, *J. Am. Chem. Soc.*, 1989, **111**, 1698.

6.8 S. Zlatogorsky, D. Ellis and A.J. Welch, unpublished results. This represents an improvement on the original synthesis; H.D. Smith, T.A. Knowles and H. Schroeder, *Inorg. Chem.*, 1965, **4**,107.

6.9 M.J. Frisch, G.W. Trucks, H.B. Schlegel, G.E. Scuseria, M.A. Robb, J.R. Cheeseman, J.A. Montgomery Jr., T. Vreven, K.N. Kudin, J.C. Burant, J.M. Millam, S.S. Iyengar, J. Tomasi, V. Barone, B. Mennucci, M. Cossi, G. Scalmani, N. Rega, G.A. Petersson, H. Nakatsuji, M. Hada, M. Ehara, K. Toyota, R. Fukuda, J. Hasegawa, M. Ishida, T. Nakajima, Y. Honda, O. Kitao, H. Nakai, M. Klene, X. Li, J.E. Knox, H.P. Hratchian, J.B. Cross, V. Bakken, C. Adamo, J. Jaramillo, R. Gomperts, R.E. Stratmann, O. Yazyev, A.J. Austin, R. Cammi, C. Pomelli, J.W. Ochterski, P.Y. Ayala, K. Morokuma, G.A. Voth, P. Salvador, J.J. Dannenberg, V.G. Zakrzewski, S. Dapprich, A.D. Daniels, M.C. Strain, O. Farkas, D.K. Malick, A.D. Rabuck, K. Raghavachari, J.B. Foresman, J.V. Ortiz, Q. Cui, A.G. Baboul, S. Clifford, J. Cioslowski, B.B. Stefanov, G. Liu, A. Liashenko, P. Piskorz, I. Komaromi, R. L. Martin, D.J. Fox, T. Keith, M.A. Al-Laham, C.Y. Peng, A. Nanayakkara, M. Challacombe, P.M.W. Gill, B. Johnson, W. Chen, M.W. Wong, C. Gonzalez and J.A. Pople, *Gaussian 03*, Gaussian, Inc., Wallingford CT, USA, 2004.

6.10 (a) H.L. Schmider and A.D. Becke, *J. Chem. Phys.*, 1998, **108**, 9624.
(b) J.P. Perdew, *Phys. Rev. B: Condens. Matter*, 1986, **33**, 8822.

6.11 (a) W.J. Hehre, R. Ditchfield and J.A. Pople, *J. Chem. Phys.*, 1972, **56**, 2257.
(b) P.C. Hariharan and J.A. Pople, *Theor. Chim. Acta*, 1973, **28**, 213.

6.12 (a) A. Bergner, M. Dolg, W. Kuechle, H. Stoll and H. Preuss, *Mol. Phys.*, 1993, **80**, 1431.

(b) M. Kaupp, P.v.R. Schleyer, H. Stoll and H. Preuss, *J. Chem. Phys.*, 1991, **94**, 1360.

(c) M. Dolg, H. Stoll, H. Preussand and R.M. Pitzer, *J. Phys. Chem.*, 1993, **97**, 5852.

6.13 C.F. Macrae, I.J. Bruno, J.A. Chisholm, P.R. Edgington, P. McCabe, E. Pidcock, L. Rodriguez-Monge, R. Taylor, J. van de Streek and P.A. Wood, *J. Appl. Crystallogr.*, 2008, **41**, 466.

6.14 P. Flükiger, H.L. Lüthi, S. Portmann and J. Weber, *MOLEKEL 4.3*, Swiss Center for Scientific Computing, Manno, Switzerland, 2002.

6.15 Bruker AXS APEX2, version 2009-5, Bruker AXS Inc., Madison, Wisconsin, USA, 2009.

6.16 Rigaku/MSC (2009). *CrystalClear-SM Expert*. Rigaku/MSC, The Woodlands, Texas, USA.

6.17 G.M. Sheldrick, *Acta Crystallogr., Sect. A: Fundam. Crystallogr.*, 2008, **A64**, 112.

6.18 O.V. Dolomanov, L.J. Bourhis, R.J. Gildea, J.A.K. Howard and H. Puschmann, *J. Appl. Cryst*., 2009, **42**, 339.

6.19 A. McAnaw, G. Scott, L. Elrick, G.M. Rosair and A.J. Welch, *Dalton Trans.*, 2013, **42**, 645.

6.20 (a) A. Burke, R. McIntosh, D. Ellis, G.M. Rosair and A.J. Welch, *Collect. Czech. Chem. Commun.*, 2002, **67**, 991.

(b) A. McAnaw, M.E. Lopez, D. Ellis, G.M. Rosair and A.J. Welch, *Dalton Trans.*, 2014, **43**, 5095.

6.21 A.R. Kudinov, D.S. Perekalin, S.S. Rynin, K.A. Lyssenko, G.V. Grintselev-Knyazev and P.V. Petrovskii, *Angew. Chem., Int. Ed.*, 2002, **41**, 4112.

6.22 (a) T.E. Paxson and M.F. Hawthorne, *J. Am. Chem. Soc.*, 1974, **96**, 4674.

(b) R.T. Baker, M.S. Delaney, R.E. King, C.B. Knobler, J.A. Long, T.B. Marder, T.E. Paxson, R.G. Teller and M.F. Hawthorne, *J. Am. Chem. Soc.*, 1984, **106**, 2965.

6.23 Z. Demidowicz, R.G. Teller and M. F. Hawthorne, *J. Chem. Soc., Chem. Commun.*, 1979, 831.

Appendix 1

Crystal Data and Structure Refinements

Crystal data and structure refinement for compound **1**.

Identification code	x82706_0m
Empirical formula	C11 H19 B10 Co
Formula weight	318.29
Temperature	100(2) K
Wavelength	0.71073 Å
Crystal system	Triclinic
Space group	*P*-1
Unit cell dimensions	a = 7.1142(5) Å, α = 75.946(3)°. b = 9.1272(6) Å, β = 88.019(3)°. c = 11.9007(7) Å, γ = 78.059(3)°.
Volume	733.29(8) $Å^3$
Z	2
Density (calculated)	1.442 Mg/m^3
Absorption coefficient	1.149 mm^{-1}
F(000)	324
Crystal size	0.42 x 0.34 x 0.30 mm^3
Theta range for data collection	2.35 to 30.98°.
Index ranges	-9<=h<=10, -13<=k<=13, -16<=l<=17
Reflections collected	15837
Independent reflections	4413 [*R*(int) = 0.0322]
Completeness to theta = 25.00°	97.9 %
Absorption correction	Semi-empirical from equivalents
Max. and min. transmission	0.7243 and 0.6533
Refinement method	Full-matrix least-squares on F^2
Data / restraints / parameters	4413 / 0 / 235
Goodness-of-fit on F^2	1.025
Final *R* indices [*I*>2sigma(*I*)]	*R*1 = 0.0314, *wR*2 = 0.0952
R indices (all data)	*R*1 = 0.0377, *wR*2 = 0.0994
Largest diff. peak and hole	0.505 and -0.508 e.$Å^{-3}$

Crystal data and structure refinement for compound **2**.

Identification code	x82690_0m
Empirical formula	C13 H23 B10 Co
Formula weight	346.34
Temperature	100(2) K
Wavelength	0.71073 Å
Crystal system	Triclinic
Space group	*P*-1
Unit cell dimensions	a = 8.0489(6) Å, α = 98.473(3)°. b = 9.0351(8) Å, β = 96.184(3)°. c = 11.9980(9) Å, γ = 101.756(4)°.
Volume	836.31(12) $Å^3$
Z	2
Density (calculated)	1.375 Mg/m^3
Absorption coefficient	1.014 mm^{-1}
F(000)	356
Crystal size	0.62 x 0.32 x 0.14 mm^3
Theta range for data collection	2.34 to 32.45°.
Index ranges	-12<=h<=12, -13<=k<=12, -16<=l<=18
Reflections collected	22402
Independent reflections	5401 [*R*(int) = 0.0297]
Completeness to theta = 25.00°	99.0 %
Absorption correction	Semi-empirical from equivalents
Max. and min. transmission	0.8711 and 0.5721
Refinement method	Full-matrix least-squares on F^2
Data / restraints / parameters	5401 / 0 / 252
Goodness-of-fit on F^2	1.041
Final *R* indices [I>2sigma(I)]	*R*1 = 0.0257, *wR*2 = 0.0663
R indices (all data)	*R*1 = 0.0292, *wR*2 = 0.0681
Largest diff. peak and hole	0.507 and -0.295 e.$Å^{-3}$

Crystal data and structure refinement for compound **4**.

Identification code	x82710_0m
Empirical formula	C13 H23 B10 Co
Formula weight	346.34
Temperature	100(2) K
Wavelength	0.71073 Å
Crystal system	Monoclinic
Space group	*C*2/*c*
Unit cell dimensions	a = 56.627(8) Å, α = 90°. b = 8.8716(10) Å, β = 100.226(4)°. c = 13.7968(19) Å, γ = 90°.
Volume	6821.0(15) $Å^3$
Z	16
Density (calculated)	1.349 Mg/m^3
Absorption coefficient	0.995 mm^{-1}
F(000)	2848
Crystal size	0.62 x 0.32 x 0.04 mm^3
Theta range for data collection	2.32 to 26.50°.
Index ranges	-70<=h<=70, -11<=k<=10, -17<=l<=17
Reflections collected	55490
Independent reflections	6994 [*R*(int) = 0.0744]
Completeness to theta = 25.00°	99.9 %
Absorption correction	Semi-empirical from equivalents
Max. and min. transmission	0.9613 and 0.7716
Refinement method	Full-matrix least-squares on F^2
Data / restraints / parameters	6994 / 0 / 517
Goodness-of-fit on F^2	0.971
Final *R* indices [*I*>2sigma(*I*)]	*R*1 = 0.0358, *wR*2 = 0.0830
R indices (all data)	*R*1 = 0.0600, *wR*2 = 0.0947
Largest diff. peak and hole	0.362 and -0.373 e.$Å^{-3}$

Crystal data and structure refinement for compound **5**.

Identification code	2676m
Empirical formula	C11 H19 B10 Co
Formula weight	318.29
Temperature	100(2) K
Wavelength	0.71073 Å
Crystal system	Orthorhombic
Space group	*Pnma*
Unit cell dimensions	a = 17.3192(17) Å, α = 90°. b = 11.7891(11) Å, β = 90°. c = 7.2997(7) Å, γ = 90°.
Volume	1490.4(2) $Å^3$
Z	4
Density (calculated)	1.418 Mg/m^3
Absorption coefficient	1.131 mm^{-1}
F(000)	648
Crystal size	0.58 x 0.32 x 0.04 mm^3
Theta range for data collection	2.35 to 28.36°.
Index ranges	-22<=h<=23, -15<=k<=15, -9<=l<=9
Reflections collected	31925
Independent reflections	1945 [*R*(int) = 0.0471]
Completeness to theta = 25.00°	99.9 %
Absorption correction	Semi-empirical from equivalents
Max. and min. transmission	0.9562 and 0.7598
Refinement method	Full-matrix least-squares on F^2
Data / restraints / parameters	1945 / 17 / 137
Goodness-of-fit on F^2	1.367
Final *R* indices [*I*>2sigma(*I*)]	*R*1 = 0.0709, *wR*2 = 0.1645
R indices (all data)	*R*1 = 0.0773, *wR*2 = 0.1663
Largest diff. peak and hole	1.231 and -2.543 e.$Å^{-3}$

Crystal data and structure refinement for compound **6**.

Identification code	x82844
Empirical formula	C13 H23 B10 Co
Formula weight	346.34
Temperature	100(2) K
Wavelength	0.71073 Å
Crystal system	Monoclinic
Space group	*P*21/*c*
Unit cell dimensions	a = 10.1626(10) Å, α = 90°. b = 10.2041(9) Å, β = 102.048(4)°. c = 16.7251(11) Å, γ = 90°.
Volume	1696.2(3) $Å^3$
Z	4
Density (calculated)	1.356 Mg/m^3
Absorption coefficient	1.000 mm^{-1}
F(000)	712
Crystal size	0.38 x 0.24 x 0.20 mm^3
Theta range for data collection	2.05 to 30.67°.
Index ranges	-13<=h<=14, -14<=k<=14, -23<=l<=23
Reflections collected	44880
Independent reflections	5232 [*R*(int) = 0.0572]
Completeness to theta = 25.00°	100.0 %
Absorption correction	Semi-empirical from equivalents
Max. and min. transmission	0.8251 and 0.7025
Refinement method	Full-matrix least-squares on F^2
Data / restraints / parameters	5232 / 0 / 222
Goodness-of-fit on F^2	0.899
Final *R* indices [*I*>2sigma(*I*)]	*R*1 = 0.0410, *wR*2 = 0.1161
R indices (all data)	*R*1 = 0.0733, *wR*2 = 0.1381
Largest diff. peak and hole	0.691 and -0.447 e.$Å^{-3}$

Crystal data and structure refinement for compound **8**.

Identification code	x82720_0m
Empirical formula	C20 H26 B10 Co2
Formula weight	492.37
Temperature	100(2) K
Wavelength	0.71073 Å
Crystal system	Triclinic
Space group	*P*-1
Unit cell dimensions	a = 7.0221(11) Å, α = 78.819(8)°. b = 9.8594(15) Å, β = 84.528(9)°. c = 15.571(2) Å, γ = 76.945(9)°.
Volume	1028.8(3) $Å^3$
Z	2
Density (calculated)	1.589 Mg/m^3
Absorption coefficient	1.620 mm^{-1}
F(000)	500
Crystal size	0.74 x 0.24 x 0.18 mm^3
Theta range for data collection	2.32 to 30.77°.
Index ranges	-10<=h<=10, -14<=k<=13, -21<=l<=22
Reflections collected	23875
Independent reflections	5934 [*R*(int) = 0.0424]
Completeness to theta = 25.00°	97.0 %
Absorption correction	Semi-empirical from equivalents
Max. and min. transmission	0.7586 and 0.6549
Refinement method	Full-matrix least-squares on F^2
Data / restraints / parameters	5934 / 0 / 326
Goodness-of-fit on F^2	1.004
Final *R* indices [*I*>2sigma(*I*)]	*R*1 = 0.0380, *wR*2 = 0.0885
R indices (all data)	*R*1 = 0.0623, *wR*2 = 0.0980
Largest diff. peak and hole	0.547 and -0.633 e.$Å^{-3}$

Crystal data and structure refinement for compound **7**.

Identification code	x82671
Empirical formula	C12 H21 B10 Cl2 Co
Formula weight	403.22
Temperature	100(2) K
Wavelength	0.71073 Å
Crystal system	Monoclinic
Space group	*P*2(1)/*n*
Unit cell dimensions	a = 11.4396(5) Å, α = 90°. b = 8.7217(3) Å, β = 107.299(2)°. c = 19.2249(9) Å, γ = 90°.
Volume	1831.36(13) $Å^3$
Z	4
Density (calculated)	1.462 Mg/m^3
Absorption coefficient	1.219 mm^{-1}
F(000)	816
Crystal size	0.78 x 0.24 x 0.18 mm^3
Theta range for data collection	2.22 to 28.50°.
Index ranges	-15<=h<=15, -11<=k<=11, -25<=l<=25
Reflections collected	46198
Independent reflections	4640 [*R*(int) = 0.0476]
Completeness to theta = 25.00°	99.9 %
Absorption correction	Semi-empirical from equivalents
Max. and min. transmission	0.8104 and 0.4497
Refinement method	Full-matrix least-squares on F^2
Data / restraints / parameters	4640 / 0 / 262
Goodness-of-fit on F^2	1.131
Final *R* indices [*I*>2sigma(*I*)]	*R*1 = 0.0349, *wR*2 = 0.0731
R indices (all data)	*R*1 = 0.0418, *wR*2 = 0.0757
Largest diff. peak and hole	0.406 and -0.345 e.$Å^{-3}$

Crystal data and structure refinement for compound **9**.

Identification code	x83030
Empirical formula	C12 H19 B9 Ru
Formula weight	361.63
Temperature	100(2) K
Wavelength	0.71073 Å
Crystal system	Monoclinic
Space group	*P*2(1)/*n*
Unit cell dimensions	a = 7.1815(4) Å, α = 90°. b = 23.7802(13) Å, β = 108.369(3)°. c = 9.2668(5) Å, γ = 90°.
Volume	1501.92(14) $Å^3$
Z	4
Density (calculated)	1.599 Mg/m^3
Absorption coefficient	1.025 mm^{-1}
F(000)	720
Crystal size	0.42 x 0.38 x 0.30 mm^3
Theta range for data collection	2.47 to 31.91°.
Index ranges	-10<=h<=10, -34<=k<=35, -13<=l<=13
Reflections collected	38403
Independent reflections	5146 [*R*(int) = 0.0278]
Completeness to theta = 25.00°	100.0 %
Absorption correction	Semi-empirical from equivalents
Max. and min. transmission	0.7485 and 0.5690
Refinement method	Full-matrix least-squares on F^2
Data / restraints / parameters	5146 / 0 / 199
Goodness-of-fit on F^2	1.113
Final *R* indices [*I*>2sigma(*I*)]	*R*1 = 0.0215, *wR*2 = 0.0484
R indices (all data)	*R*1 = 0.0231, *wR*2 = 0.0490
Largest diff. peak and hole	0.773 and -0.756 e.$Å^{-3}$

Crystal data and structure refinement for compound **10**.

Identification code	x82985
Empirical formula	C10 H21 B9 Ru
Formula weight	339.63
Temperature	100(2) K
Wavelength	0.71073 Å
Crystal system	Orthorhombic
Space group	*Pbca*
Unit cell dimensions	a = 9.8641(7) Å, α = 90°. b = 13.0864(8) Å, β = 90°. c = 22.9811(15) Å, γ = 90°.
Volume	2966.5(3) $Å^3$
Z	8
Density (calculated)	1.521 Mg/m^3
Absorption coefficient	1.032 mm^{-1}
F(000)	1360
Crystal size	0.44 x 0.35 x 0.08 mm^3
Theta range for data collection	2.72 to 29.03°.
Index ranges	-13<=h<=13, -14<=k<=17, -31<=l<=31
Reflections collected	37689
Independent reflections	3941 [*R*(int) = 0.0394]
Completeness to theta = 25.00°	99.8 %
Absorption correction	Semi-empirical from equivalents
Max. and min. transmission	0.9220 and 0.6594
Refinement method	Full-matrix least-squares on F^2
Data / restraints / parameters	3941 / 0 / 182
Goodness-of-fit on F^2	1.101
Final *R* indices [*I*>2sigma(*I*)]	*R*1 = 0.0454, *wR*2 = 0.1082
R indices (all data)	*R*1 = 0.0605, *wR*2 = 0.1175
Largest diff. peak and hole	2.594 and -0.908 e.$Å^{-3}$

Crystal data and structure refinement for compound **11**.

Identification code	X83144
Empirical formula	C16 H28 B10 O Ru
Formula weight	445.55
Temperature	100(2) K
Wavelength	0.71073 Å
Crystal system	Orthorhombic
Space group	*Pbca*
Unit cell dimensions	a = 9.2856(11) Å, α = 90°. b = 19.785(2) Å, β = 90°. c = 21.686(3) Å, γ = 90°.
Volume	3984.0(9) $Å^3$
Z	8
Density (calculated)	1.486 Mg/m^3
Absorption coefficient	0.791 mm^{-1}
F(000)	1808
Crystal size	0.41 x 0.28 x 0.10 mm^3
Theta range for data collection	2.26 to 26.83°.
Index ranges	-11<=h<=10, -24<=k<=25, -27<=l<=25
Reflections collected	42596
Independent reflections	4248 [*R*(int) = 0.0785]
Completeness to theta = 25.00°	99.9 %
Absorption correction	Semi-empirical from equivalents
Max. and min. transmission	0.9251 and 0.7374
Refinement method	Full-matrix least-squares on F^2
Data / restraints / parameters	4248 / 4 / 269
Goodness-of-fit on F^2	1.025
Final *R* indices [*I*>2sigma(*I*)]	*R*1 = 0.0451, *wR*2 = 0.1005
R indices (all data)	*R*1 = 0.0837, *wR*2 = 0.1183
Largest diff. peak and hole	0.655 and -0.497 e.$Å^{-3}$

Crystal data and structure refinement for compound **12**.

Identification code	x83222
Empirical formula	C12 H20 B10 Ru
Formula weight	373.45
Temperature	163(2) K
Wavelength	0.71073 Å
Crystal system	Monoclinic
Space group	*P*2(1)/*n*
Unit cell dimensions	a = 10.5124(7) Å, α = 90°. b = 13.7539(9) Å, β = 108.423(3)°. c = 11.4807(8) Å, γ = 90°.
Volume	1574.88(18) $Å^3$
Z	4
Density (calculated)	1.575 Mg/m^3
Absorption coefficient	0.980 mm^{-1}
F(000)	744
Crystal size	0.42 x 0.06 x 0.04 mm^3
Theta range for data collection	2.39 to 28.77°.
Index ranges	-14<=h<=14, -18<=k<=18, -15<=l<=15
Reflections collected	30467
Independent reflections	4056 [*R*(int) = 0.0563]
Completeness to theta = 25.00°	100.0 %
Absorption correction	Semi-empirical from equivalents
Max. and min. transmission	0.9619 and 0.6838
Refinement method	Full-matrix least-squares on F^2
Data / restraints / parameters	4056 / 0 / 219
Goodness-of-fit on F^2	1.035
Final *R* indices [*I*>2sigma(*I*)]	*R*1 = 0.0320, *wR*2 = 0.0646
R indices (all data)	*R*1 = 0.0521, *wR*2 = 0.0706
Largest diff. peak and hole	0.658 and -0.873 e.$Å^{-3}$

Crystal data and structure refinement for compound **13**.

Identification code	X83169
Empirical formula	C12 H20 B10 Ru
Formula weight	373.45
Temperature	100(2) K
Wavelength	0.71073 Å
Crystal system	Monoclinic
Space group	*P*21/*c*
Unit cell dimensions	a = 11.833(2) Å, α = 90°. b = 7.5610(15) Å, β = 97.11(3)°. c = 18.058(4) Å, γ = 90°.
Volume	1603.3(6) $Å^3$
Z	4
Density (calculated)	1.547 Mg/m^3
Absorption coefficient	0.962 mm^{-1}
F(000)	744
Crystal size	0.42 x 0.38 x 0.02 mm^3
Theta range for data collection	1.73 to 29.52°.
Index ranges	-14<=h<=14, 0<=k<=10, 0<=l<=24
Reflections collected	17396
Independent reflections	3623 [*R*(int) = 0.0600]
Completeness to theta = 25.00°	82.0 %
Absorption correction	Semi-empirical from equivalents
Max. and min. transmission	0.9810 and 0.6881
Refinement method	Full-matrix least-squares on F^2
Data / restraints / parameters	3623 / 30 / 213
Goodness-of-fit on F^2	1.081
Final *R* indices [*I*>2sigma(*I*)]	*R*1 = 0.0623, *wR*2 = 0.1682
R indices (all data)	*R*1 = 0.0827, *wR*2 = 0.1767
Largest diff. peak and hole	1.209 and -2.361 e.$Å^{-3}$

Crystal data and structure refinement for compound **14**.

Identification code	3308
Empirical formula	C12 H20 B10 Ru
Formula weight	373.45
Temperature	100(2) K
Wavelength	0.71073 Å
Crystal system	Orthorhombic
Space group	*Pnma*
Unit cell dimensions	a = 17.884(4) Å, α = 90°. b = 12.007(2) Å, β = 90°. c = 7.3419(16) Å, γ = 90°.
Volume	1576.5(6) $Å^3$
Z	4
Density (calculated)	1.573 Mg/m^3
Absorption coefficient	0.978 mm^{-1}
F(000)	744
Crystal size	0.74 x 0.18 x 0.04 mm^3
Theta range for data collection	2.28 to 32.27°.
Index ranges	-24<=h<=25, -17<=k<=16, -11<=l<=10
Reflections collected	21381
Independent reflections	2797 [*R*(int) = 0.0868]
Completeness to theta = 25.00°	100.0 %
Absorption correction	Semi-empirical from equivalents
Max. and min. transmission	0.9619 and 0.5313
Refinement method	Full-matrix least-squares on F^2
Data / restraints / parameters	2797 / 1 / 130
Goodness-of-fit on F^2	1.186
Final *R* indices [*I*>2sigma(*I*)]	*R*1 = 0.0669, *wR*2 = 0.1236
R indices (all data)	*R*1 = 0.1086, *wR*2 = 0.1329
Largest diff. peak and hole	2.178 and -4.641 e.$Å^{-3}$

Crystal data and structure refinement for compound **16**.

Identification code	X84341
Empirical formula	C13 H26 B10 Cl2 Fe
Formula weight	417.19
Temperature	100(2) K
Wavelength	0.71073 Å
Crystal system	Orthorhombic
Space group	*Pbca*
Unit cell dimensions	a = 9.0554(3) Å, α = 90°. b = 19.1183(7) Å, β = 90°. c = 22.2396(8) Å, γ = 90°.
Volume	3850.2(2) $Å^3$
Z	8
Density (calculated)	1.439 Mg/m^3
Absorption coefficient	1.055 mm^{-1}
F(000)	1712
Crystal size	0.42 x 0.16 x 0.08 mm^3
Theta range for data collection	2.65 to 30.15°.
Index ranges	-12<=h<=12, -26<=k<=24, -31<=l<=30
Reflections collected	75700
Independent reflections	5685 [*R*(int) = 0.0544]
Completeness to theta = 25.00°	99.9 %
Absorption correction	Semi-empirical from equivalents
Max. and min. transmission	0.9203 and 0.6656
Refinement method	Full-matrix least-squares on F^2
Data / restraints / parameters	5685 / 0 / 238
Goodness-of-fit on F^2	1.061
Final *R* indices [*I*>2sigma(*I*)]	*R*1 = 0.0563, *wR*2 = 0.1480
R indices (all data)	*R*1 = 0.0800, *wR*2 = 0.1624
Largest diff. peak and hole	1.221 and -1.830 e.Å^{-}

Crystal data and structure refinement for compound **15**.

Identification code	twin4
Empirical formula	C10 H22 B10 Ru
Formula weight	351.45
Temperature	100(2) K
Wavelength	0.71073 Å
Crystal system	Monoclinic
Space group	*P*2(1)/*c*
Unit cell dimensions	a = 11.379(2) Å, α = 90°. b = 8.9786(18) Å, β = 93.67(3)°. c = 15.157(3) Å, γ = 90°.
Volume	1545.3(5) $Å^3$
Z	4
Density (calculated)	1.511 Mg/m^3
Absorption coefficient	0.993 mm^{-1}
F(000)	704
Crystal size	0.32 x 0.14 x 0.08 mm^3
Theta range for data collection	2.69 to 32.99°.
Index ranges	-17<=h<=17, 0<=k<=13, 0<=l<=23
Reflections collected	82273
Independent reflections	5751 [*R*(int) = 0.0469]
Completeness to theta = 25.00°	99.9 %
Absorption correction	Semi-empirical from equivalents
Max. and min. transmission	0.9248 and 0.7418
Refinement method	Full-matrix least-squares on F^2
Data / restraints / parameters	5751 / 0 / 194
Goodness-of-fit on F^2	1.073
Final *R* indices [*I*>2sigma(*I*)]	*R*1 = 0.0291, *wR*2 = 0.0648
R indices (all data)	*R*1 = 0.0401, *wR*2 = 0.0681
Largest diff. peak and hole	1.623 and -0.761 e.$Å^{-3}$

Crystal data and structure refinement for compound **V**.

Identification code	2886
Empirical formula	C39 H44 B9 Cl2 P2 Rh
Formula weight	845.78
Temperature	100(2) K
Wavelength	0.71073 Å
Crystal system	Triclinic
Space group	*P*-1
Unit cell dimensions	a = 9.7670(6) Å, α = 75.731(3)°. b = 12.1220(7) Å, β = 80.599(3)°. c = 19.3752(12) Å, γ = 71.411(3)°.
Volume	2098.2(2) $Å^3$
Z	2
Density (calculated)	1.339 Mg/m^3
Absorption coefficient	0.639 mm^{-1}
F(000)	864
Crystal size	0.56 x 0.26 x 0.12 mm^3
Theta range for data collection	1.09 to 31.07°.
Index ranges	-14<=h<=11, -17<=k<=16, -28<=l<=28
Reflections collected	49055
Independent reflections	13335 [*R*(int) = 0.0447]
Completeness to theta = 25.00°	99.9 %
Absorption correction	Semi-empirical from equivalents
Max. and min. transmission	0.926 and 0.886
Refinement method	Full-matrix least-squares on F^2
Data / restraints / parameters	13335 / 0 / 482
Goodness-of-fit on F^2	1.086
Final *R* indices [*I*>2sigma(*I*)]	*R*1 = 0.0375, *wR*2 = 0.0872
R indices (all data)	*R*1 = 0.0489, *wR*2 = 0.0915
Largest diff. peak and hole	0.710 and -0.849 e.$Å^{-3}$

Crystal data and structure refinement for compound **VI**.

Identification code	x82978
Empirical formula	C20.75 H27.50 B9 Cl1.50 N O3 P Rh
Formula weight	623.28
Temperature	100(2) K
Wavelength	0.71073 Å
Crystal system	Triclinic
Space group	*P*-1
Unit cell dimensions	a = 12.4890(9) Å, α = 92.949(4)°. b = 14.5862(10) Å, β =105.014(4)°. c = 16.8809(12) Å, γ = 107.242(4)°.
Volume	2809.1(3) $Å^3$
Z	4
Density (calculated)	1.474 Mg/m^3
Absorption coefficient	0.833 mm^{-1}
F(000)	1254
Crystal size	0.58 x 0.28 x 0.08 mm^3
Theta range for data collection	1.80 to 29.89°.
Index ranges	-16<=h<=15, -19<=k<=19, 0<=l<=23
Reflections collected	74772
Independent reflections	12876 [*R*(int) = 0.0553]
Completeness to theta = 25.00°	93.8 %
Absorption correction	Semi-empirical from equivalents
Max. and min. transmission	0.9364 and 0.6437
Refinement method	Full-matrix least-squares on F^2
Data / restraints / parameters	12876 / 3 / 696
Goodness-of-fit on F^2	1.053
Final *R* indices [*I*>2sigma(*I*)]	*R*1 = 0.0555, *wR*2 = 0.1230
R indices (all data)	*R*1 = 0.1002, *wR*2 = 0.1489
Largest diff. peak and hole	0.781 and -0.917 e.$Å^{-3}$

Crystal data and structure refinement for compound **17**.

Identification code	x84397
Empirical formula	C16 H33 B9 O Ru
Formula weight	439.78
Temperature	100(2) K
Wavelength	0.71073 Å
Crystal system	Monoclinic
Space group	*P*2(1)/*c*
Unit cell dimensions	a = 20.2433(8) Å, α = 90°. b = 13.2929(5) Å, β = 93.373(2)°. c = 15.3751(6) Å, γ = 90°.
Volume	4130.2(3) $Å^3$
Z	8
Density (calculated)	1.415 Mg/m^3
Absorption coefficient	0.763 mm^{-1}
F(000)	1808
Crystal size	0.44 x 0.42 x 0.28 mm^3
Theta range for data collection	1.83 to 30.58°.
Index ranges	-24<=h<=28, -15<=k<=19, -21<=l<=21
Reflections collected	115282
Independent reflections	12608 [*R*(int) = 0.0518]
Completeness to theta = 25.00°	100.0 %
Absorption correction	Semi-empirical from equivalents
Max. and min. transmission	0.8148 and 0.7302
Refinement method	Full-matrix least-squares on F^2
Data / restraints / parameters	12608 / 0 / 557
Goodness-of-fit on F^2	1.006
Final *R* indices [*I*>2sigma(*I*)]	*R*1 = 0.0264, *wR*2 = 0.0554
R indices (all data)	*R*1 = 0.0466, *wR*2 = 0.0637
Largest diff. peak and hole	0.462 and -0.624 e.$Å^{-3}$

Crystal data and structure refinement for compound **VII**.

Identification code	x83012
Empirical formula	C39 H43 B9 Cl2 N O3 P2 Rh
Formula weight	906.78
Temperature	100.15 K
Wavelength	0.71073 Å
Crystal system	Triclinic
Space group	*P* -1
Unit cell dimensions	a = 11.2934(9) Å, α = 91.083(4)°. b = 13.0083(10) Å, β = 110.514(4)°. c = 15.8655(13) Å, γ = 99.713(4)°.
Volume	2144.0(3) $Å^3$
Z	2
Density (calculated)	1.404 Mg/m^3
Absorption coefficient	0.635 mm^{-1}
F(000)	908
Crystal size	0.56 x 0.32 x 0.08 mm^3
Theta range for data collection	2.192 to 28.525°.
Index ranges	-15<=h<=14, -17<=k<=17, -21<=l<=20
Reflections collected	40881
Independent reflections	10603 [*R*(int) = 0.0347]
Completeness to theta = 25.000°	99.6 %
Absorption correction	Semi-empirical from equivalents
Max. and min. transmission	0.7457 and 0.6599
Refinement method	Full-matrix least-squares on F^2
Data / restraints / parameters	10603 / 3 / 523
Goodness-of-fit on F^2	1.013
Final *R* indices [*I*>2sigma(*I*)]	*R*1 = 0.0354, *wR*2 = 0.0824
R indices (all data)	*R*1 = 0.0455, *wR*2 = 0.0863
Largest diff. peak and hole	1.056 and -0.758 e.$Å^{-3}$

Crystal data and structure refinement for compound **18**.

Identification code	x84491
Empirical formula	C22 H41 B9 Ru2
Formula weight	604.98
Temperature	100(2) K
Wavelength	0.71073 Å
Crystal system	Monoclinic
Space group	*P*2(1)/*n*
Unit cell dimensions	a = 8.3601(17) Å, α = 90°. b = 15.643(3) Å, β = 101.31(3)°. c = 20.547(4) Å, γ = 90°.
Volume	2634.9(9) $Å^3$
Z	4
Density (calculated)	1.525 Mg/m^3
Absorption coefficient	1.156 mm^{-1}
F(000)	1224
Crystal size	0.38 x 0.14 x 0.12 mm^3
Theta range for data collection	2.49 to 30.46°.
Index ranges	-11<=h<=11, 0<=k<=22, 0<=l<=29
Reflections collected	105880
Independent reflections	7972 [*R*(int) = 0.0674]
Completeness to theta = 25.00°	99.9 %
Absorption correction	Semi-empirical from equivalents
Max. and min. transmission	0.8737 and 0.6677
Refinement method	Full-matrix least-squares on F^2
Data / restraints / parameters	7972 / 0 / 328
Goodness-of-fit on F^2	1.045
Final *R* indices [*I*>2sigma(*I*)]	*R*1 = 0.0303, *wR*2 = 0.0601
R indices (all data)	*R*1 = 0.0424, *wR*2 = 0.0634
Largest diff. peak and hole	0.610 and -0.598 e.$Å^{-3}$

Crystal data and structure refinement for compound **19**.

Identification code	x84885
Empirical formula	C22 H41 B9 Ru2
Formula weight	604.98
Temperature	100(2) K
Wavelength	0.71073 Å
Crystal system	Monoclinic
Space group	*P*2(1)/*n*
Unit cell dimensions	a = 8.2910(6) Å, α = 90°. b = 26.1610(17) Å, β = 99.394(4)°. c = 12.0948(8) Å, γ = 90°.
Volume	2588.2(3) $Å^3$
Z	4
Density (calculated)	1.553 Mg/m^3
Absorption coefficient	1.177 mm^{-1}
F(000)	1224
Crystal size	0.48 x 0.16 x 0.12 mm^3
Theta range for data collection	2.61 to 32.60°.
Index ranges	-12<=h<=12, -39<=k<=39, -17<=l<=18
Reflections collected	67252
Independent reflections	9412 [*R*(int) = 0.0475]
Completeness to theta = 25.00°	99.9 %
Absorption correction	Semi-empirical from equivalents
Max. and min. transmission	0.8716 and 0.6019
Refinement method	Full-matrix least-squares on F^2
Data / restraints / parameters	9412 / 0 / 352
Goodness-of-fit on F^2	1.041
Final *R* indices [*I*>2sigma(*I*)]	*R*1 = 0.0269, *wR*2 = 0.0524
R indices (all data)	*R*1 = 0.0351, *wR*2 = 0.0548
Largest diff. peak and hole	0.515 and -0.714 e.$Å^{-3}$

Crystal data and structure refinement for compound **20**.

Identification code	x84654
Empirical formula	C26 H49 B9 O Ru2
Formula weight	677.08
Temperature	100(2) K
Wavelength	0.71073 Å
Crystal system	Monoclinic
Space group	*P*2(1)/*c*
Unit cell dimensions	a = 12.7008(9) Å, α = 90°. b = 14.3815(9) Å, β = 93.426(3)°. c = 16.5610(10) Å, γ = 90°.
Volume	3019.6(3) $Å^3$
Z	4
Density (calculated)	1.489 Mg/m^3
Absorption coefficient	1.020 mm^{-1}
F(000)	1384
Crystal size	0.34 x 0.14 x 0.10 mm^3
Theta range for data collection	2.83 to 28.70°.
Index ranges	-17<=h<=17, -19<=k<=19, -20<=l<=22
Reflections collected	50782
Independent reflections	7797 [*R*(int) = 0.0626]
Completeness to theta = 25.00°	99.9 %
Absorption correction	Semi-empirical from equivalents
Max. and min. transmission	0.9049 and 0.7230
Refinement method	Full-matrix least-squares on F^2
Data / restraints / parameters	7797 / 0 / 394
Goodness-of-fit on F^2	1.036
Final *R* indices [*I*>2sigma(*I*)]	*R*1 = 0.0406, *wR*2 = 0.0804
R indices (all data)	*R*1 = 0.0560, *wR*2 = 0.0874
Largest diff. peak and hole	1.224 and -0.678 e.$Å^{-3}$

Crystal data and structure refinement for compound **21**.

Identification code	2014ncs0036
Empirical formula	C20 H42 B12 Ru2
Formula weight	614.40
Temperature	100(2) K
Wavelength	0.71073 Å
Crystal system	Monoclinic
Space group	*P*2(1)/*n*
Unit cell dimensions	a = 8.4816(6) Å, α = 90°. b = 15.5241(11) Å, β = 101.3680(10)°. c = 20.8045(15) Å, γ = 90°.
Volume	2685.6(3) $Å^3$
Z	4
Density (calculated)	1.520 Mg/m^3
Absorption coefficient	1.134 mm^{-1}
F(000)	1240
Crystal size	0.11 x 0.08 x 0.01 mm^3
Theta range for data collection	2.39 to 27.51°.
Index ranges	-10<=h<=7, -19<=k<=20, -26<=l<=27
Reflections collected	30380
Independent reflections	6109 [*R*(int) = 0.0358]
Completeness to theta = 25.00°	99.9 %
Absorption correction	Semi-empirical from equivalents
Max. and min. transmission	0.8260 and 0.6690
Refinement method	Full-matrix least-squares on F^2
Data / restraints / parameters	6109 / 0 / 317
Goodness-of-fit on F^2	1.021
Final *R* indices [*I*>2sigma(*I*)]	*R*1 = 0.0366, *wR*2 = 0.0885
R indices (all data)	*R*1 = 0.0437, *wR*2 = 0.0919
Largest diff. peak and hole	1.443 and -0.722 e.$Å^{-3}$

Crystal data and structure refinement for compound **22**.

Identification code	X84914
Empirical formula	C21 H42 B11 Ru2
Formula weight	615.60
Temperature	100(2) K
Wavelength	0.71073 Å
Crystal system	Monoclinic
Space group	*P*2(1)/*n*
Unit cell dimensions	a = 8.3871(5) Å, α = 90°. b = 15.5825(9) Å, β = 101.538(3)°. c = 20.8076(13) Å, γ = 90°.
Volume	2664.4(3) $Å^3$
Z	4
Density (calculated)	1.535 Mg/m^3
Absorption coefficient	1.144 mm^{-1}
F(000)	1244
Crystal size	0.52 x 0.16 x 0.10 mm^3
Theta range for data collection	2.48 to 33.12°.
Index ranges	-12<=h<=12, -23<=k<=23, -31<=l<=31
Reflections collected	70146
Independent reflections	10070 [*R*(int) = 0.0467]
Completeness to theta = 25.00°	99.9 %
Absorption correction	Semi-empirical from equivalents
Max. and min. transmission	0.8942 and 0.5876
Refinement method	Full-matrix least-squares on F^2
Data / restraints / parameters	10070 / 0 / 355
Goodness-of-fit on F^2	1.039
Final *R* indices [*I*>2sigma(*I*)]	*R*1 = 0.0349, *wR*2 = 0.0684
R indices (all data)	*R*1 = 0.0444, *wR*2 = 0.0716
Largest diff. peak and hole	1.706 and -1.345 e.$Å^{-3}$

Crystal data and structure refinement for compound **23**.

Identification code	0037
Empirical formula	C16 H30 B6 Ru1.50
Formula weight	438.87
Temperature	100(2) K
Wavelength	0.71073 Å
Crystal system	Monoclinic
Space group	*P*2(1)
Unit cell dimensions	a = 10.9415(8) Å, α = 90°. b = 15.4104(11) Å, β = 95.5330(10)°. c = 11.1689(8) Å, γ = 90°.
Volume	1874.4(2) $Å^3$
Z	4
Density (calculated)	1.555 Mg/m^3
Absorption coefficient	1.217 mm^{-1}
F(000)	888
Crystal size	0.16 x 0.08 x 0.03 mm^3
Theta range for data collection	2.26 to 27.52°.
Index ranges	-14<=h<=14, -20<=k<=20, -13<=l<=14
Reflections collected	21510
Independent reflections	8499 [*R*(int) = 0.0441]
Completeness to theta = 25.00°	99.7 %
Absorption correction	Semi-empirical from equivalents
Max. and min. transmission	0.8260 and 0.6690
Refinement method	Full-matrix least-squares on F^2
Data / restraints / parameters	8499 / 1 / 440
Goodness-of-fit on F^2	1.107
Final *R* indices [*I*>2sigma(*I*)]	*R*1 = 0.0430, *wR*2 = 0.1134
R indices (all data)	*R*1 = 0.0446, *wR*2 = 0.1143
Largest diff. peak and hole	3.170 and -0.492 e.$Å^{-3}$

Crystal data and structure refinement for compound **24**.

Identification code	4595
Empirical formula	C19.38 H39.75 B11 Cl0.75 O Ru
Formula weight	535.33
Temperature	100.0 K
Wavelength	0.71073 Å
Crystal system	Triclinic
Space group	*P* -1
Unit cell dimensions	a = 9.4098(11) Å, α = 82.224(7)°. b = 10.1175(12) Å, β = 80.879(7)°. c = 27.785(4) Å, γ = 84.344(7)°.
Volume	2579.7(6) $Å^3$
Z	4
Density (calculated)	1.378 Mg/m^3
Absorption coefficient	0.698 mm^{-1}
F(000)	1103
Crystal size	0.34 x 0.08 x 0.04 mm^3
Theta range for data collection	0.75 to 26.02°.
Index ranges	-11<=h<=11, -12<=k<=12, 0<=l<=34
Reflections collected	27276
Independent reflections	8694 [*R*(int) = 0.0754]
Completeness to theta = 26.00°	85.4 %
Absorption correction	Semi-empirical from equivalents
Max. and min. transmission	1 and 0.605551
Refinement method	Full-matrix least-squares on F^2
Data / restraints / parameters	8694 / 166 / 612
Goodness-of-fit on F^2	1.089
Final *R* indices [*I*>2sigma(*I*)]	*R*1 = 0.0773, *wR*2 = 0.1690
R indices (all data)	*R*1 = 0.1182, *wR*2 = 0.1878
Largest diff. peak and hole	1.255 and -1.163 e.$Å^{-3}$

Crystal data and structure refinement for compound **25**.

Identification code	x84717
Empirical formula	C19 H39 B11 O Ru
Formula weight	503.48
Temperature	100(2) K
Wavelength	0.71073 Å
Crystal system	Triclinic
Space group	*P*-1
Unit cell dimensions	a = 8.8006(3) Å, α = 109.414(2)°. b = 16.3125(6) Å, β = 93.755(2)°. c = 17.6973(6) Å, γ = 92.860(2)°.
Volume	2384.08(14) $Å^3$
Z	4
Density (calculated)	1.403 Mg/m^3
Absorption coefficient	0.669 mm^{-1}
F(000)	1040
Crystal size	0.38 x 0.36 x 0.22 mm^3
Theta range for data collection	1.47 to 32.56°.
Index ranges	-13<=h<=13, -24<=k<=24, -26<=l<=26
Reflections collected	59979
Independent reflections	17109 [*R*(int) = 0.0425]
Completeness to theta = 25.00°	99.9 %
Absorption correction	Semi-empirical from equivalents
Max. and min. transmission	0.8668 and 0.7851
Refinement method	Full-matrix least-squares on F^2
Data / restraints / parameters	17109 / 61 / 727
Goodness-of-fit on F^2	1.047
Final *R* indices [*I*>2sigma(*I*)]	*R*1 = 0.0430, *wR*2 = 0.0932
R indices (all data)	*R*1 = 0.0649, *wR*2 = 0.1026
Largest diff. peak and hole	2.085 and -2.405 e.$Å^{-3}$

Appendix 2

Structures found during CSD search

* Denotes structure with two independent molecules in asymmetric unit

4.3 3-R-3,1,2-closo-$MC_2B_9H_{11}$ (R = C_5H_5/C_5Me_5/arene)

CSD Reference Code	Formula and Literature Reference	Notes
DEHFIF	3-(η-C_6H_6)-3,1,2-$RuC_2B_9H_{11}$ M.P. Garcia, M. Green, F.G.A. Stone, R.G. Somerville, A.J. Welch, C.E. Briant, D.N. Cox and D.M.P. Mingos, *J. Chem. Soc., Dalton Trans.*, 1985, 2343.	Sits on a crystallographic mirror plane.
DUBDIN	3-(η-C_5H_5)-3,1,2-$CoC_2B_9H_{11}$ D.E. Smith, A.J. Welch, *Organometallics*, 1986, **5**, 760.	N/A
DUBDIN01	3-(η-C_5H_5)-3,1,2-$CoC_2B_9H_{11}$ J.G. Planas, C. Vinas, F. Teixidor, M.E. Light and M.B. Hursthouse, *Cryst. Eng. Comm.*, 2007, **9**, 888.	N/A
KEJVEA	3-(η-C_5Me_5)-3,1,2-$RhC_2B_9H_{11}$ X.L.R. Fontaine, N.N. Greenwood, J.D. Kennedy, K. Nestor, M. Thornton-Pett, S. Hermanek, T. Jelinek and B. Stibr, *J. Chem. Soc., Dalton Trans.*, 1990, 681.	N/A
KEJVIE	3-(η-C_5Me_5)-3,1,2-$IrC_2B_9H_{11}$ X.L.R. Fontaine, N.N. Greenwood, J.D. Kennedy, K. Nestor, M. Thornton-Pett, S. Hermanek, T. Jelinek and B. Stibr, *J. Chem. Soc., Dalton Trans.*, 1990, 681	N/A
LUKKUX	3-(η-C_5Me_5)-3,1,2-$CoC_2B_9H_{11}$ A. Burke, R. McIntosh, D. Ellis, G.M. Rosair and A.J. Welch, *Collect. Czech. Chem. Commun.*, 2002, **67**, 991.	Sits on a crystallographic mirror plane.
NEJGEP	[$NPhMe_3$][3-(η-C_5H_5)-3,1,2-$FeC_2B_9H_{11}$] R.H. Herber, A.R. Kudinov, P. Zanello, I. Nowik, D.S. Perekalin, V.I. Meshcheryakov, K.A. Lyssenko, M. Corsini and S. Fedi, *Eur. J. Inorg. Chem.*, 2006, 1786.	N/A
VEMNIK	3-(η-C_6Me_6)-3,1,2-$RuC_2B_9H_{11}$ M. Bown, X.L.R. Fontaine, N.N. Greenwood, J.D. Kennedy, J. Plesek, B. Stibr and M. Thornton-Pett, *Acta Crystallogr., Sect. C: Cryst. Struct. Commun.*, 1990, **46**, 995.	Sits on a crystallographic mirror plane.
JIMXUY	3-(η-C_6H_6)-3,1,2-$FeC_2B_9H_{11}$	Sits on a

	S.S. Lee, C.B. Knobler and M.F. Hawthorne, *J. Organomet. Chem.*, 1990, **394**, 29.	crystallographic mirror plane.
LULHAB	$[N(PPh_3)_2][3\text{-}(\eta\text{-}C_5Me_5)\text{-}3,1,2\text{-}RuC_2B_9H_{11}]$ A.R. Kudinov, D.S. Perekalin, S.S. Rynin, K.A. Lyssenko, G.V. Grintselev-Knyazev and P.V. Petrovskii, *Angew. Chem., Int. Ed.*, 2002, **41**, 4112.	One cage carbon is disordered over two sites.
EQIYAF*	$[3\text{-}(\eta\text{-}C_6Me_6)\text{-}3,1,2\text{-}RhC_2B_9H_{11}][BF_4]$ D.A. Loginov, A.O. Belova, Z.A. Starikova, P.V. Petrovskii and A.R. Kudinov, *Mendeleev Commun.*, 2011, **21**, 4.	Sits on a crystallographic mirror plane.
HUSKOW	$3\text{-}(\eta\text{-}C_6Me_6)\text{-}3,1,2\text{-}FeC_2B_9H_{11}$ B. Stibr, M. Bakardjiev, J. Holub, A. Ruzicka and M. Kvicalova, *Inorg. Chem.*, 2009, **48**, 10904.	Sits on a crystallographic mirror plane.

4.4 3-R-3,1,2-closo-$MC_2B_9H_{11}$ (R = substituted arene/heterocyclic rings/four membered rings)

OPIQOU	$3\text{-}(\eta\text{-}C_5H_5BMe)\text{-}3,1,2\text{-}RhC_2B_9H_{11}$ D.A. Loginov, Z.A. Starikova, P.V. Petrovsky and A.R. Kudinov, *Izv. Akad. Nauk SSSR, Ser. Khim. (Russ.)(Russ. Chem. Bull.)*, 2010, 639.	N/A
RADCUU	$3\text{-}(\eta\text{-}NC_4H_4)\text{-}3,1,2\text{-}CoC_2B_9H_{11}$ M. Lamrani, S. Gomez, C. Vinas, F. Teixidor, R. Sillanpaa and R. Kivekas, *New J. Chem.*, 1996, **20**, 909.	N/A
BEXLAR	$3\text{-}(\eta\text{-}1,3,5\text{-}C_6Me_3H_3)\text{-}3,1,2\text{-}FeC_2B_9H_{11}$ T.P. Hanusa, J.C. Huffman and L.J. Todd, *Polyhedron*, 1982, **1**, 77.	One cage carbon is disordered over two sites.
BEXLAR01	$3\text{-}(\eta\text{-}1,3,5\text{-}C_6Me_3H_3)\text{-}3,1,2\text{-}FeC_2B_9H_{11}$ B. Stibr, M. Bakardjiev, J. Holub, A. Ruzicka, Z. Padelkova and P. Stepnicka, *Inorg. Chem.*, 2011, **50**, 3097.	One cage carbon is disordered over two sites.
EQIYEJ	$[3\text{-}(\eta^6\text{-}1,4(1,4)\text{-dibenzenacyclohexaphane})\text{-}3,1,2\text{-}RhC_2B_9H_{11}][BF_4]$ D.A. Loginov, A.O. Belova, Z.A. Starikova, P.V. Petrovskii and A.R. Kudinov, *Mendeleev Commun.*, 2011, **21**, 4.	One cage carbon wrongly assigned.
FOTLAB	$3\text{-}(p\text{-xylene})\text{-}3,1,2\text{-}FeC_2B_9H_{11}$ H.C. Kang, C.B. Knobler and M.F. Hawthorne, *Inorg. Chem.* , 1987, **26**, 3409.	N/A
FOTLEF	$3\text{-(toluene)}\text{-}3,1,2\text{-}FeC_2B_9H_{11}$	N/A

	H.C. Kang, C.B. Knobler and M.F. Hawthorne, *Inorg. Chem.* , 1987, **26**, 3409.	
HUSKUC	3-(η-1,2,4,5-$C_6Me_4H_2$)-3,1,2-$FeC_2B_9H_{11}$ B. Stibr, M. Bakardjiev, J. Holub, A. Ruzicka and M. Kvicalova, *Inorg. Chem.*, 2009, **48**, 10904.	N/A
KAXGEV	[NEt_4][3-(η-$P_2(C^tBu)_2$)-3,1,2-$RhC_2B_9H_{11}$] H.F. Dare, J.A.K. Howard, M.U. Pilotti, F.G.A. Stone and J. Szameitat, *Chem. Commun.*, 1989, 1409.	N/A
KAXGIZ	3-(η-P(P(Au(PPh_3)))($C^tBu)_2$)-3,1,2-$RhC_2B_9H_{11}$ H.F. Dare, J.A.K. Howard, M.U. Pilotti, F.G.A. Stone and J. Szameitat, *Chem. Commun.*, 1989, 1409.	N/A
ODOGAQ	3-(*p*-cymene)-3,1,2-$RuC_2B_9H_{11}$ M.E. Lopez, M.J. Edie, D. Ellis, A. Horneber, S.A. Macgregor, G.M. Rosair and A.J. Welch, *Chem. Commun.*, 2007, 2243.	N/A
TANTOR	3-(flourenyl)-3,1,2-$RuC_2B_9H_{11}$ Z.G. Lewis and A.J. Welch, *Acta Crystallogr., Sect. C: Cryst. Struct. Commun.*, 1992, **48**, 53.	N/A
XOQDAI	3-(2,5-dimethylpyrrolyl)-3,1,2-$CoC_2B_9H_{11}$ J. Llop, C. Vinas, F. Teixidor, L. Victori, R. Kivekas and R. Sillanpaa, *Organometallics*, 2002, **21**, 355.	N/A
LOPFUS	3-(η-C_4Me_4)-3,1,2-$PtC_2B_9H_{11}$ D.A. Loginov, Z.A. Starikova, E.A. Petrovskaya and A.R. Kudinov, *J. Organomet. Chem.*, 2009, **694**, 157.	N/A
UXIFOX	3-(η-C_6Me_5H)-3,1,2-$FeC_2B_9H_{11}$ B. Stibr, M. Bakardjiev, J. Holub, A. Ruzicka, Z. Padelkova, P. Stepnicka, *Inorg.Chem.*, 2011, **50**, 3097.	One cage carbon is disordered over two sites.

4.5 3,3,3-L_3-3,1,2-closo-$MC_2B_9H_{11}$

CSCREC	[Cs][3,3,3-$(CO)_3$-3,1,2-$ReC_2B_9H_{11}$] A. Zalkin, T.E. Hopkins and D.H. Templeton, *Inorg. Chem.*, 1966, **5**, 1189.	N/A
HOSGIF	[NMe_4]$_2$[3,3,3-$(CO)_3$-3,1,2-$MoC_2B_9H_{11}$] J-H. Kim, M. Lamrani and J-W. Hwang, Y. Do, *Inorg. Chim. Acta*, 1998, **283**, 145.	One cage carbon is disordered over two sites.
KISCEU	3,3,3-$(CO)_3$-3,1,2-$FeC_2B_9H_{11}$ S.S. Lee, C.B. Knobler and M.F. Hawthorne,	N/A

	Organometallics , 1991, **10**, 670.	
MOGSAC	$[NEt_4][3,3,3\text{-}(CO)_3\text{-}3,1,2\text{-}TcC_2B_9H_{11}]$ J.F. Valliant, P. Morel, P. Schaffer and J.H. Kaldis, *Inorg. Chem.*, 2002, **41**, 628.	N/A
KOBLOC	$[Cs][3,3,3\text{-}(CO)_3\text{-}3,1,2\text{-}ReC_2B_9H_{11}]$ P.A. Chetcuti, P.Moser and G. Rihs, *Organometallics*, 1991, **10**, 2895.	N/A
LAQSOL*	$3,3,3\text{-}(NMe_2)_3\text{-}3,1,2\text{-}NbC_2B_9H_{11}$ A.S. Batsanov, A.V. Churakov, J.A.K. Howard, A.K. Hughes, A.L. Johnson, A.J. Kingsley, I.S. Neretin and K. Wade, *J. Chem. Soc., Dalton Trans.*, 1999, 3867.	N/A
LAQSUR*	$3,3,3\text{-}(NEt)_3\text{-}3,1,2\text{-}TaC_2B_9H_{11}$ A.S. Batsanov, A.V. Churakov, J.A.K. Howard, A.K. Hughes, A.L. Johnson, A.J. Kingsley, I.S. Neretin and K. Wade, *J. Chem. Soc., Dalton Trans.*, 1999, 3867.	N/A
XAMPIK	$3,3,3\text{-}(N,N\text{-dimethylacetamidinato})_3\text{-}3,1,2\text{-}TaC_2B_9H_{11}$ C.K. Broder, A.E. Goeta, J.A.K. Howard, A.K. Hughes, A.L. Johnson, J.M. Malget and K. Wade, *J. Chem. Soc., Dalton Trans.*, 2000, 3526.	N/A
XAMPOQ	$3,3,3\text{-}(p\text{-fluoro-}N,N\text{-dimethylbenzamidinato})_3\text{-}3,1,2\text{-}TaC_2B_9H_{11}$ C.K. Broder, A.E. Goeta, J.A.K. Howard, A.K. Hughes, A.L. Johnson, J.M. Malget and K. Wade, *J. Chem. Soc., Dalton Trans.*, 2000, 3526.	N/A
VUPBAJ	$3,3,3\text{-}Cl_3\text{-}3,1,2\text{-}TaC_2B_9H_{11}$ R. Uhrhammer, D.J. Crowther, J.D. Olson, D.C. Swenson and R.F. Jordan, *Organometallics*, 1992, **11**, 3098.	N/A
XAMQAD*	$3,3,3\text{-}(2,6\text{-dimethylphenolato})_3\text{-}3,1,2\text{-}TaC_2B_9H_{11}$ C.K. Broder, A.E. Goeta, J.A.K. Howard, A.K. Hughes, A.L. Johnson, J.M. Malget and K. Wade, *J. Chem. Soc., Dalton Trans.*, 2000, 3526.	One cage carbon is disordered over two sites in both molecules.
SEZWUP	3-(hydrogen tris(1-pyrazolyl)borate)-3,1,2-$RhC_2B_9H_{11}$ D.M. Schubert, C.B. Knobler, S. Trofimenko and M.F. Hawthorne, *Inorg. Chem.*, 1990, **29**, 2364.	One cage carbon either wrongly assigned or disordered over two sites.

4.6 3,3-L_2-3-L'-3,1,2-closo-$MC_2B_9H_{11}$

BIHQUE	$3,3\text{-}(PPh_3)_2\text{-}3\text{-}(CO)\text{-}3,1,2\text{-}RuC_2B_9H_{11}$ D.D. Ellis, S.M. Couchman, J.C. Jeffery, J.M. Malget and	N/A

	F.G.A. Stone, *Inorg. Chem.*, 1999, **38**, 2981.	
CAZDOW	$[PHPh_3][3,3\text{-}Br_2\text{-}3\text{-}(PPh_3)\text{-}3,1,2\text{-}RhC_2B_9H_{11}]$ L. Zheng, R.T. Baker, C.B. Knobler, J.A. Walker and M.F. Hawthorne, *Inorg. Chem.*, 1983, **22**, 3350.	N/A
CEHCEX	$[NEt_4][3,3\text{-}(PPh_3)_2\text{-}3\text{-}Cl\text{-}3,1,2\text{-}RuC_2B_9H_{11}]$ I.T. Chizhevsky, I.A. Lobanova, P.V. Petrovskii, V.I. Bregadze, F.M. Dolgushin, A.I. Yanovsky, Y.T. Struchkov, A.L. Chistyakov, I.V. Stankevich, C.B. Knobler and M.F. Hawthorne, *Organometallics*, 1999, **18**, 726.	N/A
CEHCIB	$[NEt_4][3,3\text{-}(PPh_3)_2\text{-}3\text{-}H\text{-}3,1,2\text{-}RuC_2B_9H_{11}]$ I.T. Chizhevsky, I.A. Lobanova, P.V. Petrovskii, V.I. Bregadze, F.M. Dolgushin, A.I. Yanovsky, Y.T. Struchkov, A.L. Chistyakov, I.V. Stankevich, C.B. Knobler and M.F. Hawthorne, *Organometallics*, 1999, **18**, 726.	N/A
HIZQIQ	$3,3\text{-}(CO)_2\text{-}3\text{-}(\eta^2\text{-}1\text{-phenyl-prop-2-yne})\text{-}3,1,2\text{-}RuC_2B_9H_{11}$ J.C. Jeffery, P.A. Jelliss, E. Psillakis, G.E.A. Rudd and F.G.A. Stone, *J. Organomet. Chem.*, 1998, **562**, 17.	N/A
HIZQOW	$3,3\text{-}(CO)_2\text{-}3\text{-}(1\text{-phenyl-1-triethylphosphineprop-2-en-2-yl})\text{-}3,1,2\text{-}RuC_2B_9H_{11}$ J.C. Jeffery, P.A. Jelliss, E. Psillakis, G E.A. Rudd and F.G.A. Stone, *J. Organomet. Chem.*, 1998, **562**, 17.	N/A
KISBIX	$3,3\text{-}(CO)_2\text{-}3\text{-}(PPh_3)\text{-}3,1,2\text{-}FeC_2B_9H_{11}$ S.S. Lee, C.B. Knobler and M.F. Hawthorne, *Organometallics*, 1991, **10**, 670.	N/A
MEFNEQ	$3,3\text{-}(CO)_2\text{-}3\text{-}(NCMe)\text{-}3,1,2\text{-}RuC_2B_9H_{11}$ D. Ellis, P. Jelliss and F.G.A. Stone, *Private Communication*, 2002.	N/A
NITWOC	$3,3\text{-}(PPh_3)_2\text{-}3\text{-}Cl\text{-}3,1,2\text{-}RhC_2B_9H_{11}$ I.T. Chizhevsky, I.V. Pisareva, E.V. Vorontzov, V.I. Bregadze, F.M. Dolgushin, A.I. Yanovsky, Y.T. Struchkov, C.B. Knobler and M.F. Hawthorne, *J. Organomet. Chem.*, 1997, **536**, 223.	N/A
QAQQAB	$3\text{-}(dppp)\text{-}3\text{-}Cl\text{-}3,1,2\text{-}RuC_2B_9H_{11}$ D.N. Cheredilin, R. Kadyrov, F.M. Dolgushin, E.V. Balagurova, I.A. Godovikov, S.P. Solodovnikov and I.T. Chizhevsky, *Inorg. Chem. Commun.*, 2005, **8**, 614.	N/A
QEXWEW	$3\text{-}(dppe)\text{-}3\text{-}Cl\text{-}3,1,2\text{-}RuC_2B_9H_{11}$ D.N. Cheredilin, F.M. Dolgushin, I.D. Grishin, E.V.	N/A

	Kolyakina, A.S. Nikiforov, S.P. Solodovnikov, M.M. Il'in, V.A. Davankov, I.T. Tsizhevsky and D.F. Grishin, *Izv. Akad. Nauk SSSR, Ser. Khim. (Russ.)(Russ. Chem. Bull.)*, 2006, 1120.	
REQSIP	3,3-$(PPhMe_2)_2$-3-(N-phenylthioformamido)-3,1,2-$RhC_2B_9H_{11}$ P.A. McEneaney, T.R. Spalding and G. Ferguson, *J. Chem. Soc., Dalton Trans.*, 1997, 145.	N/A
BIHYOG	3,3-$(PPh_3)_2$-3-(μ^2(Au-Ru)-(H))-3-(Au(PPh_3))-3,1,2-$RuC_2B_9H_{11}$ D.D. Ellis, S.M. Couchman, J.C. Jeffery, J.M. Malget and F.G.A. Stone, *Inorg. Chem.*, 1999, **38**, 2981.	N/A
TAKCIR	[NEt_4][3,3-$(CO)_2$-3-($SnPh_3$)-3,1,2-$FeC_2B_9H_{11}$] S.S. Lee, C.B. Knobler and M.F. Hawthorne, *Organometallics*, 1991, **10**, 1054.	N/A
TELCIW	3,3-$(PPh_3)_2$-3-Cl-3,1,2-$RhC_2B_9H_{11}$ G. Ferguson, P.A. McEneaney and T.R. Spalding, *Acta Crystallogr., Sect. C: Cryst. Struct. Commun.*, 1996, **52**, 2710.	N/A
TUBLUX	3,3-$(PPhMe_2)_2$-3-Cl-3,1,2-$CoC_2B_9H_{11}$ S.L. Hendershot, J.C. Jeffery, P.A. Jelliss, D.F. Mullica, E.L. Sappenfield and F.G.A. Stone, *Inorg. Chem.*, 1996, **35**, 6561.	N/A
VENBIZ	3-(dithioformato-S,S′)-3-(PPh_3)-3,1,2-$RhC_2B_9H_{11}$ G. Ferguson, S. Coughlan, T.R. Spalding, X.L.R. Fontaine, J.D. Kennedy and B. Stibr, *Acta Crystallogr., Sect. C: Cryst. Struct. Commun.*, 1990, **46**, 1402.	N/A
YEBHOD	3-(bipy)-3-(CO)-3,1,2-$RuC_2B_9H_{11}$ P.A. Jelliss, J. Mason, J.M. Nazzoli, J.H. Orlando, A. Vinson, N.P. Rath and M.J. Shaw, *Inorg. Chem.*, 2006, **45**, 370.	N/A
YEBHUJ	3-(N,N,N′,N′-tetramethylethylenediamine)-3-(CO)-3,1,2-$RuC_2B_9H_{11}$ P.A. Jelliss, J. Mason, J.M. Nazzoli, J.H. Orlando, A. Vinson, N.P. Rath and M.J. Shaw, *Inorg. Chem.*, 2006, **45**, 370.	N/A
ZEPYIC	[$Au(PPh_3)_2$][3,3-$(CO)_2$-3-Cl-3,1,2-$RuC_2B_9H_{11}$] S. Anderson, D.F. Mullica, E.L. Sappenfield and F.G.A. Stone, *Organometallics*, 1995, **14**, 3516.	N/A
ZOTVOT	3,3-$(PMePh_2)_2$-3-Cl-3,1,2-$RhC_2B_9H_{11}$	N/A

	G. Ferguson, J. Pollock, P.A. McEneaney, D.P. O'Connell, T.R. Spalding, J.F. Gallagher, R. Macias and J.D. Kennedy, *Chem. Commun.*, 1996, 679.	
TOJROZ	[*p*-$(PPh_3CH_2)_2(C_6H_4)$][3-(μ^2-oxo)-(3,3-$(O)_2$-3,1,2-$MoC_2B_9H_{11})_2$] J-H. Kim, E. Hong, J. Kim and Y. Do, *Inorg. Chem.*, 1996, **35**, 5112.	Two cages linked by a bridging oxygen gives two ELOs which are the same by symmetry.
XODXAP	3-(μ^2-oxo)-(3,3-$(NMe_2)_2$-3,1,2-$TaC_2B_9H_{11})_2$ M.A. Fox, A.E. Goeta, A.K. Hughes, J.M. Malget, K. Wade, *Collect. Czech. Chem. Commun.*, 2002, **67**, 791.	Two cages linked by a bridging oxygen gives two ELOs.
KISBUJ	3,3-$(P(OMe)_3)_2$-3-(CO)-3,1,2-$FeC_2B_9H_{11}$ S.S. Lee, C.B. Knobler and M.F. Hawthorne, *Organometallics*, 1991, **10**, 670.	Sits on a crystallographic mirror plane.
HPRHCB	3,3-$(PPh_3)_2$-3-H-3,1,2-$RhC_2B_9H_{11}$ G.E. Hardy, K.P. Callahan, C.E. Strouse and M.F. Hawthorne, *Acta Crystallogr., Sect. B: Struct. Crystallogr. Cryst. Chem.*, 1976, **32**, 264.	One cage carbon is disordered over two sites.
TPNRHB*	3-(κ^2-nitrato)-3-(PPh_3)-3,1,2-$RhC_2B_9H_{11}$ Z. Demidowicz, R.G. Teller and M.F. Hawthorne, *Chem. Commun.*, 1979, 831.	Both cage carbons wrongly assigned in both molecules
TAKCOX*	[$N(PPh_3)_2$][3-(η-allyl)-3-(CO)-3,1,2-$FeC_2B_9H_{11}$] S.S. Lee, C.B. Knobler and M.F. Hawthorne, *Organometallics*, 1991, **10**, 1054.	Sits on a crystallographic mirror plane.
WURZUF	3-(bipy)-3-(PPh_3)-3,1,2-$RuC_2B_9H_{11}$ D.I. D'yachikhin, F.M. Dolgushin, I.A. Godovikov and I.T. Chizhevsky, *Mendeleev Commun.*, 2010, **20**, 174.	N/A
FIRHOD	3-(η-allyl)-3-(PPh_3)-3,1,2-$RhC_2B_9H_{11}$ J.A. Walker, L. Zheng, C.B. Knobler, J. Soto and M.F. Hawthorne, *Inorg. Chem.*, 1987, **26**, 1608.	N/A
UZUYEU	3-(dppb)-3-Cl-3,1,2-$RuC_2B_9H_{11}$ I.D. Grishin, D.I. D'yachihin, A.V. Piskunov, F.M. Dolgushin, A.F. Smol'yakov, M.M. Il'in, V.A. Davankov, I.T. Chizhevsky and D.F. Grishin, *Inorg. Chem.*, 2011, **50**, 7574.	N/A
ZOTVIN	[3-$(PMePh_2)_2$-3-(MeCN)-3,1,2-$RhC_2B_9H_{11}$][SbF_6]	N/A

	G. Ferguson, J. Pollock, P.A. McEneaney, D.P. O'Connell, T.R. Spalding, J.F. Gallagher, R. Macias and J.D. Kennedy, *Chem. Commun.* , 1996, 679.	
SEMZIV	3-(dpp(pentane))-3-Cl-3,1,2-$RuC_2B_9H_{11}$ I.D. Grishin, D.I. D'yachihin, E.S. Turmina, F.M. Dolgushin, A.F. Smol'yakov, A.V. Piskunov, I.T. Chizhevsky and D.F. Grishin, *J. Organomet. Chem.*, 2012, **721**, 113.	N/A
HOHDEN	3-((μ^2-4-methylphenylmethylidynyl)hydrogen-tris(pyrazol-1-yl)borate($W(CO)_2$))-3,3-$(CO)_2$-3,1,2-$RuC_2B_9H_{11}$ D.D. Ellis, J.M. Farmer, J.M. Malget, D.F. Mullica and F.G.A. Stone, *Organometallics*, 1998, **17**, 5540.	N/A
HOHDIR	3-((μ^2-4-methylphenylmethylenethio-C,S)hydrogen-tris(pyrazol-1-yl)borate($W(CO)_2$))-3,3-$(CO)_2$-3,1,2-$RuC_2B_9H_{11}$ D.D. Ellis, J.M. Farmer, J.M. Malget, D.F. Mullica and F.G.A. Stone, *Organometallics*, 1998, **17**, 5540.	N/A
HOHDAJ*	3-((μ^2-4-methylphenylmethylidynyl)(η-C_5H_5)($W(CO)_2$))-3,3-$(CO)_2$-3,1,2-$RuC_2B_9H_{11}$ D.D. Ellis, J.M. Farmer, J.M. Malget, D.F. Mullica and F.G.A. Stone, *Organometallics*, 1998, **17**, 5540.	N/A
HIZQUC	3-(dppm)-(3,3-$(CO)_2$-3,1,2-$RuC_2B_9H_{11}$)$_2$ J.C. Jeffery, P.A. Jelliss, E. Psillakis, G.E.A. Rudd and F.G.A. Stone, *J. Organomet. Chem.*, 1998, **562**, 17.	Two cages linked by a bridging dppm gives two different ELOs.
HIPQII	3-(dppe)-3-Cl-3,1,2-$CoC_2B_9H_{11}$ A.P. Tyurin, A.F. Smolyakov, F.M. Dolgushin, I.A. Godovikov and I.T. Chizhevsky, *Izv. Akad. Nauk SSSR, Ser. Khim. (Russ.)(Russ. Chem. Bull.)*, 2013, 1938.	N/A

4.7 3-L-3-L'-3-L''-3,1,2-closo-$MC_2B_9H_{11}$

LICDOQ	3-(NO)-3-(CO)-3-(4-methyl-α-methoxybenzylidene)-3,1,2-$ReC_2B_9H_{11}$ D.D. Ellis, P.A. Jelliss and F.G.A. Stone, *Chem. Commun.*, 1999, 2385.	N/A
LOBSUQ	[NEt_4][3-(CO)-3-(PPh_3)-3-I-3,1,2-$RuC_2B_9H_{11}$] S. Du, D.D. Ellis, P.A. Jelliss, J.A. Kautz, J.M. Malget and F.G.A. Stone, *Organometallics*, 2002, **19**, 1983.	N/A
KISBOD	3-(CO)-3-(PPh_3)-3-(NCMe)-3,1,2-$FeC_2B_9H_{11}$	N/A

	S.S. Lee, C.B. Knobler and M.F. Hawthorne, *Organometallics*, 1991, **10**, 670.	
BOZMUY	3-(1,4-diphenyl-2-triphenylphosphine-buta-1,3-diene-1,4-diyl)-3-(PPh_3)-3,1,2-$RhC_2B_9H_{11}$ W.C. Kalb, Z. Demidowicz, D.M. Speckman, C. Knobler, R.G. Teller and M.F. Hawthorne, *Inorg. Chem.*, 1982, **21**, 4027.	N/A
DIKFUY	3-(2-(diphenylphosphino)-phenyl-C^1,P)-3-(PPh_3)-3,1,2-$RhC_2B_9H_{11}$ C.B. Knobler, R.E. King III and M.F. Hawthorne, *Acta Crystallogr., Sect. C: Cryst. Struct. Commun.*, 1986, **42**, 159.	N/A
JEMDAG	3-(PPh_3)-3-(CO)-3-((η-C_5H_5)$(CO)_2$(μ^2-p-tolylmethylidyne)WAu)-3,1,2-$RhC_2B_9H_{11}$ N. Carr, M.C. Gimeno, J.E. Goldberg, M.U. Pilotti, F.G.A. Stone and I. Topaloglu, *J. Chem. Soc., Dalton Trans.*, 1990, 2253.	N/A
TAKCUD	$[N(PPh_3)_2]$[3-(CO)-3-(PPh_3)-3-(MeCO)-3,1,2-$FeC_2B_9H_{11}$] S.S. Lee, C.B. Knobler and M.F. Hawthorne, *Organometallics*, 1991, **10**, 1054.	N/A

4.8 2-(L_2L'/L_3)-2,1-closo-$MCB_{10}H_{11}$

RURZUZ*	2,2-$(PEt_3)_2$-2-H-2,1-$PtCB_{10}H_{11}$ S.A. Batten, J.C. Jeffery, P.L. Jones, D.F. Mullica, M.D. Rudd, E.L. Sappenfield, F.G.A. Stone and A. Wolf, *Inorg. Chem.*, 1997, **36**, 2570.	N/A
RUSBAI	2,2-$(PEt_3)_2$-2-(Au(PPh_3))-2,1-$PtCB_{10}H_{11}$ S.A. Batten, J.C. Jeffery, P.L. Jones, D.F. Mullica, M.D. Rudd, E.L. Sappenfield, F.G.A. Stone and A. Wolf, *Inorg. Chem.*, 1997, **36**, 2570.	Sits on a crystallographic mirror plane.
RUSBIQ	2,2-$(PEt_3)_2$-2-(Hg(Ph))-2,1-$PtCB_{10}H_{11}$ S.A. Batten, J.C. Jeffery, P.L. Jones, D.F. Mullica, M.D. Rudd, E.L. Sappenfield, F.G.A. Stone and A. Wolf, *Inorg. Chem.*, 1997, **36**, 2570.	N/A
VABCOQ	2,2-$(PPhMe_2)_2$-2-Cl-2,1-$PtCB_{10}H_{11}$ I. Blandford, J.C. Jeffery, H. Redfearn, L.H. Rees, M.R. Dudd and F.G.A. Stone, *J. Chem. Soc., Dalton Trans., 1998*, 1669.	N/A
SEQQIO	$[N(CH_2Ph)Et_3]_2$[2,2,2-$(CO)_3$-2,1-$ReCB_{10}H_{11}$] I. Blandford, J.C. Jeffery, P.A. Jelliss and F.G.A. Stone,	N/A

	Organometallics, 1998, **17**, 1402.	

4.9 2-($L_2L'/C_5H_5/C_5Me_5$/arene)-2,1-closo-$MXB_{10}H_{10}$ ($X \neq C$)

CIVFUJ	2,2-$(PPhMe_2)_2$-2-Cl-2,1-$RhSB_{10}H_{10}$ R. Macias, M. Thornton-Pett, J. Holub, T.R. Spalding, Y. Faridoon, B. Stibr and J.D. Kennedy, *J. Organomet. Chem.*, 2008, **693**, 435.	N/A
GEXFEU	2-(dithioformato-S,S′)-2-(PPh_3)-2,1-$RhSeB_{10}H_{10}$ G. Ferguson, Faridoon and T.R.Spalding, *Acta Crystallogr., Sect. C: Cryst. Struct. Commun.*, 1988, **44**, 1368.	N/A
KOJKUP	2,2-$(PPh_3)_2$-2-H-2,1-$RhNB_{10}H_{11}$ H-P. Hansen, J. Muller, U. Englert and P. Paetzold, *Angew. Chem., Int.Ed.*, 1991, **30**, 1377.	N/A
REQSOV	2,2-$(PPhMe_2)_2$-2-(N-phenylthioformamido)-2,1-$RhTeB_{10}H_{10}$ P.A. McEneaney, T.R. Spalding and G. Ferguson, *J. Chem. Soc., Dalton Trans.*, 1997, 145.	N/A
SABDAA	2,2-$(PPh_3)_2$-2-H-2,1-$RhTeB_{10}H_{10}$ Faridoon, O.N. Dhubhghaill, T.R. Spalding, G. Ferguson, B. Kaitner, X.L.R. Fontaine J.D. Kennedy and D. Reed, *J. Chem. Soc., Dalton Trans.*, 1988, 2739.	N/A
WIBSAB	2-(N-phenyldithiocarbamato-S,S′)-2-(PPh_3)-2,1-$RhTeB_{10}H_{10}$ G. Ferguson, D. O'Connell and T. R. Spalding, *Acta Crystallogr., Sect. C: Cryst. Struct. Commun.*, 1994, **50**, 1432.	N/A
GEBBIY	2-(toluene)-2,1-$FeSB_{10}H_{10}$ S.O. Kang, P.J. Carroll and L.G. Sneddon, *Organometallics*, 1988, **7**, 772.	N/A
SEWVAR*	2-(η-C_5Me_5)-2,1-$RhTeB_{10}H_{10}$ Faridoon, M. McGrath, T.R. Spalding, X.L.R. Fontaine, J.D. Kennedy and M. Thornton-Pett, *J. Chem. Soc., Dalton Trans.*, 1990, 1819.	N/A
SEWVEV	2-(η-C_6Me_6)-2,1-$RuTeB_{10}H_{10}$ Faridoon, M. McGrath, T.R. Spalding, X.L.R. Fontaine, J.D. Kennedy and M. Thornton-Pett, *J. Chem. Soc., Dalton Trans.*, 1990, 1819.	N/A
YOYHAV	2-(η-C_6Me_6)-2,1-$RuNB_{10}H_{11}$	N/A

	H.-P. Hansen, U. Englert and P. Paetzold, *Z. Anorg. Allg. Chem.*, 1995, **621**, 719.	

4.10 3-($L_2L'_2$/$L_2L'L''$/L_3L')-3,1,2-closo-$MC_2B_9H_{11}$

FINWIJ	$[HNMe_3][3,3\text{-}(CO)_2\text{-}3,3\text{-}(Cl)_2\text{-}3,1,2\text{-}ReC_2B_9H_{11}]$ M. J. Fischer, P. A. Jelliss, L. M. Phifer and N. P. Rath, *Inorg. Chim. Acta*, 2005, **358**, 1531.	N/A
TOJREP	$[NMe_4]_2[3,3\text{-}(CO)_2\text{-}3,3\text{-}(SPh)_2\text{-}3,1,2\text{-}MoC_2B_9H_{11}]$ J-H. Kim, E. Hong, J. Kim and Y. Do, *Inorg. Chem.*, 1996, **35**, 5112.	N/A
HOSGOL	$[N(PPh_3)_2][3,3\text{-}(CO)_2\text{-}3\text{-}$(diethyldithiocarbamato-S,S′)$\text{-}3,1,2\text{-}MoC_2B_9H_{11}]$ J-H. Kim, M. Lamrani, J-W. Hwang and Y. Do, *Inorg. Chim. Acta*, 1998, **283**, 145.	One cage carbon is disordered over two sites.
QEXWAS	$3,3\text{-}(PPh_3)_2\text{-}3\text{-}H\text{-}3\text{-}Cl\text{-}3,1,2\text{-}RuC_2B_9H_{11}$ D. N. Cheredilin, F. M. Dolgushin, I. D. Grishin, E. V. Kolyakina, A. S. Nikiforov, S. P. Solodovnikov, M. M. Il'in, V. A. Davankov, I. T. Tsizhevsky and D. F. Grishin, *Izv. Akad. Nauk SSSR, Ser. Khim. (Russ.)(Russ. Chem. Bull.)*, 2006, 1120.	N/A
TEXYUQ	$3,3\text{-}(PPh_3)_2\text{-}3\text{-}H\text{-}3\text{-}Cl\text{-}3,1,2\text{-}OsC_2B_9H_{11}$ I.T.Chizhevsky, P.V.Petrovskii, P.V.Sorokin, V.I.Bregadze, F. M. Dolgushin, A. I. Yanovsky and Yu. T. Struchkov, *Organometallics*, 1996, **15**, 2619.	N/A
HOSGUR	$[NMe_4][3,3\text{-}(CO)_2\text{-}3\text{-}$(2-sulfido-pyridyl-N,S)$\text{-}3,1,2\text{-}MoC_2B_9H_{11}]$ J-H. Kim, M. Lamrani, J-W. Hwang and Y. Do, *Inorg. Chim. Acta*, 1998, **283**, 145.	N/A
UZUYAQ	3-(dppb)$\text{-}3\text{-}H\text{-}3\text{-}Cl\text{-}3,1,2\text{-}RuC_2B_9H_{11}$ I.D. Grishin, D.I. D'yachihin, A.V. Piskunov, F.M. Dolgushin, A.F. Smol'yakov, M.M. Il'in, V.A. Davankov, I.T. Chizhevsky and D.F. Grishin, *Inorg. Chem.*, 2011, **50**, 7574.	N/A
WELNEG	$[3,3,3\text{-}(NC^tBu)_3\text{-}3\text{-}$(t-butyliminoethyl-C,N)$\text{-}3,1,2\text{-}MoC_2B_9H_{11}][SO_3CF_3]$ S.J. Dossett, S. Li, D.F. Mullica, E.L. Sappenfield and F.G.A. Stone, *Organometallics*, 1994, **13**, 822.	N/A

4.11 2-(L_2L'/$LL'L''$/C_5H_5/C_5Me_5/arene)-2,1,7-closo-$MC_2B_9H_{11}$

HABKIE*	2-(dithioformato-S,S′)-2-(PPh_3)-2,1,7-$RhC_2B_9H_{11}$ G. Ferguson, S. Couglan and T. R. Spalding, *Acta Crystallogr., Sect. C: Cryst. Struct. Commun.*, 1993, **49**, 957.	N/A
BUVBUP	[(PPh_3)$_2$N][2-(κ^2-(*m*-fluorobenzonitrile N-oxycarbonyl))-2-(PPh_3)-2,1,7-$RhC_2B_9H_{11}$ P.A. Chetcuti, J.A. Walker, C.B. Knobler and M.F. Hawthorne, *Organometallics*,1988, **7**, 641.	N/A
EDAGAS	2,2-(PPh_3)$_2$-2,2-(H)$_2$-2,1,7-$OsC_2B_9H_{11}$ E.V. Balagurova, D.N. Cheredilin, G.D. Kolomnikova, O.L. Tok, F.M. Dolgushin, A.I. Yanovsky and I.T. Chizhevsky, *J. Am. Chem. Soc.*, 2007, **129**, 3745.	N/A
ITAMAS	2-(η-1,2,3,4,5-C_6Me_5H)-2,1,7-$FeC_2B_9H_{11}$ J. Holub, B. Stibr, M. Bakardjiev, A. Ruzicka and Z. Padelkova, *Dalton Trans.*, 2011, **40**, 6623.	N/A
ITAMEW	2-(η-1,3,5-$C_6Me_3H_3$)-2,1,7-$FeC_2B_9H_{11}$ J. Holub, B. Stibr, M. Bakardjiev, A. Ruzicka and Z. Padelkova, *Dalton Trans.*, 2011, **40**, 6623.	N/A
SEZXAW*	2-(Hydrogen tris(1-pyrazolyl)borate)-2,1,7-$RhC_2B_9H_{11}$ D.M. Schubert, C.B. Knobler, S. Trofimenko and M.F. Hawthorne, *Inorg. Chem.*, 1990, **29**, 2364.	One cage carbon disordered over two sites in molecule two.
EZEZIS	2-(η^4-C_5Me_5H)-2,1,7-$CoC_2B_9H_{11}$ B.E. Hodson, T.D. McGrath and F.G.A. Stone, *Inorg.Chem.*, 2004, **43**, 3090.	
UJEYEO*	2-(η-C_5H_5)-2,1,7-$CoC_2B_9H_{11}$ M.E. Lopez, D. Ellis, P.R. Murray, G.M. Rosair, A.J. Welch and L.J. Yellowlees, *Collect. Czech. Chem. Commun.*, 2010, **75**, 853.	N/A

4.12 Subicosahedral

MOKHOJ	1-H-1-Cl-1,1-(PPh_3)$_2$-1,2,3-$RuC_2B_4H_6$ I.V. Pisareva, F.M. Dolgushin, O.L. Tok, V.E. Konoplev, K.Yu. Suponitsky, A.I. Yanovsky and I.T. Chizhevsky, *Organometallics*, 2001, **20**, 4216.	N/A
GETMAT	2-(η-C_6Me_6)-2,1,6-$RuC_2B_7H_9$	N/A

	M. Bown, T. Jelinek, B. Stibr, S. Hermanek, X.L.R. Fontaine, N.N. Greenwood, J.D. Kennedy and M. Thornton-Pett, *Chem. Commun.*, 1988, 974.	
HEPCOB	2,2-$(PEt_3)_2$-2-H-2,1,6-$RhC_2B_7H_9$ G.K. Barker, M.P. Garcia, M. Green, F.G.A. Stone, J.-M. Bassett and A.J. Welch, *Chem. Commun.*, 1981, 653.	N/A
OCEWUP	$[N(PPh_3)_2]$[2,2,2-$(CO)_3$-2,1-$FeCB_8H_9$] A. Franken, T.D. McGrath and F.G.A. Stone, *Inorg. Chem.*, 2006, **45**, 2669.	N/A
RARJUP	2,2-$(PMe_3)_2$-2-H-2,1-$IrSB_8H_8$ J. Bould, N.P. Rath and L. Barton, *Organometallics*, 1996, **15**, 4916.	N/A
XIDPEH	2,2-$(PPh_3)_2$-2-H-2,1-$RhSB_8H_8$ S. Luaces, J. Bould, R. Macias, R. Sancho, F.J. Lahoz and L.A. Oro, *Dalton Trans.*, 2012, **41**, 11627.	N/A
ZOMTOK	2-(η-C_5H_5)-2,1,6-$CoC_2B_7H_9$ W. Weinmann, F. Metzner, H. Pritzkow, W. Siebert and L. Sneddon, *Chem.Ber.*, 1996, **129**, 213.	N/A

4.13 Supraicosahedral

KAPQAU	$[N(PPh_3)_2]$[4,4,4-$(CO)_3$-4,1,6-$ReC_2B_{10}H_{12}$] B.E. Hodson, T.D. McGrath and F.G.A. Stone, *Organometallics*, 2005, **24**, 3386.	N/A
KAPQEY	$[N(PPh_3)_2]$[4,4,4-$(CO)_3$-4,1,6-$MnC_2B_{10}H_{12}$] B.E. Hodson, T.D. McGrath and F.G.A. Stone, *Organometallics*, 2005, **24**, 3386.	N/A
JACCOG	$[N(CH_2Ph)Me_3]$[4,4-$(CO)_2$-4-(η^3-allyl)-4,1,6-$MoC_2B_{10}H_{12}$] M.A. Laguna, D. Ellis, G.M. Rosair and A.J. Welch, *Inorg. Chim. Acta*, 2003, **347**, 161.	N/A
CANNOV01*	4-(*p*-cymene)-4,1,6-$RuC_2B_{10}H_{12}$ A. Burke, D. Ellis, D. Ferrer, D.L. Ormsby, G.M. Rosair and A.J. Welch, *Dalton Trans.*, 2005, 1716.	N/A
CPCOTB10	4-(η-C_5H_5)-4,1,6-$CoC_2B_{10}H_{12}$ M.R. Churchill and B.G. DeBoer, *Inorg. Chem.*, 1974, **13**, 1411.	N/A
LUKKEH	4-(η-C_5Me_5)-4,1,6-$CoC_2B_{10}H_{12}$	N/A

	A. Burke, R. McIntosh, D. Ellis, G.M. Rosair and A.J. Welch, *Collect. Czech. Chem. Commun.*, 2002, **67**, 991.	
YALZUH	$[N(PPh_3)_2]$ [4-(η^2,η^2-COD)-4,1,6-$RhC_2B_{10}H_{12}$] B.E. Hodson, T.D. McGrath and F.G.A. Stone, *Organometallics*, 2005, **24**, 1638.	N/A
XERBED	1,14-(η-$C_5H_5)_2$-1,14,2,10-$Co_2C_2B_{10}H_{12}$ A. McAnaw, M.E. Lopez, D. Ellis, G.M. Rosair and A.J. Welch, *Dalton Trans.*, 2013, **42**, 671.	One cage carbon disordered over two sites.
XERBIH	1-(*p*-cymene)-14-(η-C_5H_5)-1,14,2,10-$RuCoC_2B_{10}H_{12}$ A. McAnaw, M.E. Lopez, D. Ellis, G.M. Rosair and A.J. Welch, *Dalton Trans.*, 2013, **42**, 671.	N/A

Miscellaneous

CIDHAY	1,2-(*o*-xylylene)-3,3-$(PPh_3)_2$-3-H-3,1,2-$RhC_2B_9H_9$ C.B. Knobler, T.B. Marder, E.A. Mizusawa, R.G. Teller, J.A. Long, P.E. Behnken, M.F. Hawthorne, *J. Am. Chem. Soc.*, 1984, **106**, 2990.	N/A
UJEYIS*	2-(η-C_5H_5)-2,1,12-$CoC_2B_9H_{11}$ M.E. Lopez, D. Ellis, P.R. Murray, G.M. Rosair, A.J. Welch and L.J. Yellowlees, *Collect. Czech. Chem. Commun.*, 2010, **75**, 853.	N/A